Highly Fluorinated Model Compounds for Matter-Wave Interferometry

Inauguraldissertation

zur

Erlangung der Würde eines Doktors der Philosophie
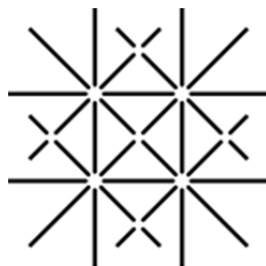
vorgelegt der

Philosophisch-Naturwissenschaftlichen Fakultät

der Universität Basel

von

Jens Tüxen

aus Weil am Rhein, Deutschland

UNI
BASEL

Basel, 2012

Genehmigt von der Philosophisch-Naturwissenschaftlichen Fakultät

auf Antrag von

Prof. Dr. Marcel Mayor

Prof. Dr. Stefan Willitsch

Prof. Dr. Willi Bannwarth

Basel, den 24.04.2012

Prof. Dr. Martin Spiess

creative commons

Namensnennung-Keine kommerzielle Nutzung-Keine Bearbeitung 2.5 Schweiz

---

Sie dürfen:

das Werk vervielfältigen, verbreiten und öffentlich zugänglich machen

Zu den folgenden Bedingungen:

Namensnennung. Sie müssen den Namen des Autors/Rechteinhabers in der von ihm festgelegten Weise nennen (wodurch aber nicht der Eindruck entstehen darf, Sie oder die Nutzung des Werkes durch Sie würden entlohnt).

Keine kommerzielle Nutzung. Dieses Werk darf nicht für kommerzielle Zwecke verwendet werden.

Keine Bearbeitung. Dieses Werk darf nicht bearbeitet oder in anderer Weise verändert werden.

- Im Falle einer Verbreitung müssen Sie anderen die Lizenzbedingungen, unter welche dieses Werk fällt, mitteilen. Am Einfachsten ist es, einen Link auf diese Seite einzubinden.

- Jede der vorgenannten Bedingungen kann aufgehoben werden, sofern Sie die Einwilligung des Rechteinhabers dazu erhalten.

- Diese Lizenz lässt die Urheberpersönlichkeitsrechte unberührt.

Quelle: http://creativecommons.org/licenses/by-nc-nd/2.5/ch/   Datum: 3.4.2009

Dedicated to:

Jasmin and Rainer

Table of Contents

1 Introduction

1.1 Matter-Wave Interferometry

In our everyday life, the macroscopic world, we are very familiar with the behavior of waves such as sound waves or waves that propagate on the surface of water. However, it seems contradictory to us to assign a wave nature to particles. The wave nature of matter, which represents one of the cornerstones of quantum mechanics, is completely excluded in the description of classical objects.

The phenomenon that microscopic particles, such as electrons, neutrons, atoms and small molecules, are able to behave like waves has been extensively studied and goes back to the findings by Louis de Broglie.[1] He was the first who proposed the wave-particle duality for electrons in 1924. According to de Broglie, for every particle with a momentum a corresponding wavelength can be assigned.

$$\lambda_{\mathrm{dB}} = \frac{h}{p} = \frac{h}{m * v}$$ 1.1

The relation is given by equation 1.1 where λ_{dB} is the de Broglie wavelength, h is the Planck constant, p is the momentum, m is the mass and v is the velocity. In 1927 de Broglie's hypotheses were experimentally confirmed by Davisson and Germer.[2] They were able to observe the wave nature of electrons by diffraction experiments on the surface of a nickel crystal. In the following years further work of Estermann and Stern revealed the wave nature of helium atoms and dihydrogen molecules.[3] In their studies diffraction on a crystal face of lithium fluoride led to the formation of interference patterns. Substantial progress in these first years of matter-wave experiments was made by Halban and Preiswerk who observed the wave nature of neutrons in 1936.[4] However, today it remains a great challenge to observe the wave-particle duality for larger objects, such as macromolecules. Furthermore, the wave nature of macroscopic objects has never been observed.

When two waves interact, the principle of superposition says that the emerging new wave is the sum of both wave functions. This phenomenon is called interference. A pioneering experimental concept to visualize interference, and thus wave behavior, has its origin more than two hundred years ago. In his double-slit experiment Thomas Young imaged an interference pattern by shining light onto a photographic screen that was placed behind a plate with two small slits cut into it (figure 1).[5] The interaction of the light behind the double slit led to intensity patterns on the screen which are not explainable if light is modeled as

consisting of particles. Only characteristics of waves with the phenomena of constructive and destructive interference were suitable to explain the obtained patterns.
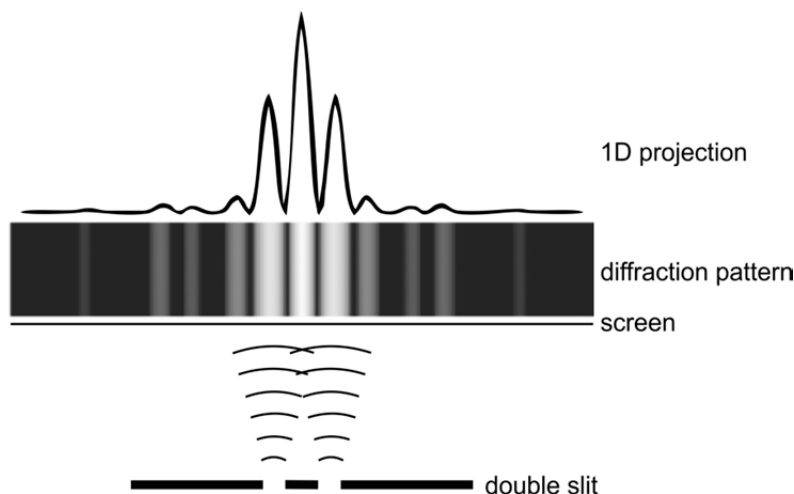
Figure 1. Demonstration of the wave nature of light in the double-slit experiment by Thomas Young from 1807. By shining light onto a thin plate with two small slits an interference pattern can be observed on a screen behind the thin plate. The interference pattern arises from constructive and destructive interference of light waves. The graphic was adopted from reference [6].

As described above the birth of matter-wave interferometry dates back to the first half of the last century. Especially the ten years after de Broglie's hypotheses in 1927, the experiments of Davisson and Germer, Estermann and Stern, and Halban and Preiswerk, represent a groundbreaking period in this field of research. However, after Young's double-slit experiment with light waves in 1807 it took more than 150 years until this type of experiments, i.e. diffraction on a double slit, was performed with other objects. In 1961 experiments with beams of electrons were conducted by Jönsson.[7] First double-slit experiments with neutrons and atoms followed in the 1980s and 1990s.[8]–[10]

Following on from the pioneering work of Estermann and Stern, who presented the first molecule (H_2) acting as a wave in 1930, a milestone in the field of molecule interferometry was published by Schöllkopf and Toennies in 1994.[11] Their experiments with cold and weakly bound helium dimers marked the starting point for a series of molecule interference experiments with other examples of small interfering molecules in the following years. Mainly cold diatomic systems, including I_2,[12] Na_2,[13] K_2[14] and D_2[15] were shown to interfere in the first years after the appearance of the work of Schöllkopf and Toennies. A breakthrough regarding the complexity of interfering objects was the first macromolecule interference experiment with the buckminsterfullerene C_{60} performed by Arndt *et al.* in 1999.[16] In the following an overview about the different types and aspects of molecule interferometry experiments is given. After a short discussion of the realization of quantum

interference experiments (QIE) with small molecules, the main focus lies on matter-wave interferometry with macromolecules with its starting point in 1999 by Arndt *et al.*.

Almost all pioneering interference experiments with electrons, neutrons, atoms and small molecules are based on Young's double-slit experiment.[7]–[9] Young's experiment is a typical example for a study of waves that operates in the far-field regime, also known as Fraunhofer regime. The far-field approximation is used when the size of the slit opening is small and the distance between the diffraction element and the screen is large as compared to the wavelength. If this is the case, the curvature of the propagating wave front can be neglected and the wave fronts are therefore seen as planar. Hence the observed interference pattern is described by the superposition of approximated planar wave fronts. The far-field approximation is valid for

$$\frac{a^2}{L * \lambda} \ll 1 \qquad\qquad 1.2$$

where a is the slit size, L is the distance between the diffraction element and the observation element and λ the wavelength. If

$$\frac{a^2}{L * \lambda} \geq 1 \qquad\qquad 1.3$$

holds, meaning that the slit size is large and the distance between the diffraction element and the screen is small in comparison with the wavelength, the curvature of the waves has to be taken into account. This situation is referred to as near-field or Fresnel regime. Near-field interferometers, which were introduced by Clauser and Li for potassium atoms,[17] were hardly present in the first years of molecule interferometry. However, they exhibit essential advantages in interference experiments with increasingly complex molecules (*vide infra*).

1.1.1 Interferometry with Large Molecules

Since the kick-off in 1999 all following matter-wave experiments with macromolecules were carried out in the laboratories of Prof. Markus Arndt (in the first years under the supervision of Prof. Anton Zeilinger). This research is driven by multiple goals. A main ambition is the exploration of the frontiers of quantum mechanics to approach the transition between the quantum world and the classical world. A second interest is to study decoherence processes in order to optimize interferometers and to gain insight into the question of why macroscopic objects do not show quantum behavior. As a third issue interferometry is a powerful tool to address molecule metrology. Since small deviations in molecule properties can have large

effects on the interference, precise measurements of these properties become accessible. In the following the progress since the year 1999 in these three areas is discussed.

1.1.1.1 Far-Field Molecule Interferometry

As described above, the first macromolecule for which the wave-particle duality has been shown was the buckminsterfullerene C_{60}.[16] The initial pioneering far-field experiment was presented by Arndt *et al.* in 1999 and afterwards discussed in more detail in two further publications.[18][19] The four main parts of the experimental setup are a source, a collimation unit, a diffraction grating and a detector (figure 2A). The whole apparatus operates under vacuum (5 x 10^{-7} mbar) to minimize collisions of the beam with background gases. To create a molecule beam the C_{60} molecules were sublimed in an oven at temperatures of 900-1000 K. In this experiment the hot molecules pass the interferometer with different velocities, the most probable one being 220 ms^{-1}. This velocity corresponds to a de Broglie wavelength of 2.5 pm. The velocity distribution was determined by a time-resolved detection of the chopped molecular beam.[18] After leaving the source, the beam passes through two collimation slits and subsequently through one diffraction grating made of silicon nitride before entering the detection unit. The detection works with a thermal photoionization stage that can be laterally shifted and an ion detector to record the flux. The interference pattern was detected by scanning the detected ions as a function of the lateral position of the photoionization stage (figure 2B).
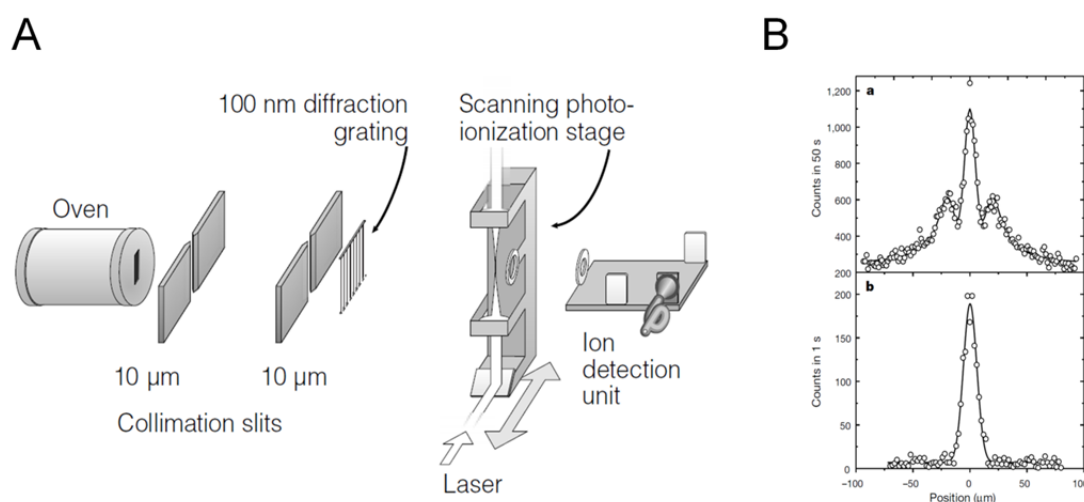
Figure 2. (A) Schematic representation of the experimental setup of the far-field interferometer suitable for experiments with C_{60} molecules. The interferometer comprises a thermal source, a collimation unit, a diffraction grating with a grating period of 100 nm and a detection unit (B) A comparison of the interference pattern of C_{60} molecules (a) and the molecule beam profile when no grating is present in the experimental setup (b).[16]

The fullerene molecules leave the oven horizontally and fly with various velocities. Owing to the Earth's gravity, different velocities correspond to different trajectories. This fact was utilized in an improved far-field setup.[20] By putting a knife edge in the molecular beam a gravitational velocity selection method narrows the velocity spread of the molecules (figure 3). This leads to a higher quality of the observed interference patterns. With this advancement the observation of interference of C_{70} in addition to C_{60} became possible.
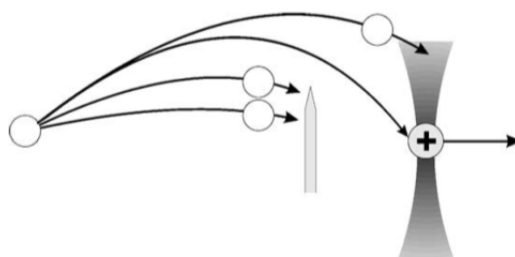
Figure 3. Sketch of the gravitational selection method. Fullerenes with undesired velocities are either blocked by the knife edge or launched under an angle which is too steep to permit the molecules to pass the effective ionization region.[20]

A further issue that decreases the quality of the observed interference pattern originates from the interactions between the molecule beam and the diffraction grating. Attractive van der Waals interactions between fullerene molecules and the grating wall can lead to dephasing. Furthermore material gratings can be blocked or destroyed by the passing molecules. A solution to this drawback of material gratings is the substitution of the silicon nitride grating by a standing light wave as the diffraction element as described by Nairz *et al.*.[21] The matter diffraction at a standing light wave was first proposed for electrons by Kapitza and Dirac in 1933 and is therefore referred to as Kapitza-Dirac effect.[22] The first experimental realization of this phenomenon was done with atoms by Moskowitz *et al.*[23] and is nowadays widely used in atom interferometry.[24] Experiments with electrons as originally proposed where only presented in 2001, almost 70 years after the theoretical description.[25] Optical phase gratings exhibit several advantages compared to material gratings: a perfect periodicity, optical gratings cannot be blocked or destroyed by the passing molecules, and there are no disturbing van der Waals or Casimir-Polder interactions between the molecule and the grating.

Although the far-field experiments with fullerenes marked an important milestone in the development of macromolecule interferometry and new concepts of far-field interferometry with large molecules have been developed recently,[26] near-field interferometry has an enormous advantage when working with large objects. The required slit openings of the used gratings, which is a critical issue in the buildup of an interferometer, are smaller in far-field

interferometry in comparison with near-field interferometry. A detailed discussion of the scaling behavior in near-field interferometry is given in the next section. The work in the Arndt group with near-field interferometers has led to an enormous progress in molecule interferometry in the last ten years.[27]

1.1.1.2 Near-Field Molecule Interferometry

Near-field interferometry profits from the so called Talbot effect. In 1936 Henry Talbot investigated the diffraction of light on a grating.[28] He found that if the screen is placed in defined distances behind the grating the obtained interference pattern is an image of the structure of the diffraction grating. The distance between grating and screen has to be a multiple of the Talbot distance L_T. The parameters that influence L_T are the grating period d and the de Broglie wavelength λ_{dB} of the incident wave.

$$L_T = \frac{d^2}{\lambda_{dB}}$$ 1.4

From equation 1.4 one key advantage of near-field interferometry becomes obvious. L_T is proportional to the square of d and inversely proportional to λ_{dB}. In a given interferometer with fixed distances between the grating and the screen ($L_T = const.$) doubling a particle's mass, which corresponds to a bisection of its wavelength, demands a decrease in grating period by a factor of $\sqrt{2}$. In contrast, the relation of grating period and de Broglie wavelength is linear in far-field interferometry and thus a decrease of the grating period by a factor of 2 would be necessary. To sum up the advantageous scaling behavior favors near-field interferometry over the experiments in the Fraunhofer regime when exploiting large objects.

The Talbot effect describes the diffraction of plane waves (figure 4A). In 1948 Lau proposed the use of a second grating, referred to as the Talbot-Lau effect (figure 4B).[29] This offers the possibility to work with sources of incoherent waves. The first grating, which is also placed in the Talbot distance to the diffraction grating acts as a collimation.
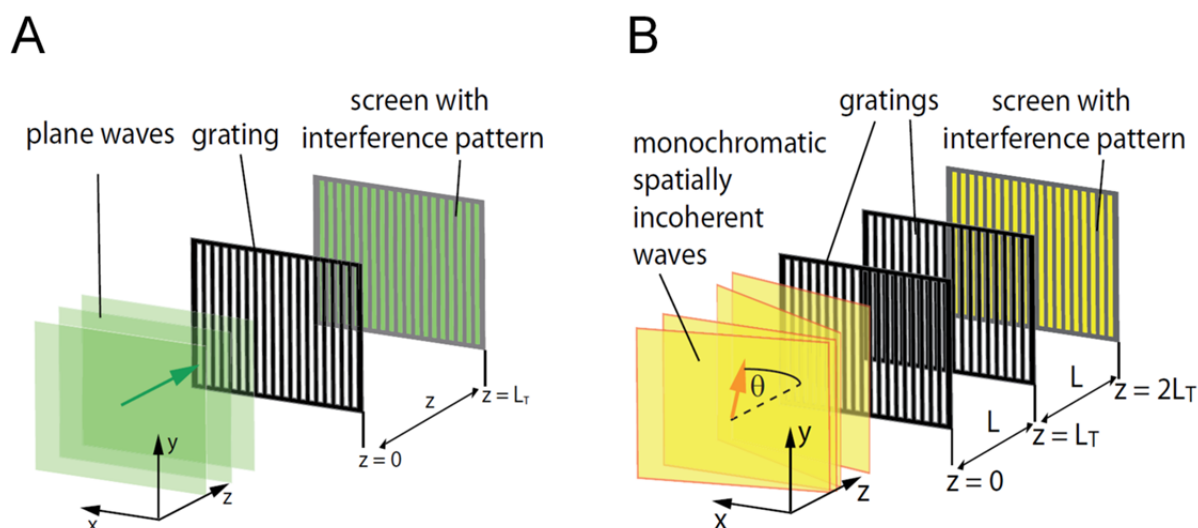
Figure 4. Schematic representation of (A) Talbot self-imaging using plane-parallel, monochromatic waves and (B) the Talbot-Lau effect using spatially incoherent waves.[30]

The quantum phenomenon of self-imaging of the grating, which was described by Talbot and Lau for light waves, is the central reason why in interferometry with large molecules near-field interferometers are the setups of choice. The possibility to work with uncollimated sources including thermal evaporation and lower requirements on the grating periods makes near-field interferometry superior to far-field interferometry.[31][32]

In 2002 Brezger *et al.* described near-field Talbot-Lau interferometry with C_{70} molecules.[33] This first near-field interferometer for macromolecules consisted of a thermal source, three gold gratings, and an ionization – ion counting scheme as detection. According to the Talbot-Lau effect the first grating acts as a collimation grating to prepare the incoherent molecule beam. Diffraction at the second grating, which is placed in a distance equal to the Talbot length behind the first grating, leads to a self-imaging phenomenon of the diffraction grating further downstream. The periodic interference fringe is recorded by transversal scanning of the third grating and detection of the transmitted flux. However, the observation of a periodic signal is not necessarily a proof of quantum interference. It is also possible that classical shadows behind the grating – Moiré fringes – are responsible for such structures. Clarity can be obtained if one investigates the fringe visibility and its dependence on different velocities of the molecules. As depicted in figure 5A the interference visibility (contrast) V is determined from the modulation of the transmitted signal according to equation 1.5.

$$V = \frac{S_{\max} - S_{\min}}{S_{\max} + S_{\min}}$$

1.5

For classical Moiré fringes the visibility is constant, or only weakly dependant on the velocity, when one takes van der Waals interactions between the molecules and the grating

walls into account. In the quantum model the visibility, in contrast, is strongly influenced by the molecules' velocity. Figure 5B shows such a comparison of experimental values obtained for C_{70} and quantum mechanical and classical predictions with and without van der Waals interactions. The experimental visibilities are in good agreement with the quantum model that includes van der Waals interactions. From the comparison of the experimental data with the theoretical simulations it can be concluded that the periodic structure originates from quantum effects and not from classical shadows behind the grating.

A

B
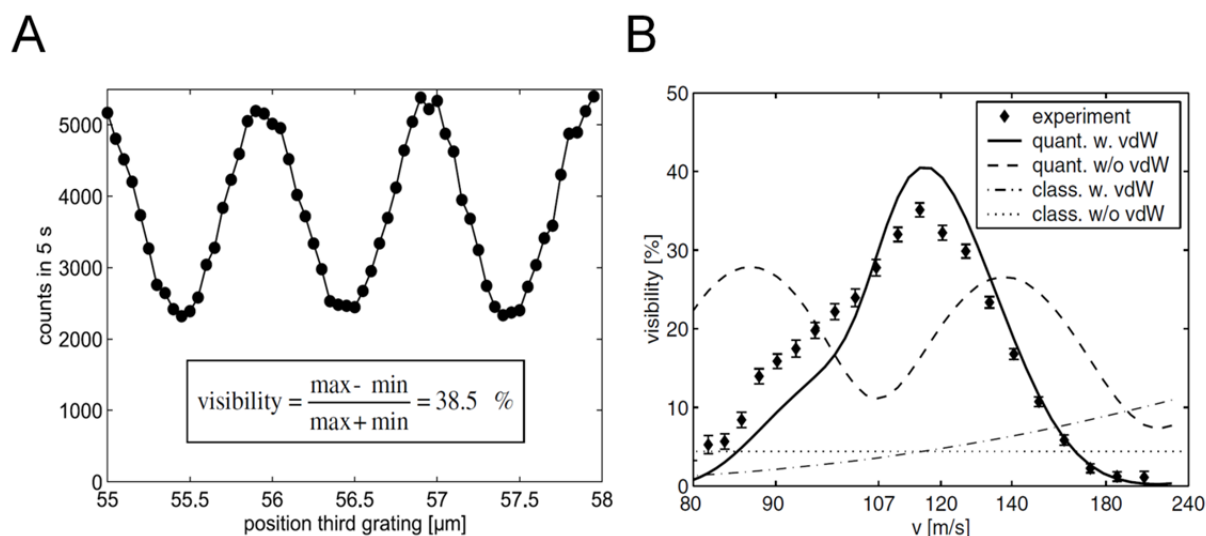
Figure 5. (A) Interference fringe obtained in a near-field interference experiment with C_{70} molecules (B) Experimental and calculated dependence of the interference visibility on the mean velocity of the molecular beam.[33]

The newly established Talbot-Lau interferometer (TLI) was shortly after exposed to beams of tetraphenylporphyrin (**TPP**, figure 6) and the fluorofullerene $C_{60}F_{48}$. The observation of the wave nature of the fluorous fullerene $C_{60}F_{48}$ represented a new mass record for quantum interferometry.[34] However, the setup of the TLI had to be adapted to the new compounds. Since thermal laser ionization, as present in the first generation TLI, turned out to not be suitable for these two structures a new detection unit was implemented. Here the detection was performed with a combination of electron impact ionization and quadrupole mass spectrometry (QMS). With the QMS unit it was also possible to ensure the stability of the interfering particles during the evaporation process and the flight through the interferometer. By integration of the QMS signal of the molecule ion peak, it is guaranteed that exclusively the flux of the desired compound is recorded.
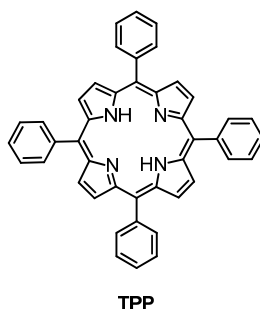
Figure 6. Structure of tetraphenylporphyrin (**TPP**).

Generally, the search for effective detection methods is an important field in the development of new setups. Ionization techniques are expected to get less effective when increasing the molecular mass of the compounds. Fluorescence imaging on a surface, however, is a promising tool to image interference patterns. Stibor *et al.* demonstrated such an interference experiment with **TPP** by imaging the interference pattern by means of fluorescence microscopy of trapped **TPP** molecules on a quartz surface.[35] The quartz surface was situated in the Talbot distance behind the diffraction grating.

During the development of suitable experiments for larger and larger molecules it was noticed in the far-field setups that material gratings can cause severe limitations. Although the requirements on the size – and therefore on the manufacturing process – of the tiny gratings are smaller in near-field interferometry compared to far-field interferometry, the molecule-wall interactions also have an increasingly negative influence. With increasing particle size the compound's polarizability generally increases. From a higher polarizability follows stronger van der Waals interactions with the grating wall. In far-field interferometry the use of optical gratings (Kapitza-Dirac effect) was therefore successfully introduced.[21] The implementation of a standing light wave as optical phase grating in a near-field interferometer was published in 2007 (figure 7A).[36] A standing light wave generated by a green laser with a wavelength of 532 nm created a diffraction element with a grating period d that equals to one half of the laser wavelength (equation 1.6).

$$d = \frac{\lambda_{\text{laser}}}{2} = 266 \, \text{nm} \qquad\qquad 1.6$$

The interferometer was named after the two important effects that it uses and is referred to as a Kapitza-Dirac-Talbot-Lau interferometer (KDTLI). In the first experiments with this setup the wave nature of C_{70} and a perfluoroalkyl functionalized azobenzene derivative (**F-alkyl AZO**) were observed (figure 7B).[36] Two years later a detailed theoretical discussion of the setup was delivered and experiments with the fullerenes C_{60} and C_{70}, and the fluorofullerenes $C_{60}F_{36}$ and $C_{60}F_{48}$ were presented.[37]
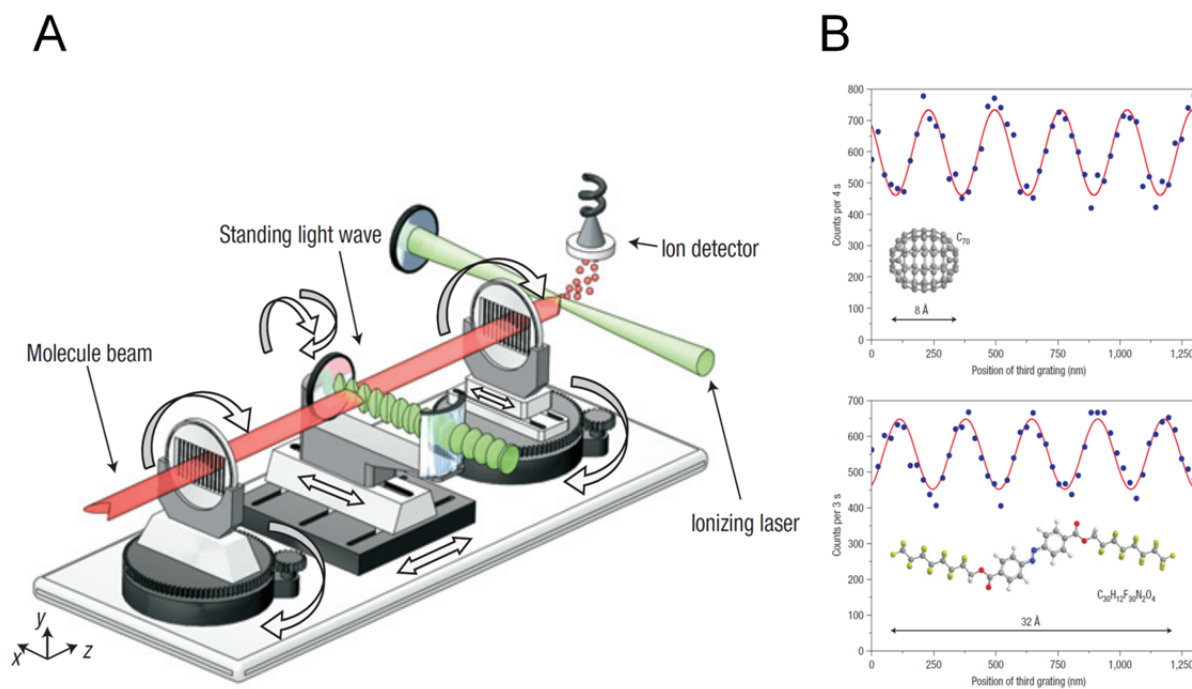
Figure 7. (A) Schematic representation of the KDTLI (B) Interference fringes obtained for C_{70} (top) and a perfluoroalkyl functionalized azobenzene (**F-alkyl AZO**) (bottom).[36]

With the realization of near-field interferometers for macromolecules it was possible to increase the mass record obtained in a far-field setup (C_{70} molecules published in 2001) by a factor of almost 2:

$$\frac{M_W(C_{60}F_{48})}{M_W(C_{70})} = \frac{1633 \text{ g/mol}}{841 \text{ g/mol}} = 1.94 \qquad\qquad 1.7$$

From the year 2003 when the near-field interference experiment with the fluorofullerene $C_{60}F_{48}$ was presented until the beginning of this doctoral thesis in 2008 this molecule remained the mass record holder for quantum interference. In the next chapter the second goal of the interference experiments in the Arndt group is discussed: the effect of decoherence processes.

1.1.2 Decoherence Studies

The study of decoherence is of enormous relevance for two principle reasons. Understanding of processes that cause the loss of quantum information is essential for the development of interferometers. Secondly the understanding of why macroscopic objects do not seem to obey quantum rules is inseparably linked to decoherence. Several studies on effects that result in dephasing of quantum interference and therefore the loss of quantum information were recently carried out in the Arndt group.[37]

Large objects can absorb energy and release it by thermal emission of photons. Emission of photons gives the possibility to determine the position of an object, which inevitably leads to decoherence. This is one of the main reasons why macroscopic objects appear classical. In two studies the effect of the internal temperature of C_{70} molecules on the visibility of quantum interference in a TLI was investigated.[38][39] Starting from T = 1000 K, which gives a perfect interference contrast, the temperature was gradually raised to T = 3000 K finally leading to a complete loss of quantum information. The conclusion of such a thermally induced quantum-to-classical transition was that thermal emission of radiation is a very important decoherence process with respect to the behavior of macroscopic objects, but not a limiting factor for interferometry in the size range of macromolecules or nanoobjects.

Hornberger *et al.* investigated decoherence originating from interactions of a quantum object with its environment, namely due to collisions with background gases.[40] For this purpose they conducted interference experiments in the TLI with C_{70} molecules and the controlled addition of various gases, e.g. methane, neon and helium. With these experiments it was possible to estimate the required vacuum conditions in the TLI to be 3 x 10^{-10} mbar for a hypothetic object with the mass 5 x 10^{7} amu. From this study and related work from Hackermüller *et al.*[41] it was concluded that with the technological possibilities of today's laboratories, it is feasible to provide suitable vacuum conditions for QIE with objects that exceed the current mass record by several orders of magnitude.

It is not only quantum decoherence, which can lead to a loss of quantum information. Classical perturbations can also make it impossible to observe quantum interference. Stibor *et al.* estimated the influence of inertial forces and vibrations.[42] The rotation of the Earth, gravitational acceleration, grating vibrations, and acoustic noise are examples that one has to be aware of when recording quantum interference.

The investigations presented in this section showed that a variety of decoherence processes play an important role in molecule interferometry. However, it was clearly demonstrated that today's technological conditions are not essentially limiting quantum experiments with objects in the current size region and above.

1.1.3 Quantum Metrology

Quantum interferometry is very sensitive to all kind of deviations. Small changes in the internal structure of the interfering objects can influence the outcome of interference

experiments drastically. Thus the measurement of the particle's properties becomes accessible by the analysis of these deviations. Various metrological examples from atom interferometry are known, e.g. the measurement of static polarizabilities.[43]

Recently Stefanov *et al.* developed a setup based on a TLI to measure electric polarizabilities of molecules.[44] As displayed in figure 8 an electrostatic field gradient was installed in between the gratings. The electric field causes a deflection of the beam, referred to as Stark deflection. Since the intensity of the deflection is dependent on the electric susceptibility of the flying molecule, a measurement of this molecular property became accessible. The measurement of static electric polarizabilities of the fullerenes C_{60} and C_{70} in this setup[45] were in good agreement with literature values, which were determined by other methods.
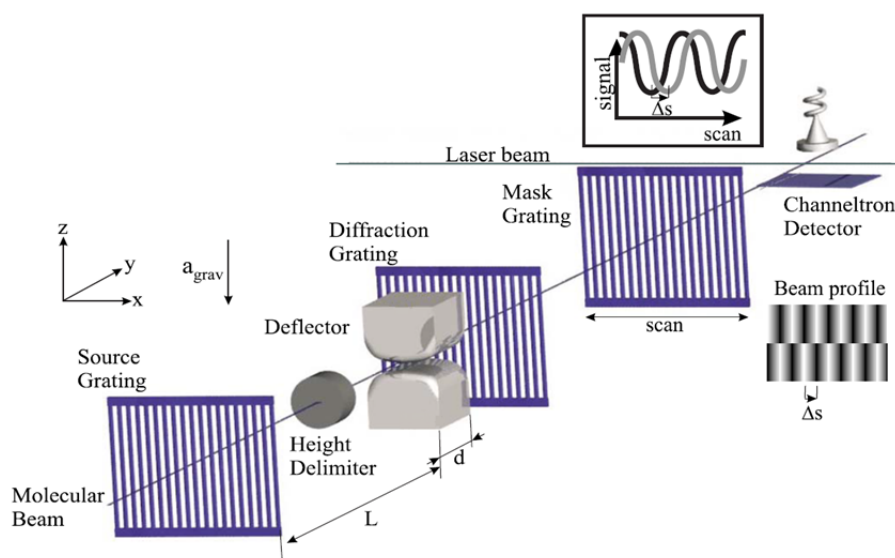
Figure 8. Schematic representation of the experimental setup to measure electric polarizabilities. The three grating setup is extended by an external electric field – a deflector – causing a deflection of the beam profile, which is directly proportional to the molecular scalar polarizability α.[45]

Besides the measurement of electric polarizabilities the principle of interferometric deflection can also be used to sort molecules that differ in their polarizabilities. This concept was theoretically examined for polypeptides and carbon nanotubes, and experimentally shown for a binary mixture of C_{60} and C_{70} molecules.[46] A polarizability ratio of $\alpha_{C_{70}}/\alpha_{C_{60}} = 1.22$ proved to be sufficient to sort these two compounds in the gas phase.

In a KDTLI the standing light wave interacts with the molecule beam via the dipole force. The induced phase modulation Φ is directly proportional to the optical polarizability α_{opt} of the molecule and the power of the laser:

$$\Phi \sim \alpha_{opt}\, P \qquad\qquad 1.8$$

Optical polarizabilities are therefore accessible by the determination of the dependence of the interference fringe on the laser power of the optical phase grating. In 2007 Hackermüller *et al.*[47] measured optical polarizabilities of fullerenes (C_{60} and C_{70}) and later measurements with fluorofullerenes were reported.[37] As shown in figure 9 the polarizability can be extracted from a fit of the theoretical quantum mechanical expectations to the measured values of the fringe visibility with dependence to the laser power. The thin lines in the figure represent the expected visibility/laser power dependence using a classical model. A clear discrepancy between the classical model and the experimental values is observed.
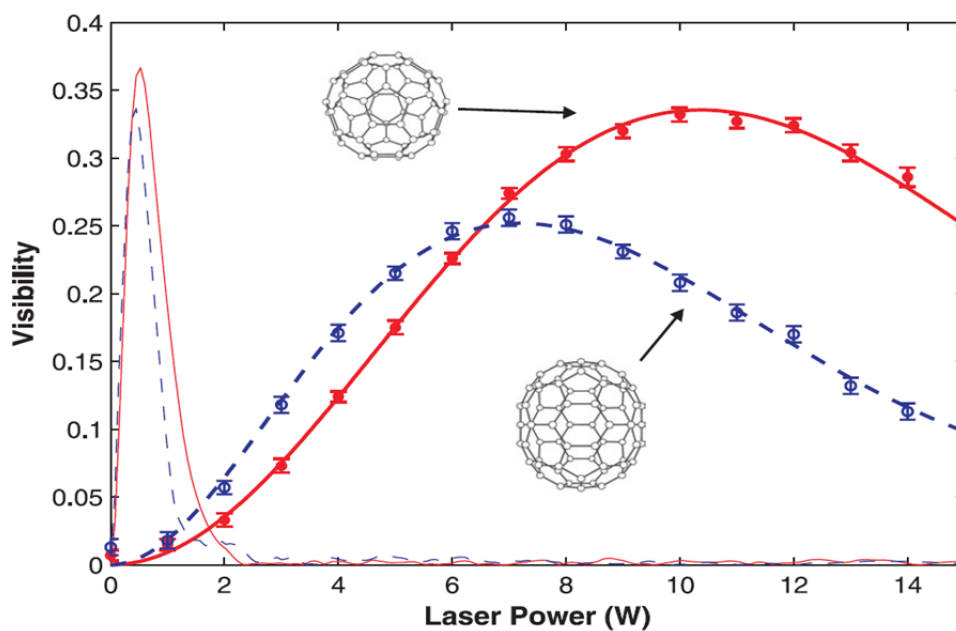
Figure 9. Determination of the optical polarizability via the dependence of the interference fringe on the laser power of the optical phase grating in a KDTLI. The polarizability can be extracted from a fit of the theoretical expectations (bold lines) to the measured values (circles) of the fringe visibility here shown using the example of the fullerenes C_{60} and C_{70}.[37]

In 2008 Nimmrichter *et al.* proposed a method to measure the absolute photon absorption cross section of molecules in the gas phase.[48] This method is based on the recoil of molecules originating from photon absorption in a near-field TLI. Although this setup has not yet been realized this example and the ones described above show that molecule interferometry opens the door to a wide variety of precise measurements of molecule properties.

A further aspect of quantum metrological investigations was described by Gring *et al.*: the influence of thermally activated dipole moments.[49] In a KDTLI the optical polarizability α_{opt} can be extracted from the dependence of the interference contrast on the laser power of

the standing light wave. In the work of Gring and coworkers a good match of experimental and theoretical values of α_{opt} for experiments with **F-alkyl AZO** was described. However, in interferometric deflection studies with this molecule the calculated values for the static electric polarizability α_{stat} were markedly lower than the experimental values. Obviously, the knowledge of α_{stat} is not sufficient to describe the behavior of these molecules in an external electric field. Instead Van Vleck's equation[50] for the electric susceptibility χ must be considered.

$$\chi = \alpha_{stat} + \frac{\langle d^2 \rangle}{3 k_B T} = \alpha_{stat} + \alpha_{dip} \qquad 1.9$$

Here, in addition to α_{stat}, the influence of dynamic dipole moments is taken into account. As shown in calculations, thermal vibrations, which mainly take place in the floppy perfluoroalkyl side arms of the molecule, induce strong fluctuating dipole moments on the nanosecond timescale. According to Van Vleck's formula the thermal average of all possible dipole moments is important. A comparison of simulated values for χ of **F-alkyl AZO** finally showed a good match with the experimental data. In conclusion, the effect of thermally activated dipole moments in QIE was described in this work. Importantly, although there is no positional information about the single particle – otherwise there would be no interference – information about internal molecular properties is accessible.

1.1.4 Experimental Improvements

The desire to approach the quantum-to-classical transition by means of quantum experiments with large objects calls for improved experimental setups. Two very important aspects of these setups are the efficiency of beam sources and of detection methods. In the Arndt group considerable effort was invested in recent years to explore new techniques on both sides of the interferometer.

Marksteiner *et al.* reported on the formation of beams of amino acid metal complexes.[51] They presented the creation of molecule beams by UV laser desorption. With this technique it was possible to obtain molecule beams with particle masses up to ~ 6500 amu. The neutral compounds consisted of tryptophan units that form complexes with various alkaline earth metals.

A further idea was exploited by Reiger *et al.*: gold nanoparticle (AuNP) beams for matter-wave interferometry.[52] Three different beam creation methods – electrospray ionization

(ESI), matrix assisted laser desorption ionization (MALDI) and thermal laser desorption (TLD) –, and three detection concepts – quadrupole mass spectrometry (QMS), time-of-flight mass spectrometry (ToF-MS) and multi-photon ionization (MUPI) ToF-MS – were investigated. In this work combinations of sources and detection schemes, respectively, were tested and finally a new tailor-made interferometer setup for AuNPs was proposed.

The sublimation of perfluoroalkyl functionalized fullerenes to form molecule beams was presented by Deachapunya et al. in 2008.[53] These molecules were identified as promising candidates for molecule interferometry because they were known to be stable and highly volatile in relation to their molecular weight.[54]

On the detection side several promising setups are being developed in the Arndt group. In an article by Juffmann et al., which appeared in 2009, scanning tunneling microscopy (STM) was implemented as the detection unit in a near-field interferometer.[55] After diffraction C_{60} molecules were deposited on a silicon(111) surface. The surface was then transferred to a STM setup. The distribution of every single C_{60} molecule was imaged and the periodic interference fringe was clearly observed as shown in figure 10.
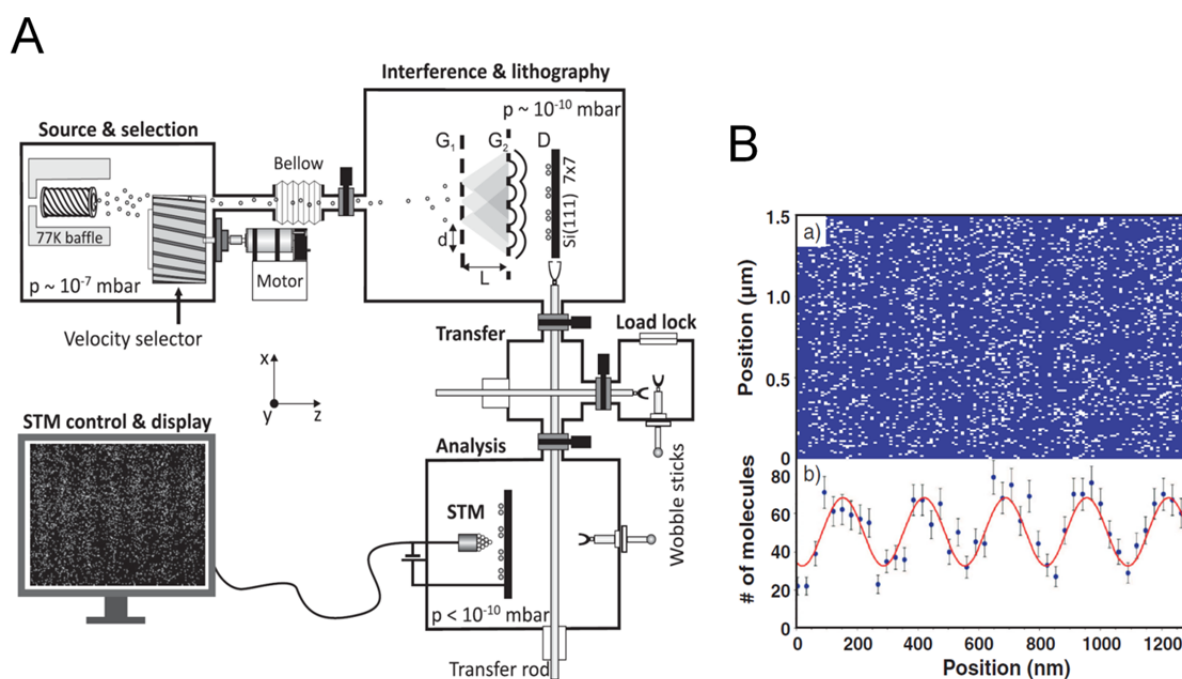
Figure 10. (A) Schematic representation of a near-field interferometer comprising a detection unit based on scanning tunneling microscopy (STM) (B) Interference image of the surface deposited fullerene molecules.[55]

Besides the established use of mass spectrometric devices for the detection, fluorescence imaging is the most promising tool for future applications. In 2004 Stefanov et al. conducted experiments with molecule beams of the fluorescent dyes tetraphenylporphyrin (**TPP**),

porphine and Nile red.[56] By the in-flight measurement of fluorescence it was possible to determine the enthalpy of sublimation of these compounds from the temperature dependence of the fluorescence signal. The implementation of such a concept into an interferometer has, however, not yet been realized. The very low beam intensity in molecule interferometry limits the applicability of the in-flight measurement.

Fluorescence microscopy on surfaces is a further concept that was investigated. A big advantage of the deposition of the interfering particles on a surface with subsequent interference readout by fluorescence measurement is that in one interferogram the interference pattern for all arriving velocities is saved. The vertical position on the surface is determined by the trajectory of the molecules, which is influenced by the gravitational field of the Earth. Thus, the position on the screen is directly related to the velocity of the arriving particles. In 2005 Goldfarb *et al.* tested several surfaces for fluorescence detection of **TPP**.[57] It turned out that the mobility of **TPP** on graphite and mica is too large for the needs of the TLI. The mobility on quartz surfaces is, by contrast, low enough to guarantee the needed spatial resolution for Talbot-Lau interferometry. With these findings it was shortly after possible to observe quantum interference patterns of **TPP** on quartz glass surfaces.[35]

In a related work by Dreas-Wlodarczak *et al.* a system that aimed at a minimal surface mobility was tested.[58] The non covalent axial binding of a pyridine unit to a zinc porphyrin complex seemed to be an ideal interaction for surface immobilization (figure 11). The deposition of zinc tetraphenylporphyrin on pyridine functionalized glass surfaces showed that the obtained spatial resolution of the fluorescence signal would be sufficient for Talbot-Lau interferometry.
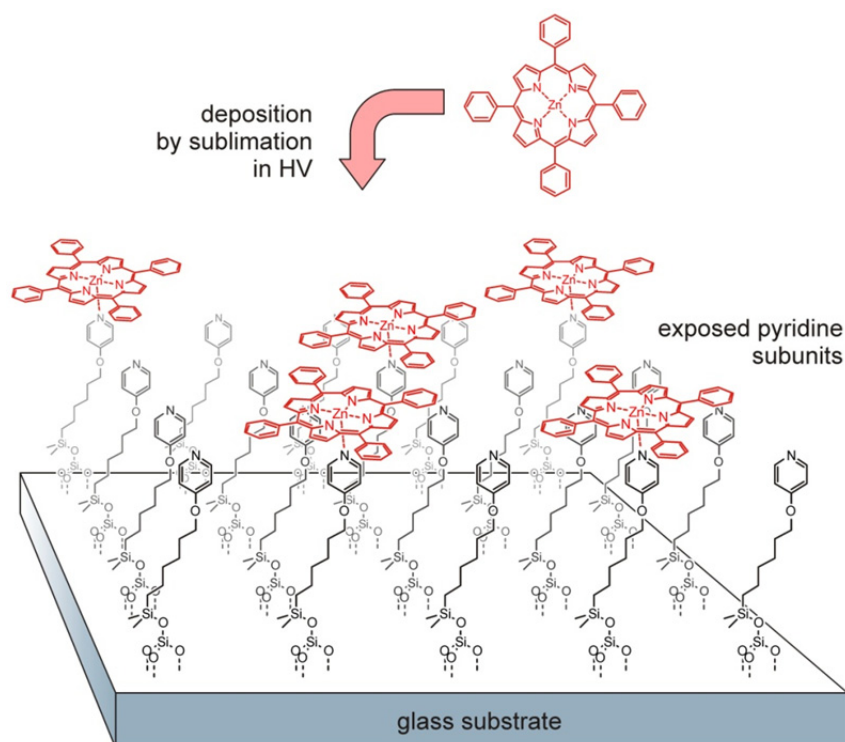
Figure 11. Schematic representation of the deposition of zinc tetraphenylporphyrin onto a pyridine functionalized glass substrate.[58]

As described in this section numerous promising ideas for novel beam creation techniques and detection schemes were examined in the last decade. A crucial role for successful QIE plays the nature of the interfering particle. In the following the trend from commercially available molecules to tailor-made molecules for QIE is described.

1.2   Highly Fluorinated Compounds

After almost one decade of QIE in the Arndt group it became obvious that further progress in interferometry with large organic molecules is only achievable in strong collaboration with synthetic chemists. The request for more complex molecules that meet the requirements of the interferometers can no longer be satisfied by compounds from the "catalog". The first matter-wave experiments were exclusively conducted with commercially available organic compounds or compounds that were not tailor-made for QIE. An overview over all organic molecules for which the wave nature had been observed until the year 2007 is given in figure 12. The fullerenes C_{60} and C_{70}, and tetraphenylporphyrin (**TPP**) were all obtained from commercial sources, whereas the fluorofullerenes $C_{60}F_{36}$ and $C_{60}F_{48}$ were purchased from the group of Prof. Sidorov from the State University Moscow.[59]–[61] The perfluoroalkyl functionalized azobenzene (**F-alkyl AZO**) that was investigated in the KDTLI was the only tailor-made compound.[36] This experiment marked the first collaborative work between the Arndt group in Vienna and chemists from the group of Prof. Mayor in Basel.
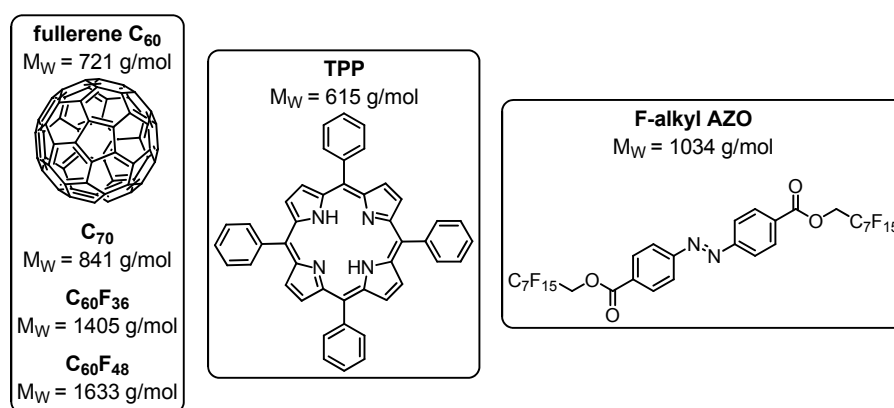
Figure 12. Overview of all organic molecules investigated in QIE in the group of Prof. Arndt between the years 1999 and 2007.

The use of F-alkyl tags (the prefix F- is an IUPAC authorized abbreviation for perfluoro) in the design of the fluorous azobenzene derivative was chosen for several reasons. A high stability, a high molecular weight, and low intermolecular interactions of these labels make them appealing building blocks for tailor-made molecules for matter-wave interferometry. A detailed discussion about the beneficial effects of F-alkyl functionalization in the context of molecule interferometry is given in section 1.2.4. In the following chapters a general introduction to the field of fluorous chemistry is provided.

1.2.1 The Birth of Fluorous Chemistry – Fluorous Biphasic Catalysis

Since many decades perfluoroalkyl functionalized substances have been used in a wide range of industrial applications. Two important segments are surface active ingredients of soil and liquid repellents, for example in textiles,[62] or the use as refrigerants. However, the birth of the term fluorous chemistry can be attributed to the use of the unique miscibility properties of perfluorinated solvents for chemical synthesis methods developed in the 1990s.[63]

Fluorous solvents such as perfluorohexane are at the same time hydrophobic and lipophobic. A ternary mixture of a common organic solvent, a fluorous solvent and water usually forms a triphasic system. However, the miscibility of the organic media and the fluorous media is increased at elevated temperatures. Exemplarily a 1:1 mixture of perfluoro-(methylcyclohexane) (PFMC) and methylcyclohexane forms two phases at room temperature and one homogeneous phase at temperatures higher than 88.6 °C.[64] Although the orthogonal miscibility and the temperature dependant phase separation had been known since 1949[64] the first publication, that reached a broad audience and drew attention to fluorous concepts for chemical syntheses, was the work of Horváth and Rábai in 1994.[63] In their seminal paper they described the concept of fluorous biphasic catalysis (FBC). The hydroformylation of alkenes, a very important industrial process, which is also known as oxo process, was chosen as a model reaction. In a transition metal catalyzed reaction a terminal alkene reacts with carbon monoxide and dihydrogen (syngas) to yield an aldehyde (scheme 1).
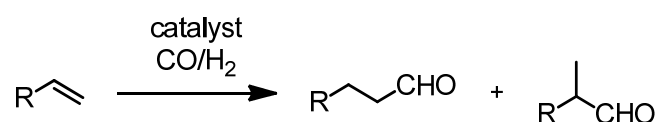
Scheme 1. Hydroformylation of alkenes with syngas to form aldehydes.

A major challenge in this process is an efficient separation and recycling of the catalyst. The idea from Horváth and Rábai was to add F-alkyl tags to the catalyst and benefit from the "like dissolves like" effect and the temperature dependant miscibility of fluorous and common organic solvents. As shown in scheme 2, the concept of FBC is based on a solvent system that is biphasic at room temperature and homogeneous at increased temperatures. This allows for a homogeneous, high yielding catalytic reaction and a very mild opportunity to separate the fluorous catalyst from the reaction products by simple cooling to room temperature and subsequent phase separation. Horváth and Rábai used the fluorous rhodium catalyst **CAT1**, that is depicted in figure 13, and a solvent mixture of toluene and PFMC for their fluorous version of the hydroformylation of alkenes.
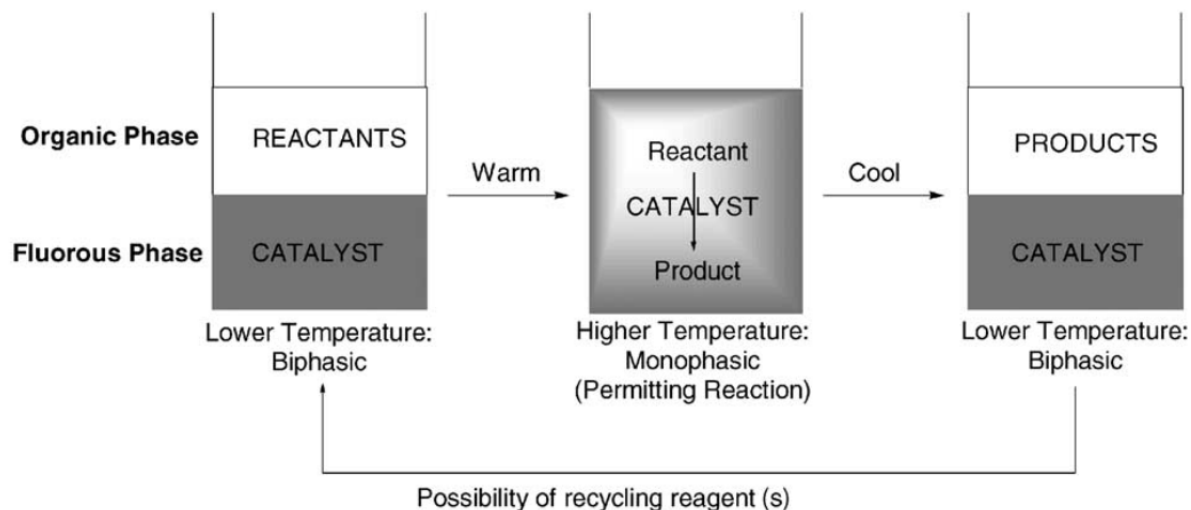
Scheme 2. The concept of fluorous biphasic catalysis (FBC).[65]

The concept of FBC was picked up by many research laboratories.[66] Figure 13 shows examples of F-alkyl tagged metal complexes that were used for various catalytic reactions. In 1997 Klement *et al.* described the nickel-catalyzed oxidation of aldehydes to carboxylic acids using a solvent mixture of toluene and perfluorodecaline and catalyst **CAT3**.[67] Catalyst **CAT2**, a fluorous version of bis(triphenylphosphine)palladium (II) chloride, was developed in the laboratories of Prof. Bannwarth in Freiburg, Germany, for Stille couplings.[68] Today a whole series of fluorous analogues of established metal catalysts, such as the fluorous counterpart to Vaska's complex **CAT4**,[69] have been prepared and some of them have even been made commercially available.
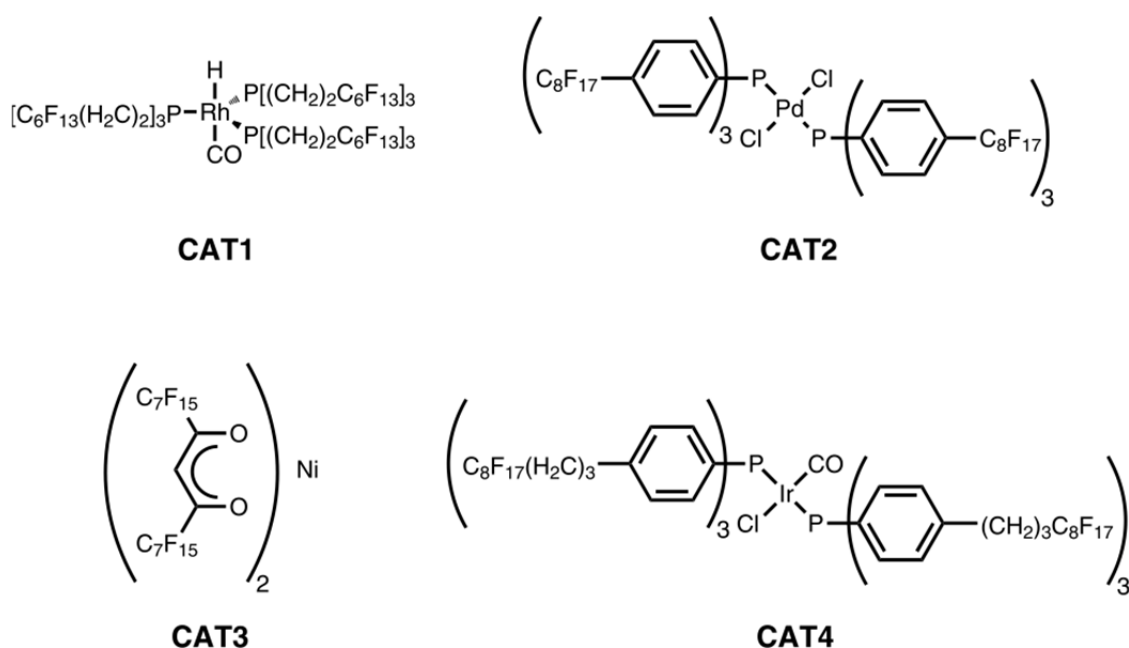
Figure 13. Various F-alkyl labeled catalysts for fluorous biphasic catalysis (FBC).

To sum up, although several publications about organic synthesis with highly fluorinated compounds already existed before, the birth of fluorous chemistry can be assigned to the work of Horváth and Rábai in 1994. Their innovative work marked the beginning of an enormous increase of research work done in the field of fluorous synthetic chemistry all over the world.[70]

1.2.2 Fluorous Separation Techniques and Fluorous Synthesis Strategies

Liquid-liquid extractions with a fluorous and a non-fluorous media were initially used in FBC to recover F-alkyl labeled catalysts.[63] In 1997 Studer *et al.* presented a synthesis strategy, where instead of a fluorine labeled catalyst the reactant is tagged.[71] The idea to immobilize the product on an additional phase is conceptually similar to solid-phase synthesis. It offers the possibility of replacing extensive purification steps, for example chromatography, by simple extraction steps. A prerequisite for the success of this concept is that every single reaction step can be brought to completion, exemplarily by the use of an excess of reagents. Otherwise the separation of the starting material and the product would become necessary which is not feasible by liquid-liquid extractions since both components share their preference for the fluorous phase. The strategy is referred to as fluorous synthesis.

One advantage of liquid-liquid extraction with fluorous solvents is that the partition coefficients of the compounds are usually very high in one of the two media. This enables efficient and clean separations. However, there are also drawbacks. Fluorous solvents are expensive and harmful to the environment. Furthermore, F-alkyl chains have high molecular weights. Consequently, large amounts of these precursors have to be introduced to the target compounds, and, in case of a detagging in a last reaction step, large amounts of waste are produced.

To circumvent these disadvantages the application of fluorous solid phase extractions was appealing. Similar to reverse phase silica gel, that is for example functionalized with C_{18} alkyl chains, fluorous counterparts were developed. Fluorous reverse phase silica gel (FRPSG) allowed for new synthetic concepts in fluorous chemistry. Before, exclusively the separation of fluorous from non-fluorous compounds was feasible by liquid-liquid extractions. Since a molecule`s fluorine content of higher than 60 wt% is required to guarantee a high partition coefficient in fluorous media, this type of fluorous chemistry is referred to as heavy fluorous synthesis. In contrast to that, chromatography with FRPSG made it possible to separate

compounds having different fluorine contents. From then on it was possible to work with lower fluorine functionalization, the field of light fluorous synthesis. Not only reagents and reactants with shorter F-alkyl labels came into the focus, but also solvents with lower fluorine content were used as reaction media. These hybrid organic/fluorous solvents such as trifluoromethylbenzene have the advantage that they are capable of dissolving a wide range of organic and highly fluorinated compounds and thus enable homogenous reactions without using mixtures of organic and fluorocarbon solvents at high temperatures.[72][73]

The first preparation of FRPSG was described by Berendsen and Galan in 1980.[74] However, they did not focus on the separation of fluorinated compounds from each other. In their work the fluorinated phase was used to analyze different herbicides with a maximum of one fluorine atom per molecule. For almost 20 years the potential of FRPSG, namely the separation of compounds according to their fluorine content, was not recognized by the community of synthetic organic chemists. All publications that picked up the work of Berendsen and Galan were restricted to molecules without a considerable fluorine content.[75]

The first fluorous solid phase extraction that was used to separate non-fluorous from fluorous compounds was presented by Curran *et al.* in 1997.[76] Since the recognition of their power fluorocarbon stationary phases found a lot applications and the step to commercialized FRPSG was made rapidly.[70] FRPSG was also implemented in high-performance liquid chromatography (HPLC) systems. With fluorous HPLC as efficient separation technique Lou *et al.* presented in 2001 a new combinatorial synthesis approach: fluorous mixture synthesis (FMS).[77] The concept is shown in scheme 3. A reaction sequence is not performed for every single starting material (blue, green and yellow circles) separately, but in one pot in order to reduce the overall synthetic effort. Prior to the first step of the reaction sequence the starting material is tagged with fluorous labels containing different amounts of fluorine atoms. After mixing and performing of the envisaged reaction sequence the obtained product mixture is finally demixed with fluorous HPLC to afford the desired pure products.
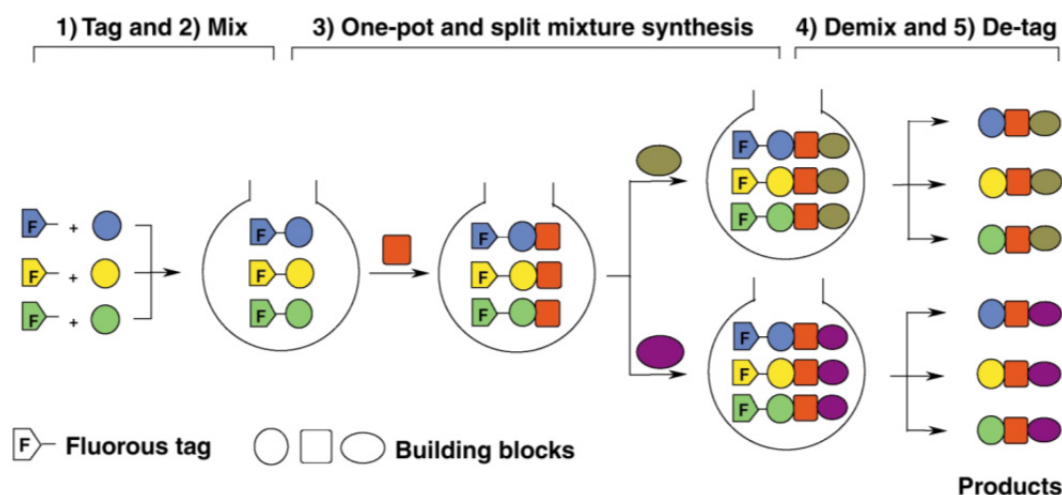
Scheme 3. Schematic diagram of the concept of fluorous mixture synthesis (FMS).[78]

In the original paper of Lou *et al.* the FMS strategy was applied to synthesize both enantiomers of the natural product mappicine. In a first step two enantiomeric pure starting materials were tagged with fluorous labels of different lengths and subsequently mixed. After a reaction sequence of four steps with the quasiracemic mixture, demixing by fluorous chromatography and detagging (R)- and (S)-mappicine were obtained enantiomerically pure.

With the commercialization of fluorous HPLC columns the number of applications that can be found in the literature increased markedly. The purification of tagged oligopeptides and oligonucleotides[79] or the synthesis of a library of diazonium functionalized oligo phenylene vinylene (OPV) derivatives for optoelectronic applications[80] are examples. Figure 14 shows a selection of four different types of fluorous stationary phases that became commercially available. Additionally, one homemade FRPSG developed by Glatz *et al.* is depicted.[81] The four commercial HPLC columns differ in the structure of the fluorinated part. Branched perfluorohexyl (Fluofix), linear perfluorohexyl (Fluophase RP) and perfluorooctyl (Fluoro*Flash*) chains show comparable retention behavior. Generally, the longer the F-alkyl part the stronger is the retention of highly fluorinated analytes. The retention characteristics of Fluophase PFP (perfluorophenyl phase) differ strongly from the other three products since the perfluorinated segment is not based on sp^3-hybridized carbon. Owing to the aromatic core other interactions, including π-π-stacking, can play a dominant role. Common to all four of these FRPSGs is the immobilization method to the silica gel. Starting from chlorodimethylsilane precursors the immobilization is performed resulting in a single bond between each chain and the silica gel. In contrast to that, the FRPSG from Glatz *et al.* is prepared starting from a fluorous triethoxysilane derivative. In an acid catalyzed reaction the

chains are immobilized on the silica gel via multiple binding sites yielding a higher stability of the FRPSG.
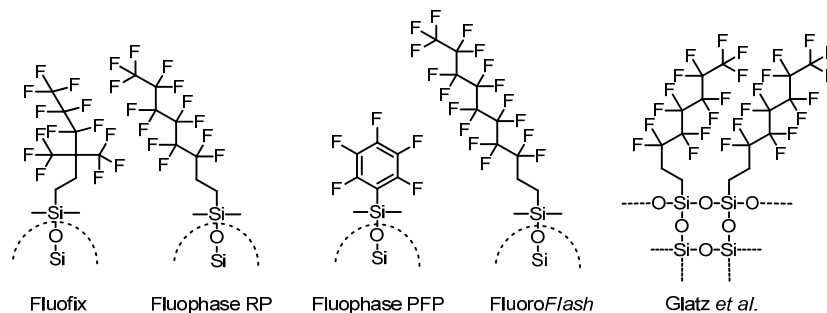
Figure 14. Schematic representation of four different types of commercial FRPSG and one non-commercial FRPSG for HPLC applications.

1.2.3 Fluorous Building Blocks: Availability and Reactivity

Since the 1990s the field of fluorous chemistry increased continuously. With the launch of the first company specialized on fluorous products in the year 2000, fluorous.com, the pool of commercially accessible fluorous building blocks grew further. F-alkyl functionalized building blocks are today available with a wide range of functional groups. In monofunctional building blocks the fluorous part is often isolated from the reactive group by a spacer. By the integration of spacers between the F-alkyl group and the reaction centre the influence of the strong electron-withdrawing effect of the fluorocarbon chain is minimized to enable common reactivities of the functional groups. The length of the perfluoroalkyl parts is variable and ranges from short trifluoromethyl substituents to perfluorododecyl moieties. Also compounds with branched fluorous segments are on the market. The spacer usually consists of methylene units, but phenyl spacers are also available. Spacer lengths of two to three methylene units are generally enough to isolate the fluorous part sufficiently and thus to guarantee the expected reactivity of the functional group. Figure 15 displays various segments that can be found in commercial fluorous building blocks.
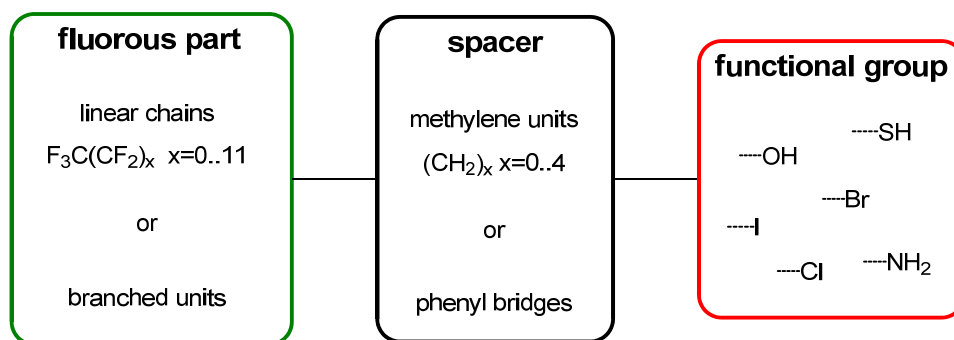
Figure 15. Schematic representation of the constitution of monofunctional commercial fluorous building blocks.

If a spacer is present highly fluorinated tags can usually be attached to target compounds by common organic synthetic methods. However, the direct perfluoroalkylation reaction without a spacer cannot be accomplished as is common when using hydrogenated alkyl counterparts. Initially perfluoroalkylations of arenes were performed as radical reactions.[82][83] This reaction suffers from a low regioselectivity and the formation of side products, e.g. the formation of diperfluoroalkyl side products. In 1969 McLoughlin and Thrower described the first metal-mediated polyfluoroalkylation of aromatic compounds (scheme 4).[84] The reactions were performed with iodofluoroalkyl chains and iodoarenes in the presence of stoichiometric amounts of copper and dimethylsulfoxide (DMSO) as solvent. Temperatures of 100-120 °C were used. A big advantage of this reaction type is that both, the iodofluoroalkanes and the aromatic compounds, can bear a wide variety of substituents. Besides fluorine and chlorine, alkyl, alkoxy, carboxylic ester and nitro groups may be present without affecting the yield to a significant extend. The high regioselectivity and a high functional group tolerance make this reaction one of the favored methods towards perfluoroalkylated aromatic compounds.[85]

$$R_f{-}I \quad + \quad Ar{-}I \quad \xrightarrow[\text{100-120°C}]{\text{Cu, DMSO}} \quad R_f{-}Ar \qquad R_f = \text{perfluoroalkyl}$$
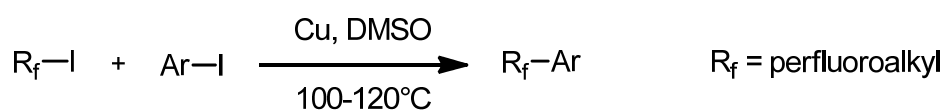
Scheme 4. Copper-mediated perfluoroalkylation of iodoarenes described by McLoughlin and Thrower.[84]

After the publication of McLoughlin and Thrower several research groups expanded and optimized the scope of this reaction. Chen *et al.* investigated solvent effects,[86] and extended the reaction to bromoaromatics[87][88] and perfluorooxaalkyl iodides[89] as starting material. Over the years DMSO and dimethylformamide (DMF) have proven to be suitable solvents for this reaction, but high yielding examples with hexamethylphosphoramide (HMPA), dimethylacetamide (DMAC), pyridine and ionic liquids are also known.[90][91] Common to all these solvents is their high Lewis basicity. The solvent's ability to coordinate to a substrate as

electron-pair donor is crucial for the stabilization of the perfluoroalkyl-copper intermediate, which is formed in a first reaction step. Hence, only solvents with high donor numbers, a qualitative measure of their Lewis basicity, are suitable reaction media for copper-mediated perfluoroalkylations.

The original paper from 1969 aimed at the introduction of long perfluoroalkyl chains. However, the vast majority of today's copper-mediated perfluoroalkylations are performed with trifluoromethyl groups.[85] This structural motif gained a lot of attention in the research field of bioactive compounds.[92][93] Trifluoromethylated aromatic compounds are active ingredients of a wide range of pharmaceuticals and agrochemicals.

As described in the last three sections the field of fluorous chemistry has grown and evolved continuously since the 1990s. Novel catalysis and combinatorial approaches, i.e. fluorous biphasic catalysis (FBC) and fluorous mixture synthesis (FMS), and efficient separation techniques were the main achievements of this period. However, the advantages of highly fluorinated compounds in the context of QIE are different than the remarkable phase behavior of these compounds. In the following section important properties of highly fluorinated compounds from the matter-wave physicist's view are discussed.

1.2.4 Highly Fluorinated Compounds for Matter-Wave Interferometry

One of the main goals of the QIE in the Arndt group is to perform experiments with increasingly heavy molecules. The incorporation of F-alkyl groups into a molecule is a very efficient way to increase a molecule's molecular weight. A simple trifluoromethyl group weighs 69 g/mol, compared to 15 g/mol for the hydrogenated counterpart, respectively. Adding a perfluorooctyl chain to a molecule would increase its mass by 419 g/mol. A quantum interference experiment with a molecule bearing four of such substituents ($4 *$ $419 \text{ g/mol} = 1\,676 \text{ g/mol}$) would mark a new mass record for matter-wave interferometry. The mass record from the time when the work on this doctoral thesis started was 1633 g/mol from the fluorofullerene $C_{60}F_{48}$.[34]

An important feature of suitable compounds for molecule interferometry is their stability. The molecules have to be brought as intact, neutral particles into the gas phase and should be stable during the flight through the interferometer. The carbon-fluorine bond is the most stable single bond known in organic chemistry. The bond-dissociation energy of a C-F bond is around 485 kJ/mol as compared with ca. 425 kJ/mol for a carbon-hydrogen bond. The exact

values are affected by the remaining substituents on the carbon atom. The high bond strength of the C-F bond, which originates from a very effective overlap of the orbitals, is the reason why highly fluorinated compounds show high thermal and chemical stabilities. Hence, the high stability of F-alkyl functionalized molecules is one of the promising features why these compounds are expected to be appropriate model compounds for QIE.

A further property of this compound class, which is very important for example in the field of environmental science is the high volatility of fluorous compounds. The element fluorine has a very low polarizability. This results in low van der Waals interactions between perfluoroalkyl chains. Owing to the small interchain forces highly fluorinated compounds show high vapor pressures in relation to their molecular weight. As poly- or perfluorinated chemicals can be found in a widespread range of industrial applications the knowledge of their atmospheric transport behavior is important for the estimation of their influence on the environment and thus subject of a lot of environmental studies.[94]–[98] In the context of QIE the high volatility is a key feature why fluorinated compounds are envisaged to be suitable compounds for molecule interferometry. As stated earlier the generation of a molecule beam of high intensity in the gas phase is a prerequisite for successful QIE. Therefore compounds with high vapor pressures are preferred as they can be evaporated more easily.

In summary, highly fluorinated molecules are proposed to be ideal model compounds for matter-wave interferometry because of their high molecular weight, thermal and chemical stability and high volatilities.

2 Research Project

Is there a defined transition between quantum mechanics and classical physics? Quantum mechanical laws describe phenomena in the size region of elementary particles, atoms or molecules whereas objects from the macroscopic world obey the rules of classical physics. Investigations at the interface of both worlds – the classical and the quantum world – are a fascinating field of interest for many scientists and the driving force for the research that is done within a collaborative project between chemists in the group of Prof. Marcel Mayor and physicists in the group of Prof. Markus Arndt in Vienna, Austria. The wave-particle duality developed by de Broglie[1] represents a paradigmatic example of a non-classical feature of quantum mechanics. We try to approach the quantum-to-classical transition by the observation of the wave nature of objects as large as possible. In other words: we use a bottom-up approach to advance to the quantum-to-classical border. Besides the exploration of the frontiers of quantum mechanics, the high sensitivity of quantum interferometry allows for a wide range of metrological investigations. This aspect of macromolecule interferometry is also addressed within this project.

In particular, this doctoral thesis focuses on the design and synthesis of suitable tailor-made molecules for quantum interference experiments (QIE). Both goals of the collaborative research project – exploration of the frontiers of QIE and quantum metrological applications – are pursued with the molecules described in this doctoral thesis.

The design criteria of the molecules are adapted according to the specific requirements of the different experimental setups in Vienna – far-field as well as near-field interferometers – and the general purpose of the envisaged QIE. Common to the vast majority of the synthesis projects is the approach to work with highly fluorinated compounds. As described in the introduction perfluoroalkyl functionalized molecules represent suitable objects for matter-wave interferometry with large and complex particles.

For the exploration of the frontiers of quantum mechanics the objective was to set new mass records for both near-field and far-field interferometry. At the time of the start of this doctoral thesis the mass record for near-field interferometry was held by the fluorofullerene $C_{60}F_{48}$ with a mass of 1 633 g/mol and for far-field interferometry by the fullerene C_{70} with a molecular weight of 841 g/mol.

On the metrological side, the focus was set on a deeper understanding of the influence of a molecule's internal structure, especially its polarizability, on quantum interference.

3   Model Compounds for Quantum Metrology

In textbooks on quantum mechanics, matter wave phenomena are often associated with the equation $\lambda_{\mathrm{dB}} = h/mv$, where the de Broglie wavelength λ_{dB} is only determined by Planck's constant h and the particle's momentum $p = mv$. It is a common conjecture in compliance with quantum theory that this relation still holds for bodies of arbitrary mass, size and complexity. But what is the role of the detailed internal molecular composition if λ_{dB} does not include any such information?

This question is one of the driving forces for the research in the Vienna group and although de Broglie quantum interference describes the center of mass motion of a massive body it has been shown to be sensitive to the internal structure of the interfering object. First experiments along this line recently allowed to apply this idea to near-field interferometry for measuring the static[45] and optical[47] polarizability α_{stat} and α_{opt} as well as the total electric susceptibility χ_{tot} of molecules. The latter may also contain additional information about static or time varying electric dipole moments.[49]

Within this doctoral thesis the focus of our research was set on two metrological aspects. In sections 3.1 and 3.2 the measurement of electric susceptibilities was envisaged. Furthermore, chapter 3.3 describes how matter-wave interferometry allows for the analysis of the thermal fragmentation behavior of highly fluorinated transition metal complexes.

3.1   Fluorous Constitutional Isomers for Quantum Interferometry

All individual atoms in a given molecular structure will add up to determine its global properties, and in particular also its electrical susceptibility. The susceptibility can couple to an external electric field and thus influence the center of mass motion of the entire particle. In this way, the internal structure becomes influential by the external motion, even though the molecule still remains widely delocalized and capable of showing de Broglie interference.

It has therefore been suggested that different molecular conformations might eventually also be distinguished in QIE. Figure 16 shows the interferometer setup in Vienna for the realization of this experiment. The working principle of the KDTLI has already been described in section 1.1.1. Additionally to the three gratings setup of the KDTLI two electrodes between grating 1 (G1) and grating 2 (G2) are installed to allow for deflectometry studies. Two constitutional isomers (in figure 16 simplified depicted as blue sphere and red cylinder), i.e. molecules with the same chemical sum formula, that differ in their susceptibilities are examined in this setup. They should become distinguishable in spite of the fact that the description of de Broglie interference contains no information about the internal structure of the molecule.

The lateral position of the quantum interference shift is determined by the interaction between the external electric field and the molecular susceptibility χ_{tot}. The susceptibility varies for different atomic arrangements even if they add up to the same chemical sum formula.

Figure 16. Sketch of the matter-wave interferometer for the distinction of structural isomers. The compounds are ejected from the effusive source to pass two nano-mechanical gratings and one optical phase grating. Quantum interference leads to a molecular density distribution at G3. Its lateral position is determined by the interaction between the external electric field and the molecular susceptibility χ_{tot}. The susceptibility varies for different atomic arrangements even if they add up to the same chemical sum formula.
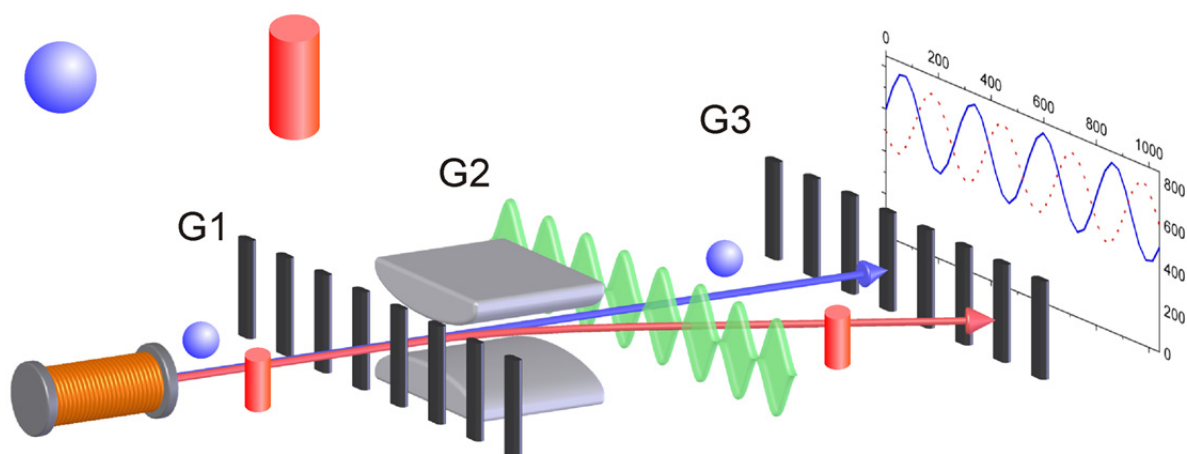
3.1.1 Molecular Design

The design of the two structural isomers is based on various aspects. In order to guarantee that the dimensions of the KDTLI, in particular the grating periods and grating distances, fit to the size of the isomers, the molecular weight was planned to be in the region of the mass record from that time, $M_W(C_{60}F_{48}) = 1\,633\,g/mol$.[34] The source consists of an oven, thus thermal stability and high vapor pressure are further indispensable properties. As described in detail in section 1.2.4 the use of perfluoroalkyl functionalized compounds helps to optimize the sublimability and molecular beam properties of the target structures with regard to their use in matter-wave interferometry. The characteristics of the source also require that the molecules can be synthesized in a scale of several hundred milligrams. As the creation of a molecule beam in a thermal source is rather inefficient these large amounts are necessary for successful QIE. Additionally, the molecules should be detectable with a quadrupole mass spectrometer (QMS), as the detection scheme of the KDTLI is based on a QMS device. Furthermore a low absorption at the wavelength of the green laser of the KDTLI ($\lambda_{laser} = 532\,nm$) is desired, since the absorption of photons could lead to decoherence.

A large difference in their total susceptibility is desired in order to be able to distinguish between both isomers. The design of both model compounds is based on recent findings in our group in the field of molecular electronics which showed a considerable delocalization of the π-system in rod-like oligo phenylene ethynylene (OPE)[99][100] on the one hand and a partition of the π-system by conjugation interrupting subunits found in platinum complexes,[101] perpendicular torsion angles[102][103] or sp^3-carbon atoms.

Therefore we proposed structure **1** with a molecular weight of 1 593 g/mol as a model compound with a low susceptibility (figure 17). The tetrahedral compound **1** consists of four perfluorohexyl functionalized phenyl rings interlinked by a central sp^3-carbon, which disables conjugation between the neighboring aromatic subunits and thus causes a low overall polarizability.

As counterpart with a high susceptibility we proposed a highly fluorinated OPE structure. A straightforward way to design a constitutional isomer of compound **1**, i.e. a structure having the same chemical sum formula, is to calculate the degree of unsaturation (DU) of isomer **1**. Molecules with identical chemical sum formulae need to have equal degrees of unsaturation. The DU is defined as the sum of all rings and π-bonds in a structure and can be calculated from the sum formula by the general equation 3.1.[104]

$$DU = 1 + \frac{1}{2}\left(\sum_i n_i(v_i - 2)\right) = \text{rings} + \pi\text{-bonds} \qquad 3.1$$

n_i is the number and v_i the formal valence of the element i. For isomer **1** with the chemical sum formula $C_{49}H_{16}F_{52}$ a DU of 16 is calculated.

An OPE structure contains alternating phenylene and ethynylene units. A phenylene unit formally consists of one ring and three π-bonds which corresponds to a DU of 4. On the other hand an ethynylene unit with its two π-bonds accounts for 2 DU units. Hence it becomes clear that an OPE structure that represents a constitutional isomer of the tetrahedral compound **1** has to consist two ethynylene and three phenylene units leading to a degree of unsaturation of 16. As shown in figure 17 the four perfluorohexyl chains are placed on the outer phenyl rings of the OPE **2**. Since they are the same for both components, they are not expected to contribute significantly to differences in the susceptibility. Finally the residual saturated alkyl moieties, three methylene units, have to be attached to the OPE. The placement as one ethyl and one methyl residue in *para*-position to each other on the central phenylene unit was chosen because of synthetic reasons and is discussed in detail in the synthetic strategy section 3.1.2. To sum up the rod-like OPE **2** contains a π-system that extends over all three phenyl rings. Thus an increased electron delocalization and polarizability is expected for model compound **2** as compared to **1**.

A simulation using the software package Gaussian 03W[105] with the basis set 3-21G yielded a static polarizability of $\alpha_{\text{stat}} = 63 \pm 2\ \text{Å}^3 \times 4\pi\varepsilon_0$ for compound **1** and $70 \pm 2\ \text{Å}^3 \times 4\pi\varepsilon_0$ for molecule **2**, i.e. a difference of about 10% between the two structures.
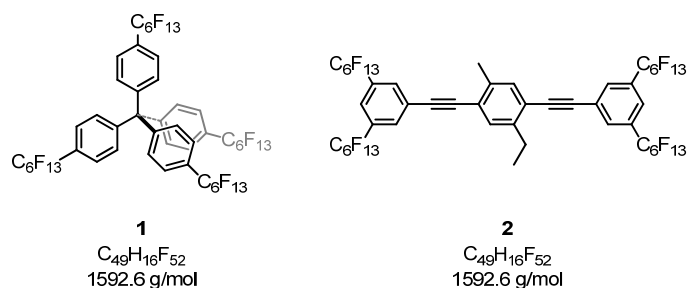
Figure 17. Fluorous constitutional isomers **1** and **2** for the application in QIE.

3.1.2 Synthetic Strategy

As shown in scheme 5 the spherical, hardly polarizable compound **1** should be accessible starting from trityl chloride (**3**). After an electrophilic aromatic substitution of trityl chloride (**3**) and aniline, and subsequent deamination the resulting tetraphenylmethane (**4**) can be brominated in the *para*-positions and finally perfluoroalkylated to yield the desired F-alkyl functionalized tetraphenylmethane derivative **1**.

The rod-like oligo phenylene ethynylene (OPE) structure **2** is supposed to be assembled starting from commercially available methyl-3,5-dibromobenzoate (**5**). The introduction of two perfluorinated alkyl chains represents the first step of the synthesis. In order to build up OPE **2** using a Sonogashira-Hagihara cross-coupling reaction as the final step, the ester functionality of compound **6** is converted into a terminal alkyne. This conversion is planned to be achieved with a reaction pathway via aldehyde **7** followed by a Corey-Fuchs reaction sequence. The central building block of the OPE, the diiodo derivative **10**, is envisaged to be synthesized from 4-ethyltoluene (**9**) by iodination.
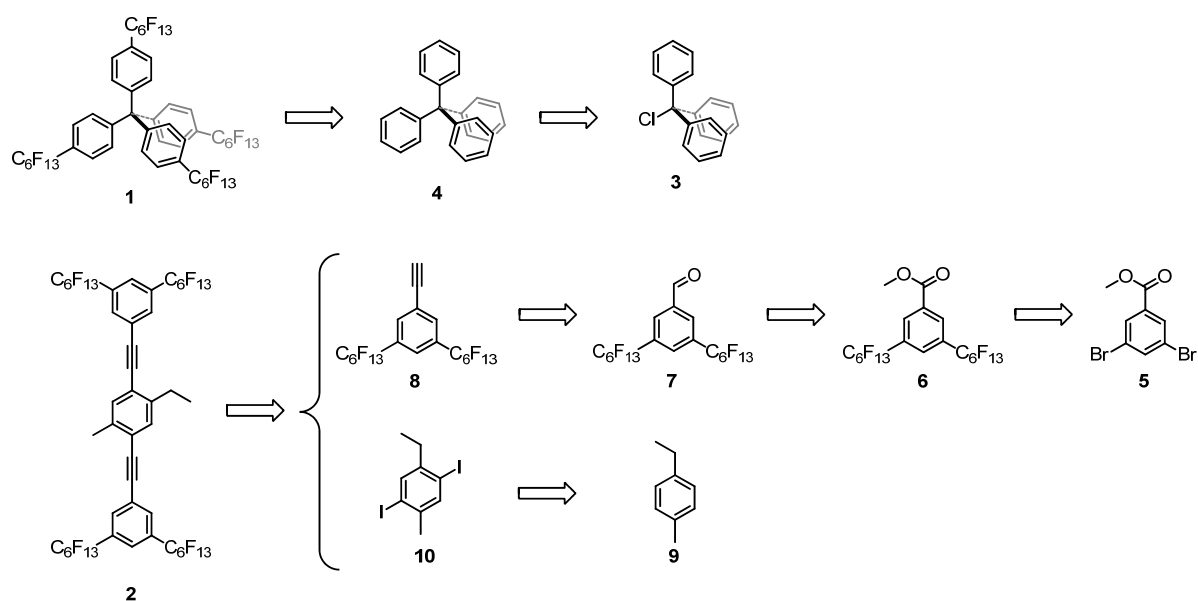
Scheme 5. Synthetic strategy towards the structural isomers **1** and **2**. The key steps are the perfluoroalkylations to introduce the fluorous ponytails, and a Sonogashira-Hagihara cross-coupling reaction as the final step in the assembly of isomer **2**.

3.1.3 Synthesis and Characterization

As displayed in scheme 6, the tetrahedral target compound **1** was synthesized in four steps starting from trityl chloride (**3**). The first two steps, initially an electrophilic aromatic substitution and a subsequent deamination leading to tetraphenylmethane (**4**), were achieved using a slightly modified literature procedure.[106] Trityl chloride (**3**) was treated with aniline at 200 °C for ten minutes. After an acidic workup the hydrochloric acid salt of tritylaniline (**11**) was used without further purification and analysis for the deamination reaction. The deamination is a two step reaction. First an acid catalyzed diazotation of tritylaniline (**11**) was performed by treatment with isoamylnitrite and sulfuric acid in ethanol at -10 °C for 30 minutes. Subsequently a nucleophilic aromatic substitution with hypophosphorous acid as hydride source led after recrystallization from hot DMF to the deaminated tetraphenylmethane (**4**) in a yield of 70% for both steps (a and b).

Bromination of all four *para*-positions of tetraphenylmethane (**4**) was done by the reaction with neat bromine according to an established procedure.[107] The reaction of tetraphenylmethane (**4**) and bromine at room temperature was completed after 25 minutes, easily judged by the stop of the evolution of gaseous hydrobromic acid. Pure tetrakis(4-bromo-phenyl)methane (**12**) was obtained after recrystallization from a mixture of chloroform and ethanol as a yellowish crystalline solid in 83% yield.

Since the copper-mediated cross-coupling of *n*-perfluoroalkyliodides and bromine substituted arenes in polar aprotic solvents at elevated temperatures (110 – 130 °C) is a common route to F-alkyl substituted aromatic compounds,[85] this reaction type was chosen to introduce the fluorous ponytails in the last reaction step. Compound **12** was reacted with 6 equivalents (1.5-fold excess) of *n*-perfluorohexyliodide in DMF containing freshly activated copper at 120 °C under an argon atmosphere for 12 hours. The copper was activated by stirring it in a mixture of acetone and a few crystals of iodine, followed by a mixture of acetone and hydrochloric acid and at last pure acetone. Impurities on the copper surface, mainly copper oxides, are effectively removed by this cleaning method.[108] These reaction conditions led to a mixture of all four differently substituted derivatives (mono-, di-, tri- and tetrasubstituted). Separation of the mixture by column chromatography with hexane as eluent afforded the desired tetrakis(4-perfluorohexyl-phenyl)methane (**1**) as a white crystalline solid in a yield of 27%. Prolonged reaction times did not increase the yield.
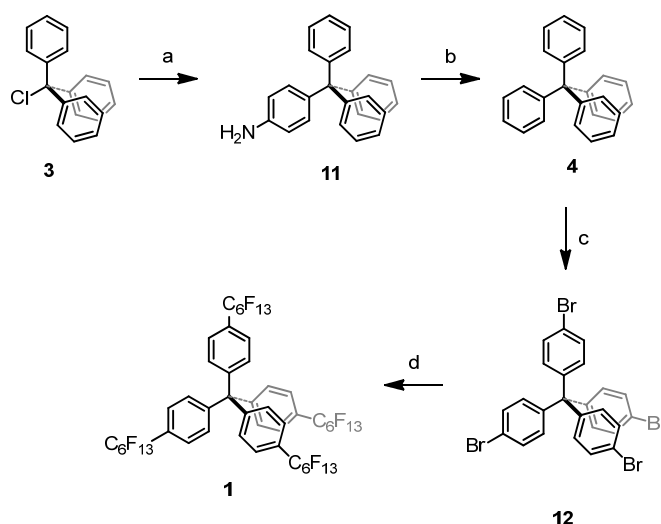
Scheme 6. Synthesis of the structural isomer **1**. *Reagents and conditions*: (a) aniline, 200 °C, 10 min (b) 1.) H_2SO_4, $C_5H_{11}ONO$, EtOH, -10 °C, 30 min, 2.) aq. H_3PO_2, reflux, 15 min, 70% (over 2 steps) (c) Br_2, rt, 25 min, 83% (d) IC_6F_{13}, Cu, DMF, 120 °C, 12 h, 27%.

Figure 18 displays the aromatic region in the ^{1}H-NMR spectra of the starting material and all four reaction products that are formed during the perfluoroalkylation of tetrakis(4-bromo-phenyl)methane (**12**). By comparing the spectra 1 and 5 the electron withdrawing effect of the perfluorohexyl chains is clearly observed. Two signals at 7.39 ppm and 7.01 ppm, respectively, for tetrakis(4-bromo-phenyl)methane (**12**) and two duplets at 7.56 ppm and 7.33 ppm indicate the lowered electron density in the aromatic rings, expressed by the shift of the signals to lower field, in the product structure. Furthermore, the isolating effect of the central sp^3-hybridized carbon atom is nicely visualized. The stepwise substitution of the bromines by perfluoroalkyl chains has only insignificant effects on the electronic structure of the remaining bromophenyl rings. Even in spectra 4 - the threefold F-alkylated product - only a small change in the chemical shift of the bromophenyl moiety is observed as compared to the starting material. The protons in *meta*-position to the bromine are only shifted from 7.01 ppm to 7.04 ppm.
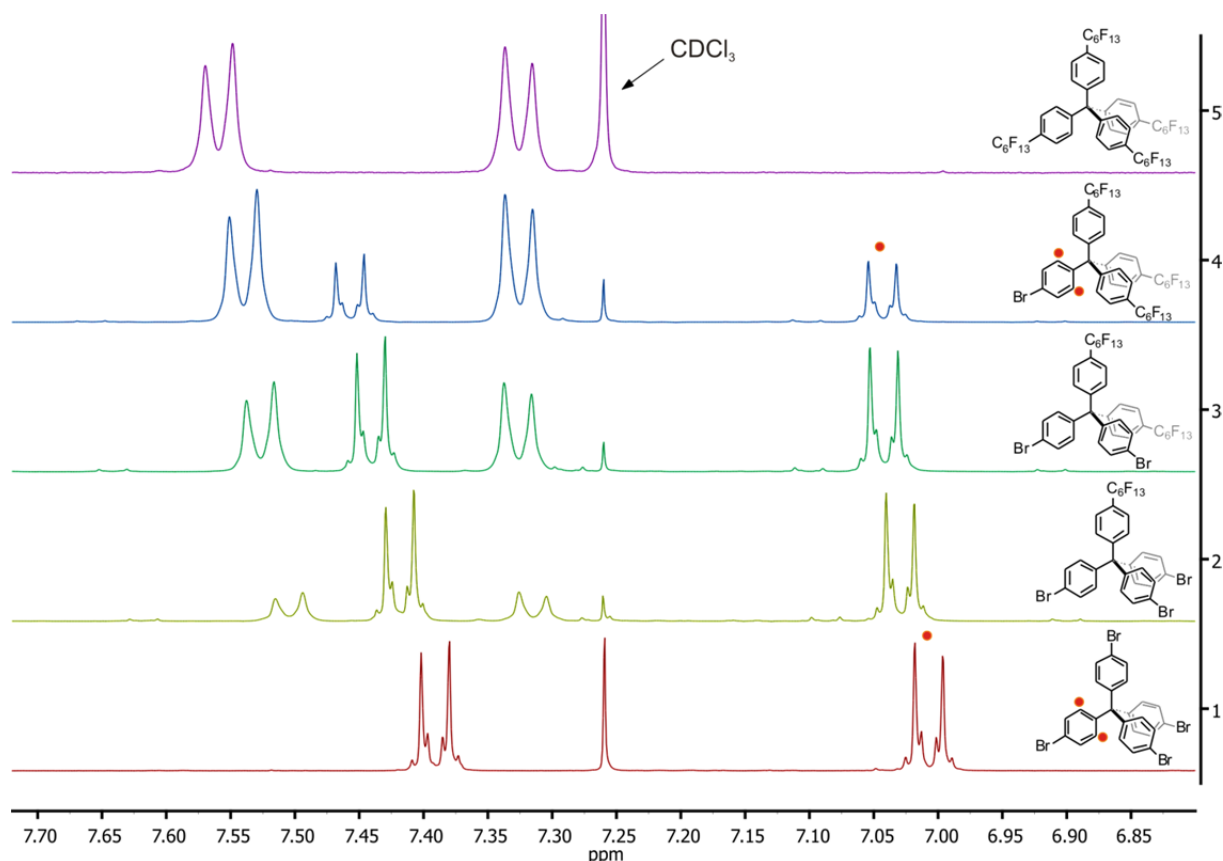
Figure 18. Aromatic region of the ^{1}H-NMR spectra (in CDCl$_3$) of tetraphenylmethane (**12**) and all four reaction products of the copper-mediated perfluorohexylation reaction. The signals that are annotated with red circles correspond to the protons in *meta*-position to the bromine in the bromophenyl units.

As displayed in scheme 7 the perfluoroalkylated ester **6** was synthesized starting from methyl-3,5-dibromobenzoate (**5**) and *n*-perfluorohexyliodide (2.5 equivalents) by heating them together with freshly activated copper in DMF at 120 °C under an argon atmosphere for 12 hours. This copper pre-treatment seemed to be very important to achieve high yields. The desired methyl ester **6** was isolated after purification by column chromatography as a white solid in 86% yield.

To convert the ester functionality of compound **6** into an aldehyde, a two-step reaction sequence via benzylic alcohol **13** was chosen. The reduction to the alcohol followed by a re-oxidation to the aldehyde is usually favored over a direct reduction of the ester to the aldehyde, generally done with diisobutyl aluminum hydride (DIBAL) as reducing agent in apolar solvents at low temperatures. The direct reduction to the aldehyde with DIBAL is usually not applied since it is often accompanied by an overreduction to the alcohol.[109][110] Furthermore, the benzylic alcohol itself is an interesting building block to functionalize molecules with a fluorophilic shell. The reduction of the ester **6** using lithium aluminum

hydride ($LiAlH_4$) in diethylether at room temperature led after aqueous workup and purification by recrystallization from hexane to the benzylic alcohol **13** as a white solid in 64% yield.

To achieve the oxidation to the aldehyde the use of a protocol developed by Corey and Schmidt in 1979 was envisaged.[111] Pyridinium dichromate (PDC) in dichloromethane as aprotic solvent oxidizes primary alcohols to the corresponding aldehydes without overoxidation to the carboxylic acid, regardless of the nature of the substrate. Alcohol **13** and a small excess of PDC were stirred at room temperature under an argon atmosphere for 24 hours. An easy workup, namely filtration of the reaction mixture to remove the chromium species and evaporation of the solvent, made this reaction very efficient. Aldehyde **7** was obtained after purification by column chromatography as a white solid in 88% yield.
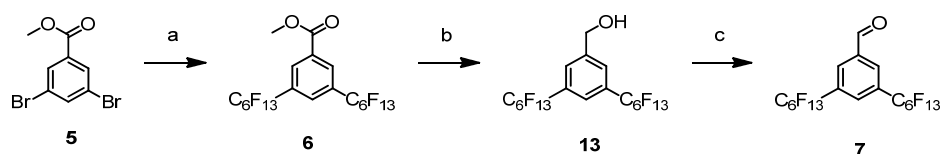
Scheme 7. Synthetic route to aldehyde **7**. *Reagents and conditions*: (a) IC_6F_{13}, Cu, DMF, 120 °C, 12 h, 86% (b) $LiAlH_4$, Et_2O, rt, 16 h, 64% (c) PDC, CH_2Cl_2, rt, 24 h, 88%.

As depicted in scheme 8 the assembly of the terminal alkyne **8** was realized in two steps from the aldehyde **7** using a Corey-Fuchs reaction sequence.[112] The first step of this transformation is a Wittig-type reaction which forms the dibromoolefin **14**. Addition of the aldehyde **7** to a phosphorous ylide - generated by mixing carbon tetrabromide and triphenylphosphine in dichloromethane at 0 °C - led to the one-carbon chain extended dibromoolefin **14** after one hour of reaction time. The crude was purified by column chromatography to give compound **14** as colorless oil in a yield of 85%. The second step was accomplished by treating the dibromoolefin **14** with 2.9 equivalents of *n*-butyllithium (*n*-BuLi) at -78 °C in tetrahydrofuran (THF) for one hour, followed by hydrolysis of the generated lithium acetylide. Alkyne **8** was obtained after purification by column chromatography as a white solid in a yield of 93%.
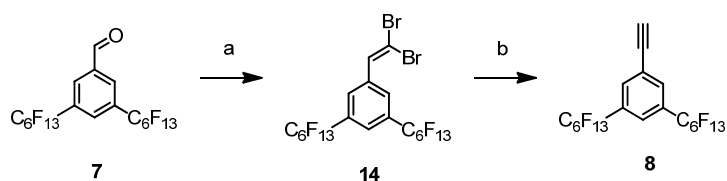
Scheme 8. Synthesis of the terminal alkyne **8**. *Reagents and conditions*: (a) CBr_4, PPh_3, CH_2Cl_2, 0 °C, 1 h, 85% (b) 1. *n*-BuLi, THF, -78 °C 2. H_2O, 93%.

The second building block for the final Sonogashira-Hagihara coupling reaction, the diiodo derivative **10**, was synthesized by iodination of commercially available 4-ethyltoluene (**9**) (scheme 9). The reaction of 4-ethyltoluene with iodine and iodic acid in a mixture of sulfuric acid, acetic acid, chloroform and water led to the diiodo compound **10** as white crystals in a yield of 53%.

9   **10**
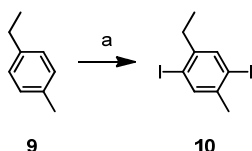
Scheme 9. Synthesis of the diiodo compound **10**. *Reagents and conditions*: (a) I_2, HIO_3, glacial AcOH, H_2SO_4, $CHCl_3$, H_2O, 85 °C, 4 h, 53%.

The Sonogashira-Hagihara coupling reaction of the free acetylene **8** and 1-ethyl-2,5-diiodo-4-methylbenzene (**10**) was performed using tetrakis(triphenylphosphine)palladium and copper iodide as catalysts, diisopropylamine as base and THF as solvent (scheme 10). After 12 hours at room temperature the crude was purified by column chromatography yielding the desired OPE **2** and considerable amounts of the homo-coupled 1,3-diacetylene **2a** as byproduct. Although the polarity of the desired OPE and the byproduct is almost identical, the separation was achieved by column chromatography (silica gel, hexane/acetone (0.2%)) to give pure OPE **2** in a yield of 22%. Homo-coupled 1,3-diynes are known byproducts in Sonogashira-Hagihara cross-coupling reactions,[113]–[115] and result from an oxidative process. Although the mixture of solvent and base (THF/diisopropylamine) was degassed by the freeze-pump-thaw procedure to exclude the presence of oxygen during the reaction the formation of considerable amounts of the side product could not be avoided. An explanation for the high tendency of alkyne **10** to dimerize in a Glaser-type reaction is the high acidity of the terminal alkyne which accelerates this type of reaction.[114] The high acidity originates from the strong electron withdrawing effect of the F-alkyl substituents which stabilizes the deprotonated species. Various other Sonogashira-Hagihara cross-coupling protocols were examined, amongst them copper-free variations to avoid acetylene homocoupling.[116] Formation of the side product **2a** was successfully reduced with these conditions, however, the yield of the desired target structure also dropped. In summary, the yield of 22% for this reaction step obtained by the standard conditions described above could not be increased.
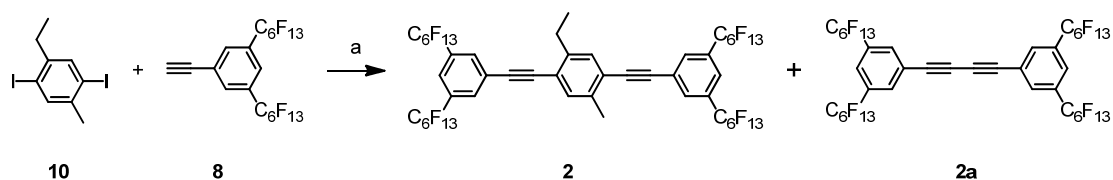
Scheme 10. Synthesis of the structural isomer **2**. *Reagents and conditions*: (a) Pd(PPh$_3$)$_4$, CuI, (*i*-Pr)$_2$NH, THF, rt, 12 h, 22%.

Scheme 11 displays the synthesis of both isomers. All precursors and the target structure **1** display reasonable solubilities in common organic solvents and were thus fully characterized by ^{1}H-, ^{13}C- and ^{19}F-NMR-spectroscopy, elemental analysis (only the elemental analysis of **7** was unrecorded due to its limited stability) and mass spectrometry. However, the dissolvation of the flat OPE **2** turned out to be challenging. Exclusively mixtures of deuterated chloroform with hybrid organic/fluorous solvents such as hexafluorobenzene or 1,1,2-trichloro-1,2,2-trifluoroethane (Freon 113) allowed recording of ^{1}H- and ^{19}F-NMR spectra of **2**. Furthermore, the identity of **2** was corroborated by MALDI-ToF mass spectrometry. Both final structures **1** and **2** could thus be made with high purity and on a scale of several hundred milligrams.
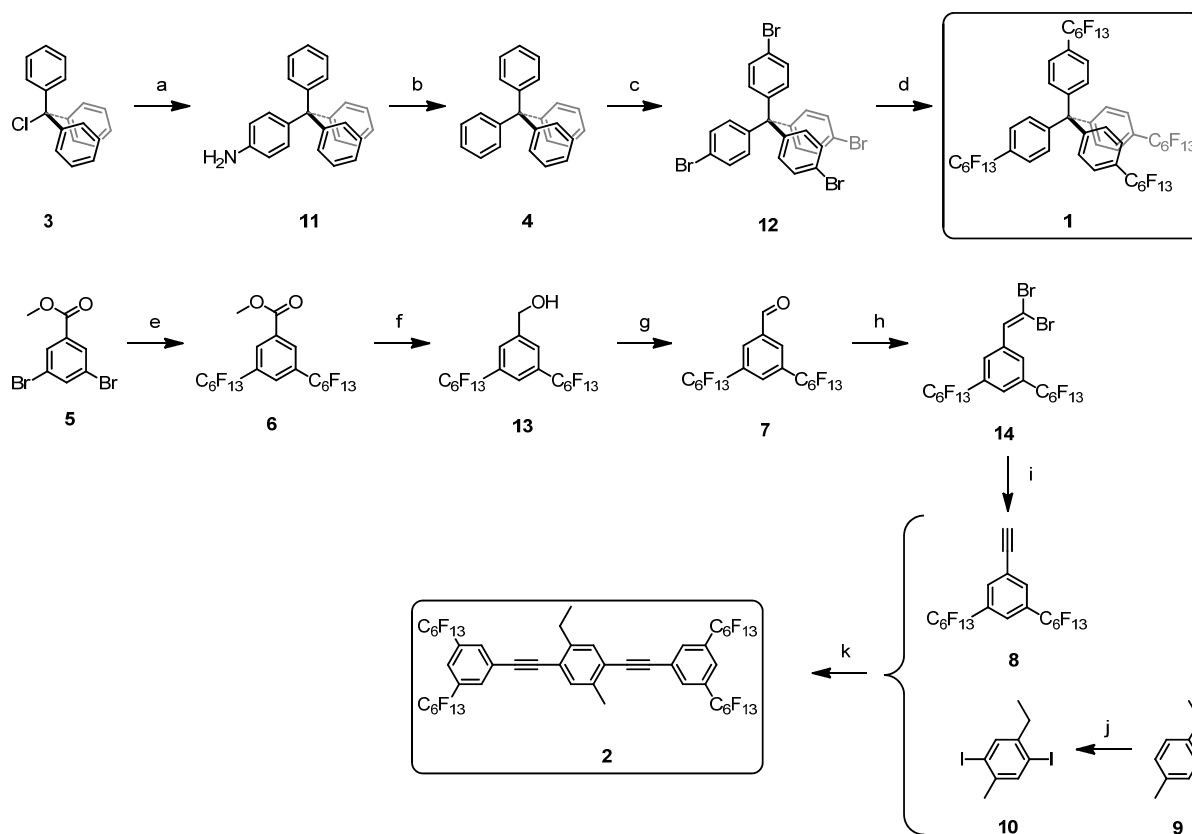
Scheme 11. Synthesis of the constitutional isomers **1** and **2**. *Reagents and conditions*: (a) aniline, 220 °C (b) 1. H$_2$SO$_4$, C$_5$H$_{11}$ONO, -10 °C, DMF 2. aq. H$_3$PO$_2$, 70% (over 2 steps) (c) Br$_2$, rt, 25 min, 83% (d) IC$_6$F$_{13}$, Cu, DMF, 120 °C, 12 h, 27%; (e) IC$_6$F$_{13}$, Cu, DMF, 120 °C, 12 h, 86% (f) LiAlH$_4$, Et$_2$O, rt, 16 h, 64% (g) PDC, CH$_2$Cl$_2$, rt, 24 h, 88%; (h) CBr$_4$, PPh$_3$, CH$_2$Cl$_2$, 0 °C, 1 h, 85% (i) 1. *n*-BuLi, THF, -78 °C 2. H$_2$O, 93%; (j) I$_2$, HIO$_3$, glacial AcOH, H$_2$SO$_4$, CHCl$_3$, H$_2$O, 85 °C, 4 h, 53%; (k) Pd(PPh$_3$)$_4$, CuI, (*i*-Pr)$_2$NH, THF, rt, 12 h, 22%.

Figure 19 displays the UV/Vis spectra of the two target structures. OPE **2** with its larger conjugated π-system absorbs at longer wavelengths as compared to isomer **1**. An important fact is that both structures do not absorb in the spectral region of the optical phase grating of the KDTLI, namely at 532 nm. The absorption of photons during the flight through the interferometer could lead to decoherence and thus to a loss of quantum interference.
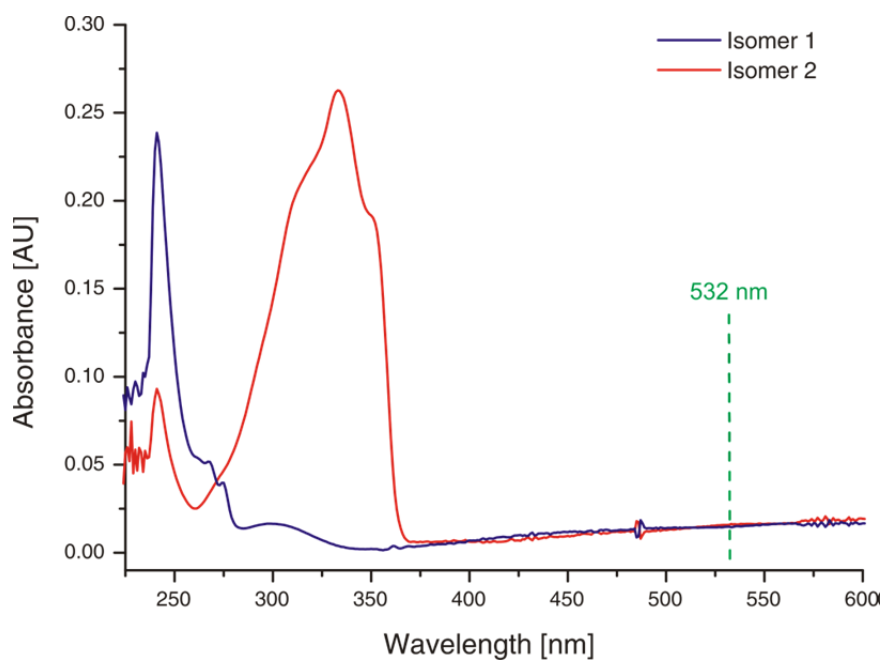
Figure 19. UV/Vis spectra of the constitutional isomers **1** ($c \approx 2 \times 10^{-5}$M) and **2** ($c \approx 9 \times 10^{-6}$M) in chloroform at room temperature.

3.1.4 Interference Experiments

To distinguish between both constitutional isomers, the substances were evaporated under high vacuum conditions in a ceramic furnace at a temperature of $T = 185 \pm 5\,°C$. The molecular beam passed through a series of delimiters that restricted the trajectory to the free-fall parabola that corresponds to the desired velocity. The particles then traversed a KDTLI, shown in figure 20, before they were ionized by electron impact and injected into a quadrupole mass spectrometer (QMS). The QMS allows to check the integrity of the molecules after the evaporation process and it discriminates the desired signal against the background gases.
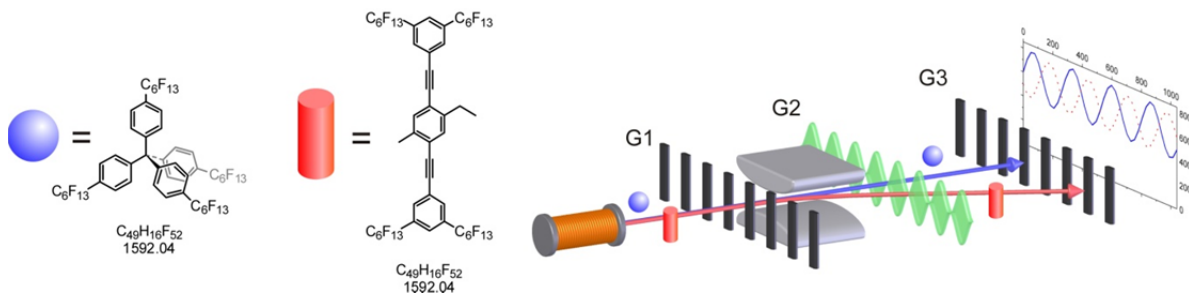
Figure 20. Schematic representation of the KDTLI for the application of two constitutional isomers.

The matter-wave interferometer consists of three gratings, G1-G3, all with identical slit periods of $d = 266$ nm and slit openings as small as about 100 nm. The first grating (G1) prepares the necessary lateral wave coherence of the molecular beam at the location of G2. Diffraction of the molecules at G2 then results in a regular density distribution of periodicity d at G3. When G3 is scanned across this molecular pattern, the detector records a sinusoidal intensity variation

$$S(x_3) = O + A \sin[2\pi(x_3 - \Delta x_3)/d] \qquad\qquad 3.2$$

as shown at the right-hand end of figure 20. Here, x_3 denotes the grating position, Δx_3 is the position offset of the interference fringe, which also depends on external forces, and we define the quantum interference visibility $V = A/O$ as the ratio of the fringe amplitude A and its vertical offset O.

The three gratings are spaced equidistant at a distance of 105 mm one from another. G1 and G3 are absorptive masks that are fabricated from a 190 nm thin SiN_x membrane. The central grating, which is responsible for diffraction, is realized as a standing light wave that is generated by a retro-reflected laser beam at $\lambda_L \approx 532$ nm. The light field imposes a position dependent phase on the matter wave that is governed by the laser power P and the optical polarizability α_{opt} at the chosen laser wavelength. For many molecules this value

approximates very closely to the static value α_{stat}, when the dipole allowed electronic resonances are sufficiently separated from the laser wavelength. This is also the case for our structures **1** and **2**.

The application of a pair of electrodes between gratings G1 and G2 allows to subject the matter wave to an inhomogeneous but constant electric field. The electric field imprints an additional phase onto the matter wave that results in a shift Δx_3 of the interference pattern at G3 parallel to the grating vector. This shift is proportional to the total electric susceptibility χ_{tot}:

$$\Delta x_3 \propto \chi_{stat}U^2/mv^2 \qquad\qquad 3.3$$

where m is the mass, v is the molecular velocity and U the voltage applied between the electrodes. In order to obtain absolute numbers, a geometry factor has to be determined experimentally, in our case in a calibration measurement with C_{60}.

Generally, the total electric susceptibility is determined by the electronic contribution to the polarizability α_{stat} and, according to the van Vleck formula[50]

$$\chi_{tot} = \alpha_{stat} + \frac{\langle d^2 \rangle}{3k_B T} \qquad\qquad 3.4$$

also by a thermal average over the square of all possible electric dipole moments, either permanent moments or those related to thermally activated vibrations.

As the polarizability is influenced by the molecular structure, in our case by the extent of delocalization of the central π-systems, we expect even constitutional isomers to behave differently under the influence of the external field. Effects of the fluorous ponytails on the polarizability are expected to be negligible mainly for two reasons: First, their electronic coupling to the aromatic subunit is poor, and second their contributions will be comparable for both constitutional isomers **1** and **2**.

Compounds **1** and **2** were examined in two separate experimental runs. They were evaporated at identical temperatures, but slightly different velocity distributions were chosen: These were centered at $v_{mean} = 110$ m/s for compound **1** and $v_{mean} = 91$ m/s for **2** with $\Delta v_{FWHM}/v_{mean} = 0.15$ and $\Delta v_{FWHM}/v_{mean} = 0.10$, respectively. This corresponds to a mean de Broglie wavelength of about 2.5 pm.

The selection of slightly different velocity classes was necessary since the two compounds exhibit different mass spectra and signal intensities. While for compound **2** the expected mass peak at $m/z = 1592$ stood out well above the background, the spectrum of compound **1**

displayed an additional dominant fragment signal at $m/z = 1197$, which is attributed to the stable trityl cation formed after loss of one fluoroalkyl substituted phenyl moiety. This fragment at $m/z = 1197$, which is also the dominant signal in the MALDI-ToF spectrum, is formed during the ionization in the QMS. Fragmentation of **1** during the beam formation was excluded by chemical analysis of the molecules deposited on an annular mask between the source and G1. The analysis corroborated with the intact parent structure **1** as the only component of the molecular beam. As shown in figure 21, the ^{1}H- and ^{13}C-NMR before and after the application in the KDTLI show no differences. Furthermore, ^{19}F-NMR spectra and MALDI-ToF-MS analysis support the thesis that isomer **1** is stable during the flight through the interferometer. The ionization fragment reduced the parent signal of **1** to about a third of the value observed for **2**. The lower signal was therefore partially compensated by choosing a different slice of the thermal velocity distribution, closer to the maximum.

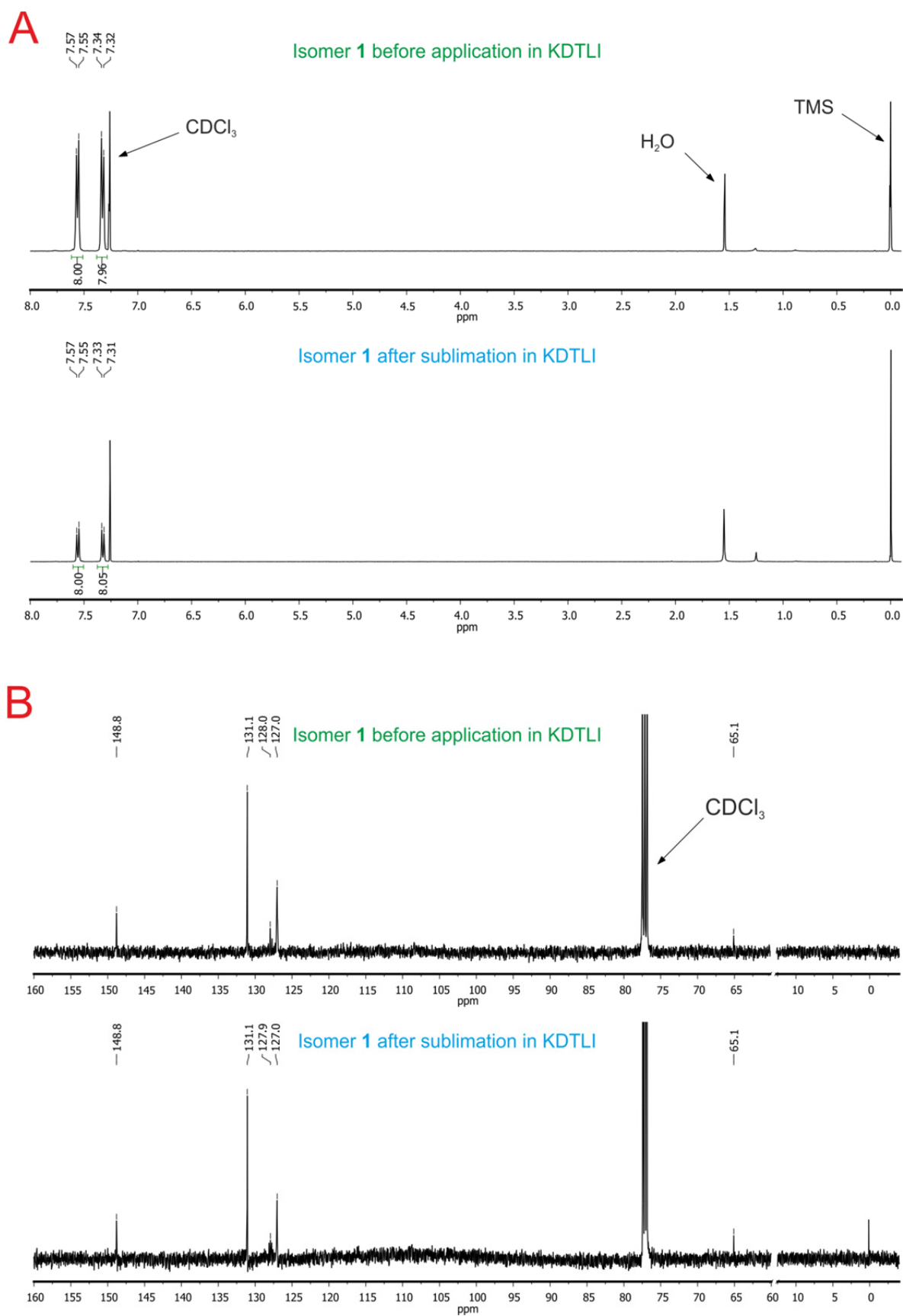**Figure 21**. NMR spectra of isomer **1** in CDCl$_3$ before and after the application in the KDTLI (A) ^{1}H-NMR spectra (B) ^{13}C-NMR spectra. For a better visualizing the spectrum between 15 ppm and 60 ppm is hidden. In this region no peaks are present.

The interference patterns were recorded at different voltage settings. At high voltages the fringe visibility is reduced by a velocity dependent dephasing of the interference pattern and the finite width of the velocity distribution. Since Δx_3 is velocity dependent (equation 3.3), a large velocity spread will blur the interference contrast.

The electric susceptibility was determined for every single voltage step by fitting equation 3.3 to the experimental value of Δx_3 with χ_{stat} as the only free parameter. The calculation included the detailed measured velocity distribution. The results of all runs for both molecules are depicted in figure 22. A weighted mean of $\chi_{stat} = 102 \pm 0.8$ Å$^3 \times 4\pi\varepsilon_0$ for compound **1** and $\chi_{stat} = 126 \pm 0.5$ Å$^3 \times 4\pi\varepsilon_0$ for OPE **2** was found. Only the statistical error bar is shown, which decreases because of the more reliable reading at high fringe deflection and high voltages. The systematic error is dominated by the uncertainty in the velocity measurement as well as the knowledge of both laser power and focal width. The drop in interference contrast at high deflection voltage rapidly spoils the fit quality at high deflection voltage. Thus the data point at $U = 10$ kV in the evaluation of the mean value of χ was excluded.
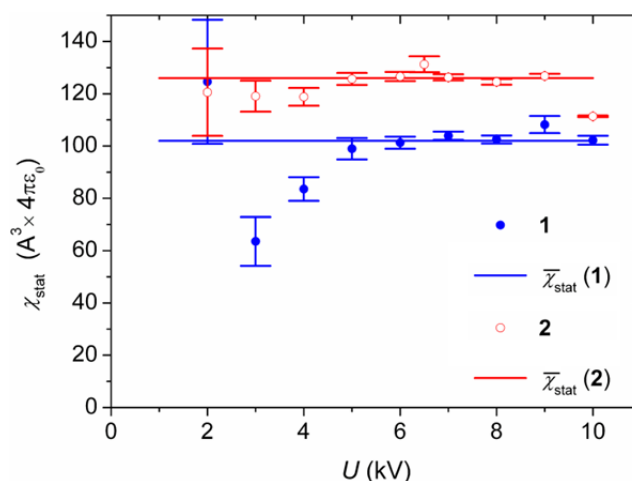
Figure 22. Experimental values of χ_{stat} for compounds **1** (blue full circles) and **2** (red hollow circles) extracted from the interference fringe shift at different settings of the deflection voltage. The error bars represent the statistical errors (1σ). The solid blue and red lines show the weighted means of the susceptibility values of **1** and **2** respectively.

Interestingly, for both isomers the susceptibility values differ from the computed static polarizabilities. This is consistent with the presence of vibration-activated electric dipole moments which emerge for flexible molecules at high temperature.[117] Based on earlier experiments with perfluoroalkyl-functionalized azobenzenes[49] a thermal contribution to the susceptibility of 10-15 Å$^3 \times 4\pi\varepsilon_0$ per side chain is expected.

3.1.5 Conclusion

To demonstrate that different molecular conformations can be distinguished in quantum interference experiments two tailor-made constitutional isomers were synthesized and applied in the Kapitza-Dirac-Talbot-Lau interferometer (KDTLI) in Vienna. Although de Broglie quantum interference describes the center of mass motion of a massive body, it was shown to be sensitive to the internal molecular structure of the constitutional isomers. The different total susceptibilities of both lead to different de Broglie interference shifts in the presence of external electric fields. The isomers thus become distinguishable in spite of their identical mass and chemical sum formula.

3.2   Non-Fluorous Constitutional Isomers and the Effect of F-alkyl Chains

In this chapter experimentally determined optical polarizabilities and electric susceptibilities are compared to computed static polarizabilities and discussed in detail.

In earlier work on the quantum interference of the fluorinated azobenzene **F-alkyl AZO**[49] and in the studies described in section 3.1 about the fluorous constitutional isomers **1** and **2**[118] it was shown that thermally excited flexible molecules may exhibit vibrationally induced electric dipole moments (figure 23). According to the Van Vleck formula such fluctuating dipole moments have a considerable effect on the electric susceptibility of a molecule. In order to obtain a deeper insight on the structural origin of these dipole moments further QIE were proposed.
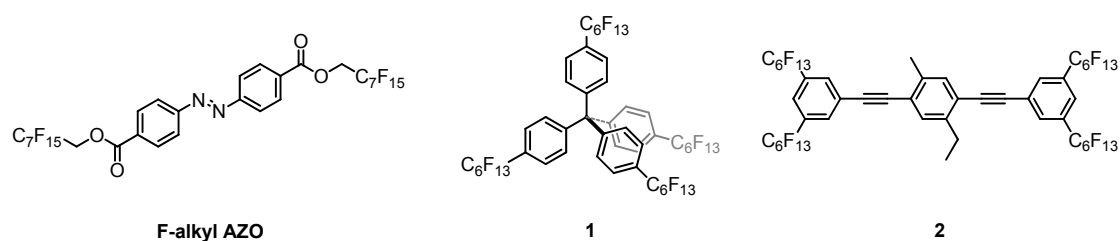
Figure 23. Structures of F-alkyl functionalized model compounds for QIE that exhibit vibrationally induced electric dipole moments. These fluctuating dipole moments influence the electric susceptibility of the molecules.

As shown in scheme 12, in a first set of QIE the comparison of the fluorous tetraphenhylmethane derivative **1** and tetraphenylmethane (**4**) was envisaged. With these experiments it was planned to assign the emerging dipole moments to a specific substructure inside the delocalized molecules. Since the non-polar tetraphenylmethane (**4**) comprises a rather rigid structure the formation of induced dipole moments from thermally activated vibrations should be negligible. As a consequence the interferometrically measured susceptibility and the computed static polarizability should ideally be equal. In contrast to that, compound **1** bears four floppy F-alkyl chains which are supposed to be the structural motif that is responsible for temporary dipole moments at high internal temperatures. For this "furry" structure **1** an increased susceptibility is expected even though this molecule is point symmetric and nonpolar in its thermal ground state. Structure **1a** (scheme 12) represents a schematic snapshot of a thermally excited state which leads to a temporary dipole moment.

In a second set of interferometric susceptibility measurements the comparison of molecules without any peripheral flexibility was proposed. Thus simpler structures like the quaterphenyl derivative **15**, a constitutional isomer of **1**, moved into our focus of investigation. Furthermore, compound **16**, which misses two hydrogen atoms to match the mass of **1**, also

represents an interesting structure. Owing to the bridging methylene unit the dihedral angle between the ring planes of the central phenyl units is fixed to an angle close to 0°. This geometry favors a high electron delocalization and thus an enlarged polarizability is expected.
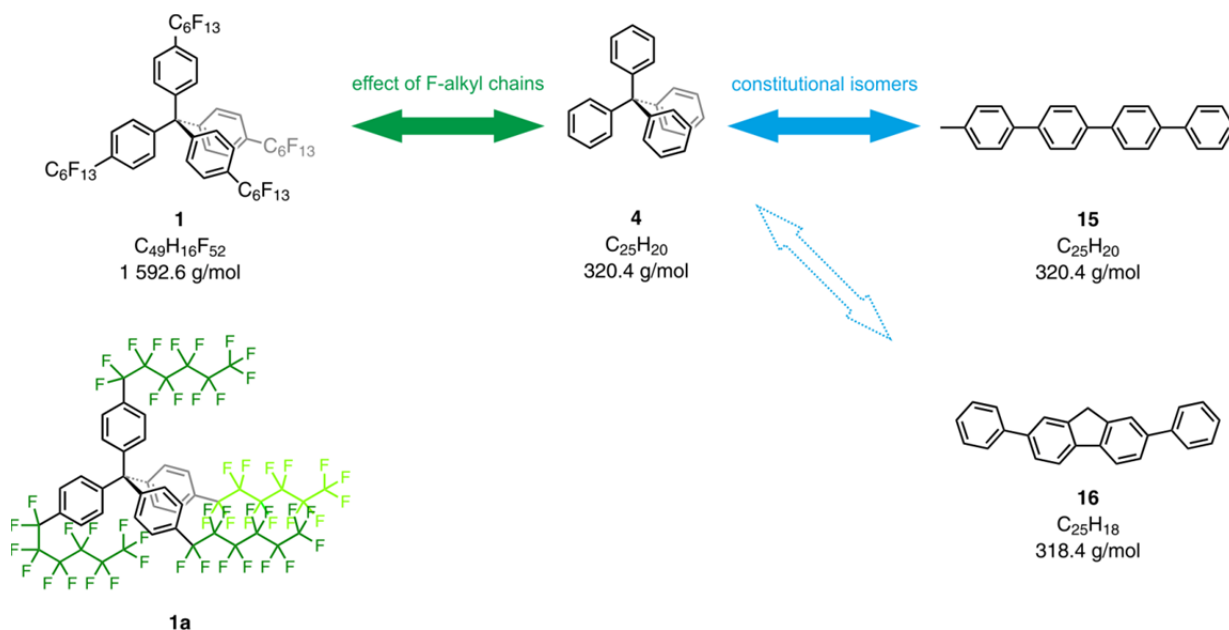
Scheme 12. Proposed target structures **1**, **4**, **15** and **16** for QIE aiming at analyzing the effect of F-alkyl chains on quantum interference and for QIE with light compounds without any peripheral flexibility. Structure **1a** displays a schematic snapshot of the thermally activated compound **1** leading to a temporary dipole moment.

3.2.1 Synthesis and Characterization

The synthesis of compound **1** was already described (*vide supra*). As tetraphenylmethane (**4**) is an intermediate in the synthetic route towards compound **1** also this structure was already synthesized in the context of the project with the fluorous constitutional isomers (see section 3.1). Before sending a sample of compound **4** to the Arndt group sublimation tests were performed to check the thermal stability and the ability to create a molecule beam. It turned out that tetraphenylmethane (**4**) can be sublimated at a pressure of 0.05 mbar and a temperature of 200 °C without any signs of decomposition. This result is a good indication that a molecule beam of sufficient intensity is achievable in the KDTLI. On the other hand a negative outcome of the sublimation test in the Basel laboratories would not mean that successful QIE are not possible because the experimental conditions of the KDTLI are much more sophisticated than the ones of the basic sublimation apparatus in the chemistry labs in Basel. The oven of the KDTLI is able to reach temperatures of more than 400 °C and works under high vacuum conditions ($p \approx 10^{-8}$ mbar), whereas the sublimation tests are performed at maximum temperatures of around 200 °C and a minimum pressure of 10^{-3} mbar.

As shown in scheme 13 compounds **15** and **16** were both assembled in one-step syntheses starting from commercially available precursors. In a palladium-catalyzed Suzuki-Miyaura cross coupling reaction 4-methylquaterphenyl (**15**) was synthesized by treating 4-bromo-4'-methylbiphenyl (**18**) and 4-biphenylboronic acid (**17**) with tetrakis(triphenylphosphine)-palladium as catalyst and potassium carbonate as base in a solvent mixture of toluene and ethanol. After 5 hours at 80 °C the desired product **15** was obtained after aqueous workup and purification by column chromatography as a white solid in a yield of 91%. Similarly, the bifunctional 2,7-dibromofluorene (**19**) was reacted with 2.2 equivalents of phenylboronic acid (**20**) using the same catalyst/base/solvent system as in step (a) to yield compound **16**. After a reaction time of 5 hours at 80 °C, an aqueous workup and purification by column chromatography pure compound **16** was obtained as a white solid in a yield of 78%. The thermal stability during a sublimation process was tested for this product. A successful sublimation was made at a temperature of 200 °C and a pressure of 0.5 mbar. Both target structures **15** and **16** were fully characterized by ^{1}H- and ^{13}C-NMR spectroscopy, mass spectrometry, elemental analysis and UV/Vis spectroscopy.
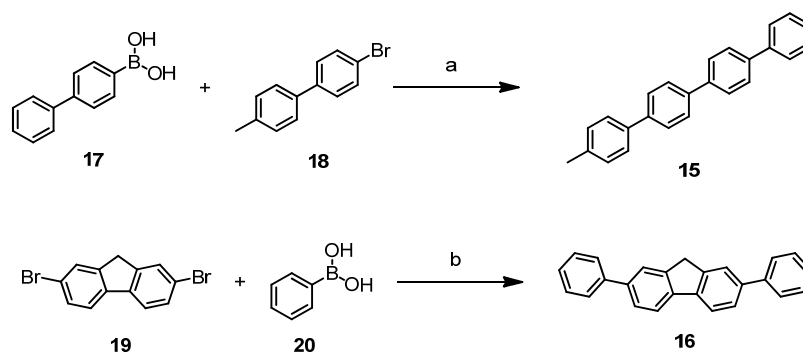
Scheme 13. Synthesis of the target structures **15** and **16**. *Reagents and conditions*: (a) Pd(PPh$_3$)$_4$, K$_2$CO$_3$, toluene, EtOH, 80 °C, 5 h, 91% (b) Pd(PPh$_3$)$_4$, K$_2$CO$_3$, toluene, EtOH, 80 °C, 5 h, 78%.

UV/Vis absorption spectra are important characteristics to estimate the suitability of molecules for the KDTLI. The optical phase grating of the KDTLI is ideally off-resonant. Although the spectra shown in figure 24 are taken in solution where solvent effects have a considerable influence on the band positions, and the QIE are performed in the gas phase, these spectra represent a good basis for the estimation of whether photon absorption must be taken into account in the QIE. The UV/Vis spectrum of tetraphenylmethane (**4**) in chloroform shows an absorption maximum at 241 nm. The quaterphenyl derivative **15** shows a maximum at 299 nm, and in the spectrum of the fluorene derivative **16** two maxima at 305 and 323 nm, respectively, are present. Consequently, all three target compounds are not expected to absorb photons when passing the standing light wave with a wavelength of 532 nm in the KDTLI.
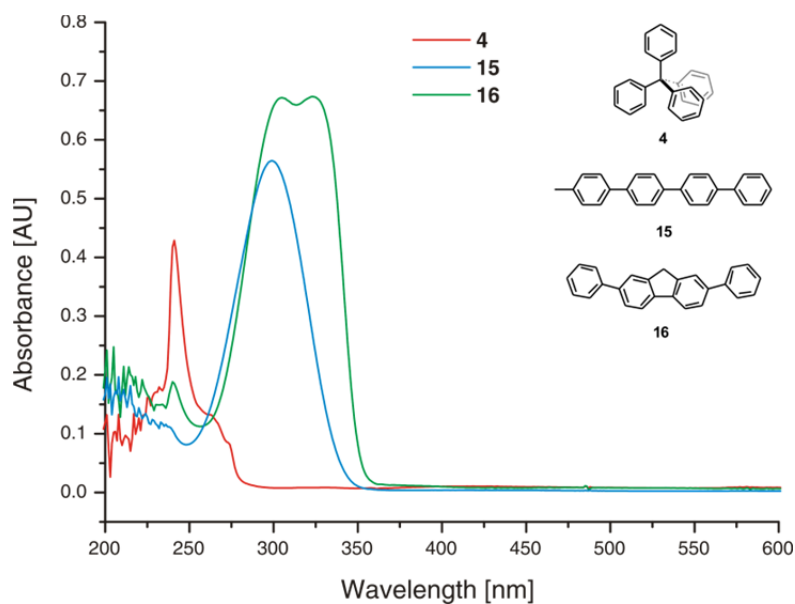
Figure 24. UV/Vis spectra of the target compounds **4** ($c \approx 2 \times 10^{-5}$M), **15** ($c \approx 1 \times 10^{-5}$M) **16** ($c \approx 9 \times 10^{-6}$M) and in chloroform at room temperature.

3.2.2 Interference Experiments

For the compounds **1** and **4** the static polarizability was computed and compared to the measured electric susceptibilities that include the presence of possible dynamical dipole moments. The two compounds differ in their structural rigidity, which influences their electric properties. Using the simulation package Gaussian09[119] with the basis set 6–31G*, the static polarizabilities were computed to be $\alpha_{stat}(\mathbf{4}) = 4\pi\varepsilon_0 \times 33 \text{Å}^3$ and $\alpha_{stat}(\mathbf{1}) = 4\pi\varepsilon_0 \times 69 \text{Å}^3$. The measurement of the electric susceptibilities was performed in the same experimental setup as the fluorous constitutional isomers (section 3.1) and is shown schematically in figure 25.
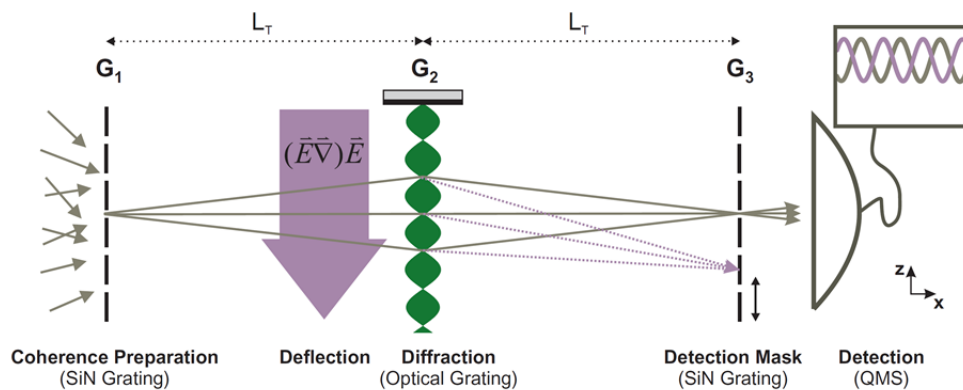
Figure 25. The KDTL metrology experiment allows one to combine matter wave interferometry with Stark deflectometry to study the internal electric properties of complex molecules.

When exposing the molecular beam to the external electric force a fringe shift is observed. To give an example, the shift of the interference pattern of compound **1** is shown in figure 26 for a deflection voltage of 5 kV.
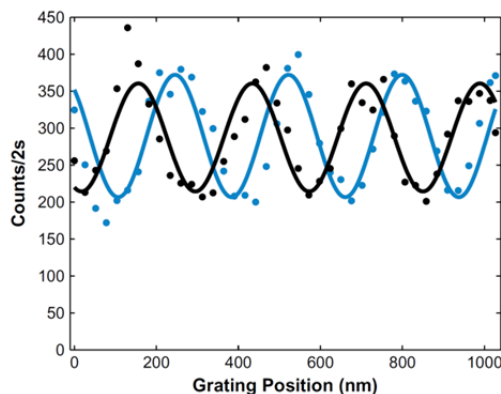
Figure 26. The quantum interference pattern is shifted when a homogeneous electric force field acts transversally on the delocalized molecules. Here: shift of compound **1** at a deflection voltage of 5 kV (blue dots) compared with the interference pattern at a reference voltage of 1 kV (black dots) applied to the electrodes. The measured dark rate is already subtracted and the solid lines represent sinusoidal fits to the data.

From a fit to the shift-versus-voltage curve, the experimental susceptibility value $\chi(\mathbf{4}) = 4\pi\varepsilon_0 \times 37(3)\text{Å}^3$ for compound **4**, which is in good agreement with the computed polarizability, can be extracted. In marked contrast to that, the susceptibility of derivative **1** shows a substantially enhanced $\chi(\mathbf{1}) = 4\pi\varepsilon_0 \times 101(4)\text{Å}^3$. This is a strong indication of the presence of thermally activated conformation changes on a short time scale. They allow for a temporary electric dipole moment whose squared projection does not average out. For both compounds **1** and **4** the fringe deflection as a function of the applied voltage is shown in figure 27. The deflection experiment thus supports the computed picture of a rigid tetraphenylmethane core and flexible side chains that enhance the susceptibility through rapidly fluctuating dipole moments.
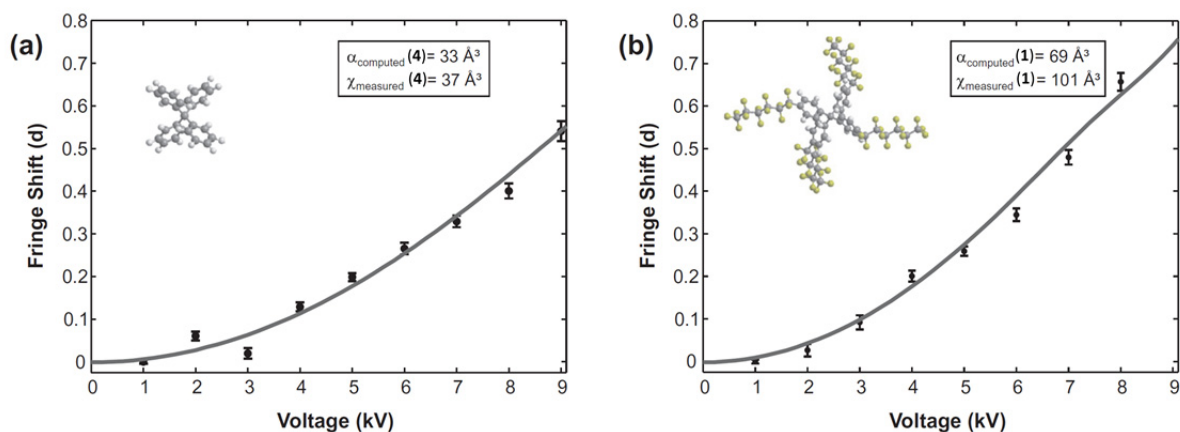
Figure 27. KDTLI-deflection experiments with compounds **1** and **4**. (a) Fringe shift of **4** measured in multiples of the grating period d as a function of deflection voltage. The computed value for the static polarizability $\alpha_{stat}(\mathbf{4}) = 4\pi\varepsilon_0 \times 33\text{Å}^3$ is in good agreement with the experimental value for the susceptibility of $\chi(\mathbf{4}) = 4\pi\varepsilon_0 \times 37(3)\text{Å}^3$, which is extracted from a numerical fit to the data (solid gray line). (b) Fringe deflection of compound **1**. In comparison to the computed static polarizability $\alpha_{stat}(\mathbf{1}) = 4\pi\varepsilon_0 \times 69\text{Å}^3$, the experiment shows a considerably enhanced susceptibility $\chi(\mathbf{1}) = 4\pi\varepsilon_0 \times 101(4)\text{Å}^3$ that can be assigned to thermally activated conformation changes and fluctuating dipole moments.

With the compounds **15** and **16** various QIE were performed in Vienna. However, for both compounds it was not possible to obtain interference patterns of good quality and thus metrological information could not be gained for these structures. The main reason was the relatively high dark rate of the mass spectrometric detection unit in the mass region of the molecular masses of the target compounds, which disabled an effective detection of the molecular flux through the KDTLI. This drawback of the QMS detection was known before, but a modification and optimization of the KDTLI towards these light compounds was not envisaged, because the experiments with these compounds were of minor importance. In future projects structures with higher masses are planned to be examined.

3.2.3 Conclusion

In conclusion, it was shown that quantum interferometry with tailored and delocalized molecules allows us to assign the rigid and the floppy components inside a molecule. For compound **4** the measured susceptibility value compares favorably with the computed polarizability, whereas it is in marked discrepancy for molecule **1**. This allows us to identify the vibrationally activated dipoles in the side arms of compound **1** as the origin of its observed susceptibility increase. The quantitative value of this contribution is sizeable and important with regard to future experiments, where long perfluoroalkyl side chains are used in an

attempt to increase the mass limits in organic interference while maintaining that the particles are sufficiently weakly bound to be able to launch them in an effusive beam.

Furthermore, in experiments with the light compounds **15** and **16** it became obvious that the current KDTLI setup is not optimized for molecules in the mass range of 300-500 g/mol as the mass spectrometric detection exhibits a bad detection efficiency in this region.

3.3   Quantum Metrology as a Complementary Tool for Mass Spectrometry

In this chapter, it is shown how a KDTLI can be employed as a complementary tool for mass spectrometry where fragmentation might occur in either the source or the ionization process. The method is based on the fact that the molecular polarizability is often a good indicator of the number of constituents in the molecule. The interference fringe contrast in the KDTLI is sensitive not only to the polarizability-to-mass ratio but also to the absolute polarizability. It thus allows addressing problems that are not easily accessible with established methods: one such example is the analysis of polymers that decay into fragments of nearly identical polarizability-to-mass ratios.

This fact was exploited to perform a fragment analysis of the commercially available F-alkylated palladium complex **21**, shown in figure 28, which has been developed as a palladium catalyst for cross-coupling reactions in fluorinated media.[68][120] The intact molecule has a mass of 3 379 amu, but quadrupole mass spectrometry reveals predominantly a compound with a mass of 1 601 amu, which corresponds to the mass of the fluorous triphenylphosphine ligand **22**. Matter-wave interferometry allows us to answer the question as to whether fragmentation occurs in the source or in the electron impact ionization stage. Our procedure measures the dynamic polarizability α, which differs by a factor of two for the intact molecule and its fragments, whereas α/m remains about the same.

At a wavelength greatly shifted from all optical resonances, the dynamic polarizability can be approximated well by the static polarizability. A Hartree–Fock simulation with Gaussian 03W,V6[105] using the basis set 3–21G results in a static polarizability of 66 Å^3 for the fluoroalkyl-functionalized triphenylphosphine ligand **22** at 1 601 amu. A value about twice as large is expected for the intact palladium complex **21** at 3 379 amu.
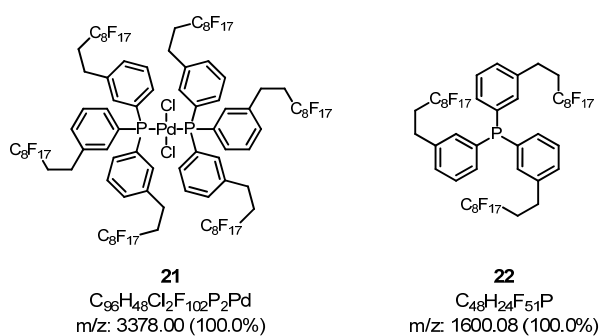
Figure 28. Molecular structure of the palladium complex **21** and the fluorous triphenylphosphine ligand **22**.

3.3.1 Interference Experiments

Figure 29A shows a typical quantum interferogram that was recorded when using complex **21**. The quantum wave properties of the palladium complex **21** are of particular interest, owing to its mass of 3 379 amu, which is about twice as high as the fluorinated fullerene derivative $C_{60}F_{48}$ (1 632 amu).[34]
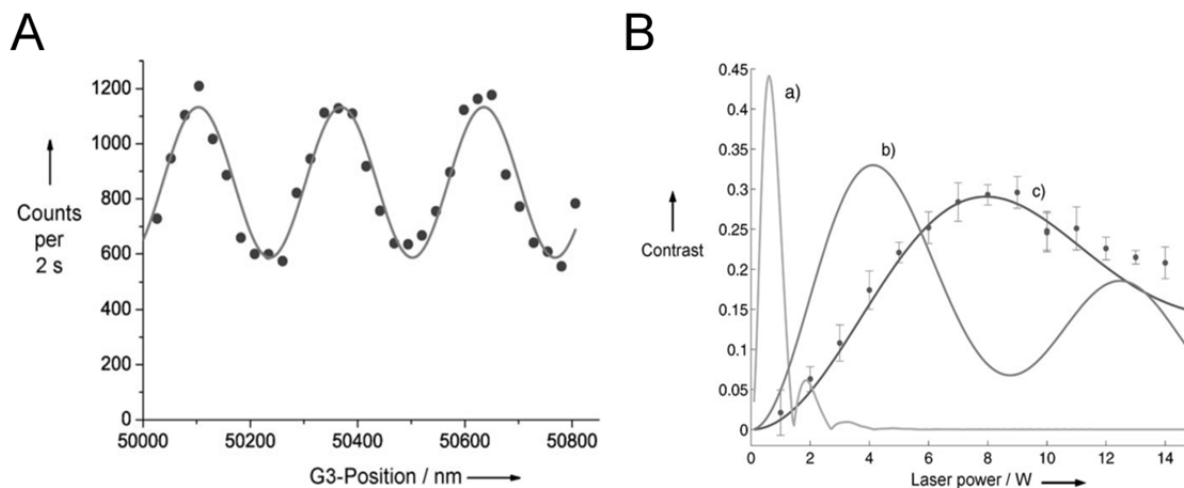
Figure 29. (A) Quantum interferogram of **21** recorded at the mass of 1601 amu. (B) Dependence of the interference fringe contrast (visibility, V) on the diffracting laser power. • experimental values, a) classical expectation for $m = 1\,601$ amu and $\alpha = 66$ Å^3, b) theoretical prediction for $m = 3\,378$ amu and $\alpha = 132$ Å^3, and c) theoretical prediction for $m = 1\,601$ amu and $\alpha = 66$ Å^3. The good agreement between the quantum expectation (c) and experiment allows a unique assignment of the molecule.

In contrast to far-field diffraction experiments, the fringe spacing in Talbot–Lau interferometry is predetermined by the experimental setting, and does not reveal mass information. However, the fringe visibility is a clear indicator for mass and polarizability, in particular when it is traced as a function of the diffracting laser power P of the optical phase grating (figure 29B). The experimental points are marked as full circles, where each point represents the average of three consecutive measurements. The error bars indicate the standard deviation. In the same figure a classical simulation is shown with Newtonian trajectories of billiard balls in an external potential for the fragment (a). This model clearly fails to describe the experiment. The same holds for a quantum wave model based on the mass and polarizability of the intact particle (b). However, a quantum model based on the mass and polarizability of ligand **22**, a likely fragment of the palladium complex **21**, is in very good agreement with the experimental data (c). This implies that the fragments are already present in the beam before the electron impact ionization, and it points to fragmentation of **21** during the beam formation.

3.3.2 Chemical Analysis

To confirm the hypothesis of fragmentation of the palladium complex **21** during sublimation, we chemically analyzed both the parent palladium complex **21** and the sublimated species which were collected on a cold copper plate in the molecular beam (figure 30).
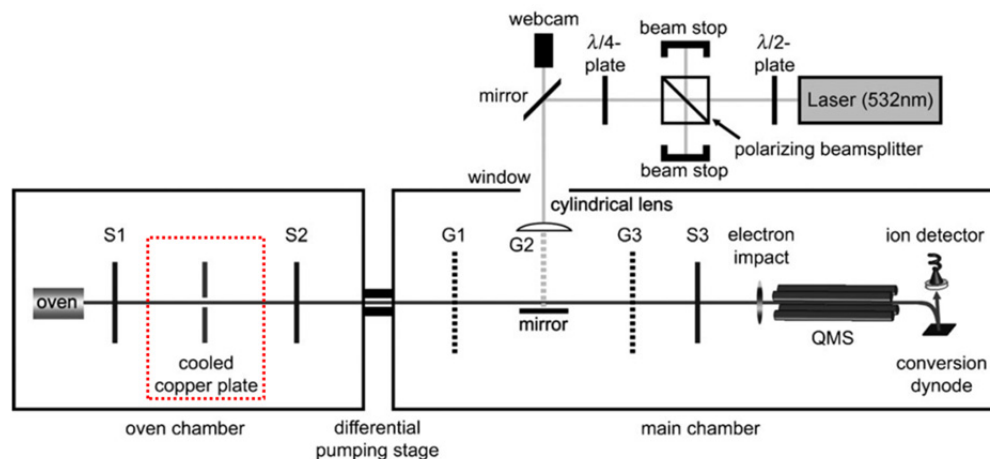
Figure 30. Schematic representation of the KDTLI. The cooled copper plate (pointed in red) is located inside the oven chamber between two velocity selectors (S1 and S2).

Extensive washing with hexafluorobenzene delivered the material from the copper plates. Qualitative analyses were performed by ^{1}H-, ^{19}F-, and ^{31}P-NMR spectroscopy as well as MALDI-ToF mass spectrometry. Whereas the ^{19}F-NMR spectra of both samples resemble each other and allowed us only to attest the presence of the 1H,1H,2H,2H-perfluorodecane chains, minor variations in the aromatic region of the ^{1}H-NMR spectrum pointed to the presence of two different compounds. Pronounced differences were observed in the ^{31}P-NMR spectra of both samples. Whereas the intact complex **21** has a ^{31}P-NMR signal at 20.9 ppm, the sample collected from the copper plate has a peak at 10.8 ppm. Thus, the sublimated species creating the molecular wave is not the entire palladium complex **21**, but rather a fragment. Further analysis of the extract from the copper plate by MALDI-ToF mass spectrometry gave a strong signal at $m/z = 1\,618$, corresponding to the water adduct of the triphenylphosphine ligand **22**. Thus, chemical analysis further corroborates the hypothesized fragmentation of **21** during sublimation.

3.3.3 Conclusion

In summary, the analytical capabilities of the KDTLI were demonstrated. The instrument may complement mass spectrometry, as it allows molecular properties of neutral particles to be probed in free flight before possibly being perturbed by ionization.

4 Model Compounds for New Size Records in Near-Field Molecule Interferometry

Exploration of the frontiers of quantum mechanics is the ultimate goal of the work presented in this chapter. In particular, efforts to set new size records for quantum interferometry and thus to approach the quantum-to-classical transition are described. As discussed in the introduction near-field Kaptitza-Dirac-Talbot-Lau interferometry seems to be an ideal concept for QIE with objects of large size and complexity. The advantages of this technique are shortly summarized (a) a favorable scaling behavior of the gratings (b) uncollimated beams can be used because of the Talbot-Lau effect and (c) the optical phase grating provides a perfect periodicity and is undestroyable. In principle, the current KDTLI in Vienna (figure 31) is constructed for objects with masses up to 15 000 g/mol, currently limited by the detection range of the QMS device. All other components of the interferometer are designed for even higher masses. The design criteria for tailor-made molecules for QIE with objects as large as possible are similar to the ones described in chapter 3 for the metrological applications in the KDTLI. The key properties are volatility, stability and detectability. Additionally, a modular synthesis strategy was desired in order to be able to gradually increase the size and complexity of the target structures. The aim was to find a suitable core structure, which can be coated with a fluorous shell of increasing thickness. As thermal evaporation is used as the source in the KDTLI, it is essential that the target structures are synthesized on a scale of several hundreds of milligrams.
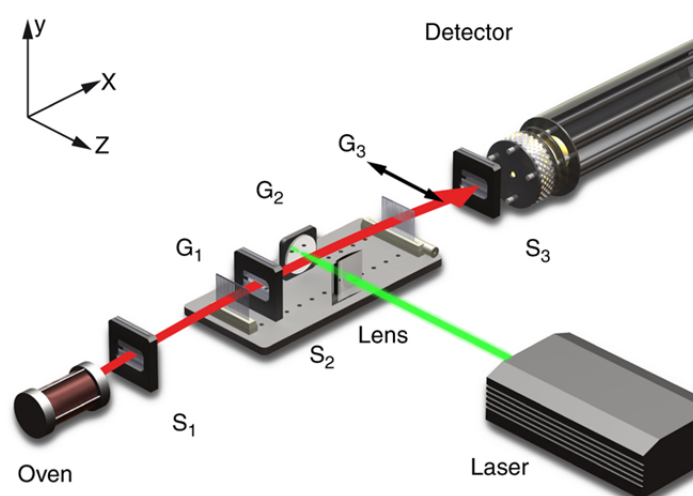

Figure 31. Schematic representation of the KDTLI. In extension to earlier experiments, various technological refinements were added: the oven was adapted to liquid samples, a liquid-nitrogen-cooled chamber became essential to maintain a low source pressure, a new mass analyzer allows increasing the detected molecular flux by a factor of four.

4.1   Fluorous Fullerenes

Fullerenes proved to be appropriate candidates for QIE.[27] They were initially chosen for several reasons. The two main aspects were that they are stable and commercially available in sufficient quantities. The thermal stability offers the possibility of working with high temperatures in the source chamber to create intense beams. In the first far-field experiments with C_{60} the oven temperature was kept between $900 - 1\,000$ K.[16] Stability is also an issue in the detection unit. The fullerenes were capable of being ionized by photoionization without being fragmented.[18] Furthermore, directly fluorinated fullerenes[59][60] set a new benchmark for mass in quantum interferometry[34] and F-alkyl functionalized fullerenes, which were synthesized in radical reactions,[54] showed promising beam properties.[53]

The favorable stability, volatility and detectability features of this compound class were the motivation for us to synthesize new tailor-made F-alkyl functionalized compounds with fullerenes as core units. Chemical functionalization of fullerenes is possible by various methods, including Diels-Alder [4+2] cycloadditions, radical reactions, oxidations, halogenations and the Bingel-Hirsch reaction.[121] We identified the Bingel-Hirsch cyclopropanation as a promising synthetic method towards fullerenes that are coated with a fluorous shell. Bingel described in 1993 the monofunctionalization of fullerenes by the reaction of C_{60} with diethyl bromomalonate (**24**) in the presence of sodium hydride as base in toluene (scheme 14).[122] Deprotonation in the α-position of diethyl bromomalonate (**24**) by the base is followed by attack of the resulting anionic nucleophile to a double bond of C_{60}. Elimination of Br⁻ leads to the formation of the cyclopropanated methanofullerene derivative **25**. Hirsch and coworkers extended the Bingel reaction to form multifunctionalized fullerene derivatives with up to six substituents with an octahedral addition pattern referred to as the Bingel-Hirsch reaction.[123]
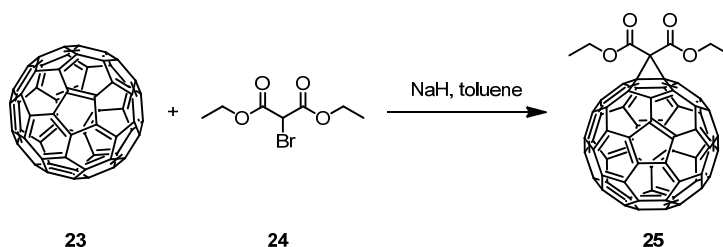
Scheme 14. Cyclopropanation of fullerenes as described by Bingel.[122] The reaction proceeds via an addition-elimination mechanism.

Wilson *et al.* described the synthesis of fluorous fullerenes by one- and threefold Bingel reactions.[124][125] However, the work of Wilson *et al.* and examples of fluorous fullerenes,

where other reaction types than Bingel-Hirsch reactions were used,[126] describe synthetic procedures on the rather small scale of milligrams and the use of fluorous and/or hybrid solvents for reactions and purification steps. Fluorous solvents are not excluded in our synthetic strategies but should be reduced to a minimum for economical and ecological reasons,[127][128] as large amounts of the target compound have to be synthesized for the QIE. Thus a main issue was the question of whether the synthesis of fluorous fullerenes is feasible on a larger scale than previously described in the literature. Nowadays, unfunctionalized malonates are used as reactants instead of bromofunctionalized derivatives as in the original reaction procedure described by Bingel.[122] Unfunctionalized malonates represent easily accessible starting materials and can be in situ converted to the halide functionalized species by the reaction with carbon tetrabromide.[129][130] Figure 32 depicts the three envisaged fluorous malonates **26-28** which were planned to be attached to the fullerene C_{60}. We aimed for first monofunctionalization and later a multiple attachment up to hexakisadducts.
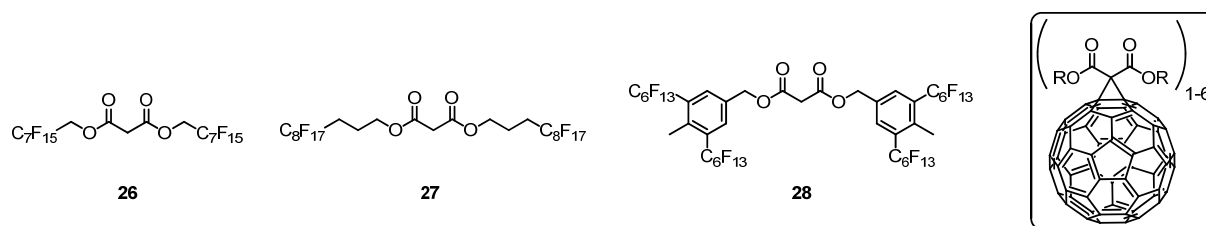
Figure 32. Structures of the envisaged fluorous malonates **26-28**, which were intended to be attached to C_{60} leading to fluorous methanofullerene derivatives.

4.1.1 Synthesis and Characterization

The fluorous malonates **26-28** were synthesized from malonyl dichloride (**33**) and the corresponding alcohols (scheme 16). The linear fluorous precursors for the malonates **26** and **27** are commercially available. The benzylic alcohol **31** was synthesized in two steps as shown in scheme 15. The chemistry that leads to the alcohol **31** is already described in section 3.1.3. Only a small variation in the structure of the starting material was chosen as compared to the reaction sequence described in scheme 7. Instead of methyl 3,5-dibromobenzoate (**5**), the methylated derivative methyl 3,5-dibromo-4-methylbenzoate (**29**) was chosen as a starting point. In consideration of the fact that an arene, which bears two F-alkyl chains and a functional group in benzylic position, represents a very versatile building block for current and future projects, the methylated form **29** was chosen because it is 1/6th

the price of methyl 3,5-dibromobenzoate (**5**). Furthermore, it was anticipated that the physical and chemical properties are not significantly different.

The two step synthesis of the alcohol **31** is shown in scheme 15. A copper-mediated perfluoroalkylation yielded the ester **30** as a white solid in a yield of 91%. Reduction to the benzylic alcohol **31** was achieved by treatment of ester **30** with lithium aluminum hydride in diethylether affording the alcohol **31** in a yield of 90%. Already in section 3.1 it was demonstrated that the benzylic functional group can be easily varied by common functional group transformations and thus a wide range of functional groups in benzylic position of this fluorous structure are accessible. Ester, alcohol, aldehyde, dibromoolefin and acetylene functionalities were synthesized on the way to the fluorous OPE **2** (see page 34 for its structure). A further functional group which can be used, for example in amide bond formations, is the free carboxylic acid. This compound was obtained by basic ester hydrolysis of ester **30** and broadens the scope of applications of this building block. Ester **30** was stirred in a methanolic potassium hydroxide solution at room temperature for 12 hours. After an acidic workup the free acid **32** was obtained as a white solid in a yield of 96%.
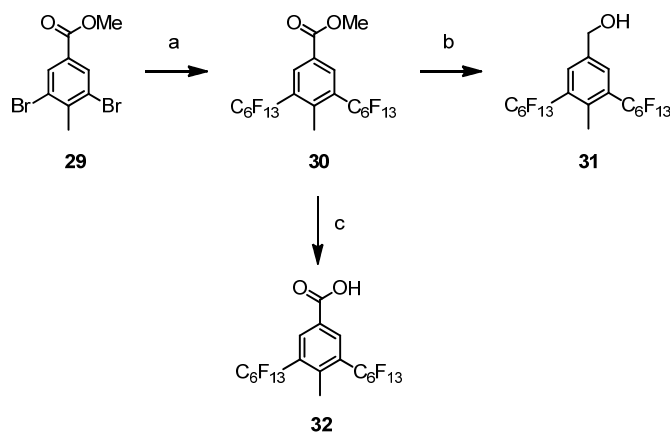
Scheme 15. Synthetic route to the alcohol **31** and the carboxylic acid **32**. *Reagents and conditions*: (a) IC$_6$F$_{13}$, Cu, DMF, 120 °C, 12 h, 91% (b) LiAlH$_4$, Et$_2$O, rt, 16 h, 90% (c) KOH, MeOH, rt, 12 h, 96%.

With the two commercially available fluorous alcohols **34** and **35**, and the synthesized alcohol **31** in hand, the malonates **26-28** were synthesized as shown in scheme 16. The alcohols were reacted with malonyl dichloride (**33**) in the presence of the organic base triethylamine in dichloromethane for 12 hours. After an aqueous workup and purification by column chromatography the fluorous malonates were isolated in 42% (**26**), 34% (**27**) and 32% (**28**) yield, respectively. As the obtained yields were rather poor, other reaction conditions were tested. However, the exchange of the base triethylamine by 4-dimethylaminopyridine (DMAP) did not improve the obtained yield (24%) in case of the malonate **28**.
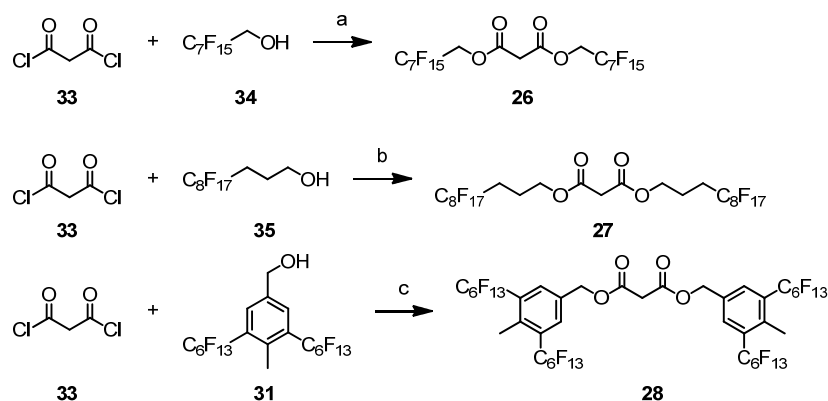
Scheme 16. Synthesis of the fluorous malonates **26-28** *Reagents and conditions*: (a) NEt$_3$, CH$_2$Cl$_2$, 0 °C → rt, 12 h, 42% (b) NEt$_3$, CH$_2$Cl$_2$, rt, 12 h, 34% (c) NEt$_3$, CH$_2$Cl$_2$, rt, 12 h, 32%.

Attempts to synthesize the fluorous fullerenes **36** and **37** are displayed in scheme 17. The monoadduct **36** was envisaged to be assembled by the reaction of C$_{60}$ (**23**), the malonate **26**, carbon tetrabromide and 1,8-diazabicyclo[5.4.0]undec-7-ene (DBU) as base in toluene. After 5 hours at room temperature and a subsequent three-phase extraction (water/toluene/perfluorohexane) it was tried to purify the crude obtained from the organic (toluene) and the fluorous (perfluorohexane) phases. However, purification by column chromatography on silica gel did not afford the desired product, instead the whole mixture stuck to the column and it was not possible to elute any product. The assembly of the hexakisadduct **37** was explored in a similar way. However, a large excess of the alcohol **27** and the base was used. Additionally, the solvent was changed from toluene to 1,2-dichlorobenzene, which should provide a higher solubility for fullerenes as compared to toluene. Also here, it was not possible to obtain the target structure or to identify the structure of the side products that were formed according to thin layer chromatography (TLC).
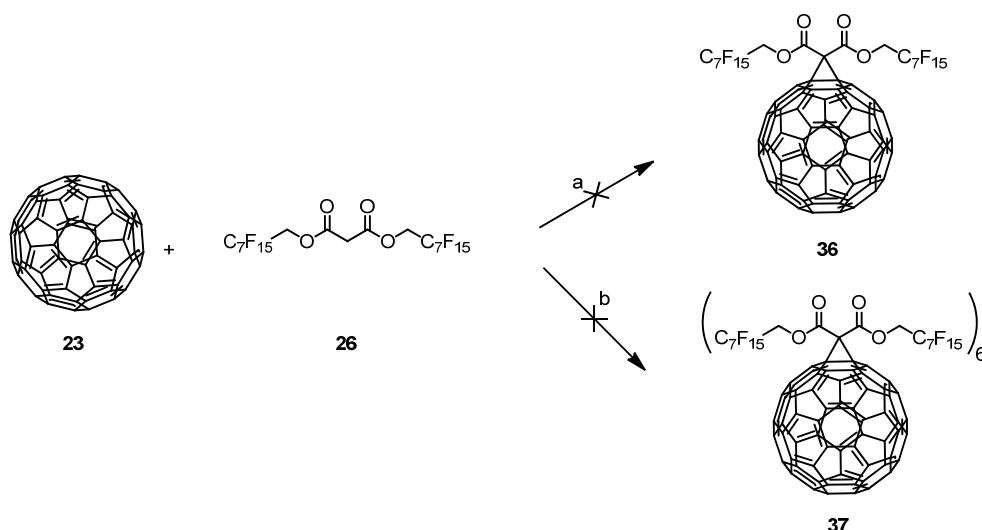
Scheme 17. Attempts to synthesize the fluorous fullerenes **36** and **37**. *Reagents and conditions*: (a) CBr$_4$, DBU, toluene, rt, 5 h (b) CBr$_4$, DBU, 1,2-dichlorobenzene, rt, 5 h.

Although it was not possible to obtain detailed information about the side reactions that took place, a possible reason for the fail of the Bingel reactions towards the fullerenes **36** and **37** could be the short insulating methylene unit between the F-alkyl chain and the ester functionality in molecule **26**. Similar problems were reported by Wilson *et al.* when using a fluorous malonate containing an ethylene spacer between the ester group and the F-alkyl chain.[124] Therefore, malonate **27** with a propylene spacer was investigated next (scheme 18). By applying reaction conditions similar to the ones described by Wilson *et al.*[124] it was possible to assemble the fluorous fullerene **38** in a yield of 14%. C$_{60}$, the malonate **27**, carbon tetrabromide and DBU were stirred at room temperature for 2.5 hours. The reaction was monitored by TLC. After a reaction time of 2 hours a third spot slowly appeared besides the two spots of the starting material **23** and the desired product **38**. According to MALDI-ToF-MS analysis this product was not, as expected, the product of a twofold Bingel reaction but an unknown side product. Thus the reaction was stopped after 2.5 hours although considerable amounts of the starting material **27** were still present in the reaction mixture. Column chromatography delivered the product **38** as brown solid in a yield of 14%. 11% of the starting material **23** was recovered as a purple solid.
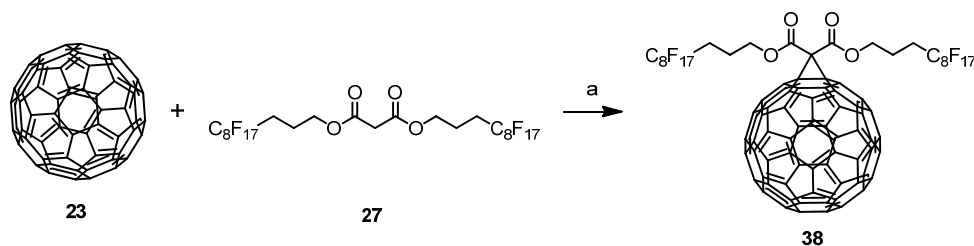
Scheme 18. Synthesis of the fluorous fullerene **38**. *Reagents and conditions*: (a) CBr$_4$, DBU, toluene, rt, 2.5 h, 14%.

Because of the low yield obtained for compound **38** and the formation of an unknown side product it was not tried to synthesize the corresponding six fold substituted fluorous fullerene. Instead the monoaddition of the malonate **28** to C$_{60}$ was envisaged (scheme 19). In this case a solvent mixture of toluene and Freon 113 (1,1,2-trichloro-1,2,2-trifluoroethane) was used as reaction medium to provide homogeneous reaction conditions. Freon 113 is an organic/fluorous hybrid solvent which is able to dissolve a wide range of common organic as well as highly fluorinated compounds. However, the reaction process was quite similar as that described for derivative **38**. Product formation was observed by TLC immediately after the start of the reaction. After a reaction time of two hours a third spot appeared which is again attributed to an unknown side product. After a reaction time of 2.75 hours the reaction was quenched with water and the crude was purified by column chromatography to afford the fluorous fullerene **39** in a yield of 13%.
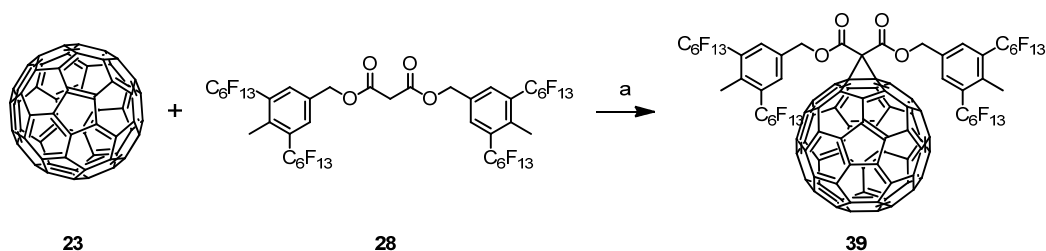
Scheme 19. Synthesis of the fluorous fullerene **39**. *Reagents and conditions*: (a) CBr$_4$, DBU, toluene, Freon 113, rt, 2.75 h, 13%.

The precursors **26-28** and the target compounds **38** and **39** were characterized by ^{1}H- and ^{19}F-NMR spectroscopy, and MALDI-ToF mass spectrometry. For the precursors also ^{13}C-NMR spectra were recorded. In the case of the fluorous fullerenes **38** and **39** the solubility was not sufficient for ^{13}C-NMR spectroscopy. The NMR spectra of compound **39** were recorded in deuterated chloroform (CDCl$_3$) whereas a mixture of CDCl$_3$ and Freon 113 was used for compound **38**. In both cases the ^{19}F-NMR spectra reveal the presence of the F-alkyl chains and the ^{1}H-NMR spectra corroborate the cyclopropanation because of the disappearance of

the proton signals for the α-position of the diester. Furthermore the MALDI-ToF spectra show the molecule ion peaks of the formed monoadducts **38** and **39**.

4.1.2 Conclusion

The pool of promising fluorous building blocks was broadened with the synthesis of the alcohol **31** and the acid **32** that are both derived from a rather cheap precursor (**29**). However, the attempts to develop large scale synthesis routes towards multiple F-alkyl functionalized fullerenes via Bingel-Hirsch reactions were not successful. Monofunctionalized fluorous fullerenes were only isolated in low yields. The formation of considerable amounts of side products and a low solubility of the reaction products make this approach unsuitable as strategy for the assembly of model compounds for QIE.

4.2   Fluorous Porphyrins – Monodisperse Compounds

As fluorous fullerene derivatives (section 4.1) did not open the window to QIE in new mass regions we moved our focus to fluorous porphyrins. The heterocyclic macrocycle of porphyrins is present in numerous naturally occurring compounds. A very important structural motif is the heme group, an iron porphyrin derivative, which can be found in many proteins, including hemoglobin, myoglobin and cytochrome P450 enzymes.[131] Also porphyrin derivatives were already successfully applied in matter-wave interferometry. In a first study with tetraphenylporphyrin (**TPP**) in a near-field TLI containing an electron impact (EI) – QMS detection scheme[34] the good detectability features when using such a mass spectrometric detection unit were noticed. Furthermore, porphyrins proved to be suitable candidates for the application in interferometer setups with detection units that are based on fluorescence microscopy as demonstrated by Stibor *et al.*.[35] Additionally, porphyrin derivatives were investigated in metrological interferometry studies.[132][133] Because of the promising stability, volatility and detectability features of **TPP** we proposed to assemble **TPP** derived highly fluorinated compounds.

4.2.1   Molecular Design

In earlier studies, perfluoroalkyl substituted tetraarylporphyrins were achieved by the arrangement of the porphyrin framework using fluorinated starting materials.[134][135] An alternative approach is the derivatization of functionalized tetraarylporphyrins either by linking perfluoroalkylated carboxylic acids to amino-functionalized **TPP** via an amide bond[136] or by the formation of ether bonds starting from hydroxy-functionalized **TPP** and fluorous benzyl bromides.[137] In order to prepare a variety of molecular weights, a modular approach to peripherally functionalized **TPP**s was particular appealing. We considered the fluorinated derivative tetrakis(pentafluorophenyl)porphyrin (**TPPF20**) as an ideal starting point for a modular synthesis that is geared towards derivatives with many peripheral fluorous chains because the four *para*-fluorine atoms can easily be substituted by various nucleophiles.[138] The nucleophilic aromatic substitution reactions of the *para*-fluorine substituents in pentafluorophenyl moieties is not limited to porphyrin systems.[139]–[141] The first example for the fourfold substitution reaction of **TPPF20** with a nucleophile was reported by Kadish *et al.*.[142] Examples with non-fluorous alcohols,[143]–[146] amines,[143][144][147]–[149] or thiols[143][150]–[152] as well as the introduction of fluorous nucleophiles, namely alcohols[153] and thiols,[154][155] are also known.

In our work we planned to synthesize and investigate four-fold functionalized porphyrins coated with a fluorous shell. As shown in scheme 20, a wide variety of different fluorous peripheries were envisaged. The aim was to cover a specific mass range and to optimize the design of the structures towards high volatility by varying the structural motifs of the fluorous part. The amount of fluorous chains in the target structure ranges from four in the linear approach over eight (1st generation branched) to 16 (2nd generation branched). To the best of our knowledge, there is only one example of a fluorous porphyrin derivative that bears more than 16 fluorinated ponytails (24 chains) from Bříza *et al*..[153] The length of the perfluoroalkyl parts was also varied. Perfluorohexyl and perfluorooctyl chains were proposed. Although F-alkyl chains with a length of up to 12 perfluorinated carbons are also commercially available, these are expected to decrease the solubility drastically and therefore to prevent syntheses and purification steps in common organic solvents. In order to investigate correlations between the molecular structure and the thermal stability of the compounds, the nature of the interlinking between the parent tetraarylporphyrin and the fluorous substituents was varied by introducing different hetero atoms as the linkage. Although the *para*-fluorine substitution with alcohols as nucleophiles is also known exclusively thiols and amines were envisaged, because they usually deliver the substitution products in high yields.[139] The *para*-fluorine substitution reaction with thiols was even categorized as click reaction because of the high yields and the mild reaction conditions observed for this reaction type.[139] Furthermore, the branching unit was varied. The branching occurs either in an aliphatic segment or in 1,3,5-trisubstituted benzene units.
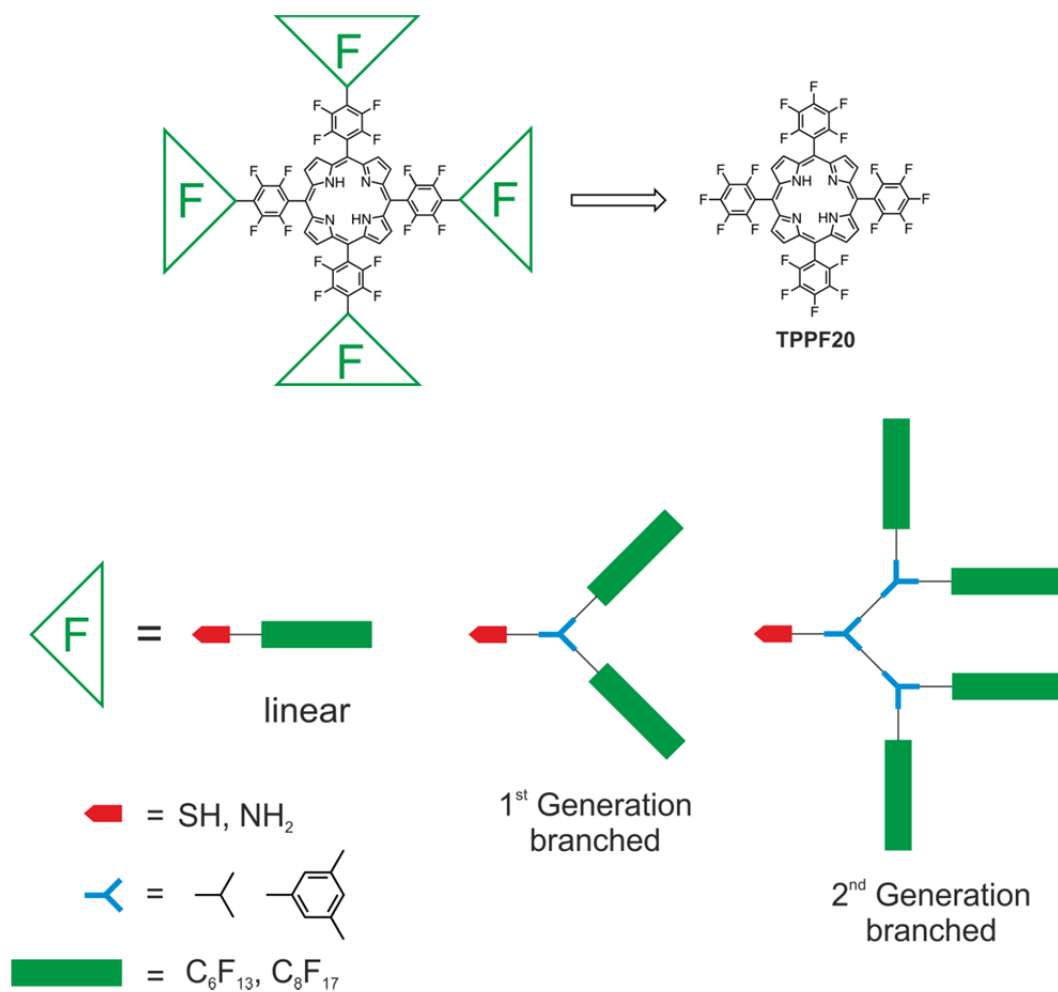
Scheme 20. Concept of the functionalization of **TPPF20** with a fluorous shell.

The nine proposed target structures **40-48** are depicted in figure 33. The series covers a molecular weight range from 2 803 g/mol (**41**) to 7 682 g/mol (**47**) and contains two amine derived structures and seven thiol based fluorous porphyrin derivatives.
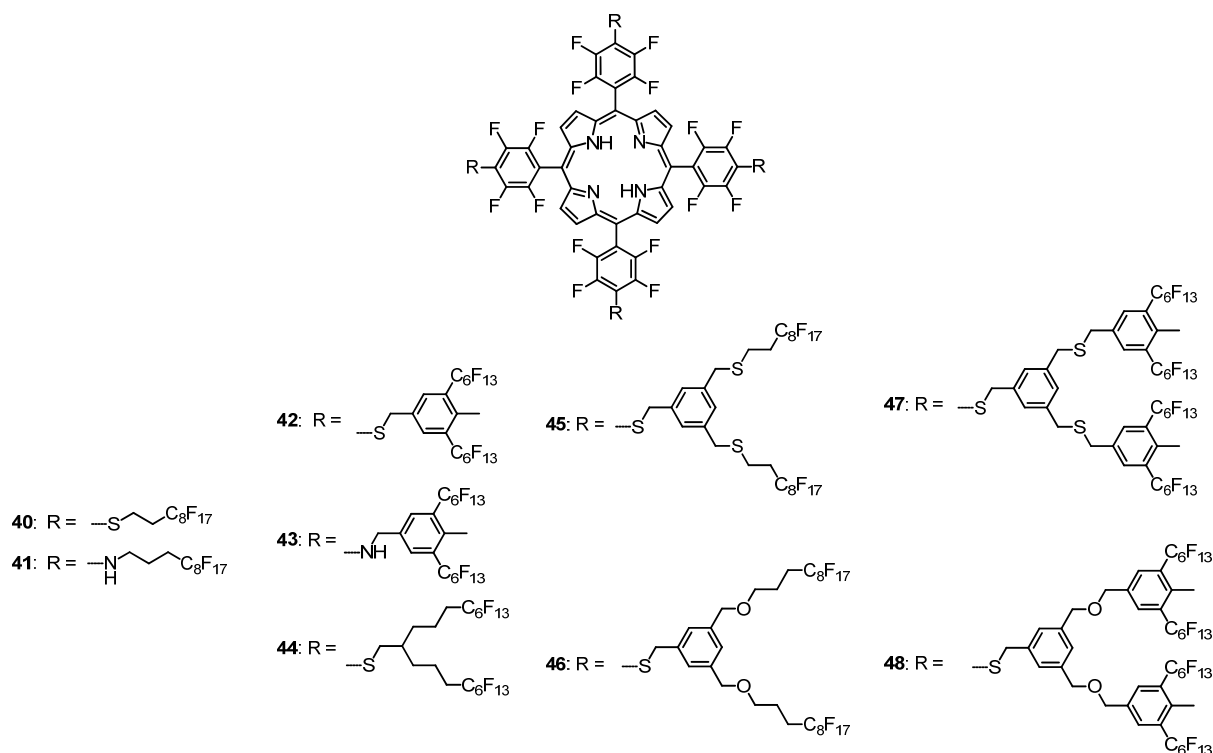
Figure 33. Highly fluorous porphyrin derivatives **40-48**.

4.2.2 Synthetic strategy

In order to be able to explore a large diversity of different designs of the fluorous periphery, a modular synthetic concept was pursued. As depicted in scheme 21, the fluorous outer parts of the porphyrin derivatives were introduced in the last step of the reaction pathway allowing for easy modification of these moieties. The key step on the way towards all nine target structures is the nucleophilic aromatic substitution reaction to introduce the fluorous building blocks. Both thiols and primary amines as nucleophiles usually give substitution products in good to excellent yields.[139] Commercially available fluorinated nucleophiles can be used for the synthesis of the porphyrins **40** and **41** allowing us to improve the reaction conditions with purchased starting materials. In all other cases the building blocks were synthesized prior to their attachment to the porphyrin centre.

The synthesis of the building blocks **49** and **50** starts with the attachment of two F-alkyl chains to the dibromide **29**. Classical functional group transformation provides access to the thiol **49** and the amine **50**. It was anticipated that the thiol **51** can be assembled from the triflate **58**, which is known to be accessible in five steps starting from the fluorous iodide **57** and diethyl malonate (**56**).[156] The starting point for the synthesis of building blocks **52** and **53** is the tribromide **59**. Monothiolation, introduction of the fluorous ponytails in a S_N2

reaction with either a fluorous alcohol or thiol and the deprotection step represent the pathway to building blocks **52** and **53**. In the reaction sequence towards the thiols **54** and **55**, alcohol **31** and thiol **49**, respectively, as fluorous part were planned to be attached to the dibromide **60**, the central unit of these two building blocks.
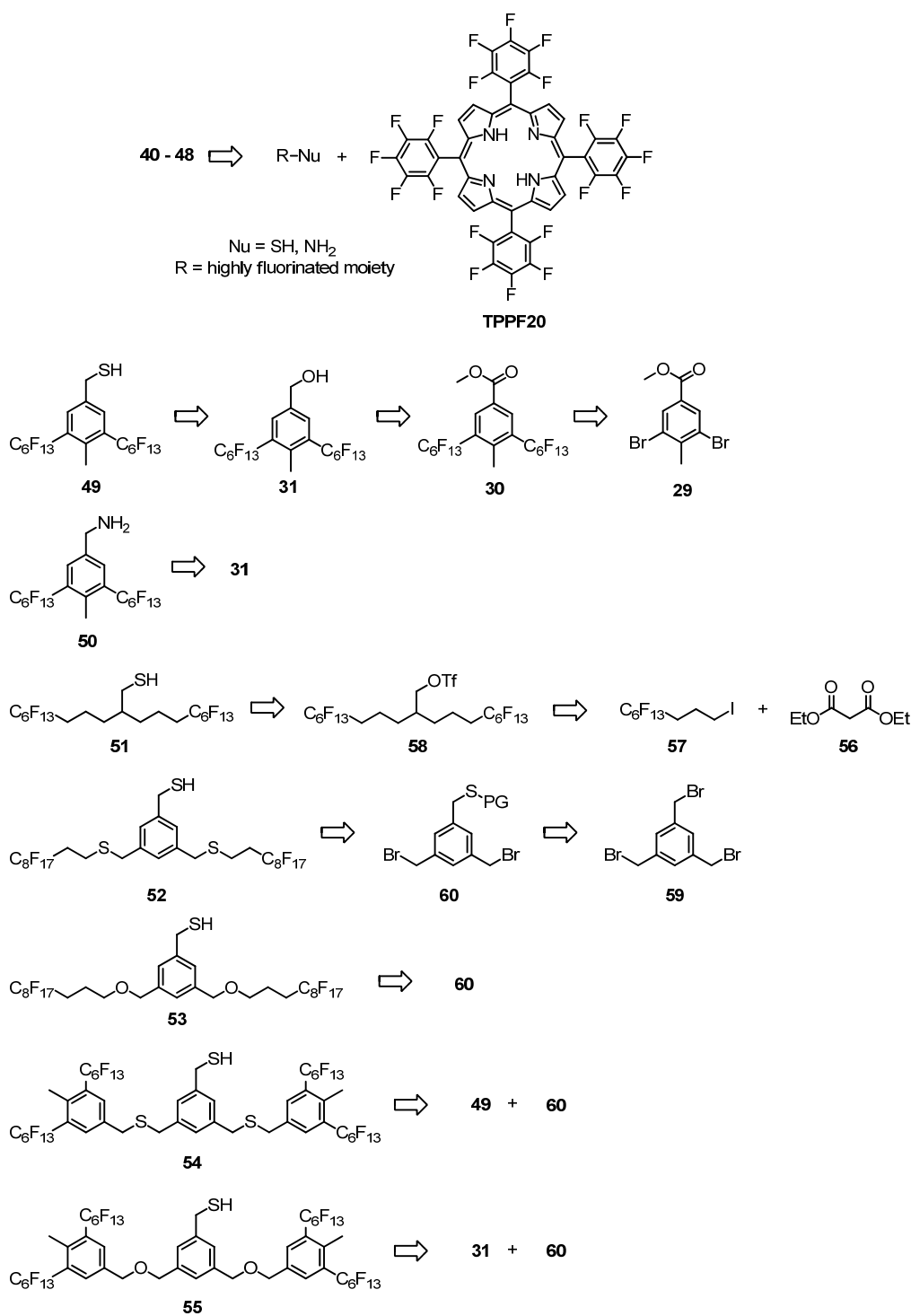
Scheme 21. Synthetic strategy towards the target compounds **40-48**. A nucleophilic aromatic substitution reaction is the key step to the desired porphyrin derivatives. The first step towards the thiols **52-55** is the introduction of the sulfur functionality bearing a protecting group (PG) to the tribromide **59**.

4.2.3 Synthesis and Characterization

The two building blocks **49** and **50** comprise two perfluorohexyl chains that are directly attached to the aromatic core. The reaction conditions for the introduction of these chains and the subsequent reduction to the benzylic alcohol **31** were already described in section 4.1.1. The fluorous ponytails were introduced in a copper-mediated cross-coupling reaction of *n*-perfluorohexyliodide and the dibromide **29** to afford the ester **30** in a yield of 91%. The reduction of the ester **30** using lithium aluminum hydride (LiAlH₄) led to the benzylic alcohol **31** in 90% yield.

The conversion of the alcohol to a thiol functionality was achieved in two steps and is shown in scheme 22. In order to convert the benzylic alcohol **31** to the corresponding benzylic thioacetate a modification[157] of the Mitsunobu reaction[158] was performed. A mixture of alcohol **31** and thioacetic acid in tetrahydrofuran (THF) was treated with a solution containing the preformed adduct of triphenylphosphine and diisopropyl azodicarboxylate (DIAD). The pure acetylsulfanyl derivative **61** was obtained after column chromatography as a colorless oil in a yield of 61%. The formation of the betaine derived from triphenylphosphine and DIAD prior to the addition of the alcohol and thioacetic acid is crucial for the formation of the product. When using the common Mitsunobu procedure, which is the slow addition of the azodicarboxylate to a solution of the alcohol, the nucleophile, and triphenylphosphine in THF, yields of only 5-10% were obtained.
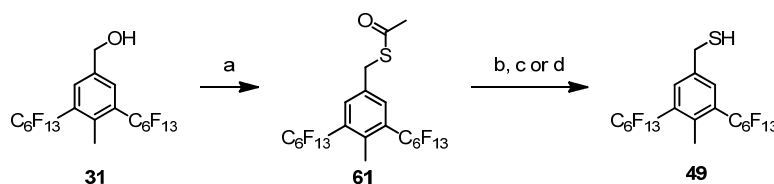
Scheme 22. Preparation of the fluorous thiol **49**. *Reagents and conditions*: (a) DIAD, PPh₃,THF, 0 °C, 2 h, then **31**, thioacetic acid, 0 °C to rt, 3 h, 61%; (b) LiAlH₄, Et₂O, 12 h, traces of product; (c) K₂CO₃, MeOH, THF, rt, 20 min, 59%; (d) acetyl chloride, MeOH, CH₂Cl₂, rt, 5 h, 72%.

The final step towards building block **49** was the removal of the acetyl protection group of the sulfur to obtain the free thiol **49**. The thioacetate was treated with LiAlH₄ in diethylether at room temperature for 12 hours. However, only traces of the product were isolated, instead large amounts of the corresponding disulfide were formed. In a second attempt the deprotection was performed under basic conditions. Thioacetate **61** was added to a mixture of THF, methanol and potassium carbonate. After a reaction time of 20 minutes the reaction mixture was quenched with aqueous hydrochloric acid. After purification by column chromatography the thiol **49** was isolated in a yield of 59%. A further improvement of the

yield was obtained by an acidic cleavage of the protecting group, which was realized by the *in situ* generation of hydrochloric acid. The addition of acetyl chloride to a solution of thioacetate **61** in a solvent mixture of methanol and dichloromethane (CH_2Cl_2) led to the formation of the desired product. After a reaction time of five hours the crude product was purified by column chromatography to afford **49** as a white solid in a yield of 72%.

Scheme 23 displays the synthesis of the benzylic amine **50**. Initially it was tried to assemble the amine **50** in a two step synthesis via the benzylic bromide **62**. However, the treatment of the benzylic alcohol **31** with phosphorous tribromide, a standard reagent for the conversion of alkyl alcohols into the corresponding bromides, in dichloromethane at room temperature did not show any conversion as judged by TLC. Thus, for the synthesis of the benzylic amine **50** the same strategy as for the benzylic thiol **49** was envisaged. The nitrogen was - identical to the sulfur of building block **49** – introduced in a Mitsunobu reaction.[158] DIAD was slowly added to a solution of alcohol **31**, triphenylphosphine and phthalimide in THF at -5 °C. The reaction mixture was stirred at room temperature for 12 hours. An aqueous workup and purification by column chromatography afforded the desired phthalimide derivative **63** as a white solid in a yield of 87%. Cleavage of the *N*-benzylphthalimide was achieved with the help of the Ing-Manske procedure.[159] The benzylic amine was obtained by the hydrolysis of compound **63** with hydrazine in a solvent mixture of ethanol and toluene. After 12 hours at reflux and an aqueous workup the free benzylic amine **50** was isolated as a white solid in quantitative yield with no need for further purification.
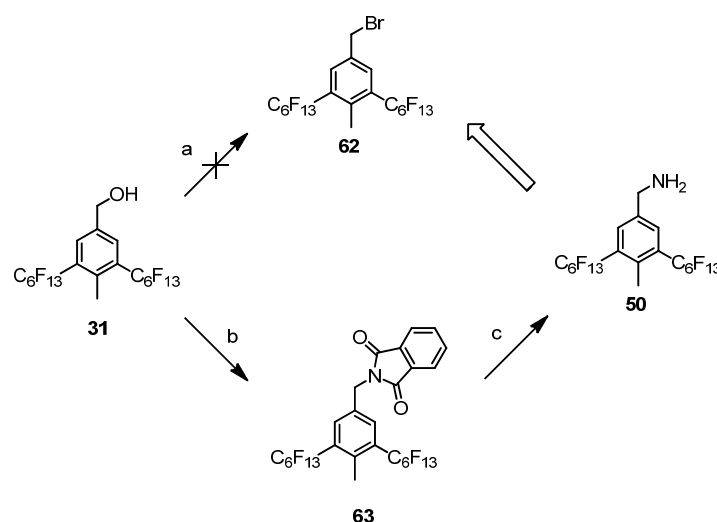
Scheme 23. Synthesis of the fluorous amine **50**. *Reagents and conditions*: (a) PBr$_3$, CH$_2$Cl$_2$, rt, 4 h; (b) phthalimide, DIAD, PPh$_3$,THF, -5 °C to rt, 12 h, 87%; (c) hydrazine hydrate, EtOH, toluene, reflux, 12 h, quant.

The alkyl thiol **51** was synthesized in seven steps. Starting from 3-(perfluorohexyl)propyl iodide (**57**) and diethyl malonate (**56**), the triflate **58** was assembled in five steps according to a literature procedure.[156] The propylene spacer in compound **57** was chosen to guarantee a high reactivity in the S_N2 reaction. Fluorous iodides with shorter alkyl spacers become progressively less reactive.[70][160][161] The literature protocol yielded the triflate **58** in a high overall yield of 84% over the five steps including only two purification steps (scheme 24). In a first step a twofold substitution reaction in the α-position of diethyl malonate (**56**) was performed. Treatment of the malonate with sodium hydride as base in DMF at room temperature for 1 hour followed by the addition of 3-(perfluorohexyl)propyl iodide (**57**) and stirring at 80 °C for 12 hours yielded the fluorous malonate **64** quantitatively. A basic ester hydrolysis with potassium hydroxide in a solvent mixture of water and ethanol led after acidification to the formation of the diacid **65**. Purification by recrystallization afforded pure diacid **65** as a yellow solid in a yield of 88%. Subsequently a pyrolysis was performed by heating the diacid **65** to 190 °C for 45 minutes. The decarboxylated monoacid **66** was obtained as a yellow solid in a yield of 99%. The reduction of the acid **66** to the alcohol **67** was achieved by reaction with borane-THF complex in THF at reflux for 16 hours. The alcohol **67** was obtained after aqueous workup as a white solid in a quantitative yield. The conversion to the triflate **58** was accomplished by treating the alcohol **67** with trifluoromethanesulfonic acid anhydride in the presence of pyridine in dichloromethane at low temperatures. Purification by column chromatography afforded the triflate **58** as colorless oil in a yield of 96%.
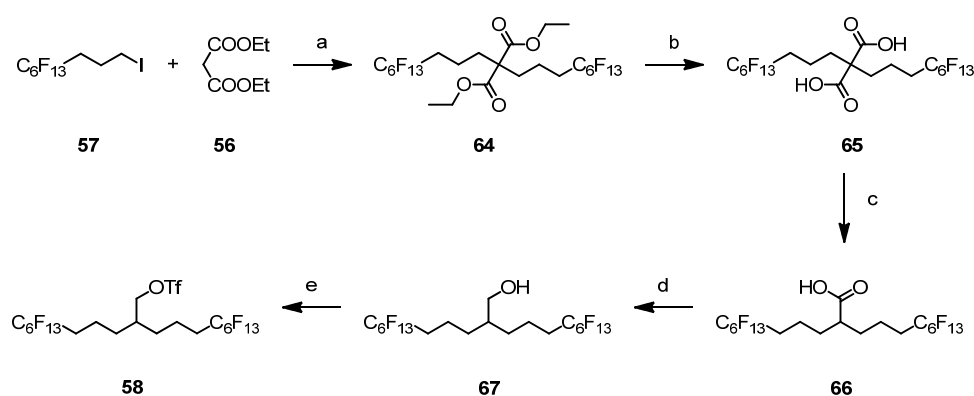
Scheme 24. Synthesis of the fluorous triflate **58**. *Reagents and conditions*: (a) NaH, DMF, rt, 1 h → reflux, 12 h, quant.; (b) KOH, EtOH, 80 °C, 12 h, 88%; (c) 190 °C, 45 min, 99%; (d) BH$_3$·THF, THF, reflux, 16 h, quant.; (e) Tf$_2$O, pyridine, CH$_2$Cl$_2$, -15 °C → rt, 15 min, 96%.

With the triflate in hand the sulfur was efficiently introduced as a trityl protected functionality by the reaction of the triflate **58** with trityl thiol and an excess of sodium hydride stirred in THF at room temperature for two hours (scheme 25). Purification by column chromatography

led to the desired compound **68** as a colorless oil in a yield of 95%. By following a procedure developed by Moreau *et al.* the trityl protection group was removed under acidic conditions in the presence of a cation scavenger.[162] Trifluoroacetic acid (TFA) was added to a solution of the protected thiol **68** and 1.5 equivalents of triethylsilane in CH_2Cl_2. The deprotection reaction is fast even at low acid concentrations (4 vol.-% related to the amount of CH_2Cl_2). After stirring for 25 minutes at room temperature and an aqueous workup, the free thiol **51** was obtained after column chromatography as a white solid in a yield of 88%. In summary, the thiol **51**, which comprises two perfluorohexyl chains and an alkyl based branching unit was synthesized in a multigram scale in seven steps with a high overall yield of 70%.
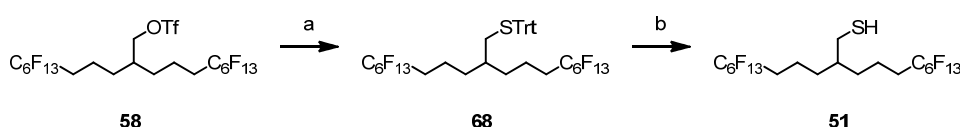
Scheme 25. Synthesis of the fluorous thiol **51**. *Reagents and conditions*: (a) trityl thiol, NaH, THF, rt, 2 h, 95%; (b) HSiEt₃, TFA, CH_2Cl_2, rt, 25 min, 88%.

The branched thiol building blocks **52** and **53** were synthesized in three reaction steps (scheme 26). A reaction sequence including mono-functionalization of tris(bromomethyl)-benzene (**59**) with a protected thiol, introduction of two fluorous ponytails and a final deprotection of the thiol functionality yielded the desired fluorous thiols suitable for the envisaged substitution reaction.
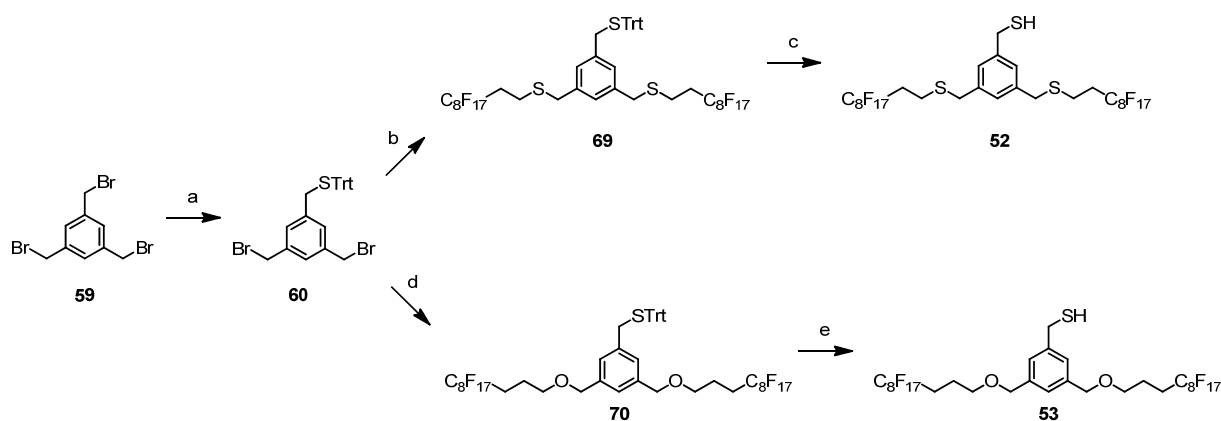
Scheme 26. Synthesis of the thiols **52** and **53**. *Reagents and conditions:* (a) trityl thiol, K₂CO₃, THF, reflux, 20 h, 33%; (b) HS(CH₂)₂C₈F₁₇ (**71**), Na₂CO₃, DMF, microwave irradiation, 150 °C, 20 min, 82%; (c) HSiEt₃, TFA, CH_2Cl_2, rt, 5 min, 83%; (d) HO(CH₂)₃C₈F₁₇ (**72**), NaH, THF, reflux, 4 h, 52%; (e) HSiEt₃, TFA, CH_2Cl_2, rt, 1 h, 77%.

The trityl protected thiol derivative **60** was assembled by the reaction of the tribromide **59** with one equivalent of trityl thiol in the presence of potassium carbonate as base in THF at

reflux for 20 hours. An aqueous workup and purification by column chromatography afforded compound **60** as a white solid in a yield of 33%. In contrast to all other precursors described in this section, compound **60** is not stable upon storage at room temperature over several weeks. Probably a nucleophilic attack of the sulfur moiety to the remaining bromines causes the degradation to the products shown in scheme 27. This phenomenon was already observed for a similar compound by Peterle.[163] He describes in his dissertation the degradation of compound **73** comprising a benzylic methyl sulfide and a benzylic bromide functionality, however, on a much shorter time scale. The degradation of compound **73** occurs within several hours. The increased stability of the trityl protected compound **60** as compared to the methyl sulfide **73** can be explained by the steric shielding of the sulfur functionality by the trityl group. When stored at 4 °C compound **60** is stable over months.
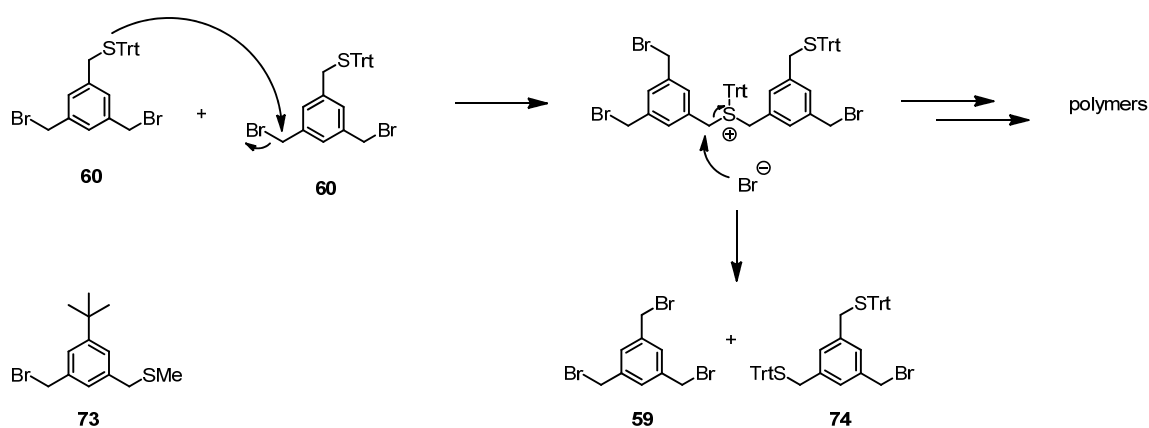
Scheme 27. Hypothesized mechanism of the degradation of compound **60** upon storage at room temperature over several weeks. No degradation is observed when stored at 4 °C.

With the monofunctionalized compound **60** in hand the introduction of the fluorous ponytails was performed. For the nucleophilic substitution reaction with the fluorous thiol microwave heating was applied. Dibromide **60** was heated together with 3 equivalents of the fluorous thiol **71** and sodium carbonate as base in DMF in a microwave apparatus to 150 °C for 20 minutes. After an aqueous workup compound **69** was purified by column chromatography to afford pure **69** as a pale yellow solid in a yield of 82%. A final deprotection step led to the highly fluorous benzylic thiol **52**. Identical trityl deprotection conditions as described above for the alkyl based thiol **51** were used to obtain pure thiol **52** after column chromatography as a white solid in a yield of 83%.

3-Perfluorooctylpropanol (**72**) as fluorous part was attached to the dibromide **60** by using harsher conditions as compared to the fluorous thiol (**71**). Generation of an alcoholate by the addition of the alcohol to a suspension of sodium hydride in THF and a subsequent S$_N$2

reaction of the alcoholate and the dibromide **60** led to the highly fluorinated trityl-protected thiol **70**. The desired product was isolated in a yield of 52% after purification by column chromatography. The final deprotection was achieved in an analogous manner as described for the trityl derivative **69** leading to thiol **53**. Purification by column chromatography afforded pure thiol **53** as a white solid in a yield of 77%.

For the second generation of branched fluorous building blocks the same strategy as in the first generation was pursued (scheme 28). The reaction of the dibromide **60** with the thiol **49** in the presence of sodium carbonate as base under microwave irradiation in DMF led to compound **75** which was isolated as a white solid in a yield of 74%. However, the deprotection of building block **75** to the free thiol **54** was not performed for reasons that are discussed later.

For the alcohol **31** as fluorous part the treatment with sodium hydride in THF at reflux was applied. Compound **76** was isolated in a yield of 67% after purification by column chromatography. The final acidic deprotection using TFA and triethylsilane in dichloromethane afforded pure thiol **55** as a white solid in a yield of 72%.
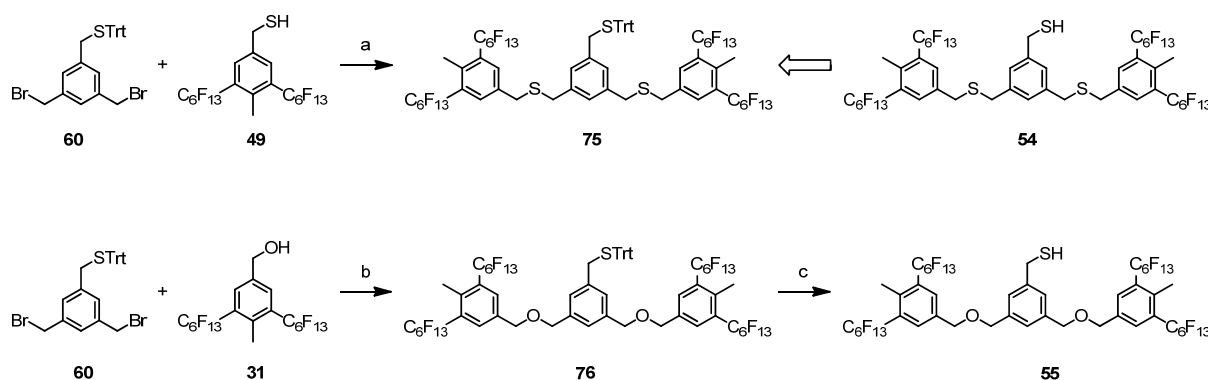
Scheme 28. Synthesis of the thiols **54** and **55**. *Reagents and conditions:* (a) Na_2CO_3, DMF, microwave irradiation, 150 °C, 20 min, 74%; (b) NaH, THF, reflux, 4 h, 67%; (c) $HSiEt_3$, TFA, CH_2Cl_2, rt, 20 min, 72%.

All precursors were characterized by NMR spectroscopy (^{1}H, ^{13}C and ^{19}F), mass spectrometry and elemental analysis. With the thiol dendrons **49**, **51-53** and **55** in hand the envisaged target porphyrins comprising several peripheral fluorous ponytails became accessible. Table 1 gives an overview of the nucleophilic aromatic substitution reactions carried out to assemble the target structures **40**, **42**, **44-46** and **48**. The five sulfur substituted porphyrin derivatives were synthesized in a similar way as described by Samaroo *et al.* in the substitution reaction of **TPPF20** with 1*H*,1*H*,2*H*,2*H*-perfluorododecane-1-thiol. In their protocol the porphyrin and
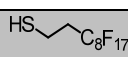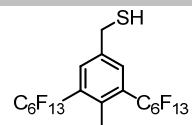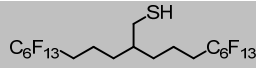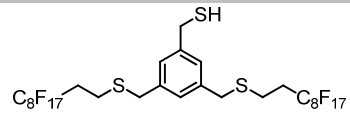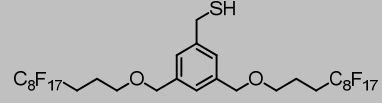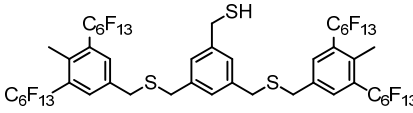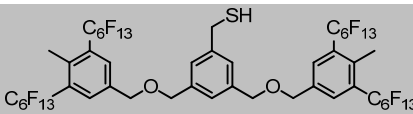
the thiol are treated at room temperature in a mixture of ethyl acetate and DMF with a dialkylamine derivative as base.[154][155]

In the cases of the target products **40**, **42**, **44** and **45** (entries 1-4) a solution of **TPPF20** in DMF was added to a solution of 6-10 equivalents of the thiol (**49**, **51**, **52** or **71**) and diethyl amine in a mixture of ethyl acetate and DMF. Stirring at room temperature for 1 to 4 hours was followed by quenching with water. After extraction with diethylether and a subsequent wash with brine, purification by column chromatography was performed. For the porphyrin derivative **40** recrystallization from acetone or precipitation from an ethanol/acetone mixture were also successfully applied as alternative purification procedures.

The three thiol based target compounds **40**, **42** and **44** were isolated as intensely purple colored solids. The yield obtained for derivative **40** bearing four perfluorooctyl moieties was 81%. Compound **42** with eight perfluorohexyl chains was isolated in a yield of 89%. Derivative **44**, having eight perfluorooctyl parts in its periphery, afforded a yield of 70%. In the case of porphyrin **45** (entry 4) the product formation was confirmed by MALDI-ToF-MS and NMR analyses and of the crude. However, this compound was not stable and degraded on the time scale of some hours. The degradation was accompanied by a color change from purple to dark brown. Furthermore, the solubility of the crude in acetone dropped from good solubility directly after the aqueous workup to completely insoluble within one day. After 24 hours it was no longer possible to detect the molecule ion signal in MALDI-ToF mass spectrometry. We hypothesized that the benzylic thioether moieties could be the origin of the instability and thus we went on with the dendrons having benzylic ethers as structural motifs. For this reason the synthetic efforts towards the porphyrin **47**, the heaviest derivative in our series, were stopped. The large number of benzylic thioether moieties would presumably cause similar stability problems as observed for porphyrin **45**.

The target compounds **46** and **48** were synthesized by using similar conditions as described above (table 1, entries 5 and 7). Remarkably, both derivatives did not show any signs of instability, corroborating the hypothesis that the benzylic thioether units were responsible for the degradation of compound **45**. Porphyrin **46** with eight and derivative **48** with 16 perfluorohexyl chains were obtained in yields of 64% and 31%, respectively.

Table 1. *Para*-fluoro-thiol substitution reactions towards the target compounds **40**, **42** and **44-48**.
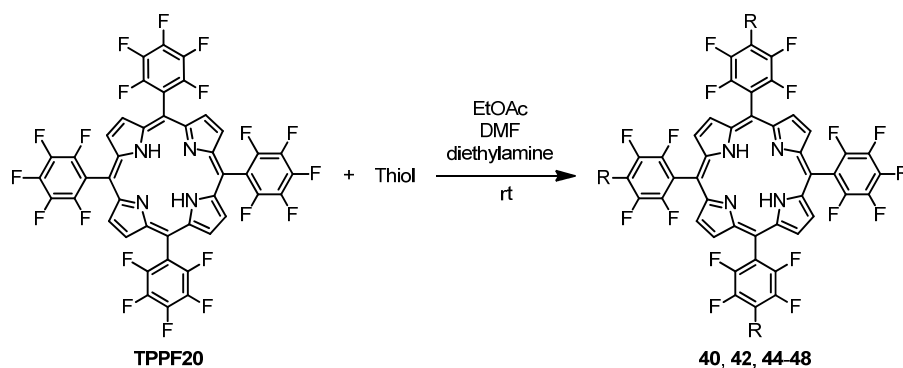
Entry		Thiol (R-H)	Eq.	Reaction time [h]	Yield (%)	Product
1	**71**		10	1.5	81	**40**
2	**49**		6	1	89	**42**
3	**51**		10	4	70	**44**
4	**52**		6	2.5	product unstable	**45**
5	**53**		8	3.5	64	**46**
6	**54**			reaction not performed		**47**
7	**55**		8	6.5	31	**48**

For the substitution of the *para*-fluoro groups by the amines **77** and **50** a slightly modified general method for the reaction of primary amines and **TPPF20** developed by Samaroo *et al.*[164] was applied (scheme 29). They used microwave irradiation and *N*-methyl-pyrrolidone (NMP) as solvent. A mixture of **TPPF20** and ten equivalents of the amine (**50** or **77**) in NMP was heated in a microwave apparatus at 250 °C for two hours. The reaction time was optimized by checking the conversion after several reaction times (3, 20, 90 and 120 minutes) by TLC. Quenching with water and an extraction with diethylether yielded the crude product

which was purified by column chromatography. Porphyrin derivatives **41** and **43** were obtained as intensely purple colored solids in yields of 75% and 50%, respectively.
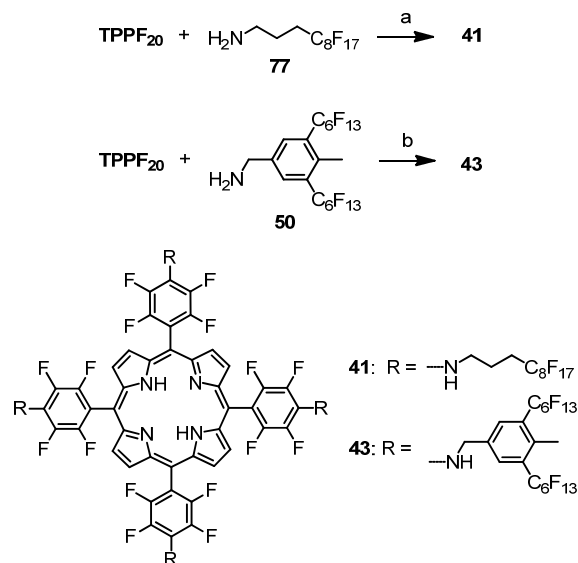
Scheme 29. Synthesis of the target compounds **41** and **43**. *Reagents and conditions*: a) NMP, microwave irradiation, 250 °C, 2 h, 75%; b) NMP, microwave irradiation, 250 °C, 2 h, 50%.

The purity of the porphyrin derivatives **40-44** and **46** was monitored by analytical HPLC on a fluorous column (FluoroFlash). These columns are packed with perfluorooctyl functionalized silica gel as stationary phase (see figure 34C). Therefore the retention time of analytes is primarily determined by their fluorine content.[75] In figure 34A the chromatograms of the derivatives **40-44** and **46** are shown. The integrals of the main peaks are between 97.0% and 97.6%. The retention times of these compounds are strongly dominated by the nature of the fluorous part of the molecules. The porphyrins **40** and **41** with each four perfluorohexyl chains are eluted after less than two minutes. The derivatives having eight perfluorohexyl ponytails have similar retention times of around 7 minutes and porphyrin **46** with eight perfluorooctyl chains exhibits strong interactions with the stationary phase leading to a retention time of 21.7 minutes.
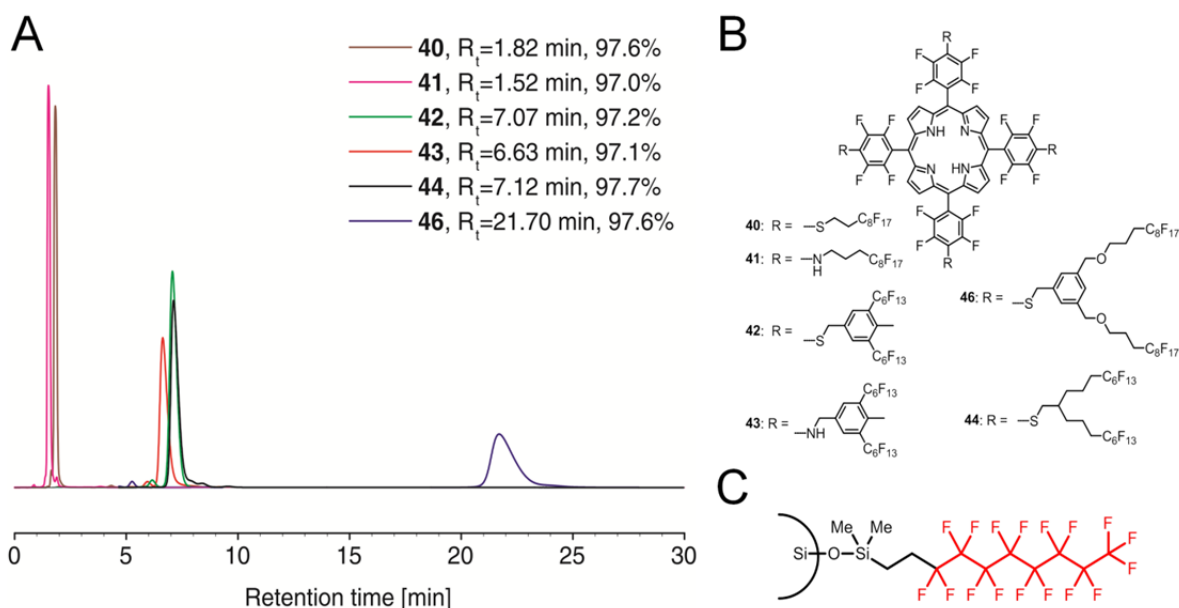
Figure 34. (A) Overlaid HPLC chromatograms of porphyrin derivatives **40-44** and **46**. Stationary phase: FluoroFlash HPLC column (4.6 mm i.d., 50 mm length, 5 μm); mobile phase: tetrahydrofuran (100%); flow rate: 1.4 mL/min; column temperature: 50 °C. (B) Structure of the analyzed fluorous porphyrins. (C) Structure of the stationary phase of the FluoroFlash HPLC column that was used for the analysis.

Fluorous HPLC is an ideal tool for the analysis of the porphyrins **40-44** and **46** as the side products of the nucleophilic aromatic substitution reactions, mainly three- or fivefold substituted derivatives, can be easily distinguished due to their varying fluorine content. For example, the retention times of porphyrin **44** and the major side product of the final reaction step, which is the threefold substituted derivative, are 7.50 minutes for the product and 2.58 minutes for the impurity on a FluoroFlash column (50 mm, 1.4 mL/min, 100% THF, 50 °C). A comparison of the chromatograms of **1** and **5**, and their corresponding side products **1**$_{fivefold}$ and **5**$_{threefold}$ is displayed in figure 35.
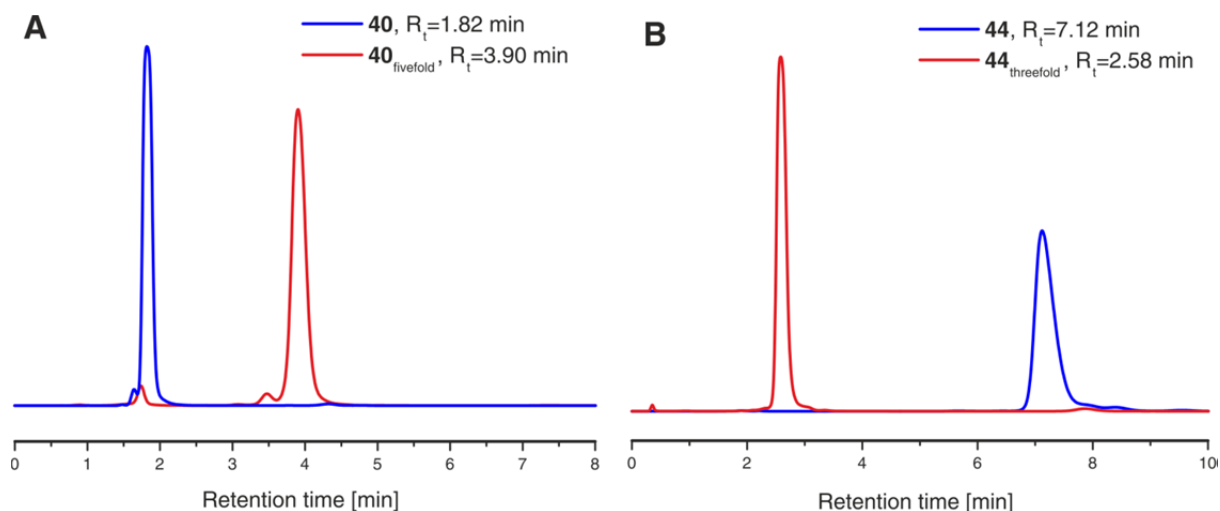
Figure 35. Overlaid HPLC chromatograms of the target porphyrin derivatives **40** and **44** and their major side products. Stationary phase: *FluoroFlash* HPLC column (4.6 mm i.d., 50 mm length, 5 μm); mobile phase: tetrahydrofuran (100%); flow rate: 1.4 mL/min; column temperature: 50 °C. (A) Overlaid HPLC chromatograms of porphyrin derivative 40 and the fivefold substituted side product **40**fivefold. (B) Overlaid HPLC chromatograms of porphyrin derivative **44** and the threefold substituted side product **44**threefold.

However, porphyrin **48** was not eluted under the conditions we tested, although THF is known to be the most powerful eluent in the class of common organic non-fluorous solvents in fluorous HPLC applications. Even a flow rate of 3 mL/min did not lead to the elution of porphyrin **48** within 90 minutes. We hypothesize that the interactions between the stationary phase and porphyrin **48** bearing 16 perfluorohexyl chains are too strong and thus prevent elution. The purity of this derivative can be seen in the chromatogram of the recycling gel permeation chromatography (GPC) that was used to purify this compound. The signal was detected with a UV/Vis detector at 415 nm. The baseline separated peaks of **48** and the side product **48**threefold were collected during the last two of 34 cycles. In figure 36A the complete chromatogram is shown and figure 36B displays a zoom on the last two cycles.
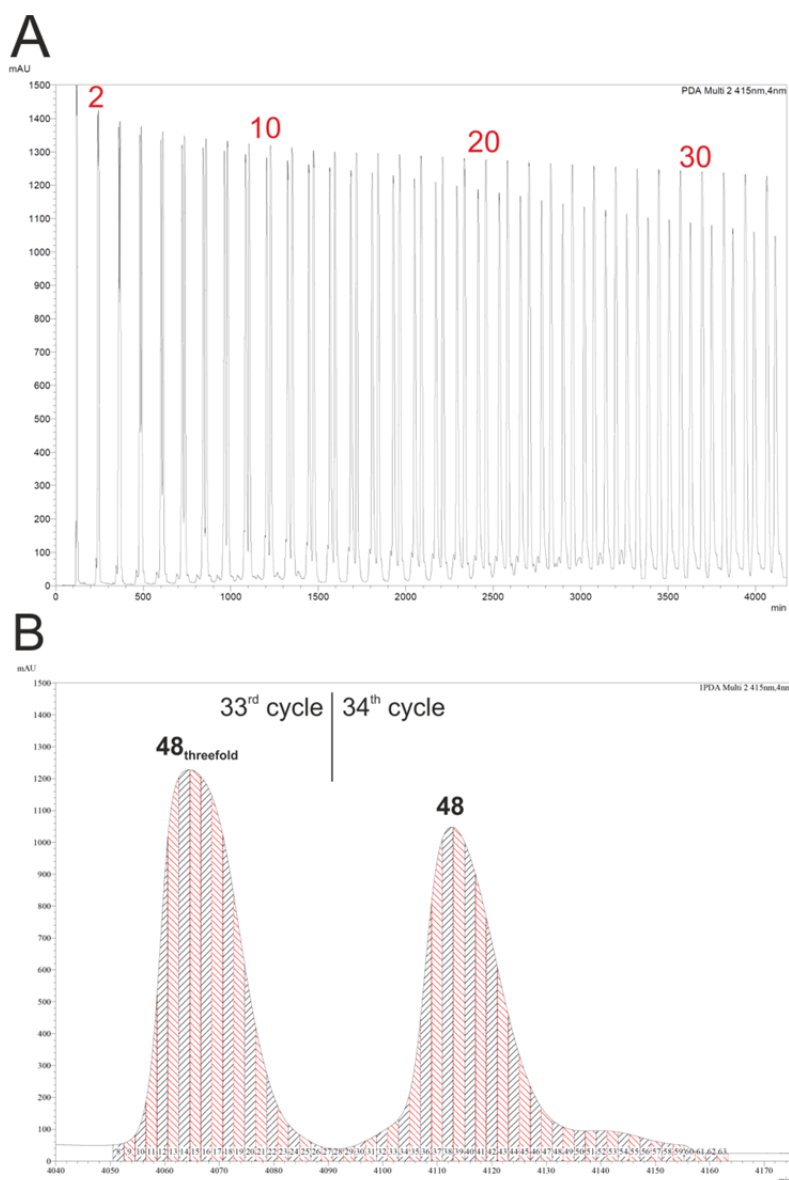
Figure 36. (A) Recycling gel permeation chromatogram of derivative **48**. Stationary phase: *PSS SDV* preparative columns (2 columns in series: 600 mm x 20.0 mm, 5 μm, linear porosity "S", operating ranges: 100 – 100 000 g mol^{-1}); mobile phase: chloroform (100%); flow rate: 2.0 mL/min. (B) Last two cycles of the recycling gel permeation chromatogram of derivative **48**.

Furthermore, the porphyrins were characterized by NMR spectroscopy (^{1}H and ^{19}F), mass spectrometry (MALDI-ToF) and UV/Vis spectroscopy. The mass spectra of all target compounds show exclusively the molecule ion peak M$^+$. The absence of the peak for the three- and fivefold substituted porphyrins corroborates that only the desired fourfold substituted derivatives were isolated. Note that the MALDI-ToF mass spectra of the target compounds were recorded in their neat form without additional matrices. It is known that porphyrin derivatives can serve as their own matrices.[165] From the rather simple ^{19}F- and ^{1}H-NMR spectra it is furthermore evident that the four substituents are attached exclusively in the *para*-positions of the four fluorinated phenyl rings leading to highly symmetrical structures.

As exemplarily shown for porphyrin **46** in figure 37 a singlet for the eight pyrrole protons of the porphyrin core in the ^{1}H-NMR spectrum points at the expected *para*-substitution pattern. Furthermore, two distinct signals for the aromatic fluorine atoms in the ^{19}F-NMR spectra indicate the expected substitution pattern.
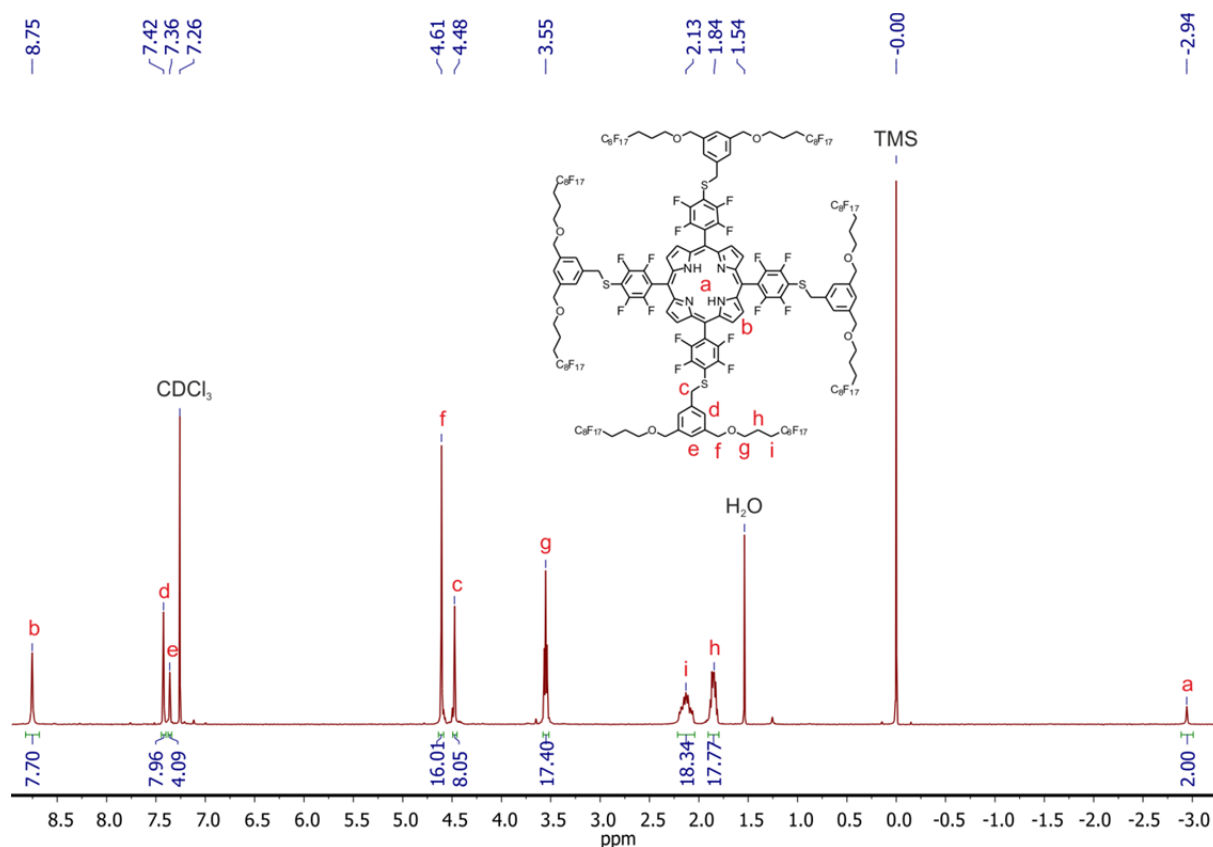
Figure 37. ^{1}H-NMR spectrum (400 MHz) of porphyrin **46** in CDCl$_3$ at room temperature.

The absorption spectra of the free base porphyrins **40-44**, **46** and **48** in CH$_2$Cl$_2$ at room temperature show the expected bands (figure 38).[166][167] For all derivatives an extremely intense Soret band (or B band) at 415 – 420 nm and four Q bands in the region 500 – 675 nm were observed. The position of the bands is strongly dominated by the central chromophore. The fluorous shell has no influence on the absorption spectra. A small effect of the linking heteroatom between the core and the periphery is observed. The maxima of the Soret bands of the thiol based porphyrins (**40**, **42**, **44**, **46**, **48**) are at 415 nm. In contrast, the maxima of the amine derived derivatives are slightly shifted to the red and show maxima at 419 nm (**43**) and 420 nm (**41**), respectively. With regard to the suitability for QIE in the KDTLI, the series of porphyrin derivatives is expected not to absorb strongly at the wavelength of the optical phase grating (532 nm). Thus these model compounds should be suitable candidates with respect to their optical properties.
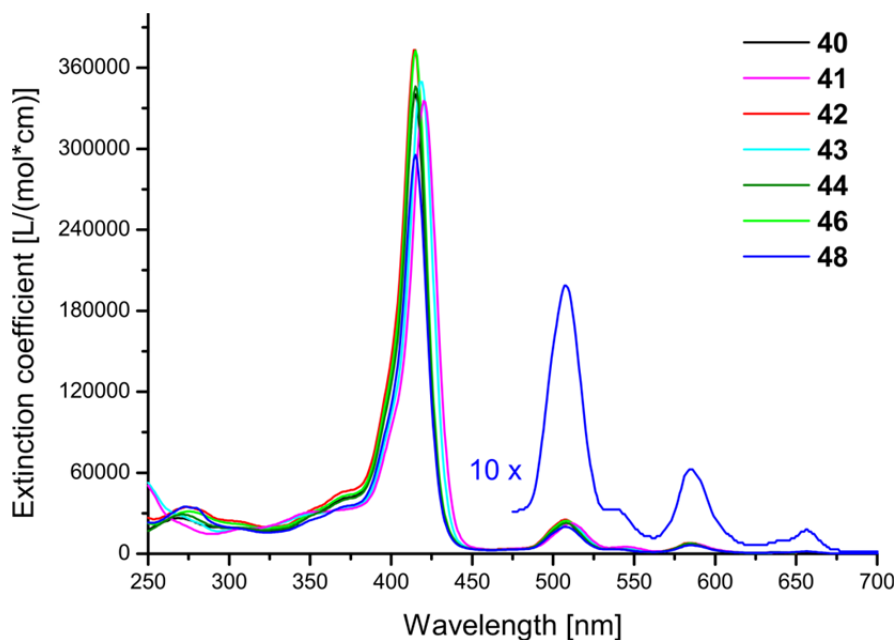
Figure 38. UV/Vis spectra of the porphyrin derivatives **40-44**, **46** and **48** in CH_2Cl_2 at room temperature. The spectrum of porphyrin **48** is additionally displayed enlarged by a factor of ten between 475 nm and 700 nm for a better visibility of the weak Q bands.

Remarkably, all fluorous porphyrins remain perfectly processable with common techniques in organic synthesis despite their high fluorine content. No fluorinated solvents were necessary to synthesize, purify or characterize the target compounds as they are all soluble in common organic solvents including acetone, chloroform and ethers (diethylether and THF).

4.2.4 Suitability for QIE – Thermal investigations

The generation of free molecular beams is a prerequisite for successful quantum experiments. Therefore this process was analyzed in Vienna by determining the enthalpy of evaporation exemplarily for porphyrin **40**. For the measurement an effusive molecular beam is generated in a resistively heated ceramic furnace. A signal, which is proportional to the temperature dependent molecular vapor pressure, is recorded in an electron impact QMS about 2.5 m behind the source.[132] The signal is attenuated by the gratings of a matter-wave interferometer which is inserted between the source and the detector but is of no relevance for the volatilization experiments. The enthalpy of evaporation ΔH_{vap} can be determined by recording the QMS counting signal N at the given mass as a function of the source temperature T. Based on an adapted Clausius-Clapeyron equation the following relation is expected to hold:

$$\ln(N \cdot T) = \frac{(\Delta H_{\mathrm{vap}})}{RT} - const$$

<div align="right">4.1</div>

with $R = 8.314\ \text{Jmol}^{-1}\text{K}^{-1}$. This includes the exponential temperature dependence of the vapor pressure and assumes a hydrodynamic flow from the thermal source.[56]   Figure 39 shows the measured QMS signal at the mass of porphyrin **40** ($M_W = 2\,815$ g/mol). Three independent measurements were conducted of which one is given by the black triangles. A linear fit to $\ln(N \cdot T)$ as a function of $1/T$ is shown as a solid line, and its slope b allows us to determine the molecular enthalpy of evaporation $\Delta H_{\text{vap}} = -b \cdot R$. Its mean value between 543 K and 590 K is 298 ± 34 kJ/mol, where we only denote the statistical uncertainty of three independent measurements. The temperature uncertainty is estimated to be 10 K on an absolute scale, but rather 2 K on a relative scale.
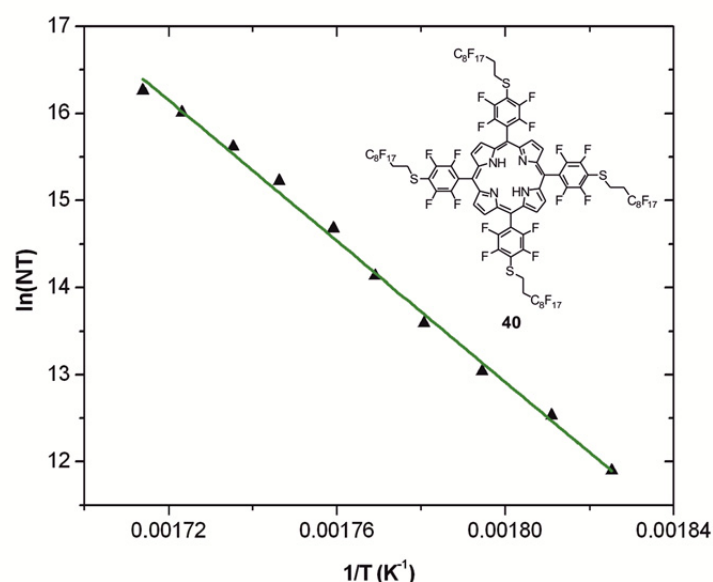
Figure 39. The detected molecular beam intensity of **40** reveals the expected exponential dependence as a function of the temperature. The triangles represent the data for one out of three independent experiments with different batches produced by the same synthesis. The solid line is a linear fit to the data. Only one of three data sets used for the extraction of the enthalpy value is shown.

4.2.5 Quantum Interference Experiments

Samples of the fluorous porphyrins **40-44** and **46** were sent to Vienna for QIE with the KDTLI (figure 40). Matter-wave interferometry with the heaviest fluorous porphyrin of our series was however not possible. Porphyrin **48** with a mass of 7 553 g/mol was synthesized in amounts of only a few tens of milligrams. In particular, in consideration of the fact that the amount of material needed for the current setup in Vienna is expected to increase with increasing molecular weight, this amount was not sufficient for QIE. However, as the development of more efficient sources is an ongoing process, porphyrin **48** could become an interesting candidate for future QIE.
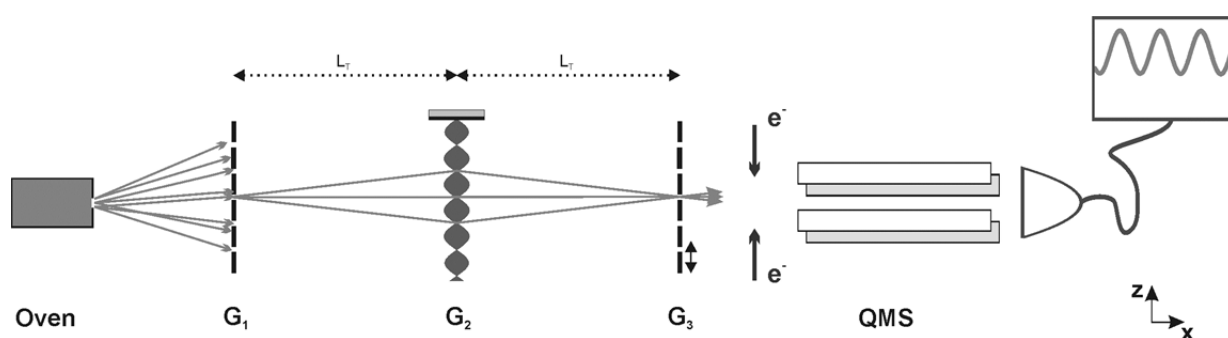
Figure 40. Sketch of the experimental setup of the KDTLI. The porphyrin derivative is evaporated in the oven, the molecules fly through three subsequent gratings, G_1, G_2, and G_3, in the interferometer and are detected in an electron impact quadrupole mass spectrometer (QMS).

It was possible to record quantum interferograms for the three porphyrin derivatives shown in figure 41A. In all cases the measured fringe visibility V, that is, the amplitude of the sinusoidal modulation normalized to the mean of the signal, exceeds the maximally expected classical Moiré fringe contrast by a significant multiple of the experimental uncertainty. This is best shown for porphyrin **40**, which reached the highest observed interference contrast in these high-mass experiments, with individual scans up to $V_{obs} = 33\%$ (figure 41C). The interferogram of porphyrin **41** is shown in figure 41B. A fringe visibility of $V_{obs} = 24 \pm 3\%$ was observed for this amine linked fluorous derivative. In addition, we have observed a maximum contrast of $V_{obs} = 16 \pm 2\%$ for porphyrin **46**, in which the classical model predicts $V_{class} = 1\%$ (figure 41D). This supports our claim of true quantum interference for all these complex molecules.
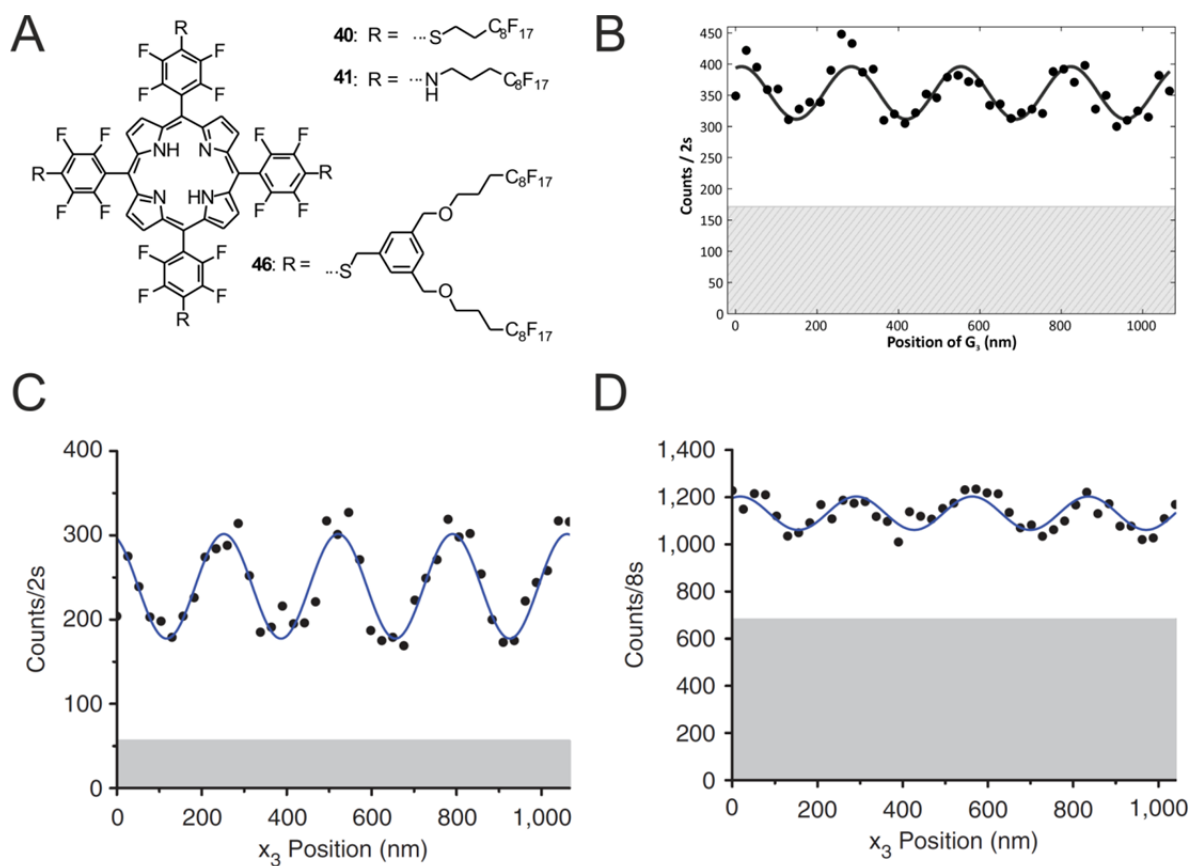
Figure 41. (A) Structures of the tailor-made fluorous porphyrins for which the wave nature has been observed. (B)-(D) Quantum interferograms of tailor-made large fluorous porphyrins. Quantum interference well beyond the classical expectations has been observed for all molecules in the set. In all panels, the black circles represent the experimental result, the solid line is a sinusoidal fit to the data and the shaded area indicates the detector dark rate. (B) Interferogram of compound **41**. (C) Interferogram of porphyrin **40**. (D) Interferogram of porphyrin **46**.

The experimental values were compared with the theoretical predictions based on a classical and a quantum model.[37] The measured interference visibility is plotted as a function of the diffracting laser power P in figure 42 for porphyrin **40**. The data are in very good agreement with the full quantum calculation and in clear discrepancy with the classical prediction. The abscissa scaling of the $V(P)$ curve is a good indicator for this. The quantum prediction mimics the classical curve qualitatively, but it is stretched in the laser power by a factor of about six.
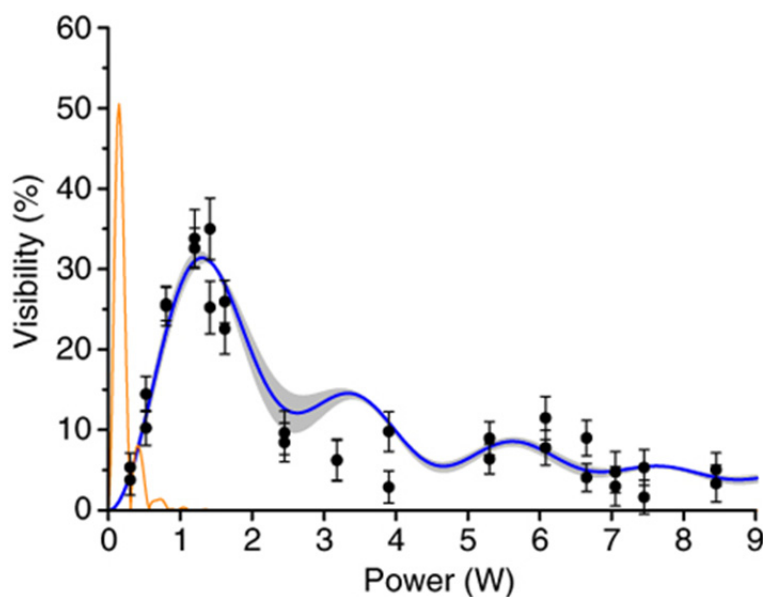
Figure 42. Quantum interference visibility as a function of the diffracting laser power. The best distinction between quantum and classical behavior is made by tracing the interference fringe visibility as a function of the laser power, which determines the phase imprinted by the second grating. Each of the two experimental runs is represented by full circles and the error bar provides the 68% confidence bound of the sinusoidal fit to the interference fringe. The blue solid line is the quantum fit in which the shaded region covers a variation of the mean molecular velocity by $\Delta v = \pm 2$ m s^{-1}. The data of porphyrin **40** are well reproduced by the quantum model and completely missed by the classical curve (orange line on the left). The following parameters were used for the models: $v = 95$ ms $- 1 \pm 16\%$, $\alpha = 200$ Å$^3 \times 4\pi\varepsilon_0$ (fit), $\sigma_{opt} = 10^{-21}$ m^{-2}, $w_x = 34 \pm 3$ μm and $w_y = 500 \pm 50$ μm.

The quantitative agreement of the experimental and expected contrast is surprisingly good, given the high complexity of the molecules. Various factors contribute to the remaining small discrepancies. The interference visibility is highly sensitive to apparatus vibrations, variations in the grating period on the level of 0.5 Å and a misalignment below 100 μrad in the grating roll angle.

4.2.6 Conclusion

We have presented a modular synthesis of seven perfluoroalkyl-substituted porphyrin derivatives with up to 16 fluorous alkyl chains as model compounds for molecular interferometry experiments. To meet the requirements of quantum studies with complex organic molecules – high volatility, high stability, and high molecular mass – we chose the functionalization of tetraarylporphyrins with perfluoroalkyl moieties. With this series in hand it was possible to observe interference patterns for the derivatives **40**, **41** and **46**. The experiments reveal the quantum wave nature of tailor-made organic molecules in an unprecedented mass and size domain and provided major contributions to the exploration of

the frontiers of quantum mechanics. Additionally, the creation of the free molecular beam which is a prerequisite for successful quantum experiments with the KDTLI was analyzed in detail by determining the enthalpy of evaporation for porphyrin **40**. Porphyrin **46** as the heaviest molecule of this series for which the wave nature could be observed has a 3.3 fold higher molecular weight than the preexisting mass record for quantum interference from the year 2003 ($C_{60}F_{48}$, 1 633 g/mol).[34] Furthermore, porphyrin **46** contains 430 atoms covalently bound in one single particle. This is ~350% more than that in all previous experiments.[118] These experiments open a new window for quantum experiments with nano-objects in a complexity class comparable to that of small proteins, and they demonstrate that it is feasible to create and maintain high quantum coherence with initially thermal systems consisting of more than 1,000 internal degrees of freedom. However, a big increase of complexity seems to be very challenging with this synthesis approach. Porphyrin **48** with a mass of 7 553 g/mol is already quite troublesome to synthesize and handle in sufficient quantities. Owing to the large amounts that are needed for the experiments new synthetic approaches are necessary to increase the size of interfering particles.

46
$C_{168}H_{94}F_{152}N_4O_8S_4$
M_W = 5 313 g/mol
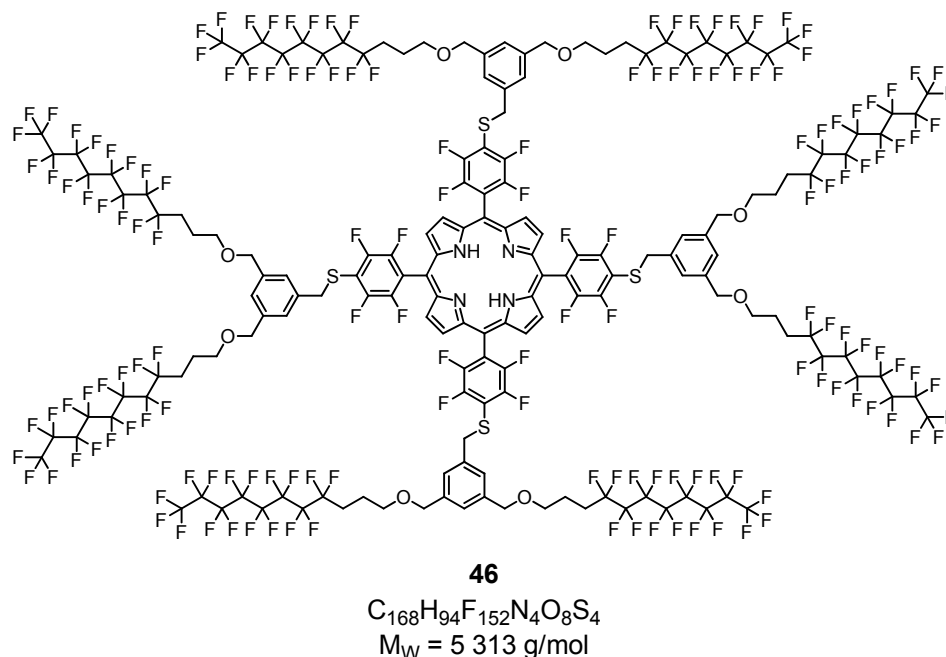
Figure 43. Chemical structure of the heaviest member of our series of tailor-made monodisperse fluorous porphyrins for which the wave nature has been observed. Porphyrin **46** has a molecular weight of 5 313 g/mol and exceeds the old mass record ($C_{60}F_{48}$, 1 633 g/mol)[34] for quantum interference by a factor of 3.3.

4.3   Fluorous Porphyrins – Library Approach

So far, our synthetic efforts were geared towards large monodisperse fluorous model compounds for QIE. This strategy was pursued with the substitution of the four *para*-fluorine substituents of **TPPF20** (figure 44) by dendritically branched fluorous moieties. Porphyrin derivative **46** with a molecular weight of 5 313 g/mol was successfully synthesized in sufficient quantities for QIE. However, a further increase of the compounds' size by means of this approach turned out to be troublesome because of the large number of reaction steps that are required and the increasing working effort that is needed to purify the target compounds.
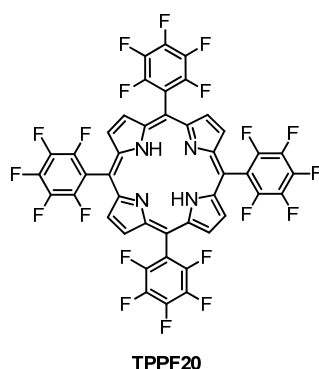
TPPF20

Figure 44. Structure of 5,10,15,20-tetrakis(pentafluorophenyl)porphyrin (**TPPF20**).

The experimental setup of the KDTLI is not restricted to monodisperse and pure starting compounds. It also allows for experiments with compound mixtures because individual components of compound libraries can be detected in the mass spectrometric detection unit. Working with mixtures has several advantages as well as disadvantages. One advantage of pure monodisperse compounds is that these can in principle also be used for interferometer setups with alternative detection schemes. Since the continuous development of new interferometers is considerably influencing the synthetic approaches towards model compounds for QIE, the development of monodisperse compounds offers a broader range of possible applications. Detection based on fluorescence microscopy is an example of a method, which is not reliable when working with compound mixtures. Furthermore, having pure compounds in the beginning gives the opportunity to observe quantum interference even if the signal of the molecule ion is not detectable with the mass spectrometer. If the stability of the target compound during the evaporation process can be proven by chemical analysis of samples that passed through the interferometer, signal counting at fragment peaks is also a feasible technique to observe quantum interference. This method was successfully applied in the sections 3.1 and 3.3. On the other hand, this procedure is not applicable when working with mixtures. When using impure samples it is crucial to detect the signal of the molecule

ion to have clear evidence of the identity of the interfering particle. A big advantage of the library approach is that the synthetic effort is considerably reduced.

As a promising approach towards compounds with high molecular masses we tried to benefit from the fact that nucleophilic aromatic substitution (S_NAr) reactions are not limited to the *para*-position of pentafluorophenyl moieties, but are theoretically possible for every fluorine substituted aromatic position. Indeed, already during the synthesis of the monodisperse series of fluorous porphyrins, which was described above, side products originating from over-substitution were observed.

The mechanism of the S_NAr reaction of a pentafluorophenyl moiety and a thiolate is depicted in scheme 30A. The RC_6F_5 group is highly activated towards nucleophilic aromatic substitution reactions because of the electron-withdrawing -I-effect of the fluorine substituents. If the R group is electronically of minor relevance the regioselectivity of the nucleophilic attack is determined by the +M-effect of the fluorine substituents, which favors an attack in *meta*-position with respect to every fluorine substituent. Thus, the fluorine in *para*-position to the R group is substituted first.[168]–[170] After the formation of a Meisenheimer complex, where a negative charge is stabilized by resonance, fluoride acts as leaving group and the rearomatized substitution product is formed. The resulting thioether compound itself can undergo further S_NAr reactions. However, the reactivity is lowered as compared to the pentafluorophenyl starting material because of the one missing activating fluorine substituent. This is the reason why the *para*-positions in **TPPF20** can be substituted under mild conditions and, on the other hand, the residual fluorines are expected to be replaced when applying harsher conditions.

Substitution reactions at the porphyrin **TPPF20** with its 20 potentially reactive fluorine substituents were expected not to yield pure twenty-fold reaction products. Besides the increase of electron density in the aromatic rings by the introduction of thioether substituents, two other effects probably markedly decrease the efficiency of the complete substitution. Firstly, steric shielding[171] due to the perfluoroalkyl chains can hinder the attack of the thiolates. Perfluoroalkyl chains are sterically more demanding than their hydrogenated counterparts. Carbon-fluorine bonds are with a bond length of around 135 nm considerably longer than sp^3-carbon-hydrogen bonds with around 109 nm.[172] Furthermore, the carbon-fluorine bond, due to the differences in electronegativity, is strongly polarized with a partial negative charge on the fluorine (scheme 30B). As a consequence, the perfluoroalkyl chain can electronically be seen as consisting of a positively charged carbon backbone and a negatively

charged outer shell. As shown in scheme 30C, an attacking anionic thiolate is not only sterically hindered but also electronically repelled by the fluorous chains.
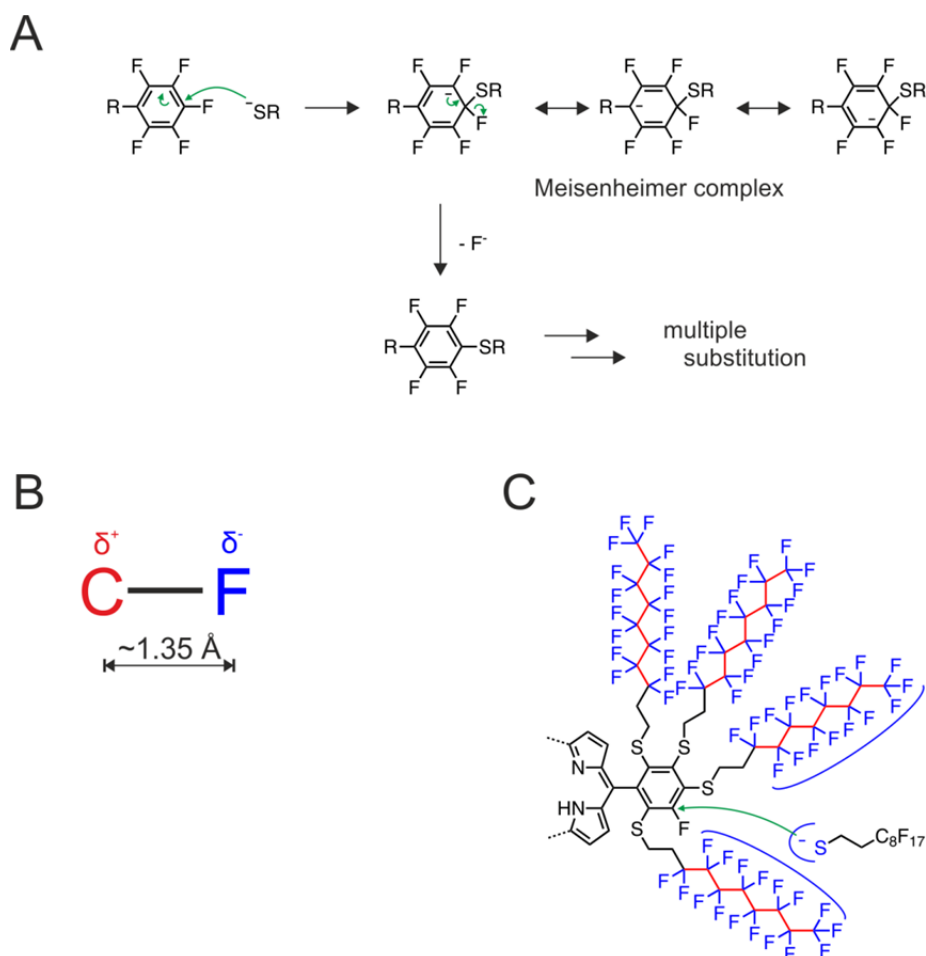
Scheme 30. (A) Mechanism of the S_NAr reaction of a pentafluorophenyl moiety and a nucleophilic thiolate. The addition-elimination mechanism proceeds via a Meisenheimer complex. (B) Average bond length and charge distribution of a carbon-fluorine bond.[172] (C) Schematic representation of a nucleophilic attack of the fluorous thiolates on a fluoroalkyl substituted phenyl moiety. The attack is hindered due to the electronic repulsion of the anionic nucleophile and the electron rich shell of the perfluoroalkyl chain.

Additionally, it is not expected that an isolation of any of the reaction products as pure compounds is feasible. The single substitution products will show only negligible polarity differences which excludes chromatography based on silica gel as an appropriate separation technique. The size differences between the individual reaction products are also expected to be of minor relevance. Thus, gel permeation chromatography (GPC) is not an adequate method towards pure products. Instead, inseparable product mixtures were expected but, as explained above, a library approach for QIE in the KDTLI represents a promising concept. The new approach is depicted in scheme 31. In a first step **TPPF20** as core unit was envisaged to be substituted with 1*H*,1*H*,2*H*,2*H*-perfluorodecane-1-thiol (**71**). In a second step the complexity of the fluorous part was planned to be increased by the use of the branched

alkyl thiol **51**. Thirdly, the application of the expanded core unit **TPPF28** to offer more reactive sites was intended.
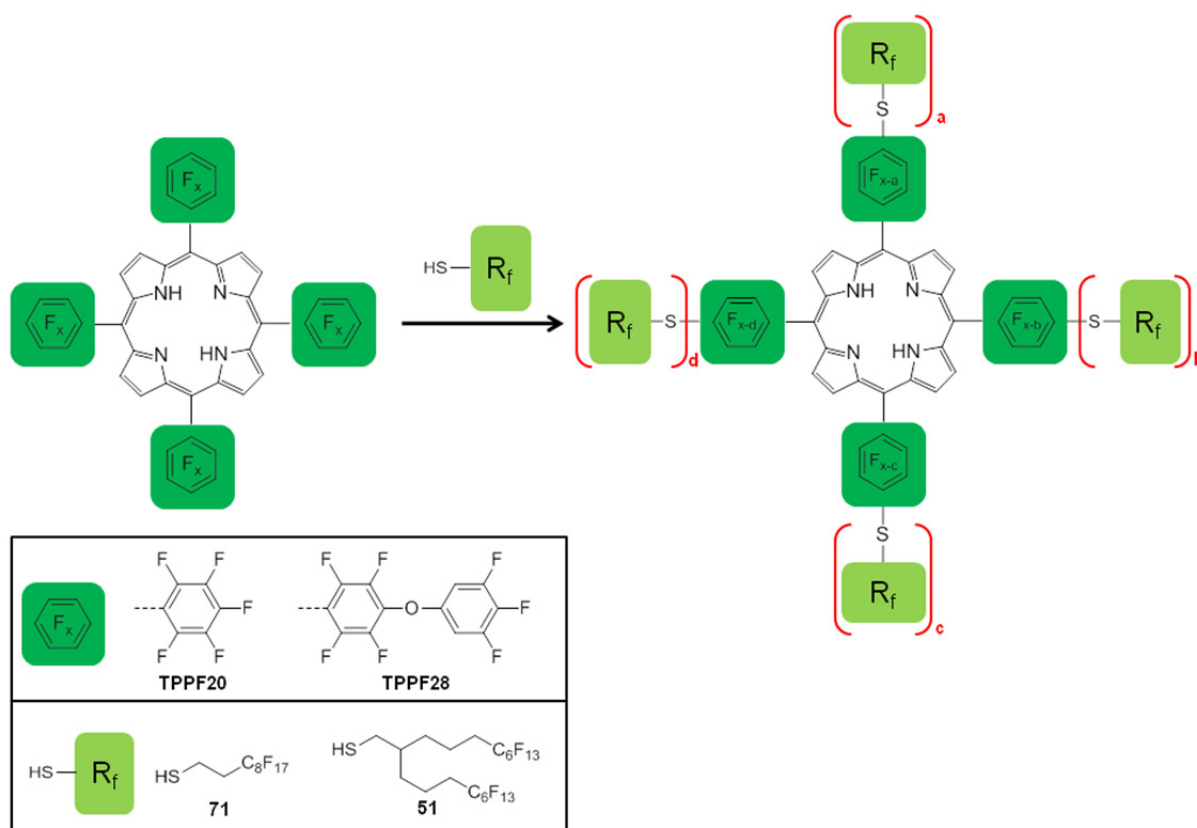
Scheme 31. Concept of the library approach towards highly fluorous porphyrin derivatives. The variable x gives the number aromatic fluorines of each *meso*-substituent in the starting material (x = 5 for **TPPF20** and x = 7 for **TPPF28**). The variables a-d stand for the number of added fluoroalkyl moieties.

4.3.1 1st Generation Library

The **TPPF20** core with twenty potential reaction centers and commercially available 1*H*,1*H*,2*H*,2*H*-perfluorodecane-1-thiol (**71**) as nucleophile were chosen for the preparation of the first generation library **TPPF20-x+17x**. As described in section 4.2.3, the substitution of the four *para*-fluorine substituents in **TPPF20** with various thiol nucleophiles was performed in a solvent mixture of ethyl acetate and DMF in the presence of the organic base diethylamine at room temperature. In order to substitute as many fluorine atoms as possible, we proposed harsher conditions. The base diethylamine was exchanged for sodium hydride to effectively generate highly nucleophilic thiolates from the corresponding thiols. Furthermore, we chose microwave irradiation as a powerful heating source.[173] In our microwave apparatus (Biotage Initiator 8, 400 W) pressure vials are used which can handle pressures up to about 20 bar. In these sealed vials it is possible to reach reaction temperatures considerably higher than the boiling points of the solvents used at ambient pressure. The maximum temperature is restricted by the apparatus to 250 °C. The effective heating by microwaves and the ability to work at high temperatures and high pressure seemed to be ideal for our library concept. For the solvent system we tested two approaches. First, two solvents that are known to effectively support nucleophilic aromatic substitution reactions in general were investigated. These were DMF and 1,3-dimethyl-2-imidazolidinone (DMI). Several examples where polyfluoroarenes were completely substituted by nucleophiles in DMI are known in the literature.[174] The substitution of all six fluorines of perfluorobenzene by the S_NAr reaction of nucleophilic thiolates and perfluorobenzene in DMI was described by Lowe *et al.*.[175] A further example is the five-fold substitution reaction of thiolates and pentafluorobenzaldehyde in DMI.[176]–[178] On the other hand, we tested fluorophilic solvents in order to provide homogeneous reaction conditions as far as possible and thus to help to drive the reaction towards completion. Common organic solvents that are known to dissolve fluorous compounds are solvents containing ether functionalities. We therefore chose THF and diethylene glycol dimethyl ether (diglyme). In particular the use of diglyme was appealing. Besides its dissolution power it shows a high boiling point of 162 °C allowing for high reaction temperatures. Furthermore, it is able to act as a chelate ligand for small cations, including lithium, sodium and potassium. By chelating the cations the reactivity of the corresponding anions, in our case thiolates, can be enhanced. This is why diglyme is a powerful solvent for reactions where organometallics are involved, including Grignard reactions, reductions with sodium borohydride and nucleophilic substitution reactions. Diglyme is stable at high temperatures and high pH

values, which enables reactions in a strong basic surrounding. Figure 45 shows all tested solvents.
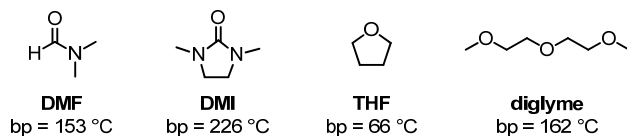
Figure 45. Structures and boiling points of the four solvents that were tested for the S_NAr reactions of the fluorous thiol **71** with **TPPF20**.

As shown in table 2 a screening of different reaction parameters (reaction time, temperature, amount of base, solvent, equivalents of thiol) to optimize the substitution reaction were performed. A mixture of **TPPF20**, 1*H*,1*H*,2*H*,2*H*-perfluorodecane-1-thiol (**71**), sodium hydride (used as a dispersion in mineral oil) and the solvent were heated in a sealed vial in a microwave apparatus. After cooling to room temperature the reaction mixture was quenched with water and subsequently extracted with diethylether. The organic layer was washed with brine and water, dried over sodium sulfate and evaporated to dryness. The resulting product mixture was finally analyzed by MALDI-ToF mass spectrometry.

The screening was started with DMF as solvent. The first attempt (entry 1) with 40 equivalents of the thiol **71**, 80 equivalents of sodium hydride, a reaction temperature of 150 °C and a reaction time of 5 minutes afforded a product mixture comprising 4- to 14-fold substituted derivatives according to MALDI-ToF MS analysis. Increasing of all reaction parameters (entry 2) improved the results and yielded a mixture with 10- to 16-fold substituted porphyrin derivatives. However, a further increase of the temperature and the reaction time was seen critically since it is known that DMF is unstable at high temperatures. DMF can degrade to form dimethylamine which can act as a nucleophile and attack **TPPF20**. Indeed, this undesired side reaction was already observed for **TPPF20**. Remarkably, the formation of the fourfold dimethylamino substituted porphyrin derivative in the presence of DMF at elevated temperatures represents the first example in literature for the fourfold *para*-fluoro substitution of **TPPF20**.[142] DMI with a boiling point of 225 °C is obviously better suited for reactions at higher temperatures. Firstly, a reaction in DMI at a temperature of 250 °C, the maximum temperature of the microwave apparatus, was investigated (entry 3). Similar results as compared to the second try with DMF (entry 2) were obtained. The next series of experiments (entries 4 to 8) were performed in THF. We started with almost identical conditions as in the first run with DMF, but much better results were obtained (entry 4). Ten to 16 attached fluorous chains and the strongest signal for the derivative containing 13

fluorous ponytails were detected by mass spectrometry. An increase of the temperature from 150 °C to 160 °C changed the results for the worse (entry 5). Staying at 150 °C and a stepwise increase of the amounts of the thiol and the base improved the obtained results. With 120 equivalents of the thiol and the base, a reaction temperature of 150 °C and a reaction time of 3 minutes a product mixture comprising 10- to 18-fold substituted derivatives were detected, the best result so far. A further increase of the amounts of the thiol and the base was not reasonable. Furthermore, a raise of the reaction temperature showed poor results. Thus, we identified the results of entry 8 as optimum for the use of THF. Finally, the two experiments with diglyme (entries 9 and 10) as solvent gave the best results for this screening of reaction parameters. According to MALDI-ToF mass spectra these conditions gave mixtures of derivatives with 10 up to 19 added fluorous chains. The strongest signals in the mass spectra of these mixtures were obtained for the derivatives with 14 (entry 9) and 15 (entry 10) fluorous chains, respectively.

Table 2. Optimization of reaction parameters for the synthesis of the 1st generation library **TPPF20-x+17x**.
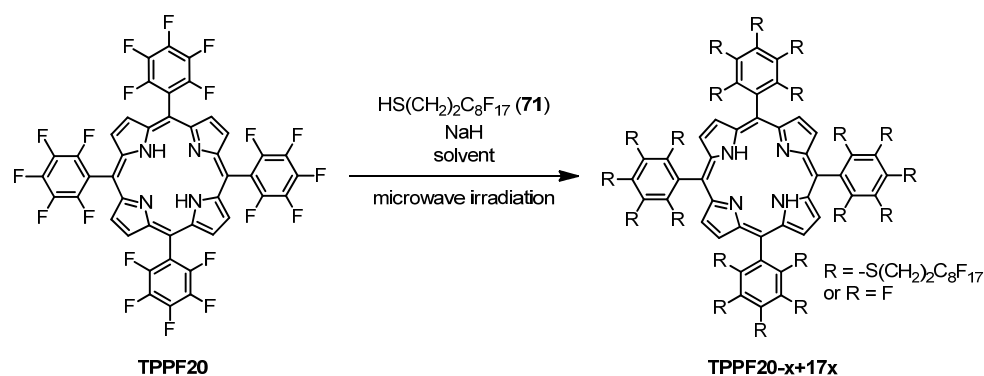
Entry	Thiol [eq.]	NaH [eq.]	Solvent	Temp. [°C]	Time [min]	№ of substituents x (range)	№ of substituents x (strongest signal)
1	40	80	DMF	150	5	4 – 14	12
2	100	120	DMF	180	10	10 – 16	12
3	50	100	DMI	250	10	10 – 14	12
4	40	80	THF	150	10	10 – 16	13
5	50	80	THF	160	15	8 – 13	11
6	60	80	THF	150	10	8 – 14	12
7	80	100	THF	150	10	10 –17	14
8	120	120	THF	150	3	10 – 18	14
9	70	100	diglyme	200	3	10 – 19	14
10	70	100	diglyme	220	6	10 – 18	15

In the following a summary of the solvent screening is given. Reactions in DMF gave moderate results but were not further optimized because of the known instability of this solvent at higher temperatures. The reactions in DMI were not further analyzed because reactions in THF led to better results at much lower reaction temperatures. Good results were obtained for THF. However, the room for optimization was limited as a large excess of the base and the nucleophile was already used and an increase of the reaction temperature did not lead to improved results. Diglyme with its higher boiling point as compared to THF gave the best results. Table 3 shows the molecular weights of the individual components of the resulting compound libraries.

Table 3. Molecular weights of the individual components of **TPPF20-x+17x**. The variable x stands for the number of fluoroalkyl substituents.

x	M_W [g/mol]	x	M_W [g/mol]	x	M_W [g/mol]	x	M_W [g/mol]
1	1 435	6	3 736	11	6 037	16	8 337
2	1 895	7	4 196	12	6 497	17	8 798
3	2 355	8	4 656	13	6 957	18	9 258
4	2 815	9	5 116	14	7 417	19	9 718
5	3 275	10	5 576	15	7 877	20	10 178

The MALDI-ToF mass spectrum obtained from the reaction of **TPPF20**, 70 equivalents of the thiol **71**, 100 equivalents of sodium hydride, a reaction temperature of 200 °C and a reaction time of 3 minutes (entry 9) is shown in figure 46. It displays the molecule ion peaks of the components of the obtained product mixture. With this reaction a compound library that covers a mass range of ca. 5 500 to 9 500 g/mol was obtained. Quantum interference of objects in this mass region would considerably exceed the mass of our heaviest interfering monodisperse porphyrin derivative **46** with a molecular weight of 5 313 g/mol.

Remarkably, all mass spectra obtained in the screening reveal similar signal intensity patterns. The strongest signal is always symmetrically neighbored in both directions of the spectrum by signals of lower intensity. The distribution is almost Gaussian. The position of the strongest signal is obviously exclusively influenced by the reaction parameters. Initially, we expected a preference for a specific number of attached chains due to differences in the reactivities of different substitution positions. In particular, strong signals for derivatives containing a multiple of four attached fluorous chains were expected. We estimated that always four substitution reactions (one on each ring) would proceed with equal rates, whereas the next fluorous chain (5th, 9th, 13th and 17th substitution) is harder to attach. Obviously, this behavior was not observed here.
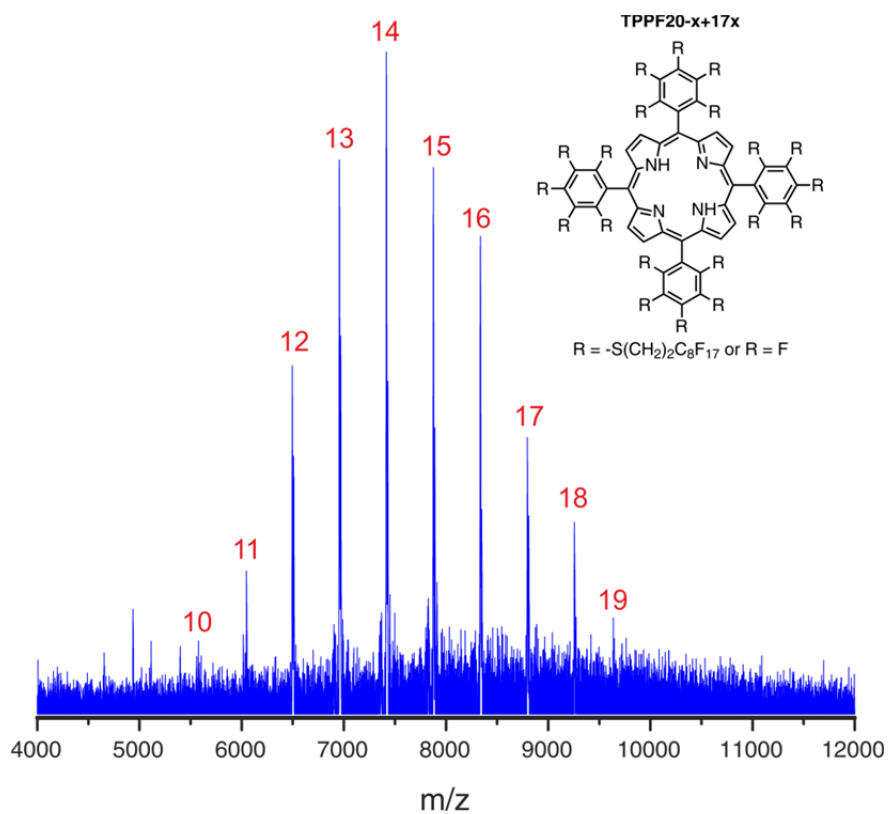
Figure 46. MALDI-ToF mass spectrum of the S_NAr reaction of **TPPF20** with thiol **71**. *Reaction conditions*: **TPPF20**, **71** (70 eq.), NaH (100 eq.), diglyme, microwave irradiation, 200 °C, 3 minutes. The numbers in red give the amount of polyfluoroalkyl substituents at the porphyrin core.

4.3.2 2nd Generation Library

To further increase the mass range of the libraries a tailor-made fluorous thiol as nucleophile was used in the second generation library **TPPF20-x+26x**. The branched thiol **51** was synthesized in seven reaction steps in an overall yield of 70%. The synthesis was described in section 4.2.3. The porphyrin core **TPPF20** as starting material remained the same as for the first generation. Also here a screening of reaction conditions was performed (table 4). However, the focus was set exclusively on ether derived solvents, because these showed promising results in the preparation of the first generation library. Reactions in THF at 150 °C with different stoichiometries of the thiol and the base led to libraries in the mass range of 6 311 g/mol to 10 885 g/mol, which corresponds to 7 to 13 attached fluorous moieties (entries 1-3). The number of aromatic fluorines that were substituted was lower as compared to similar reaction conditions in the first generation libraries. However, with the larger fluorous thiol **51** the mass range was increased at the same time. Probably steric reasons and electronic repulsion as discussed above caused the lower number of substitutions that took place in the reaction with the bulkier branched fluorous thiol **51**. As in the first generation library, reactions in diglyme at temperatures of 200 °C and 220 °C, respectively, gave the best results (entries 4 and 5). A reaction at 220 °C for 5 minutes led after workup to a mixture where the number of perfluoroalkyl substituents ranges from 9 to 15 (entry 5).

Table 4. Optimization of reaction parameters for the 2nd generation library **TPPF20-x+26x**.
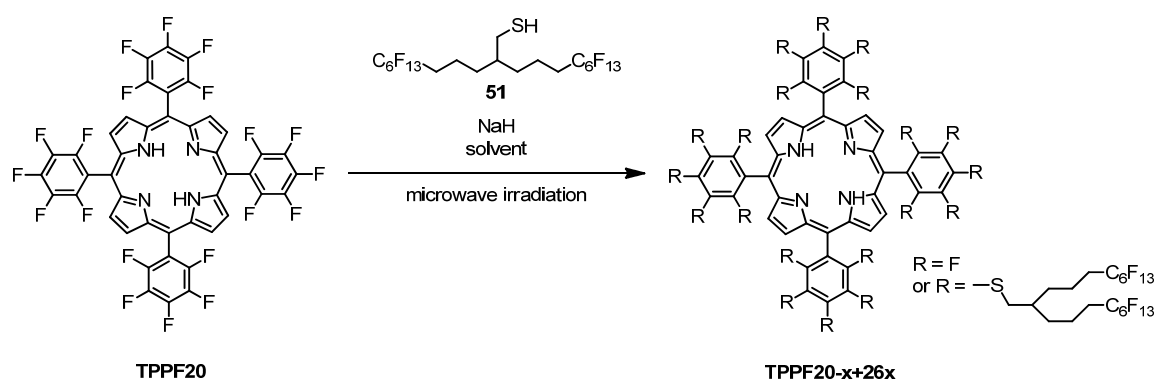
Entry	Thiol [eq.]	NaH [eq.]	Solvent	Temp. [°C]	Time [min]	№ of substituents x (range)	№ of substituents x (strongest signal)
1	40	80	THF	150	10	8 – 12	11
2	60	100	THF	150	10	7 –13	11
3	60	80	THF	150	10	8 –13	11
4	60	90	diglyme	200	3	6 – 15	13
5	60	90	diglyme	220	5	9 – 15	13

As shown in table 5, the molecular weights of the individual components of the second generation library **TPPF20-x+26x** exceeded for the first time the ceiling of 10 000 g/mol. The strongest signal in the MALDI-ToF mass spectrum obtained after reaction in diglyme is attributed to a 13-fold substituted fluorous porphyrin which has a mass of 10 885 g/mol. Remarkably, all components of the library still remain soluble to a certain degree in diethylether, which is surprising considering the fact that up to 30 perfluorohexyl ponytails ($x = 15$) are present in the target structures. At least the solubility suffices for an effective workup including a diethylether extraction.

Table 5. Molecular weights of the individual components of the 2nd generation library **TPPF20-x+26x**. The variable x stands for the number of fluoroalkyl substituents.

x	M_W [g/mol]	x	M_W [g/mol]	x	M_W [g/mol]	x	M_W [g/mol]
1	1 737	6	5 549	11	9 360	16	13 172
2	2 499	7	6 311	12	10 123	17	13 935
3	3 262	8	7 073	13	10 885	18	14 697
4	4 024	9	7 836	14	11 648	19	15 459
5	4 786	10	8 598	15	12 410	20	16 222

The MALDI-ToF mass spectrum of the best reaction conditions of the second generation library **TPPF20-x+26x** is displayed in figure 47. This library covers a mass range of ca. 8 000 to 12 500 g/mol, a considerable improvement in comparison to the first generation library **TPPF20-x+17x**.
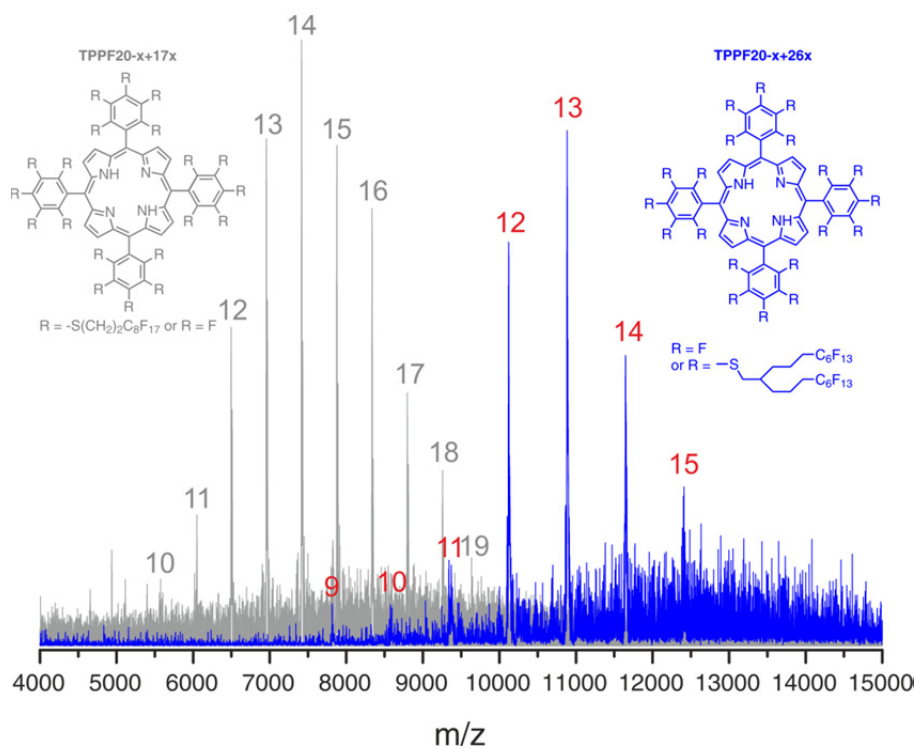
Figure 47. The MALDI-ToF mass spectrum of the S_NAr reaction of **TPPF20** with thiol **51** is shown in blue. The applied reaction conditions were: **TPPF20**, **51** (60 eq.), NaH (90 eq.), diglyme, microwave irradiation, 220 °C, 5 minutes. The numbers in red assign the amount of polyfluoroalkyl substituents at the porphyrin core. The MALDI-ToF mass spectrum of the first generation library **TPPF20-x+17x** is shown in grey for comparison.

4.3.3 3rd Generation Library

In the third generation library an expanded porphyrin derivative as a starting point was considered in order to increase the number of potential reaction centers. It was planned to enlarge the core unit by the introduction of further polyfluoroarene units, which can subsequently be substituted by fluorous chains. First, it was tried to attach pentafluorophenol (**76**) to the *para*-positions of **TPPF20** to assemble **TPPF36** with 36 potential reactive sites. It was clear that a nucleophilic introduction to **TPPF20** with a reactant, which itself can be attacked by nucleophiles, could yield numerous side products. However, the substitution of the four *para*-positions in **TPPF20** was expected to be faster than all other possible undesired substitution reaction. All fluorine substituted positions in pentafluorophenol (**78**) are less reactive towards S$_N$Ar reactions as compared to the *para*-positions in **TPPF20** because of the electron-donating effect of the hydroxyl group, which increases the electron density in the aromatic ring and thus decreases the reactivity towards nucleophilic attacks. If a *para*-substitution in **TPPF20** occurs the resulting fluorinated diphenylether moiety should also show a lowered reactivity because of the ether bridge which donates electrons to both aromatic rings. Several reaction conditions towards **TPPF36** were investigated (scheme 32). Different bases, temperatures and stoichiometries were tested but TLC and MALDI-ToF MS analysis revealed wild product mixtures in all cases. Surprisingly, none of the mixtures contained the desired product **TPPF36**.
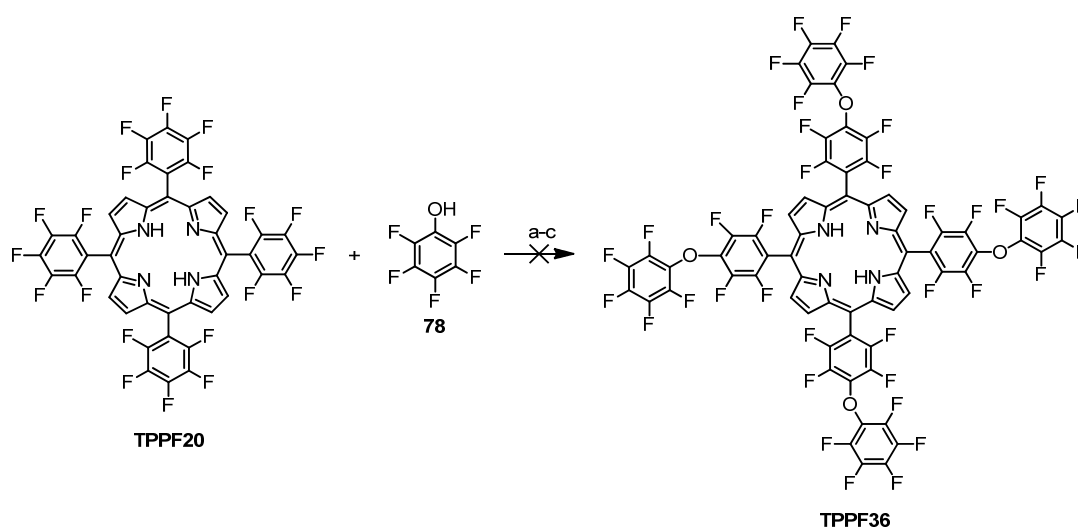
Scheme 32. Attempts to synthesize **TPPF36**. *Reagents and conditions*: (a) NaH, THF, reflux, 12 h; (b) NaH, diglyme, microwave irradiation, 200 °C, 10 min; (c) K$_2$CO$_3$, DMSO, 80 °C, 2.5 days.

In a next step it was tried to find suitable reaction conditions to introduce a phenolic structure to the *para*-positions of **TPPF20**. Thus, test reactions with phenol (**79**) as the nucleophile were performed. It turned out that the in situ generation of sodium phenolate by the reaction

of phenol (**79**) and sodium hydride as base in DMF at room temperature and subsequent addition of **TPPF20** and a raise of the temperature to 90 °C led after a reaction time of 17 hours to the formation of the desired porphyrin derivative **80** (scheme 33). Purification by column chromatography afforded compound **80** as a purple solid in a yield of 56%.
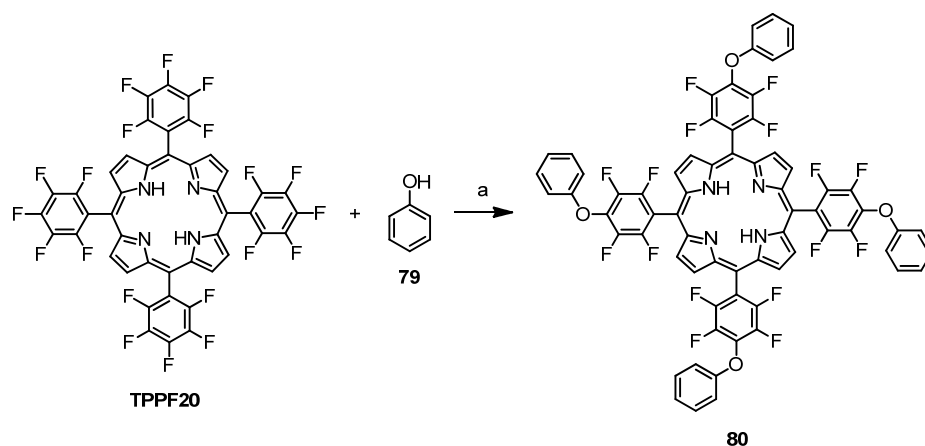
Scheme 33. Synthesis of the porphyrin derivative **80**. *Reagents and conditions*: (a) NaH, DMF, 90 °C, 17 h, 56%.

After having found suitable conditions for the $S_N Ar$ reaction of **TPPF20** and phenol (**79**), the assembly of **TPPF28** as expanded core unit was envisaged (scheme 34). The starting material 3,4,5-trifluorophenol (**81**) should be less prone to the formation of side products as the electron density in the aromatic core is considerable lower than in the pentafluoroarene rings in **TPPF20**. **TPPF20** was added to a mixture of sodium hydride and 7 equivalents of 3,4,5-trifluorophenol (**81**) in DMF. Stirring under argon at 90 °C overnight and subsequent purification by column chromatography followed by recrystallization from acetone gave the desired compound **TPPF28** as purple crystals in a yield of 36%.
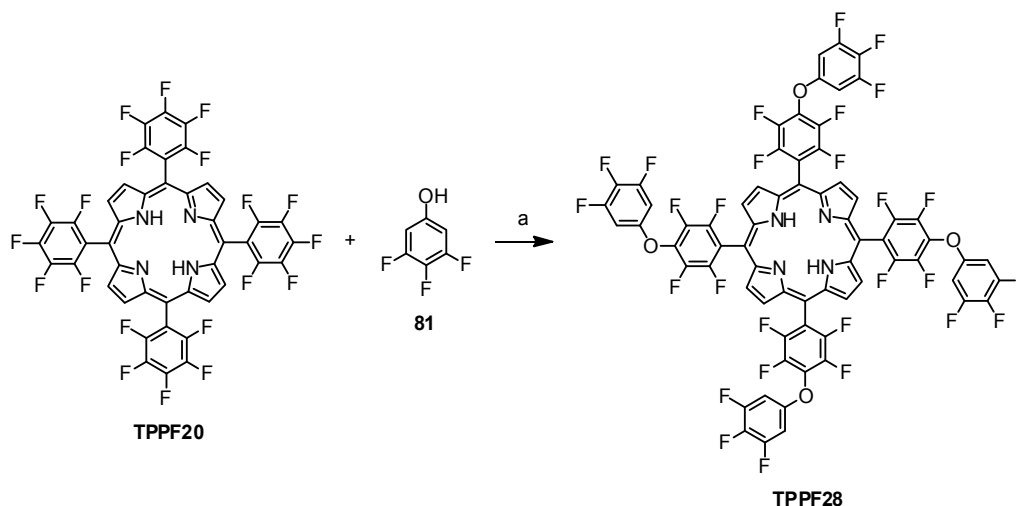
Scheme 34. Synthesis of **TPPF28**. *Reagents and conditions*: (a) NaH, DMF, 90 °C, 12 h, 36%.

The recrystallization of **TPPF28** from acetone yielded deep purple crystals suitable for X-ray analysis. Figure 48A displays the obtained centrosymmetric solid state structure. The two rings of the polyfluorodiphenyl ether units show a torsion angle close to 90°. Such a geometry offers a good accessibility of the fluorine substituents. Hence, the present conformation should be ideal for nucleophilic substitutions of these substituents. Furthermore, the phenyl units which are attached in the *meso*-position of the porphyrin core are almost perpendicular to the plane of the porphyrin core. Thus, the electronic influence of the substituents on the chromophore is very low due to the missing conjugation of the π-systems originating from the twisted position of the *meso* substituents. This is nicely reflected by the UV/Vis spectra of **TPPF28** and **TPPF20** (figure 48B). Both spectra are very similar. The band positions are determined by the central porphyrin chromophore and only tiny shifts are observed when substituents in the periphery are altered.
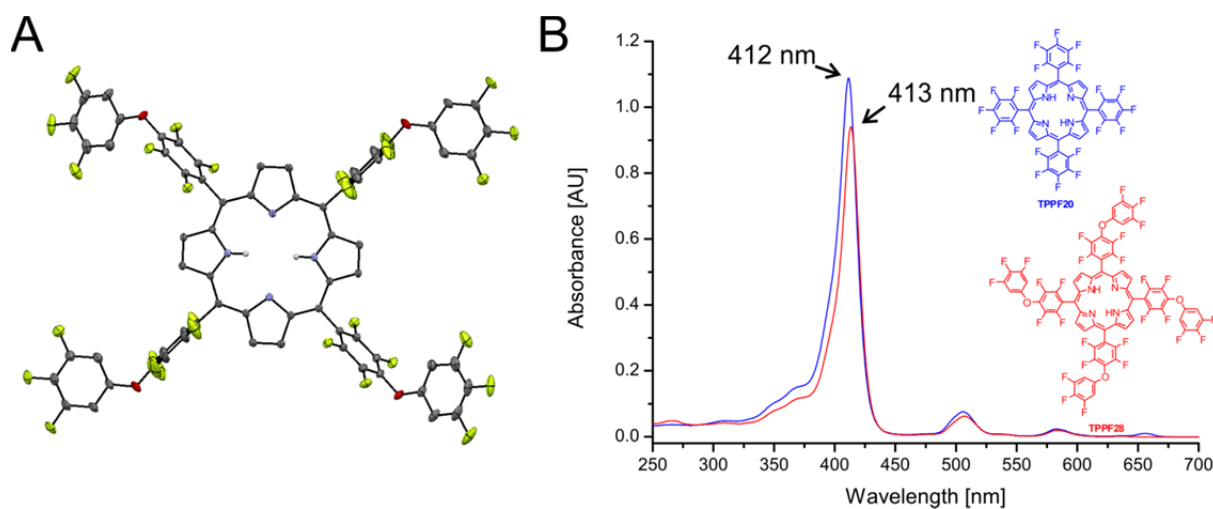
Figure 48. (A) Solid state structure of **TPPF28**. (B) UV/Vis spectra of the porphyrin derivatives **TPPF20** (blue line) and **TPPF28** (red line) in CH$_2$Cl$_2$ at room temperature.

With **TPPF28** in hand, the formation of the next generation library was envisaged. **TPPF28** was reacted with the branched thiol **51** under the reaction conditions which were optimized for the second generation library **TPPF20-x+26x**. Sodium hydride as base, diglyme as solvent, microwave heating to 220 °C and a reaction time of 5 minutes were chosen. However, the obtained MALDI-ToF mass spectrum that was recorded after workup was almost identical to the mass spectra obtained for the second generation library **TPPF20-x+26x**. From the spectra it was evident that the 3,4,5-trifluorophenol substituent acts as a leaving group under the applied reaction conditions. **TPPF28** does not represent a stable core unit under these harsh conditions. Thus, it was necessary to search for reaction conditions that are harsh enough to add many fluorous thiols but mild enough to prevent substitution of 3,4,5-trifluorophenol moieties. For these optimization reactions, the commercially available fluorous thiol **71** was used instead of the branched thiol **51**. Scheme 35 displays the reaction towards the third generation library **TPPF28-x+17x**.
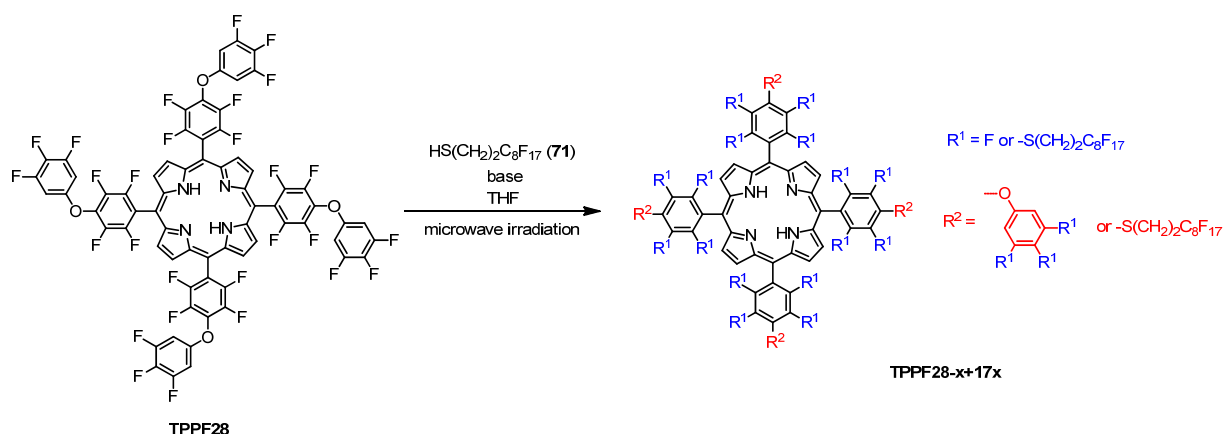
Scheme 35. Assembly of the 3rd generation library **TPPF28-x+17x**.

An overview of the screening of the reaction parameters for the formation of the library **TPPF28-x+17x** is given in table 6. Reactions with **TPPF28** and thiol **71** as starting material in THF led after workup to product mixtures, where the number of attached fluorous chains as well as the number of residual 3,4,5-trifluorophenyl moieties varied. The compositions of the obtained product mixtures are depicted in table 7. In this table the observed mass signals for each reaction are marked in the same color as the corresponding entry in table 6 and the labels are assigned with the entry number from table 6.

Table 6. Optimization of the reaction parameters for the 3rd generation library **TPPF28-x+17x**.

Entry	Thiol [eq.]	Base	Equivalents of Base	Temp. [°C]	Time [min]
1	50	K$_2$CO$_3$	100	100	8
2	50	K$_2$CO$_3$	100	160	10
3	120	K$_2$CO$_3$	120	160	20
4	70	NaH	80	150	10
5	120	NaH	120	150	10
6	70	NaH	80	100	5
7	150	NaH	120	160	2
8	160	NaH	120	170	1
9	160	NaH	120	180	0.5

Besides sodium hydride as base we also tested potassium carbonate as a milder alternative. In a first attempt with potassium carbonate at 100 °C (entry 1) exclusively the molecule ion peak of the starting material **TPPF28** was detected indicating that these conditions were mild enough to prevent degradation of the core unit, but also too mild for any substitution reaction. Two further reactions with potassium carbonate as base were performed (entries 2 and 3). In both cases signals originating from derivatives with the intact core structure as well as structures with less than four phenol residues were observed. The number of attached fluorous thiols was rather low with a maximum of nine substituents. Switching to sodium hydride as base led to improved results. Reactions in THF at 150 °C for 10 minutes (entries 4 and 5) revealed the formation of products with up to 19 fluorous ponytails. However, structures with intact core units were not observed for this reaction temperature. A decrease of the reaction temperature to 100 °C and the reaction time to 5 minutes (entry 6) delivered derivatives with the intact core but the number of attached chains was considerably lower. At a reaction temperature of 160 °C and a shortened reaction time of 2 minutes (entry 7) similar results as for the entries 4 and 5 were obtained. A further increase of the temperature to 170 °C and a decrease of the time to 1 minute (entry 8) finally gave highly fluoroalkyl substituted derivatives with the intact core unit. The last reaction with temperatures of 180 °C and a reaction time of 30 seconds (entry 9) did not afford derivatives with undegraded core units but also a high number of fluoroalkyl chains. Thus we identified the following reaction conditions as best suited for the S$_N$Ar reaction of **TPPF28** with fluorous thiols: a reaction with 160 equivalents of the thiol, 120 equivalents of sodium hydride in THF at 170 °C for 1 minute. Note that the stated reaction time does not include the warming and cooling phase in the microwave process. At such short reaction times as described here, the warming and

cooling phases are important factors and have an influence on the outcome of the reaction. As shown in figure 49 the "real" reaction time is considerably longer than one minute.
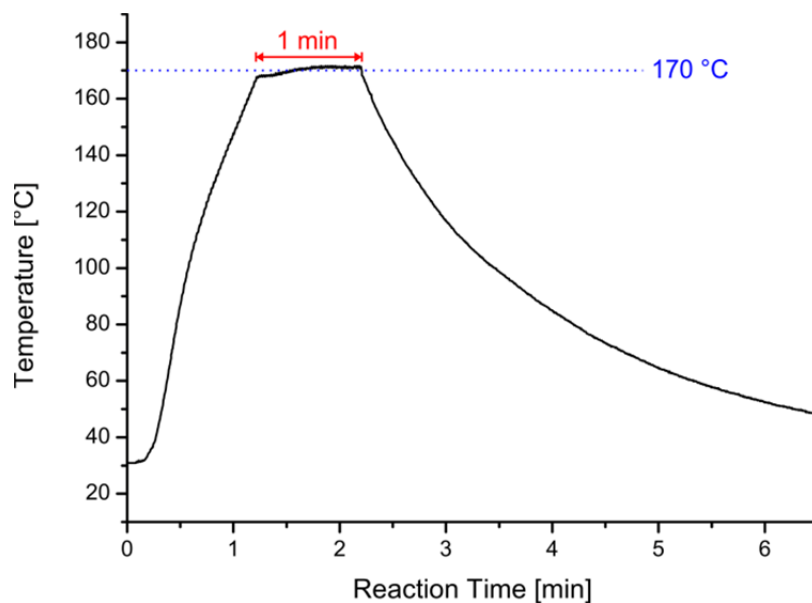
Figure 49. Temperature characteristics of the microwave reaction towards the 3rd generation library **TPPF28-x+17x.** The following parameters were used: **TPPF28**, **71** (160 eq.), NaH (120 eq.), THF, 170 °C, 1 min.

Table 7. Results of the reaction screening towards the 3rd generation library **TPPF28-x+17x**. The table displays the molecular weights of possible reaction products. The results of the specific reactions that are described in table 6 are represented by the colored labels.

№ of Chains	TPPF28 [g/mol]	3 Phenol Residues [g/mol]	2 Phenol Residues [g/mol]	1 Phenol Residue [g/mol]	0 Phenol Residues [g/mol]
0	1486	1358	1230	1102	974
1	1946	1818	1690	1562	1434
2	2406	2278	2150	2022	1894
3	2866	2738	2610	2482	2354
4	3326	3198	3070	2942	2814
5	3786	3658	3530	3402	3274
6	4246	4118	3990	3862	3734
7	4706	4578	4450	4322	4194
8	5166	5038	4910	4782	4654
9	5626	5498	5370	5242	5114
10	6086	5958	5830	5702	5574
11	6546	6418	6290	6162	6034
12	7006	6878	6750	6622	6494
13	7466	7338	7210	7082	6954
14	7926	7798	7670	7542	7414
15	8386	8258	8130	8002	7874
16	8846	8718	8590	8462	8334
17	9306	9178	9050	8922	8794
18	9766	9638	9510	9382	9254
19	10226	10098	9970	9842	9714
20	10686	10558	10430	10302	10174
21	11146	11018	10890	10762	

The third generation compound library **TPPF28-x+17x** did not lead to porphyrin derivatives in higher mass regions as compared to the previously described libraries. Instead, the reactions performed in this section served to find optimized conditions for the functionalization of the new core unit **TPPF28**. **TPPF28** is markedly more unstable as compared to **TPPF20** under harsh reaction conditions and thus milder conditions had to be found in order to pave the way to new libraries based on **TPPF28**.

4.3.4 4th Generation Library

The assembly of the fourth library **TPPF28-x+26x** was performed with the adapted reaction conditions found in the last section. **TPPF28**, the branched thiol **51** and sodium hydride in THF were heated in a microwave apparatus to 170 °C for 1 minute (scheme 36). Quenching with water, extraction with diethylether, washing with water and brine, and drying over sodium sulfate afforded the new library.
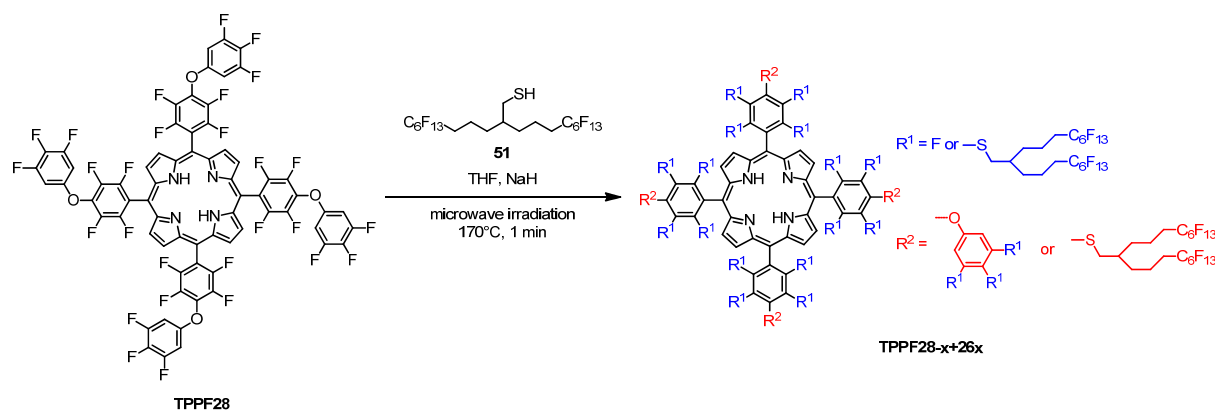
Scheme 36. Assembly of the 4th generation library **TPPF28-x+26x**.

The obtained mass spectrum is shown in figure 50. The observed signals can unambiguously be assigned to the molecule ion peaks of the depicted structures. The library covers a mass range from ca. 8 000 g/mol to almost 14 000 g/mol, which represents a further improvement.
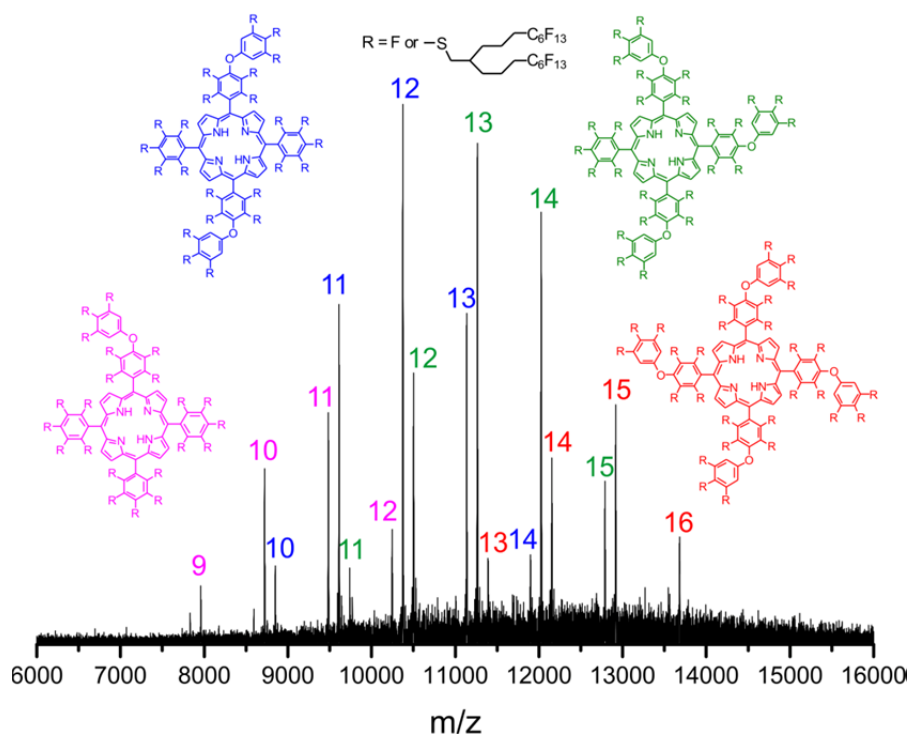
Figure 50. MALDI-ToF mass spectrum of the S_NAr reaction of **TPPF28** with thiol **51**. *Reaction conditions*: **TPPF28**, **71** (80 eq.), NaH (90 eq.), THF, microwave irradiation, 170 °C, 1 minute. The numbers give the amount of polyfluoroalkyl substituents.

4.3.5 Quantum Interference Experiments

Samples of the libraries **TPPF20-x+17x**, **TPPF20-x+26x** and **TPPF28-x+26x** in gram quantities were prepared for QIE in Vienna. The experiments are currently ongoing. Preliminary studies revealed suitable beam properties in the KDTLI for the first and the second generation libraries. It was possible to detect intact molecules of the libraries in the QMS of the KDTLI after their flight through the interferometer.

4.3.6 Conclusion

With the series of monodisperse highly fluorous porphyrins as model compounds for molecule interferometry it was possible to set new records for mass, linear extension and number of atoms in quantum interferometry. However, further enlargements of the complexity of these compounds turned out to be too time-consuming from the synthetic point of view. The work with compound libraries gave access to compounds in a new mass region (> 10 000 g/mol). Figure 51 shows the mass spectra of the assembled porphyrin libraries. With this approach masses up to 20 000 g/mol are a realistic goal for the future. The design of

new porphyrin platforms and fluorous thiol building blocks, as well as the optimization of reaction conditions should enable further advancements in this field.
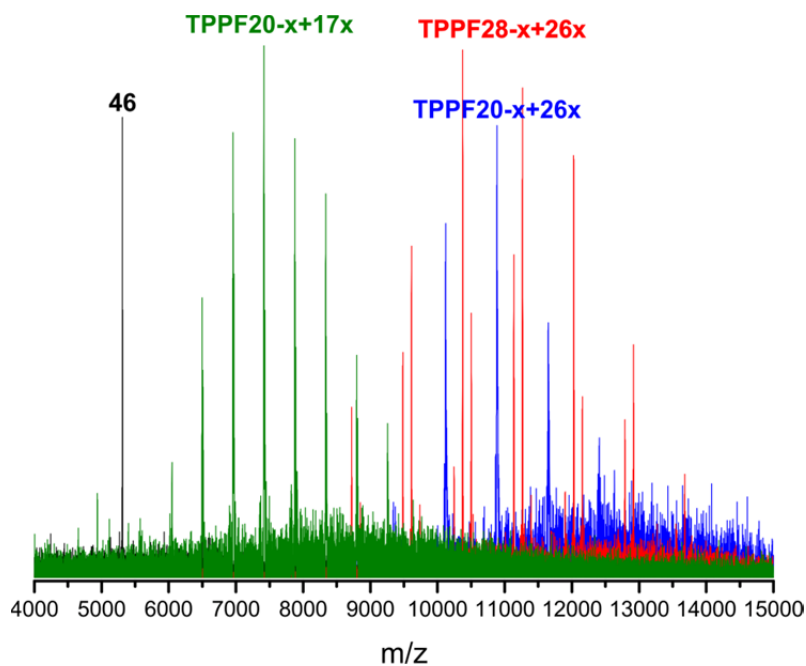
Figure 51. Overlaid MALDI-ToF mass spectra of the libraries **TPPF20-x+17x** (green), **TPPF20-x+26x** (blue) and **TPPF28-x+26x**, and the porphyrin derivative **46** (black).

5 Model Compounds for New Size Records in Far-Field Molecule Interferometry

Far-field matter-wave experiments with the fullerenes C_{60} and C_{70} can be seen as milestones in quantum interference experiments.[16][20] However, these experiments, which were first described in 1999, had remained the only demonstrations of far-field experiments with objects in these dimensions. As described in the previous chapters, substantial progress in the field of matter-wave interferometry with complex objects was exclusively accomplished in near-field setups. These setups profit from their advantageous requirements on the interferometer design.

Nevertheless, the research focus in the Arndt group was not only set on new near-field concepts. The ultimate demonstration of the quantum behavior of an object is attributed to the observation of interference in double-slit experiments operating in the far-field regime. Such matter-wave interference has been observed for electrons,[7] neutrons,[8] atoms,[10][179] and molecules[11][16][180] and it differs from classical wave-physics in that it can even be observed when single particles arrive at the detector one by one. The build-up of such patterns in experiments with electrons has been described as the "most beautiful experiment in physics".[181]–[183] Thus, considerable efforts towards far-field experiments with objects larger than the fullerenes C_{60} and C_{70} have been made within this collaborative research project.

In contrast to the earlier experiments, where ion detectors or mass spectrometric devices were used, the development of far-field setups with fluorescence detection was proposed. The efficiency of setups that are based on ion detection will dramatically decrease when the mass and complexity of the particles increase because of the difficulty of detecting ionized complex molecules. The new idea was to trap fluorescent molecules on a surface and image the interference pattern with the help of fluorescence spectroscopy. The feasibility of this detection scheme was already demonstrated in a near-field TLI with beams of **TPP** and a detection on quartz surfaces.[35]

For the realization of new far-field experiments with fluorescence detection we aimed at new large model compounds with a particular focus on tailor-made optical properties. Perfluoroalkyl functionalization was kept as design concept because it proved its value to provide good beam properties even for large organic molecules. Furthermore, molecules that are fluorescent were crucial for the success of this project. Desirable, but not crucial, was a very low absorption of the new tailor-made molecules at a wavelength of 532 nm. Although it

would not be of relevance in the targeted far-field QIE where a material grating acting as diffraction element is used, a low absorption at 532 nm would theoretically also enable the application of the new model compounds in near-field setups containing an optical phase grating with this wavelength. This would broaden the scope of possible applications.

In the following sections several approaches to meet the requirements of far-field interferometry with detection units based on fluorescence are discussed. Different fluorophores were investigated towards their functionalization with a fluorous shell, and their absorption and emission properties are presented.

5.1   Fluorous Naphthalene Diimides

Suitable model compounds for far-field experiments in an interferometer comprising a thermal source and a detection unit based on fluorescence microscopy on a screen should have the following properties. Firstly, a high volatility to reach the required beam intensities is needed. Secondly, thermal stability to guarantee the flight of intact particles through the interferometer is crucial since, in contrast to MS based interferometers, fluorescence as readout signal to observe the interference pattern cannot unambiguously be attributed to the targeted particle. All fluorescent impurities for example originating from degraded molecule fragments would also cause a signal in the detector. Chemical analysis of the trapped molecules after the quantum interference experiment is a possibility to check the nature of the arriving structures. To broaden the scope of applications the targeted model compound should preferably not or at the least weakly absorb light at a wavelength of 532 nm.

We proposed fluorous core substituted naphthalene diimides (NDIs) to be suitable candidates for such applications. NDIs are widely used in supramolecular chemistry as building blocks for rotaxanes and catenanes,[184]–[186] foldamers,[187][188] and host-guest assemblies.[189] Furthermore, applications in the field of materials chemistry, where NDIs are implemented as components of electronic devices,[190] sensors[191][192] and synthetic biomaterials,[193] are known in the literature.

NDI derivatives without any core substituents are usually colorless and non-fluorescent.[194][195] On the other hand, if donor substituents are present in the 2- and 6-position, NDIs are strongly colored.[196] Furthermore, these compounds are highly fluorescent as long as the substituent is not hetero aryl based.[197] In core substituted NDIs comprising heteroatom-aryl-groups in 2- and 6-position a fast quenching of the fluorescence is observed originating from a charge transfer from the aryl substituent to the naphthyl core.[198] An outstanding property of core substituted NDIs is that the absorption and emission properties can be tuned by the nature of the heteroatom in the 2- and 6-position.[196][197][199]–[202] In contrast to this, functional groups at the imide position have only a negligible influence on the optical properties of NDI dyes.[203]

2,6-Core substituted NDIs are accessible starting from 2,6-dichloronaphthalene-1,4,5,8-tetracarboxylic acid dianhydride (**82**) which itself can be synthesized in four steps from pyrene (**83**) (scheme 37).[200][204] The assembly of NDIs from the dianhydride **82** allows for the introduction of four substituents. The two imide functionalities require amine precursors for the conversion of the dianhydride to the imide functionality. The core functionalization via

nucleophilic aromatic substitution reactions can be realized with various nucleophiles, including thiols, amines and alcohols.[196][197][199]
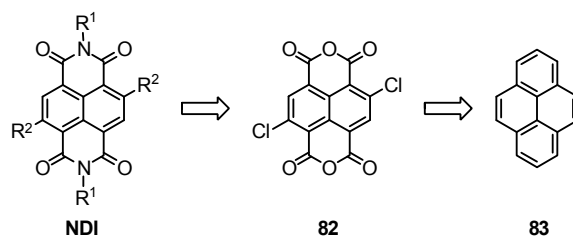
Scheme 37. Synthetic strategy towards core substituted NDIs.

As already mentioned, the absorption bands of core substituted NDIs can be tuned by the nature of the heteroatom linkage. Figure 52 shows the absorption spectra of nitrogen, oxygen and sulfur derived NDI derivatives.[205] Remarkably, the longest wavelength absorption in the visible region is strongly influenced by the nature of the core substituents. The nitrogen derivative **N$_2$NDI**, which is a blue dye, shows a broad band with a maximum at 615 nm and a shoulder at shorter wavelengths. The corresponding band of the red sulfur derivative is shifted hypsochromically as compared to **N$_2$NDI**. The longest wavelength absorption of the yellow dye **O$_2$NDI** is even further shifted to shorter wavelengths.
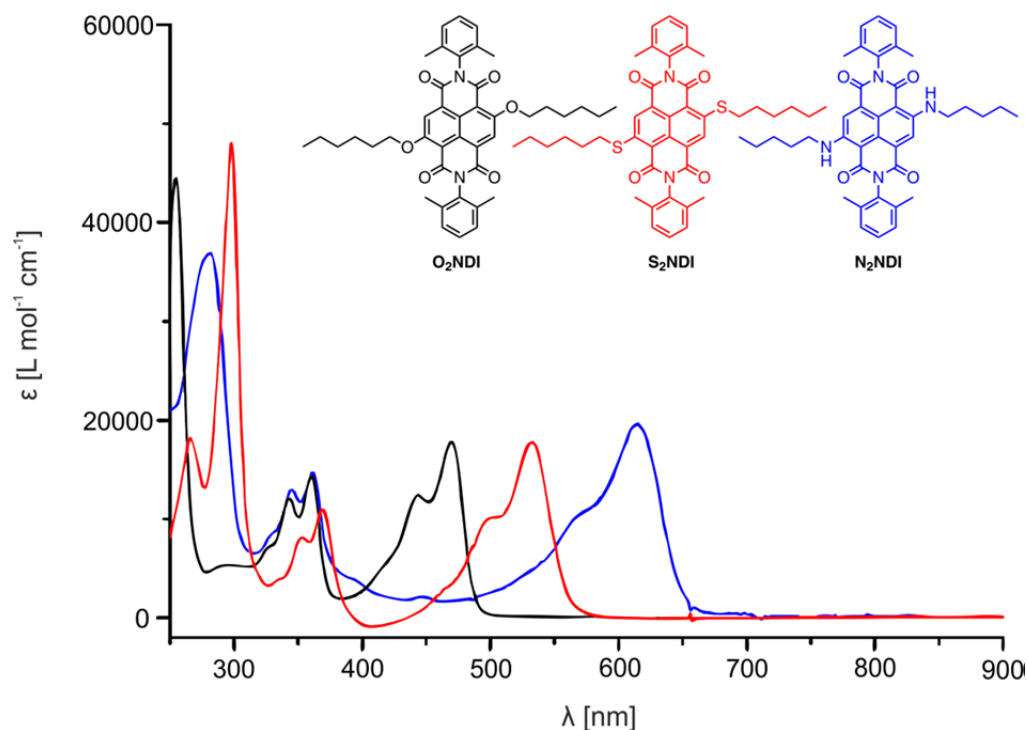

Figure 52. UV/Vis absorption spectra of three core substituted NDIs (sulfur, oxygen and nitrogen substituted) in dichloromethane at room temperature. These NDIs were synthesized and analyzed by Sandro Gabutti in the course of his PhD work in the Mayor group. The spectra were reproduced from reference [205].

For our needs NDIs with a nitrogen substituted core seem to be ideal compounds to meet the requirements described above. With the choice of nitrogen as core substituent it should be possible to shift the absorption band of the model compounds bathochromically enough to have no or only a low absorption at a wavelength of 532 nm and thus to open a wide range of possible applications in far-field as well as near-field interferometers. Oxygen based derivatives were not envisaged. Although their absorption properties are also expected to allow for applications in KDTLI setups with the optical phase grating, alcohols are usually introduced at the core position in rather poor yields.[196] Sulfur substituted NDIs are expected to be exclusively applicable in setups containing material gratings as in the envisaged far-field setup. Nevertheless, these are interesting target compounds because the high nucleophilicity of thiols should enable an efficient introduction of substituents to the NDI core.

The targeted fluorous compounds **84-86** for far-field QIE and their retro syntheses are shown in scheme 38. It was planned to use the fluorous amine **50** as building block for the imide formation in all three cases. This precursor was already synthesized in the course of the porphyrin project (section 4.2) starting from the dibromo derivative **29**. For target structure **84** *n*-pentylamine (**88**) as the nucleophile was proposed for the core substitution. This would lead to a fluorous NDI with a molecular weight of 1 945 g/mol, which would represent a doubling in mass related to the heaviest interfering object in far-field experiments (C_{70} fullerene). By choosing an amine substituted core with solubilizing alkyl chains it was expected to assemble an NDI derivative which is still processable with common organic solvents. Compound **85** with fluorous core substituents would be the next step towards large fluorous NDIs. Target structure **85** with a thioether functional group at the core is presumably not applicable in near-field experiments because of its expected strong absorption at 532 nm. However, this fluorous NDI derivative was aimed at because high yields for the introduction of thiols to the NDI core are expected. The third target structure **86** with a mass of 3 257 g/mol bears identical fluorous moieties in both, the imide and the core position.
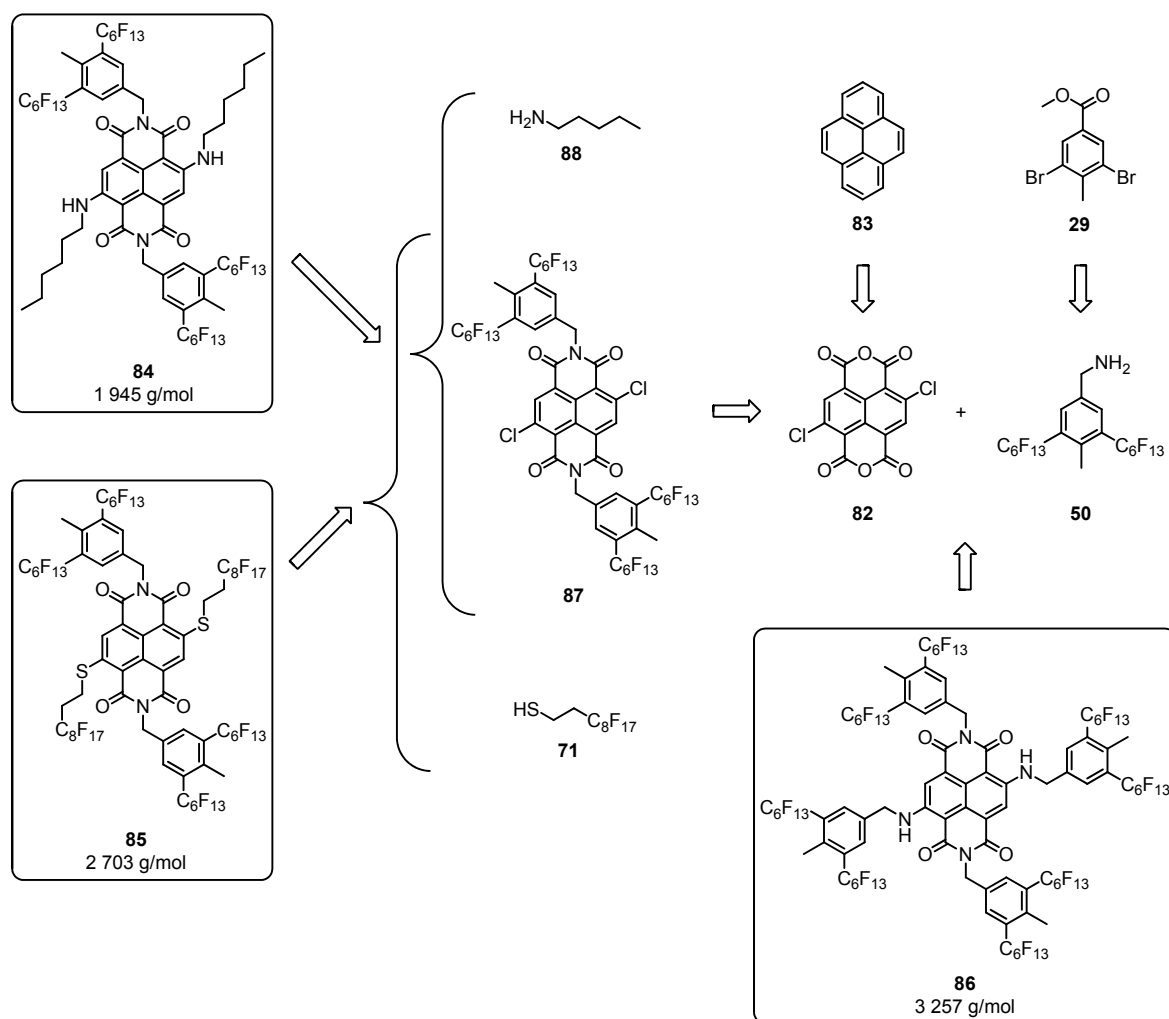
Scheme 38. Synthetic strategy towards the fluorous NDIs **84–86**.

The formation of the imide functionalities was planned to be performed by the reaction of the dianhydride **82** and the amine **50**. For conversions of this type in acidic media, selective reactions of amines with the carbonyl anhydride were observed by Würthner *et al.*.[196] A nucleophilic attack at the core is usually not observed, because in an acidic surrounding the amine functionalities are present in their protonated form. With the dichloro substituted NDI **87** nucleophilic aromatic substitutions were envisaged to introduce the amine **88** or the thiol **71**, respectively, leading to the target structures **84** and **85**. The fluorous NDI **86** was planned to be assembled in one step from the dianhydride **82** and the amine **50**. As both groups in the imide and the core position are identical a two step sequence for their introduction is not necessary.

5.1.1 Synthesis and Characterization

The synthesis of the dichloro substituted fluorous NDI **87** is displayed in scheme 39. The assembly of the amine precursor **50** was already described in section 4.2.3. The amine was synthesized in four steps including the introduction of fluorous chains to the dibromide **29**, reduction to the alcohol, introduction of a protected amine and a final deprotection step.

The free amine **50** was reacted with the dianhydride **82**, which was available in the group of Prof. Mayor, in acetic acid at reflux for 90 minutes. Upon cooling to room temperature a pale orange precipitate formed. After washing with cold acetic acid and water the fluorous NDI **87** was isolated as a pale yellow solid. The product was obtained in a yield of 57% without any further purification and was directly used for the next reaction steps. Compound **87** exhibits a very low solubility in common organic solvents and was exclusively analyzed by MALDI-ToF mass spectrometry. The mass spectrum displayed the molecule ion peak of the desired compound **87**. Furthermore, possible side products originating from a core substitution can be excluded as these species would be strongly colored and the obtained product showed only a pale yellow color.
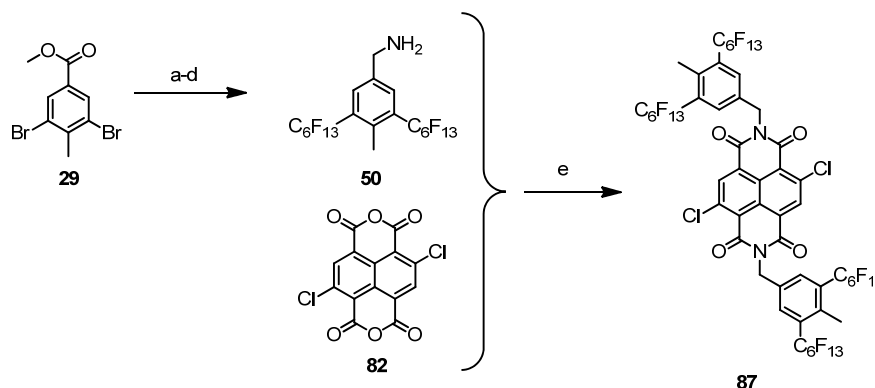
Scheme 39. Synthesis of the fluorous NDI **85**. *Reagents and conditions*: (a) IC_6F_{13}, Cu, DMF, 120 °C, 12 h, 91%; (b) $LiAlH_4$, Et_2O, rt, 16 h, 90%; (c) phthalimide, DIAD, PPh_3, THF, -5 °C to rt, 12 h, 87%; (d) hydrazine hydrate, EtOH, toluene, reflux, 12 h, quant.; (e) AcOH, reflux, 1.5 h, 57%.

The target compound **84** was assembled by the reaction of the fluorous NDI **87** with neat *n*-pentylamine (**88**) acting as solvent and reactant as shown in scheme 40. Stirring of compound **87** in *n*-pentylamine at room temperature led to a red reaction mixture. This indicates the substitution of one chloro substituent by *n*-pentylamine. Obviously the second chlorine is considerably less reactive as compared to the first one. Substitution at the second core position was only achieved when heating to 85 °C for 30 minutes. The color of the reaction mixture turned from red to blue. After cooling to room temperature, the crude was dissolved in dichloromethane, absorbed on silica gel and purified by column chromatography

using silica gel and a solvent mixture of dichloromethane and hexane (1:1). Target structure **84** was isolated as a blue solid in a yield of 72%. The purification of several hundred milligrams of the target structure, which are necessary for QIE with the current thermal source, was very laborious. The low solubility of the compound necessitated that the crude was divided into smaller portions and purified chromatographically by multiple columns.
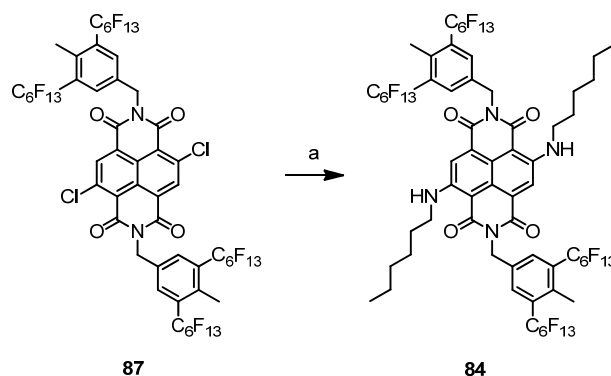
Scheme 40. Synthesis of the fluorous NDI **84**. *Reagents and conditions*: (a) *n*-pentylamine (**88**), 1.) rt, 15 min, 2.) 85 °C, 30 min, 72%.

For the characterization by nuclear magnetic resonance spectroscopy, ^{1}H- and ^{19}F-NMR spectra were recorded in deuterated benzene with several thousand scans. Furthermore, the fluorous NDI **84** was analyzed by MALDI-ToF MS, which shows exclusively the molecule ion peak, and UV/Vis and fluorescence spectroscopy. The UV/Vis spectrum in dichloromethane shows the expected bands with the longest wavelength absorption having a maximum at 623 nm and a shoulder at 580 nm. The absorption at 532 nm is low, which, in principle, enables quantum experiments in a KDTLI. Excitation at the three absorption maxima 364 nm, 580 nm and 623 nm, respectively, leads to an emission at 648 nm. The strongest fluorescence was observed for the excitation at 623 nm.

Sublimation tests were performed in the laboratories in Basel. Heating to 200 °C at a pressure of 0.05 mbar did not lead to observable sublimation of the blue dye **84**. However, it was shown that the compound is stable under these conditions.
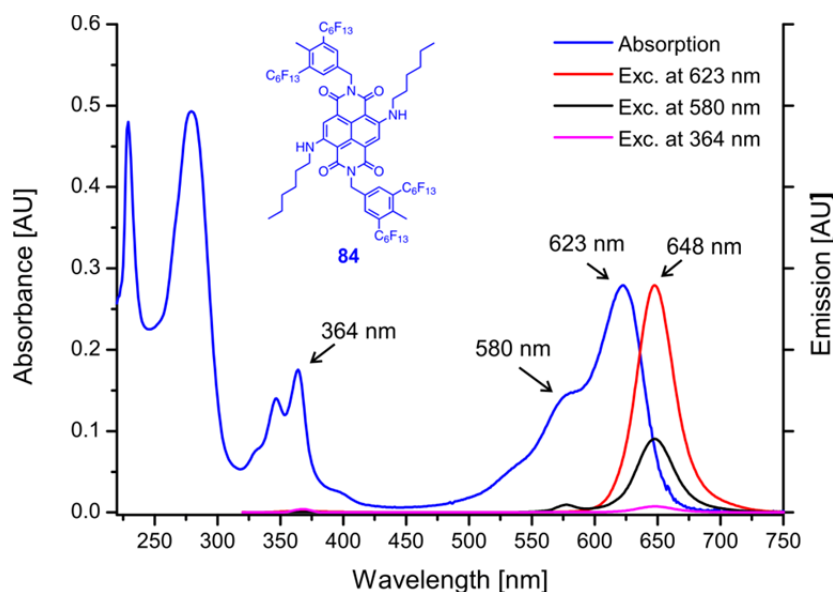
Figure 53. Absorption and emission spectra of NDI **84** ($c \approx 1 \times 10^{-5}$M) in dichloromethane at room temperature. The absorption is shown in blue. The emission is shown in red (excitation at 623 nm), black (excitation at 580 nm) and pink (excitation at 364 nm).

As next step it was tried to assemble the thiol derived NDI **85**. A suspension of the diimide derivative **87**, potassium carbonate as base and the fluorous thiol **71** in DMF was stirred under an atmosphere of argon at room temperature for 12 hours. Already after a few minutes the reaction mixture turned from colorless to red. The red color clearly indicates the formation of the doubly thiol substituted desired product. After cooling to room temperature a triphasic extraction using water, dichloromethane and perfluorohexane (FC-72) was performed. The dark red colored fluorous phase was evaporated to dryness and the crude was purified by column chromatography using silica gel and a solvent mixture of ethyl acetate and hexane (1:5). According to TLC the sample obtained after column chromatography still contained various impurities. Numerous other eluents were tested to purify the mixture but none of them yielded the pure NDI **85**.
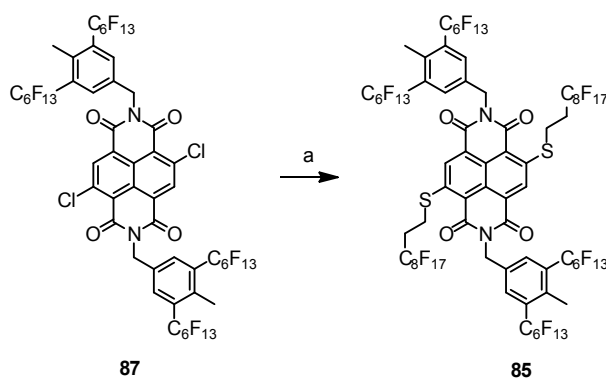
Scheme 41. Synthesis towards the fluorous NDI **85**. *Reagents and conditions*: (a) 1*H*,1*H*,2*H*,2*H*-perfluorodecanethiol (**71**), K$_2$CO$_3$, DMF, rt.

It was then attempted to purify NDI **85** with the help of fluorous reversed phase silica gel, which is able to separate compounds primarily according to their fluorine content. The silica gel was obtained from the group of Prof. Bannwarth from the University of Freiburg, Germany. As shown in figure 54A, the FRPSG, which was prepared by Dr. Hartmut Rapp, comprises perfluorohexyl chains.
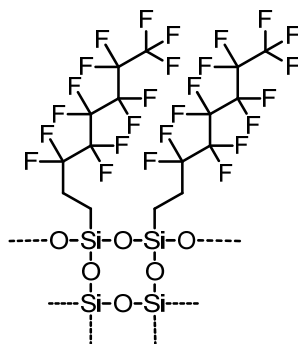
Figure 54. Structure of the fluorous reverse phase silica gel (FRPSG) from the research group of Prof. Bannwarth.

The impure sample was absorbed on the FRPSG using diethylether. The column was conditioned with a 1:1 mixture of acetonitrile and diethylether. The content of the fluorophilic eluent diethylether was gradually increased from 50% to 100%. With this gradient a separation of a yellow impurity from the red product was achieved. However, a large quantity of the deposited sample was still on the column even after elution with pure diethylether. By elution with perfluorohexane the residual product was washed from the column. As indicated by TLC analysis (silica gel, dichloromethane/hexane 1:1), all obtained fractions contained still some impurities. The findings from the TLC analysis were also corroborated by MALDI-ToF mass spectrometric analysis. The spectrum showed, besides the molecule ion peak of the desired structure **85**, additionally the peak for the mono core substituted side product. The main drawback, which made an efficient purification of the target structure very difficult, was the very low solubility of the product in common organic solvents. Chromatography with FRPSG was developed to effectively separate fluorine containing species that are still soluble in common organic solvents. The high elution power of fluorous solvents, which are suitable solvents for our target structures, is too strong for the use in chromatography with FRPSG. To sum up, the substitution reaction with fluorous thiols at the core of the fluorous NDI **87** took place, but the obtained product suffers from its very low solubility in non-fluorous solvents and was thus not isolated as a pure compound.

As already mentioned, the fluorous NDI **86** can be synthesized in one step starting from the dianhydride **82** and the amine **50**. Microwave conditions were chosen to assemble target

structure **86** (scheme 42). The reaction of the amine **50** and the dianhydride **82** was performed in DMF. After a reaction time of 10 minutes at a temperature of 180 °C, the reaction was stopped and the conversion was checked by TLC. After an additional 10 minutes at 200 °C the dark blue reaction mixture was worked up. A biphasic liquid-liquid extraction using water and perfluorohexane was performed, followed by purification by column chromatography using the F-hexyl functionalized silica gel.
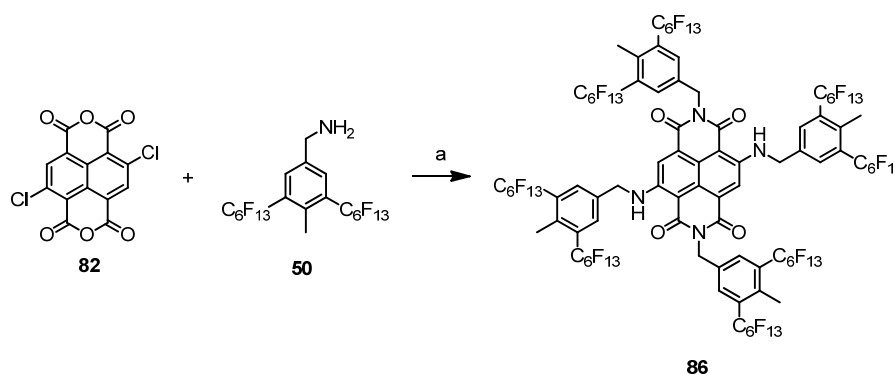
Scheme 42. Synthesis towards the fluorous NDI **86**. *Reagents and conditions*: (a) DMF, microwave irradiation, 1.) 180 °C, 10 min; 2.) 200 °C, 10 min.

Figure 55A displays the eluent gradient of the performed column with the FRPSG. In figure 55C the corresponding TLC analysis (silica gel, dichloromethane/hexane 1:1) of the obtained fractions is shown. As indicated by TLC most of the impurities could be removed. However, the product containing fraction still showed additional spots on the TLC. The presence of side products was corroborated by MALDI-ToF MS. Besides the signal for the molecule ion of the targeted NDI **86**, a small signal of the threefold substituted derivative was also found. In the ^{1}H-NMR spectrum all expected signals of the product were found. However, a competent knowledge about the purity of the compound was not obtained from these analytical data. Thus, it was decided not to send a sample of this compound to the Arndt group for QIE.
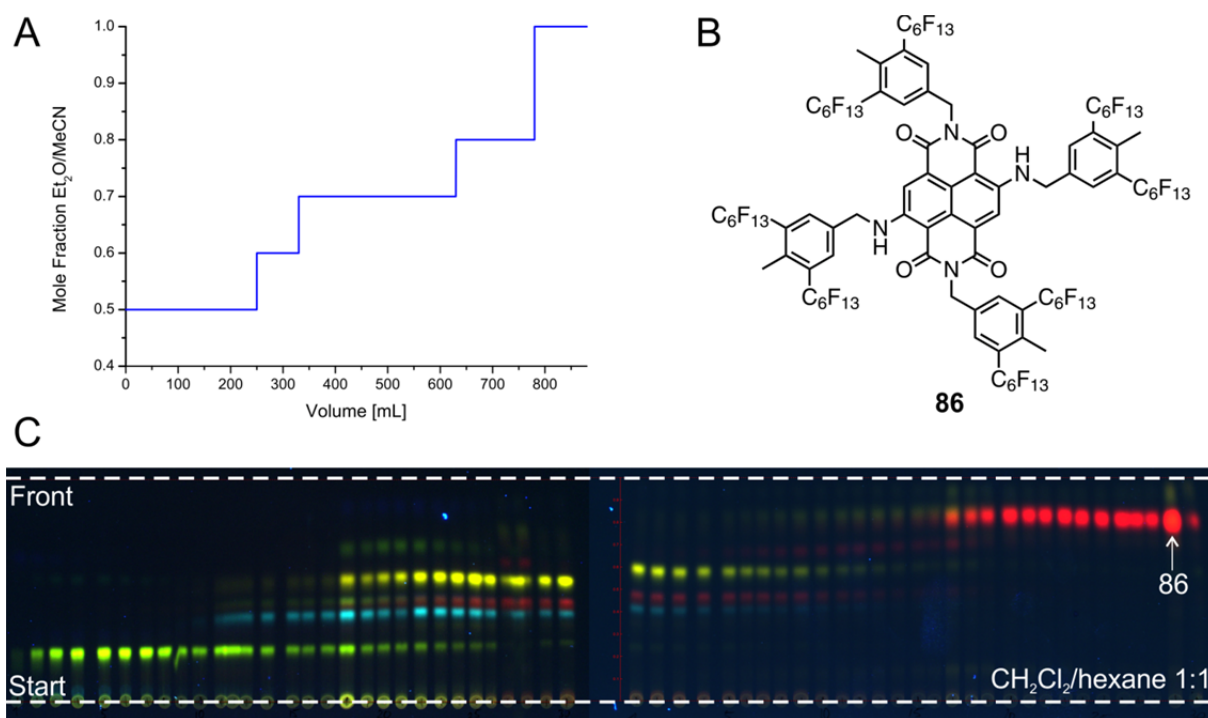
Figure 55. (A) Eluent gradient of the attempted purification of NDI **86** using FRPSG. (B) Chemical structure of the target NDI **86**. (C) Photograph of the TLC plates (silica gel, dichloromethane/hexane 1:1) when irradiating with light at 366 nm.

The synthetic efforts towards the fluorous NDI derivatives **84-86** clearly showed that the very low solubility in common organic solvents does not allow for the efficient synthesis and purification of these compounds in quantities that are required for the envisaged QIE. Exclusively NDI **84** was successfully prepared in sufficient quantities. However, the purification was laborious as multiple columns with small portions of the crude were necessary. NDI **84** was characterized by ^{1}H- and ^{19}F-NMR, UV/Vis and fluorescence spectroscopy, and MALDI-ToF mass spectrometry.

5.1.2 Quantum Interference Experiments

The NDI **84** was sent to the group of Prof. Arndt for the envisaged far-field matter-wave experiments. Numerous experiments in an interferometer with a thermal source and a fluorescence microscope at the detector level were performed. Although fluorescent particles were detected with the help of the fluorescence microscope, it was not possible to observe interference patterns and thus the wave nature of the NDI **84**. A possible reason for the failure of these experiments could be a degradation of the NDI **84** during the evaporation process. When particles of different kinds fly through the interferometer, each of them can interfere with itself. However, an interference pattern can only be observed if the vast majority of

interfering particles has an identical mass and velocity, and therefore produces a consistent interference pattern.

5.1.3 Conclusion

Fluorous naphthalene diimides derivatives seemed to be suitable model compounds for far-field matter-wave interferometry. With tunable absorption and emission properties and four possible positions where functionalization with fluorous moieties is possible, these structures were very appealing for our purposes. However, the very low solubility of the compounds made it impossible to isolate large fluorous NDIs purely and in sufficient quantities for our needs. Exclusively the smallest NDI of our proposed structures was successfully prepared. It was isolated in quantities of several hundreds of milligrams and showed the expected absorption and fluorescence properties. The far-field QIE with this model compound did not yield the desired quantum interference pattern. It was assumed that fragmentation of the molecules, which possibly occurred during the thermal evaporation process, is responsible for the failure of the experiments.

5.2   Fluorous Metalloporphyrins

Fluorescence imaging of interference patterns is a very promising detection technique for future QIE with large organic molecules. Trapping of molecules on a surface gives the possibility to simultaneously record the interference pattern of molecules having different velocities during their flight through the interferometer. The trajectory of the particles is influenced by the Earth's gravitational field and is defined by their velocity. A crucial point for the quality of the readout of the fluorescence signal is the mobility of the molecules on the surface. As the fluorescence readout has to be integrated over a certain period of time a strong movement of molecules on the surface would lead to a loss of the initial position information of the molecules and thus would make it impossible to observer interference patterns.

Porphyrin derivatives are sufficiently fluorescent to be detectable in QIE with the help of the discussed method. In 2005, Stibor *et al.* described fluorescence imaging of near-field interference patterns of **TPP** on quartz surfaces.[35] The mobility of these molecules was obviously low enough for successful QIE. Our approach to use highly fluorinated compounds aims at minimizing the intermolecular forces in order to provide high volatilities. However, this concept not only leads to good beams properties, at the same time, it increases the surface mobility of the molecules by lowering the interaction between the molecules and the surface. One approach to solve this issue was presented in 2010 by Dreas-Wlodarczak *et al.*.[58] The idea was to immobilize the fluorescent dyes by a strong metal ligand binding on a surface. Zinc porphyrins are able to axially coordinate to nitrogen atoms of heterocycles.[206][207] This binding motif was already used to immobilize metalloporphyrins on surfaces including silica[208] and gold[209] surfaces, and TiO_2 nanoparticles.[210] Dreas-Wlodarczak and coworkers successfully demonstrated the immobilization of zinc tetraphenylporphyrin (**ZnTPP**) to pyridine functionalized glass surfaces by complex formation providing a spatial resolution of the fluorescence detection which allows for far-field QIE.

Our ambition was now to combine the two concepts of perfluoroalkylation of model compounds and the immobilization of metalloporphyrins on pyridine functionalized surfaces. Both concepts already proved their bests but were never realized in one single experiment. Thus we proposed the fluorous zinc porphyrin **89** for the described experiments. Its synthesis is shown in scheme 43. The attachment of the fluorous ponytails to the free base porphyrin **TPPF20** was already described in section 4.2.3. The nucleophilic aromatic substitution reaction led to the intensely colored purple porphyrin **40** in a yield of 81%. The zinc insertion was performed in a solvent mixture of chloroform and methanol and zinc acetate as metal

source. Stirring for 40 hours at room temperature and additional 5.5 hours at a temperature of 45 °C afforded the metalloporphyrin **89** after purification by column chromatography as a pink solid in a yield of 93%.
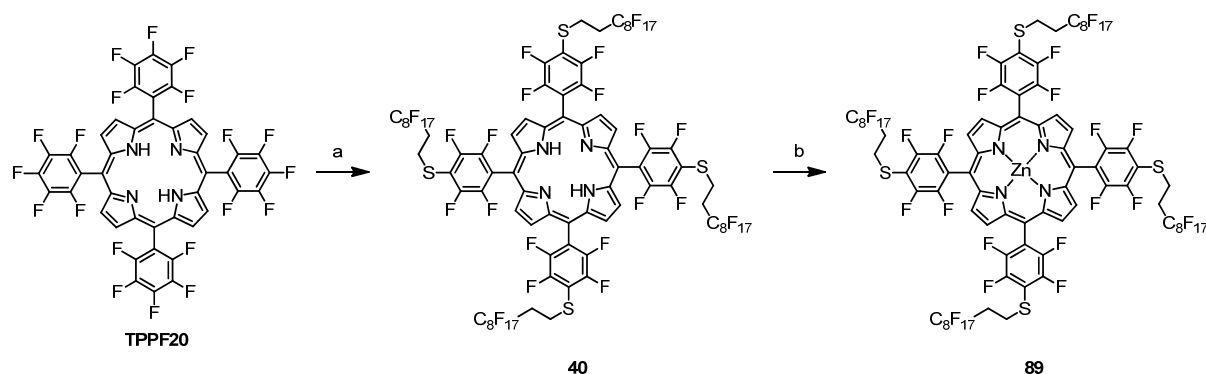
Scheme 43. Synthesis of the fluorous zinc porphyrin **89**. *Reagents and conditions*: (a) 1*H*,1*H*,2*H*,2*H*-perfluorodecanethiol (**71**), ethyl acetate, DMF, HNEt$_2$, rt, 1.5 h, 81%; (b) Zn(OAc)$_2$, MeOH, CHCl$_3$, 1.) rt, 40 h 2.) 45 °C, 5.5 h, 93%.

The metallated porphyrin **89** was characterized by NMR spectroscopy (^{1}H and ^{19}F), mass spectrometry (MALDI-ToF), elemental analysis, and UV/Vis and fluorescence spectroscopy. The mass spectrum of the target compound shows exclusively the molecule ion peak. From the ^{1}H-NMR spectra it is furthermore evident that the two hydrogens at the central nitrogens were replaced by the metal as these proton signals disappeared. The absorption and emission spectra of the zinc porphyrin **89** are displayed in figure 56. The absorption spectrum (shown in blue) shows a very strong Soret band at 416 nm. In contrast to the four Q bands observed for the free base porphyrins described in section 4.2, the zinc porphyrin **89** has only two Q bands at 544 nm and 578 nm . The reduced amount of Q bands is due to the higher symmetry of this metalloporphyrin (D$_{4h}$) as compared to the free base derivatives (D$_{2h}$). Qualitative fluorescence investigations revealed emissions at 595 nm and 647 nm when irradiating at 416 nm (shown in red) and 544 nm (shown in green), respectively.

With the described optical properties, zinc porphyrin **89**, which can be synthesized in gram quantities, is a promising candidate for the envisaged QIE. The fluorescent compound could be excited with a green laser in the region of the high energy Q band (544 nm) for the detection in the interferometer setup as was done in the studies of Dreas-Wlodarczak and coworkers with **ZnTPP**.[58] Although the conditions in the interferometer differ from the situation of the spectroscopic analyses that were performed in solution, only slight changes in the optical properties are expected for compound **89** deposited on a surface and with an axial coordination of the zinc to a pyridine ligand.[58][211]
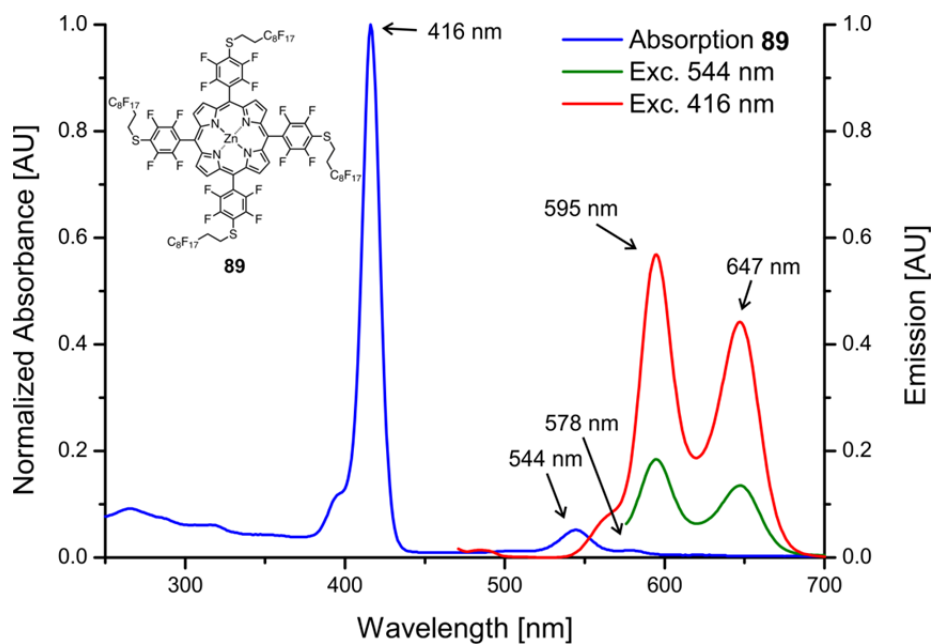
Figure 56. Absorption and emission spectra of the zinc porphyrin **89** in dichloromethane at room temperature.

The synthetic part of this project was completed. The quantum experiments with the metalloporphyrin **89** are still ongoing and results are not yet available.

5.3 Fluorous Phthalocyanines

Besides naphthalene diimide and metalloporphyrin derivatives as model compounds for far-field experiments we set our synthetic efforts on new fluorous phthalocyanine derivatives. This compound class has played a very important role in dye industry. Since the start of the technical production of copper phthalocyanine in the 1930s these pigments have constantly been used in the class of blue colorants. In addition to their interesting photophysical properties, the high chemical and thermal stability made them appealing industrial dyes. Various metallophthalocyanine are known to be sublimable *in vacuo* at temperatures between 550 °C and 600 °C without degradation.[212]

Besides the huge field of applications as dyes, phthalocyanine derivatives are nowadays also used as catalysts,[213] as components in dye-sensitized solar cells,[214] and as photosensitizers in photodynamic therapy (PDT) for cancer treatment.[215][216] Several examples of perfluoroalkyl functionalized phthalocyanines are also known in the literature.[217]–[220] Qiu *et al.* prepared fluorous derivatives as catalysts for oxidations using the concept of fluorous biphasic catalysis (FBC).[221] Other studies revealed the potential of fluorous phthalocyanines as photosensitizers for PDT.[222][223] Pozzi *et al.* reported on fluorinated phthalocyanines and their implementation in solar cells.[224]

Appealing absorption and emission properties, and a high stability made fluorous phthalocyanines promising candidates to reach our goal of increasing the mass record in far-field QIE using a fluorescence-based interferometer setup. Figure 57 shows the envisaged three target structures. They share the phthalocyanine motif and the fluorous periphery. Different central atoms, including zinc, magnesium and the hydrogenated derivative, were chosen in order to have model compounds with varying physical properties. The optical properties, including the fluorescence behavior, as well as the stability and solubility features are expected to be considerably influenced by the central atom.[225] As the success of the interference experiments is strongly dependent on the described properties, the phthalocyanine approach, where all these features can be altered by the change of the central atom, is particularly appealing.

F24PcH2, M = 2H, M$_W$ = 1 299 g/mol
F24PcMg, M = Mg, M$_W$ = 1 321 g/mol
F24PcZn, M = Zn, M$_W$ = 1 362 g/mol
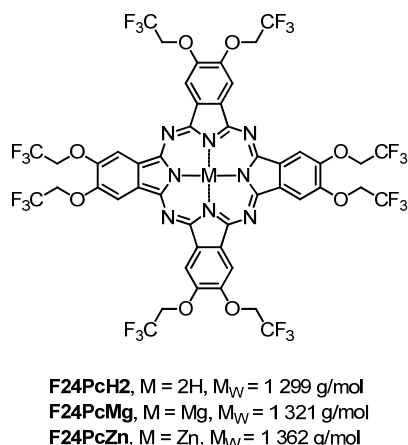
Figure 57. Structures of the envisaged fluorous phthalocyanine derivatives **F24PcH2**, **F24PcMg** and **F24PcZn** for far-field QIE. The preexisting mass record was held by the fullerene C$_{70}$ with a molecular weight of 841 g/mol.

5.3.1 Synthetic Strategy

Numerous synthetic methods for the preparation of phthalocyanines are known.[226][225] Possible precursors are exemplarily phthalamides, phthalimides, phthalic anhydrides or phthalonitriles. Conventional methods include reactions in solvent and solvent-free conditions. Our synthetic strategy towards the three envisaged octa-substituted phthalocyanine derivatives is depicted in scheme 44. 4,5-Dichlorophthalonitrile (**91**) was chosen as a starting point for our route towards the target compounds. In a first step the two chloro-substituents were planned to be substituted by 2,2,2-trifluoroethanol. With the fluorous phthalonitrile **90** in hand, metal promoted cyclotetramerization reactions to form the metallophthalocyanines **F24PcMg** and **F24PcZn** were planned. Metal-free phthalocyanines can also be directly synthesized from phthalonitrile derivatives, but often only low yields are reported for the cyclotetramerization reactions when no coordinating metal ions are involved.[227]–[229] Thus, we intended the formation of the free base derivative **F24PcH2** in a demetallation reaction from one of the two target compounds **F24PcMg** and **F24PcZn**.
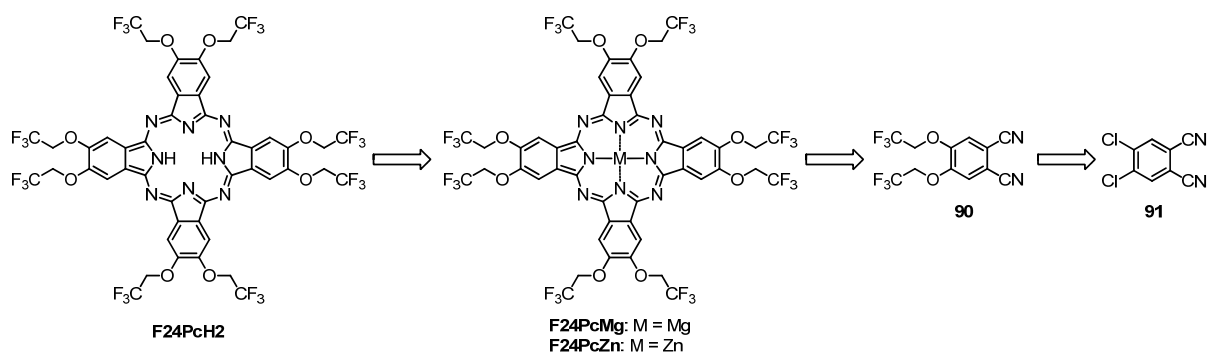
Scheme 44. Synthetic strategy towards the three fluorous phthalocyanines **F24PcH2**, **F24PcMg** and **F24PcZn**.

5.3.2 Synthesis and Characterization

The synthesis of the target structures **F24PcH2**, **F24PcMg** and **F24PcZn** is shown in scheme 45. The nucleophilic aromatic substitution reaction between 4,5-dichlorophthalonitrile (**91**) and 2,2,2-trifluoroethanol was effectively carried out under microwave heating. Compound **91** was reacted with four equivalents of the alcohol and six equivalents of potassium carbonate in DMSO at a temperature of 100 °C for one hour. An aqueous workup and purification by column chromatography afforded the fluorous phthalonitrile **90** as a white solid in a yield of 88%. For the buildup of the phthalocyanine framework, we used a solvent/base system which was described by Wöhrle *et al.* for the synthesis of various unsubstituted and substituted phthalocyanine derivatives.[230] In their work phthalonitrile precursors were reacted in penaton-1-ol, which has a boiling point of 138 °C, at reflux in the presence of the strong organic base DBU. They showed that the use of alcohols with lower boiling points as solvent and weaker bases gave much lower yields. For the assembly of the zinc phthalocyanine derivative **F24PcZn**, we used this solvent/base combination but applied microwave heating to reach higher reaction temperatures. Phthalonitrile **90**, 0.25 equivalents of zinc acetate and one equivalent of the base DBU were heated in pentan-1-ol in a microwave apparatus to 170 °C for 12 hours. After an aqueous workup and purification by column chromatography the product **F24PcZn** was obtained as a blue solid in a yield of 78%. Similarly, the magnesium derivative **F24PcMg** was synthesized using magnesium dichloride as the metal source. Identical reaction conditions as compared to the zinc derivative led after purification by column chromatography to the target structure **F24PcMg** as a blue solid in a yield of 49%. The free base phthalocyanine **F24PcH2** was prepared by the demetallation of the zinc derivative **F24PcZn**. A general procedure for the demetallation of zinc phthalocyanines developed by Alzeer *et al.* was used for this reaction step.[231] The zinc

derivative **F24PcZn** was reacted with pyridine hydrochloride in pyridine at a temperature of 120 °C for 18 hours. The blue dye **F24PcH2** precipitated while cooling to room temperature. It was collected by centrifugation and washed with numerous solvents to afford pure free base phthalocyanine **F24PcH2** as a blue solid in a yield of 76%.
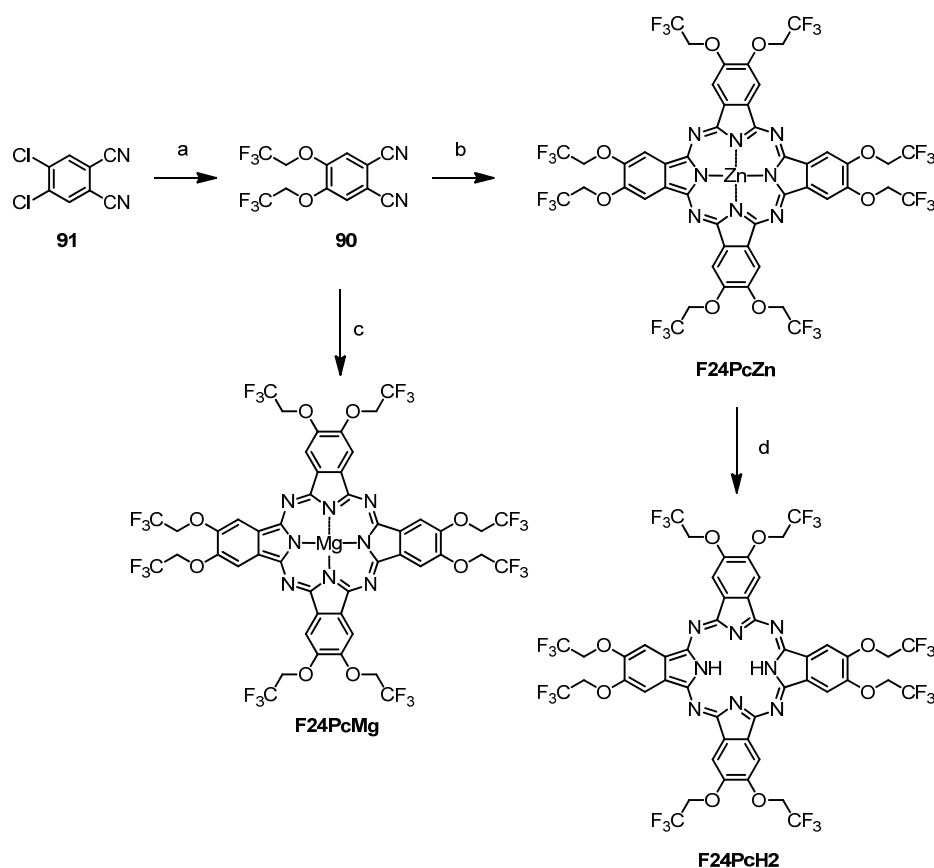
Scheme 45. Synthesis of the fluorous phthalocyanines **F24PcH2**, **F24PcMg** and **F24PcZn**. *Reagents and conditions*: (a) HOCH₂CF₃, K₂CO₃, DMSO, microwave irradiation, 1 h, 100 °C, 88%; (b) Zn(OAc)₂, DBU, pentan-1-ol, microwave irradiation, 12 h, 170 °C, 80%; (c) MgCl₂, DBU, pentan-1-ol, microwave irradiation, 12 h, 170 °C, 49%; (d) pyridine·HCl, pyridine, 18 h, 120 °C, 76%.

The two metallophthalocyanines **F24PcMg** and **F24PcZn** are passably soluble in common organic solvents and were characterized by NMR (^{1}H- and ^{19}F-), UV/Vis and fluorescence spectroscopy, and mass spectrometry (MALDI-ToF). The mass spectrum of **F24PcZn** is shown in figure 58A. It shows exclusively the signal of the molecule ion at $m/z = 1\,360$ and is well resolved (figure 58B). The signal pattern found matches very well with the calculated isotopic pattern for the sum formula $C_{48}H_{24}F_{24}N_8O_8Zn$, which is depicted in figure 58C.
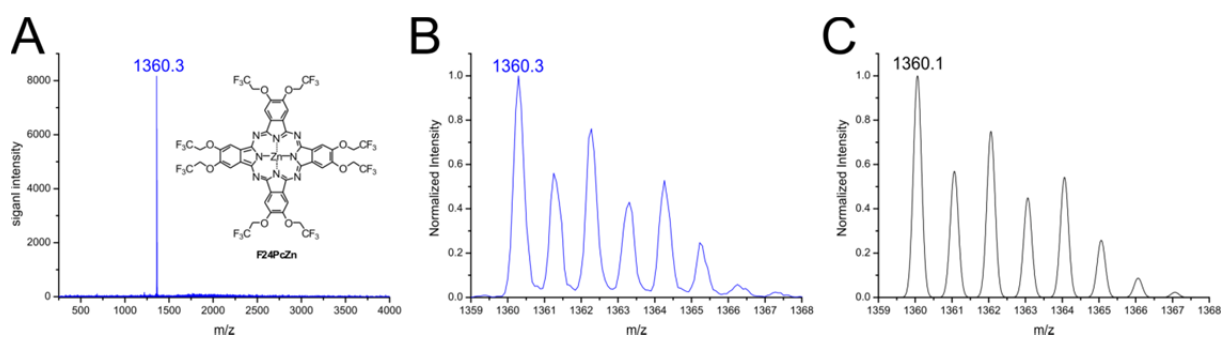
Figure 58. (A) Complete MALDI-ToF mass spectrum of **F24PcZn**. (B) MALDI-ToF mass spectrum of **F24PcZn** between m/z = 1359 and m/z = 1368. (C) Calculated isotopic pattern for the sum formula $C_{48}H_{24}F_{24}N_8O_8Zn$.

The absorption and emission spectra of the target structures **F24PcZn** and **F24PcMg** in acetone are shown in figure 59. The absorption spectra show the characteristic bands for metallophthalocyanines. The B bands are located at 360 nm (**F24PcZn**) and 356 nm (**F24PcMg**), respectively. A very intense narrow band at 664 nm for **F24PcZn** and 663 nm for **F24PcMg** can be found in the Q band region between 600 nm and 700 nm. When exciting at the wavelength of the Q and B band absorption maxima, fluorescence emission was observed. The emission wavelength of **F24PcZn** lies at 682 nm and a Stokes shift of 14 nm leads to an emission at 677 nm for the compound **F24PcMg**.
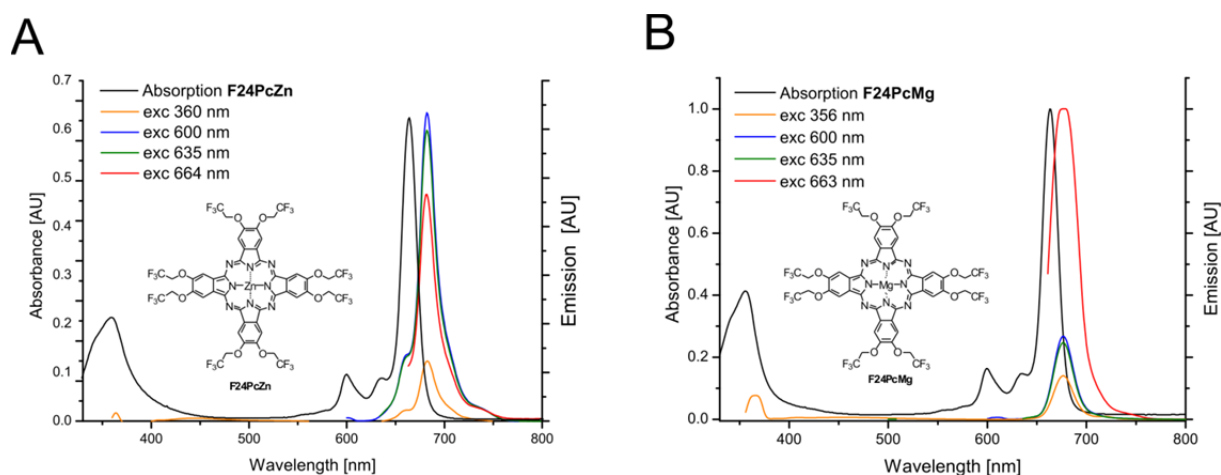
Figure 59. Absorption and emission spectra of the metallophthalocyanine derivatives **F24PcZn** and **F24PcMg** in acetone at room temperature. (A) Spectra of **F24PcZn**. (B) Spectra of **F24PcMg**.

In contrast to the metallophthalocyanines **F24PcMg** and **F24PcZn**, the metal-free derivative **F24PcH2** is completely insoluble in common organic solvents and was thus exclusively characterized by solid-state analytical methods like MALDI-ToF mass spectrometry and elemental analysis.

5.3.3 Quantum Interference Experiments

Samples of all three target structures **F24PcH2**, **F24PcMg** and **F24PcZn** were provided for far-field interference experiments at the University of Vienna. The free base phthalocyanine **F24PcH2** showed the best results in experiments in the laboratories of the Arndt group. Thus, exclusively the quantum interference of this tailor-made fluorous phthalocyanine is described here. In addition to the highly fluorinated derivatives, which were prepared in our laboratories, commercially available phthalocyanine **PcH2** with a molecular weight of 515 g/mol was also investigated in a series of far-field matter-wave interference experiments with the new setup. The two compounds, whose wave nature is discussed here, are depicted in figure 60.
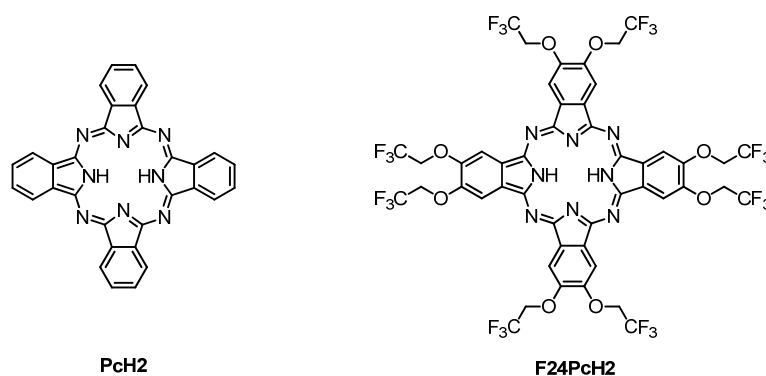
Figure 60. Structures of two phthalocyanines that were investigated in far-field QIE in the laboratories of Prof. Arndt in Vienna. **PcH2** is commercially available, whereas **F24PcH2** was synthesized in three reaction steps.

The extension of far-field diffraction to large molecules requires a sufficiently intense and coherent beam of slow and neutral molecules, a nanosized diffraction grating and a detector with both a spatial accuracy of a few nanometers and a molecule specific detection efficiency of close to 100%.

Besides the integration of fluorescence microscopy as detection unit in the new setup, a second important development was crucial for the success of the experiments. An alternative evaporation method was implemented. So far, thermal evaporation from a Knudsen cell was performed to create molecule beams. However, for thermo-labile compounds, a milder technique, namely laser evaporation, was applied.

The whole interferometer setup is shown in figure 61. It is divided into three parts: the beam preparation, coherent manipulation and detection. The molecules have to be prepared such that each of them interferes with itself and that all of them lead to similar interference patterns on the screen. For thermo-labile organic molecules which may decompose when heated to

their evaporation temperature a laser micro-source (figure 61a) which reduces the heat-load to a minimum was implemented. A blue diode laser (445 nm) is focused onto a thin layer of molecules deposited on the inside of the entrance vacuum window W_1. Although high temperatures can be reached locally, this affects only the particles within the focus area. In comparison to a Knudsen cell the heat-load to the sample is thus reduced considerably. Note that although highly fluorescent dyes are needed for a successful detection of the interference pattern, at the evaporation stage, a strong fluorescence emission after excitation with the laser would lead to a cooling of the molecules on the window W_1 and thus hinder their evaporation. Therefore the wavelength of the evaporation laser was chosen to be 445 nm which does not cause a considerable fluorescence emission at the source when using the phthalocyanine derivative **F24PcH2**. Stable molecules can be evaporated in a Knudsen cell as shown in figure 61b. The collimation slit S defines the spatial coherence of the molecular beam. The slit and the grating width further downstream narrow the beam divergence to less than the diffraction angle θ. The silicon nitride grating G has a period of d = 100 nm. In order to minimize the dispersive van der Waals interaction between the molecules and the grating wall the grating thickness was reduced from 160 nm in earlier diffraction experiments[11][19] to as little as 10 nm in the present setup. Each individually diffracted molecule finally arrives at the 170 μm thin quartz plate W_2 that seals the detector vacuum chamber against the ambient air. The gradual emergence of the quantum interference pattern is then observed in wide-field fluorescence microscopy of W_2. Spectral coherence is achieved by sorting the arriving molecules according to their longitudinal velocity and their respective free-fall height in the Earth's gravitational field.
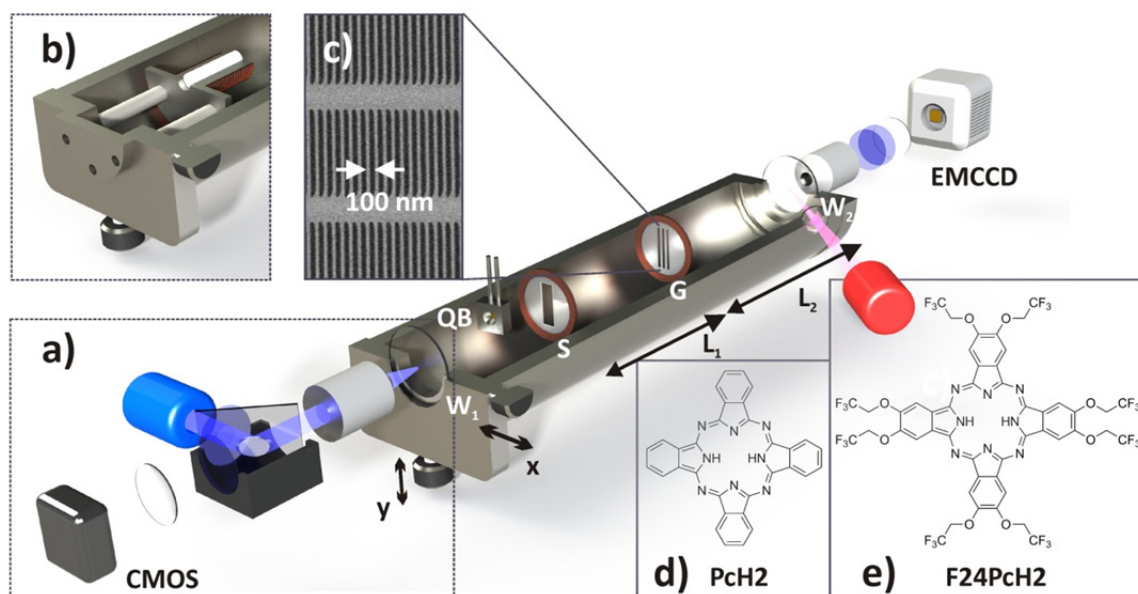
Figure 61. Setup for the laser-evaporation, diffraction and nanoimaging of complex molecules (a) Thermo-labile molecules are ejected by laser micro-evaporation: A blue diode laser (445 nm, 50 mW) is focused onto the window W_1 to evaporate the molecules that are coated on its inner surface. A CMOS camera and a quartz balance (QB) monitor the evaporation area and the molecular flux. (b) Stable molecules can be evaporated in a Knudsen cell. The collimation slit S defines the beam coherence. The grating has a period of d = 100 nm. (c) The vacuum system is evacuated to 10^{-8} mbar. The molecules on the quartz window W_2 are excited by a red diode laser (661 nm). High-resolution optics collects, filters and images the light onto an EMCCD camera. The molecules used in this study are (d) phthalocyanine derivatives **PcH2** and (e) **F24PcH2**.

The detection efficiency of the here described fluorescence detection exceeds that of electron-impact quadrupole mass spectrometry (EI-QMS) by more than a factor 100. This large gain allowed for the first time to optically visualize the real-time build-up of a 2D quantum interferogram from stochastically arriving single molecules, as shown in figure 62. This series was recorded with beams of **PcH2**, which were created in an effusive source (figure 61b) at temperatures of 750 K. A typical velocity of 150 m/s then corresponds to a de Broglie wavelength of $\lambda_{dB} = 5.2$ pm.
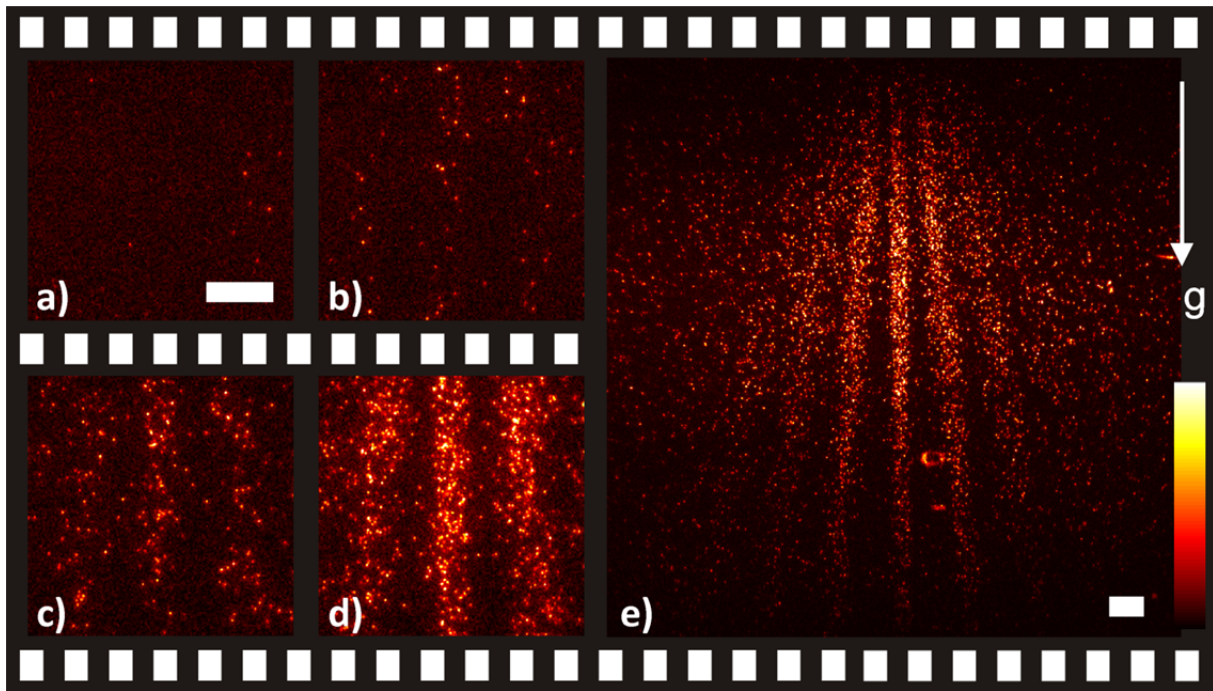
Figure 62. Nanoimaging is the key to visualizing the build-up of a deterministic interference pattern from stochastically arriving single molecules. The images were recorded a) before deposition and after **PcH2** deposition for b) 2 min, c) 20 min, d) 40 min and e) 90 min. The scale bar in figure 62e is 20 μm wide. The color bar ranges from 0 to 100 photons for (a-d) and from 0 to 600 photons in e).

The distance between the interference maxima on the screen can be easily calculated when using the assumption of arriving planar wave fronts (far-field approximation). Constructive interference, and thus an interference maximum, is observed if the path difference of waves equals to a multiple of the wavelength λ. As shown in figure 63, the following two relations hold:

$$\tan \theta = \frac{x}{L} \qquad\qquad 5.1$$

and

$$\sin \theta' = \frac{\lambda}{d} \qquad\qquad 5.2$$

In these equations θ is the angle to the first order diffraction maximum, x the distance between the interference maxima, L the distance between the grating and the screen, d the grating period and λ the wavelength. Considering that $L \gg d$ leads to the assumption that $\theta \approx \theta'$. For angles close to zero, trigonometric functions can be generally approximated as following:

$$\tan \alpha = \sin \alpha = \alpha \qquad\qquad 5.3$$

with α being the angle in radians. With this small angle approximation a simplification of the above mentioned functions leads to equation 5.4.

$$x = \frac{L * \lambda}{d}$$ 5.4

For the example of **PcH2** with a de Broglie wavelength of 5.2 pm ($v = 150$ m/s), the following distance between the interference maxima on the screen can be calculated for the described interferometer setup:

$$x = \frac{56.4 \text{ cm} * 5.2 \text{ pm}}{100 \text{ nm}} = 29 \text{ μm}$$ 5.5
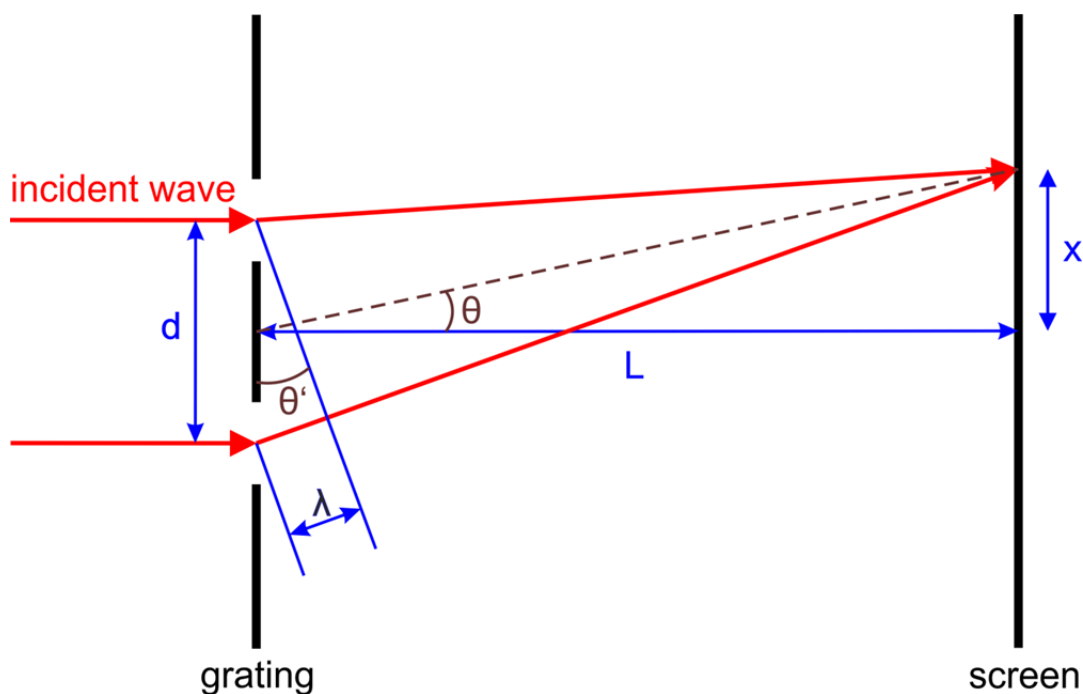
Figure 63. Schematic representation of the diffraction of planar wave fronts at a double slit. θ is the angle to the first order diffraction maximum, x the distance between the interference maxima, L the distance between the grating and the screen, d the grating period and λ the wavelength.

From these equations one can see that the distances between the interference maxima depend on the de Broglie wavelength of the interfering objects, and thus on their velocities during the flight through the interferometer. As the trajectory of the particles is influenced by the gravitational field of the Earth, fast objects hit the screen in the upper part of the vertical detection window and slow objects land in the lower region of the screen. With increasing velocity the molecules have smaller de Broglie wavelengths, which leads to a smaller distance between the interference maxima x. This phenomenon is nicely observed in the described experiment as the distance between the maxima continuously increases from top to bottom.

In figure 64 a comparison of the interferogram of the fluoroalkylated phthalocyanine **F24PcH2** with that of **PcH2** is shown. In this case both compounds were evaporated from the new laser microevaporation source which allowed to record the interferograms with a material consumption 100 times smaller than using the Knudsen cell. To account for the higher polarizability of **F24PcH2** this experiment was performed with wider collimation slits (75 nm) than used for figure 62 ($s = 50$ nm). Again, clear quantum interference was seen.

1D-projections were retrieved from the 2D diffraction patterns by vertically integrating over a part of the velocity distribution (figure 64c and d). The solid lines in these diagrams represent the textbook-like diffraction of plane waves at a grating. The lower contrast of the interferogram of **F24PcH2** as compared to **PcH2** may be attributed either to surface diffusion or to a low contribution of fragmented molecules within the molecular beam. Diffusion would actually be consistent with the design specifications of this molecule: the fluoroalkyl functionalization is made to reduce the binding to its surroundings, to facilitate the molecular evaporation. Note that in contrast to figure 63 the patterns of figure 64 show high contrast only to the first diffraction order. This is related to the larger grating slit width used in this experiment.
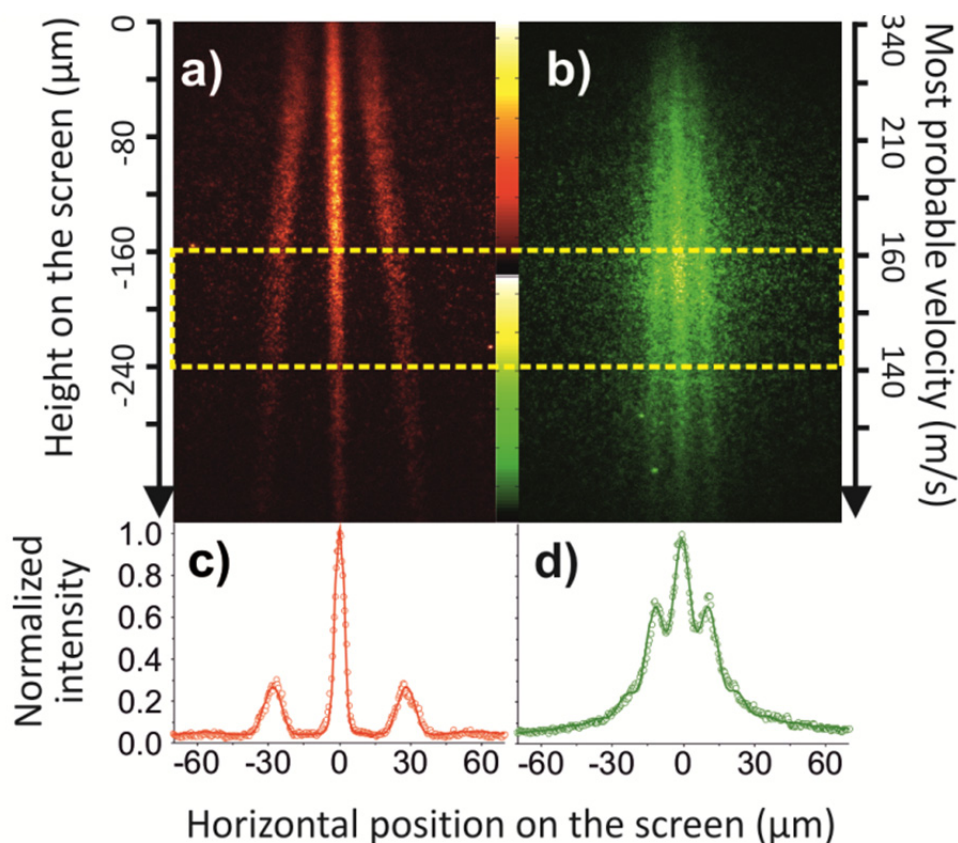
Figure 64. Comparison of the interference patterns of **PcH2** and **F24PcH2**. Quantum diffraction fans out the molecular beam in the horizontal direction. Gravity sorts the molecular beam by velocity from fast at the top to slow at the bottom. *Top:* Fluorescence images of the quantum interferograms of a) **PcH2** and b) **F24PcH2**. From these images we deduce both the mass and the velocity of the molecules. *Bottom:* Integration over $\Delta h = 80$ μm, corresponding to $\Delta v/v = 0.27$, results in a 1D diffraction curve. The **PcH2** quantum interference pattern (c) shows a fringe contrast close to 100% and is well reproduced by a numerical model that takes into account the finite source size and van der Waals forces. The **F24PcH2** diffraction curve (d) is well reproduced by allowing for an additional 3 μm small spread on the detector. The false colors serve to distinguish the two molecular species. Their true fluorescence of both starts in the range beyond 700 nm.

5.3.4 Conclusion

In summary, a series of three tailor-made fluorous phthalocyanine derivatives were synthesized and applied in far-field QIE. All three fluorescent compounds showed promising optical properties in solution. With the help of a new laser-controlled micro-evaporation source it was possible to produce a beam of molecules with the required intensity and coherence. It was shown how a combination of devices produced by nanotechnology permitted for the first time optical visualization of a real-time movie of the wave-particle duality in a textbook-like experiment for large molecules. Compared to earlier molecular far-field experiments,[16] the source economy was improved by a factor of 1000, the grating

thickness and the corresponding van der Waals phase shift were reduced by a factor of 16 and the detection efficiency was increased to the level of single molecules.

With the phthalocyanine **F24PcH2** (figure 65) having a molecular weight of 1 299 g/mol a new mass record for far-field QIE was set.[232]
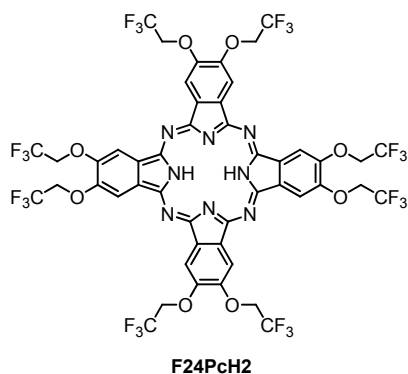
Figure 65. The phthalocyanine **F24PcH2** represents the largest object for which the wave nature has been observed so far in far-field matter-wave interferometry.

From the organic synthetic chemist's point of view, in particular, the development of the new source technique, which shows a markedly lower material consumption, offers new possibilities for the synthesis of new and larger model compounds for future applications. The rather large quantities that were required for QIE with effusive thermal sources limited the scope of accessible target structures considerably.

The feasibility of making nanometer thin absorptive gratings promises to push far-field diffraction experiments to new mass limits in the future.[26] While the van der Waals force is still visible for a membrane as thin as 10 nm, its influence shall be further reduced or completely eliminated in future experiments with masks of double layer graphene or gratings made of light.[21]

Grating diffraction of single molecules is an unambiguous and conspicuous demonstration of the wave-particle duality of quantum physics. It is only explicable in quantum terms, independent of the absolute value of the interference contrast. In contrast to photons and electrons which are irretrievably eliminated in the detection process, fluorescent molecules stay in place and can be observed and analyzed over days to show this paradigm of quantum physics.

6 Summary and Outlook

In order to explore the quantum-classical borderline, the ambition of this thesis was the design and synthesis of tailor-made molecules for matter-wave interference experiments.

In the introduction an overview of the field of matter-wave interferometry with a focus on interferometry with organic molecules is presented. Different concepts, including far-field and near-field interferometry, interferometer setups, and quantum experiments were discussed. Furthermore, the main synthesis concept of this work, i.e. the assembly of highly fluorinated compounds, was introduced. The historical background, smart synthesis concepts, including fluorous biphasic catalysis (FBC) and fluorous mixture synthesis (FMS), and the properties of fluorous compounds were described.

The synthetic work described in this thesis is part of an interdisciplinary research collaboration between chemists from the group of Prof. Mayor and the group of physicists of Prof. Arndt. Two main goals were pursued within this research project. Firstly, the focus was set on a deeper understanding of the influence of a molecule's internal structure, especially its polarizability, on quantum interference. Furthermore, the limits of quantum mechanics, the quantum-to-classical transition, were addressed by increasing the size of the interfering objects.

The metrological aspect of molecule interferometry - to measure influences of molecule properties on their wave nature - was explored in the first part of this thesis. A pair of two highly fluorinated constitutional isomers was synthesized in order to demonstrate that different molecular conformations can be distinguished in quantum interference experiments (figure 66). The tetrahedral isomer **1** was synthesized in four reaction steps including a copper mediated introduction of perfluoroalkyl chains. The rod-like derivative **2** was assembled in seven reaction steps. The two tailor-made isomers were applied in a near-field Kapitza-Dirac-Talbot-Lau interferometer. Although de Broglie quantum interference describes the center of mass motion of a massive body, it was shown to be sensitive to the internal molecular structure of the constitutional isomers. The different total susceptibilities of both isomers lead to different de Broglie interference shifts in the presence of external electric fields. The isomers thus become distinguishable in spite of their identical mass and chemical sum formula.[118]
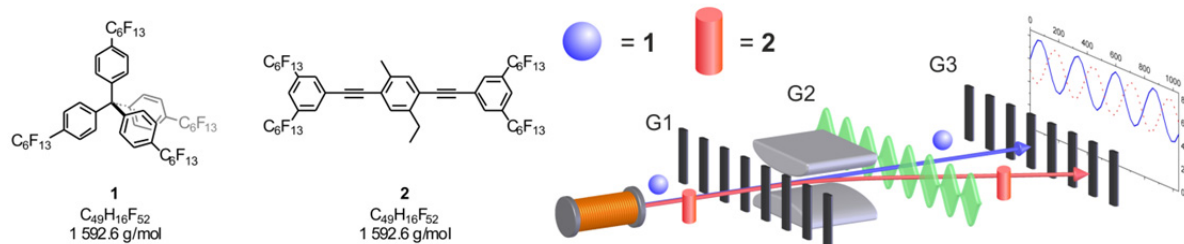
Figure 66. The structures of the two fluorous constitutional isomers **1** and **2** are shown on the left. On the right a schematic representation of the used near-field Kapitza-Dirac-Talbot-Lau interferometer is depicted.

Earlier work on the quantum interference of perfluoroalkyl functionalized molecules[49] and the here presented studies of the fluorous constitutional isomers **1** and **2**[118] revealed that thermally excited flexible molecules may exhibit vibrationally induced electric dipole moments that contribute to the molecules' electric susceptibility. In order to obtain a deeper insight on the structural origin of these dipole moments further matter-wave experiments with the non-fluorous compounds **4**, **15** and **16** were proposed (figure 67). Tetraphenylmethane (**4**) was synthesized in two steps starting from trityl chloride. The target structures **15** and **16** were each assembled in one reaction step from commercially available precursors using Suzuki-Miyaura cross coupling reactions. A comparison of the quantum interference of compound **4** with the corresponding fluorinated derivative **1** allowed the assignment of the rigid and the floppy components inside the molecules.[133] For compound **4** the measured susceptibility value is in good agreement with the computed polarizability, whereas it is in marked discrepancy for molecule **1**. According to the van Vleck formula these findings point at vibrationally induced electric dipole moments for isomer **1**. This allows to identify the vibrationally activated dipoles in the perfluoroalkyl side arms of compound **1** as the origin of its observed susceptibility increase. Furthermore, in experiments with the non-fluorous compounds **15** and **16** it became obvious that the existing Kapitza-Dirac-Talbot-Lau interferometer setup is not optimized for molecules in the mass range of 300-500 g/mol as the mass spectrometric detection exhibits a bad detection efficiency in this region.
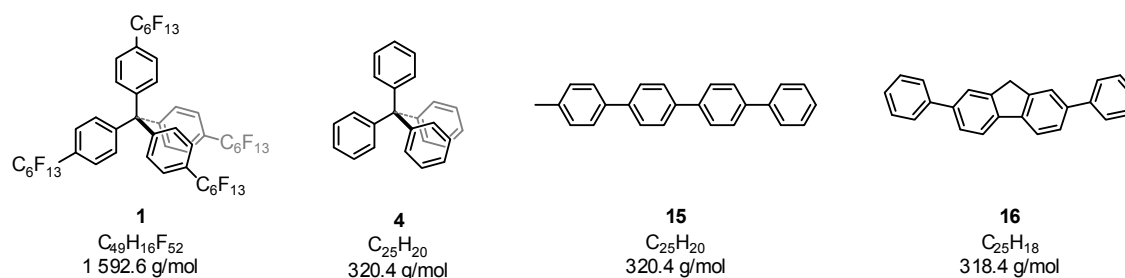

Figure 67. Target structures for investigations on the structural origin of vibrationally induced electric dipole moments.

In a last metrological project, the analytical capabilities of the Kapitza-Dirac-Talbot-Lau interferometer were demonstrated. The instrument may complement mass spectrometry, as it allows molecular properties of neutral particles to be probed in free flight before possibly being perturbed by ionization. In these studies it was shown how chemical analytical methods can help to interpret the outcome of matter-wave experiments. The investigated commercially available fluorous palladium complex was chemically analyzed after its flight through the interferometer. These analyses supported the findings of the interference experiment that indicated a fragmentation of the transition metal complex during the evaporation process and not at the ionization stage of the interferometer.[233]

Besides metrological applications, a main goal of this thesis was to synthesize model compounds for molecule interferometry to increase the preexisting mass record for quantum interferometry, which was held by the fluorofullerene $C_{60}F_{48}$ with a molecular weight of 1 633 g/mol. Near-field interferometry is a promising concept to set new records and thus to approach the quantum-to-classical transition. Firstly, it was tried to develop efficient synthesis routes towards multiple F-alkyl functionalized fullerenes via Bingel-Hirsch reactions (figure 68). However, monocyclopropanated fluorous fullerenes were only isolated in poor yields. The formation of considerable amounts of side products and a low solubility of the reaction products make this approach unsuitable as strategy for the assembly of model compounds for near-field quantum interference experiments.
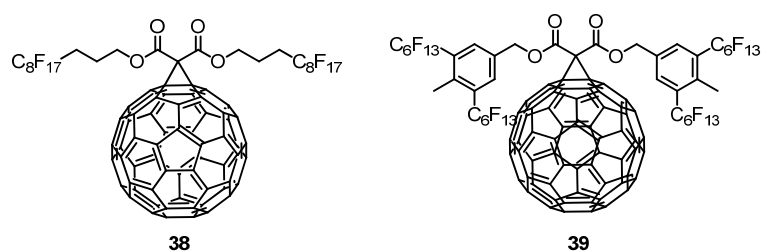
Figure 68. Structures of the fluorous fullerenes **38** and **39** which were synthesized for near-field matter-wave interferometry.

As fluorous fullerene derivatives did not open the window to quantum interference experiments in new mass regions, we moved our focus to fluorous porphyrins. A modular synthesis of seven perfluoroalkyl-substituted porphyrin derivatives with up to 16 fluorous alkyl chains was presented (figure 69).[234] To meet the requirements of quantum studies with complex organic molecules − high volatility, high stability, and high molecular mass − we chose the functionalization of tetraarylporphyrins with perfluoroalkyl moieties. With this series in hand, it was possible to observe interference patterns for three of the seven

derivatives. The matter-wave experiments reveal the quantum wave nature of tailor-made organic molecules in an unprecedented mass and size domain and provided major contributions to the exploration of the frontiers of quantum mechanics.[235] Porphyrin **46** as the heaviest molecule of this series (figure 69 right side) for which the wave nature has been observed has a 3.3 fold higher molecular weight than the preexisting mass record for quantum interference from the year 2003 ($C_{60}F_{48}$, 1 633 g/mol).[34] These experiments open a new window for quantum experiments with nanoobjects in a complexity class comparable to that of small proteins. However, a further increase of complexity seems to be very challenging with this synthetic approach. The heaviest porphyrin of the series with a mass of 7 553 g/mol was already quite laborious to synthesize and handle in sufficient quantities. Owing to the large amounts that are needed for the quantum experiments in the current near-field interferometer new synthetic approaches to increase the size of interfering objects were developed.
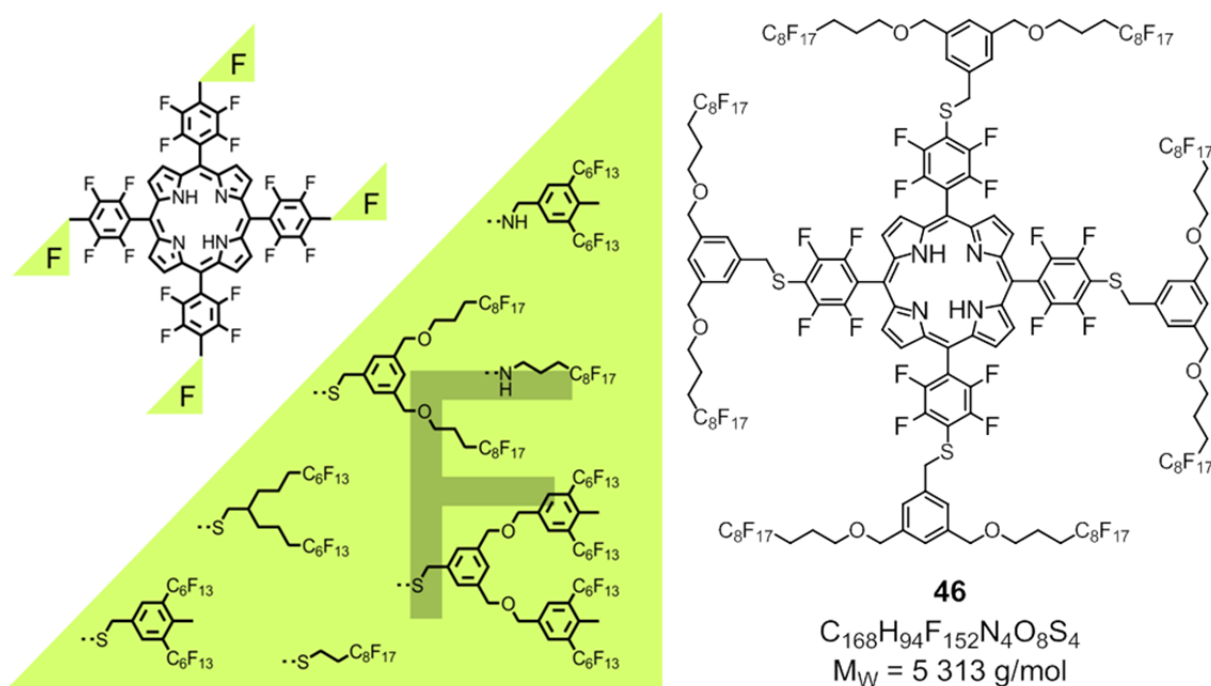
Figure 69. Left: Structures of the seven fluorous porphyrin derivatives that were prepared for quantum interference experiments in a Kapitza-Dirac-Talbot-Lau interferometer. Right: Structure of the heaviest porphyrin of this series for which the wave nature has been observed.

The experimental setup of the near-field Kapitza-Dirac-Talbot-Lau interferometer is not restricted to monodisperse and pure starting compounds. It also allows for experiments with compound mixtures because individual components of compound libraries can be detected in the mass spectrometric detection unit. The preparation of porphyrin libraries gave access to compounds in a new mass region (> 10 000 g/mol). A library containing components in the

mass range between 8 000 g/mol and 14 000 g/mol was successfully prepared (figure 70). Preliminary investigations in near-field interferometers with these structures revealed suitable molecule beam properties. With these porphyrin libraries in hand, it is expected to exceed for the first time the ceiling of 10 000 g/mol for an interfering object in the near future. Furthermore, with this synthetic approach, masses of up to 20 000 g/mol are a realistic goal. The design of new porphyrin platforms and larger fluorous thiol building blocks, as well as the optimization of reaction conditions should enable further advancements in the field of near-field matter-wave interferometry.
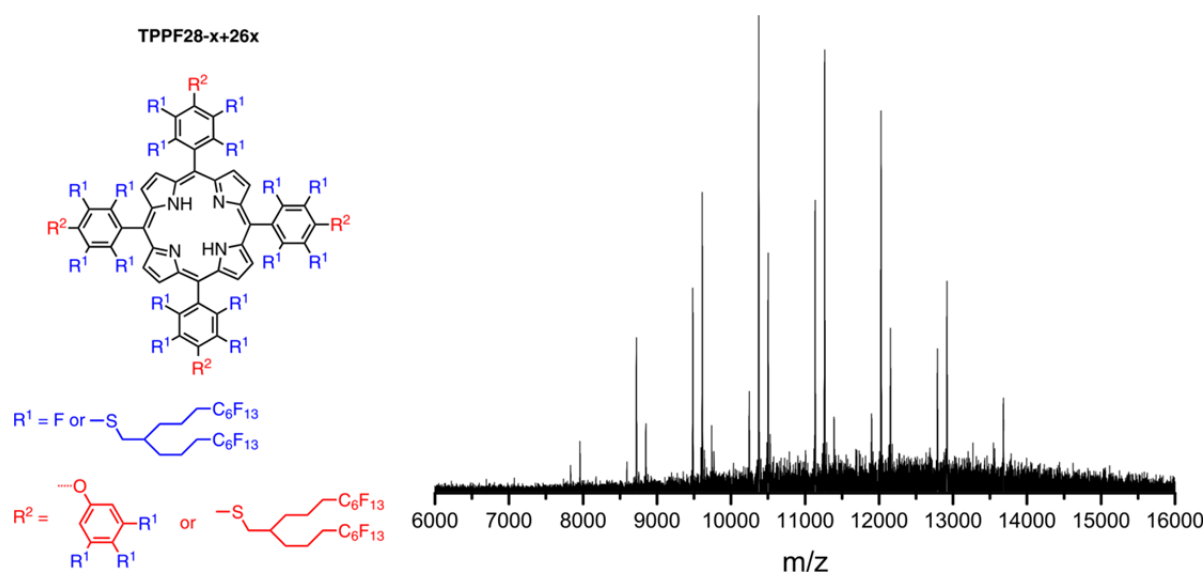
Figure 70. Left: Structure of the porphyrin library **TPPF28-x+26x**. Right: MALDI-ToF mass spectrum of the library **TPPF28-x+26x**.

Large, stable, highly volatile and fluorescent molecules were the goal of synthetic work that was performed for new far-field interference experiments in a setup based on fluorescence detection.

In a first approach fluorous naphthalene diimides derivatives were envisaged. Such compounds seemed to be appropriate model compounds for far-field matter-wave interferometry because of their tunable absorption and emission properties. However, the very low solubility of the compounds made it troublesome to isolate large fluorous naphthalene diimide derivatives purely and in sufficient quantities for our needs. Exclusively the derivative **84** (figure 71 left) with a molecular weight of 1 945 g/mol was successfully prepared. It was isolated in quantities of several hundreds of milligrams and showed the expected absorption and fluorescence properties. However, the far-field quantum interference experiments with this model compound did not yield the desired quantum interference

pattern. It was assumed that fragmentation of the molecules which presumably occurred during the thermal evaporation process led to these unsuccessful experiments.
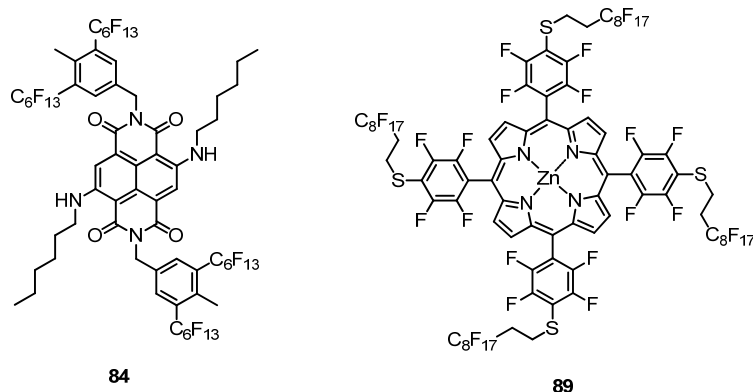
Figure 71. Structures of the synthesized target compounds **84** and **89**. Both structures were assembled for far-field experiments using fluorescence detection. The naphthalene diimide derivative **84** was envisaged to be detected on a quartz surface, whereas the metalloporphyrin **89** should be trapped on a pyridine functionalized glass surface.

The zinc porphyrin **89** (figure 71 right) was synthesized for a far-field setup that comprises a pyridine functionalized glass surface on the detector level. The axial coordination of the zinc porphyrin to the pyridine units should minimize its mobility on the surface and thus yield a high contrast interference pattern. The synthetic part of this project was completed. So far, the quantum experiments with the metalloporphyrin **89** are still ongoing and results are not yet available.

A further concept for far-field experiments aimed at the synthesis of tailor-made fluorous phthalocyanine derivatives. The three prepared fluorescent compounds **F24PcH2**, **F24PcMg** and **F24PcZn** showed promising optical properties in solution.

F24PcH2, M = 2H, M_W = 1 299 g/mol
F24PcMg, M = Mg, M_W = 1 321 g/mol
F24PcZn, M = Zn, M_W = 1 362 g/mol
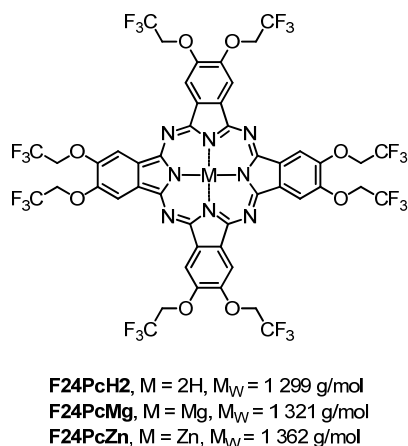
Figure 72. Structures of the three proposed fluorinated phthalocyanine derivatives for far-field matter-wave interferometry.

With the help of a new laser-controlled micro-evaporation source it was possible to produce a beam of molecules with the required intensity and coherence. At the same time, the new beam source reduces the required quantities of the organic molecules to several milligrams which gives new possibilities from the synthetic chemist's point of view. The observation of the wave nature of the phthalocyanine **F24PcH2** (figure 73) having a molecular weight of 1 299 g/mol set a new mass record for far-field molecule interferometry.[232] The preexisting record was held by the fullerene C_{70} with a mass of 841 g/mol.[20]
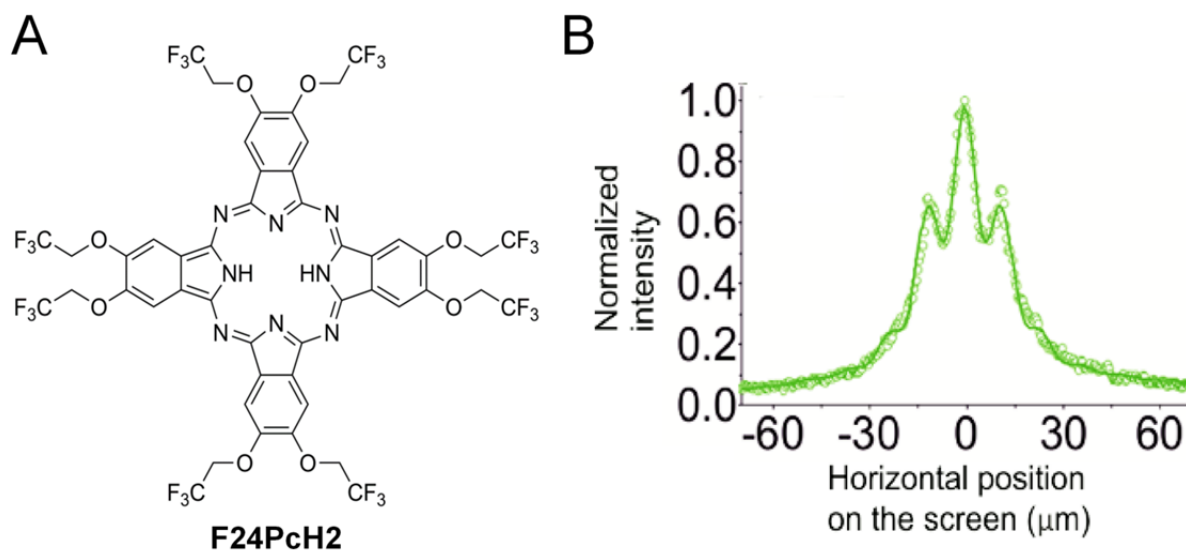
Figure 73. (A) Structure of the largest object for which the wave nature has been observed so far in far-field matter-wave interferometry. (B) Observed interference pattern for the free base phthalocyanine **F24PcH2**.

In summary, major contributions to the exploration of the frontiers of quantum mechanics were achieved by matter-wave interferometry using the perfluoroalkyl-functionalized molecules described in this thesis. Near-field experiments with libraries of fluorous porphyrins should lead in the near future to new size records in matter-wave experiments. Moreover, the current focus of the research in the field of interferometry with large objects is set on the development of new sources to bring neutral nanoobjects efficiently into the gas phase. The development of metal nanoparticle sources, which produce particles that considerably exceed the masses of the current tailor-made organic molecules, is a promising approach towards interference experiments in new size regions.

7   Experimental Part

7.1   General Remarks

Reagents and Solvents

All commercially available starting materials were of reagent grade and used as received from *Fluka AG* (Buchs, Switzerland), *Acros AG* (Basel, Switzerland), *Merck* (Darmstadt, Germany), *Alfa Aesar* (Karlsruhe, Germany), *ABCR* (Karlsruhe, Germany), *Aldrich* (Buchs, Switzerland), *fluorochem* (Hadfield, United Kingdom) and *Porphyrin Systems GbR* (Norderstedt, Germany). The solvents for chromatography and crystallization were distilled once before use, the solvents for extraction were used in technical grade. The solvent for HPLC analyses was of HPLC grade. Dry THF, dry DMF and dry CH_2Cl_2 were purchased from *Fluka*, stored over 4 Å molecular sieves, and handled under argon. For an inert atmosphere *Argon 4.8* from *PanGas AG* (Dagmersellen, Switzerland) was used.

Synthesis

All reactions with reagents which are sensitive to air or moisture were performed under an argon atmosphere using Schlenk technique, only dry solvents were used and the glassware was heated out before use. In reactions where highly fluorinated compounds were involved the use of glass coated magnetic stirring bars was favored over PTFE (Teflon) bars.

^{1}H-Nuclear Magnetic Resonance (^{1}H-NMR)

Bruker DRX-NMR (600 MHz or 500 MHz), *Bruker DPX-NMR* (400 MHz) and *Bruker BZH-NMR* (250 MHz) instruments were used to record the spectra. Chemical shifts (δ) are reported in parts per million (ppm) relative to residual solvent peaks ($CDCl_3$: 7.26 ppm) or trimethylsilane (TMS: 0.00 ppm), and coupling constants (J) are reported in Hertz (Hz). The bond distance of the coupling constant is stated with a superscript number (^nJ). NMR solvents were obtained from *Cambridge Isotope Laboratories, Inc.* (Andover, MA, USA). The measurements were done at room temperature. The multiplicities are written as: s = singlet, d = doublet, t = triplet, q = quartet, *quin* = quintet, m = multiplet and *br* = broad.

^{13}C-Nuclear Magnetic Resonance (^{13}C-NMR)

Bruker DRX-NMR (126 MHz) and *Bruker DPX-NMR* (101 MHz) instruments were used to record the spectra. Chemical shifts (δ) are reported in parts per million (ppm) relative to residual solvent peaks ($CDCl_3$: 77.0 ppm or TMS: 0.0 ppm). The measurements were done at room temperature. The multiplicities are written as: s = singlet, d = doublet, t = triplet, q = quartet, *quin* = quintet, m = multiplet. The coupling constants (J) are reported in Hertz (Hz) and are just stated in fluorine containing molecules. The signals of perfluoroalkyl segments were not assigned due to the coupling to fluorine.

^{19}F-Nuclear Magnetic Resonance (^{19}F-NMR)

A *Bruker DPX-NMR* (377 MHz) instrument was used to record the spectra. Chemical shifts (δ) are reported in parts per million (ppm), uncorrected. The measurements were done at room temperature. Coupling constants (J) are reported in Hertz (Hz). The multiplicities are written as: s = singlet, d = doublet, t = triplet, q = quartet, *quin* = quintet, m = multiplet.

Mass Spectrometry (MS)

Matrix Assisted Laser Desorption Ionization Time of Flight (MALDI-ToF) mass spectra were performed on an *Applied Bio Systems Voyager-De™ Pro* mass spectrometer or a *Bruker microflex* mass spectrometer. Electron-impact quadrupole mass spectra (EI-QMS) were recorded on a *GCMS-QP2010 SE* from *Shimadzu*. ESI-ToF mass spectra were recorded on a *Bruker MicrOTOFQ* instrument. Electron Impact (EI) mass spectra were recorded on a *Finnigan MAT 95Q*. Fast Atom Bombardment (FAB) mass spectra were recorded on a *Finnigan MAT 8400*. Significant signals are given in mass units per charge (*m/z*) and the relative intensities are given in brackets. EI-MS and FAB-MS measurements were performed by Dr. H. Nadig.

Elemental Analysis (EA)

Elemental analyses were measured by W. Kirsch on a *Perkin-Elmer Analysator 240*. The values are given in mass percent.

Melting Points (T$_M$)

Melting points were determined in °C using a *Stuart SMP3* apparatus and are uncorrected.

Ultraviolet Spectroscopy (UV)

UV/Vis-spectra were recorded on an *Agilent* 8453 diode array detector spectrophotometer or on a *UV-1800* spectrophotometer from *Shimadzu* using optical 114-*QS Hellma* cuvettes (10 mm light path) at room temperature and ambient conditions.

Fluorescence Spectroscopy

Emission spectra were recorded on a *Shimadzu* RF-5301 PC spectrofluorophotometer under ambient conditions.

Gel Permeation Chromatography (GPC)

Gel Permeations Chromatography (GPC) was performed on a *Shimadzu Prominence* System with *PSS SDV* preparative columns from *PSS* (2 columns in series: 600 mm x 20.0 mm, 5 μm particles, linear porosity "S", operating ranges: $100 - 100\,000$ g mol^{-1}) using chloroform as eluent.

High-Performance Liquid Chromatography (HPLC)

Analytical HPLC was performed on an *Agilent* HPLC system (series 1100) using a *FluoroFlash* HPLC column (4.6 mm i.d., 50 mm length, 5 μm) from *Fluorous Technologies Inc*.

Column Chromatography (CC)

For CC *silica gel 60* (particle size 40-63 μm) from *Merck* or *silica gel 60* (particle size 40-63 μm) from *Fluka* was used.

Thin Layer Chromatography (TLC)

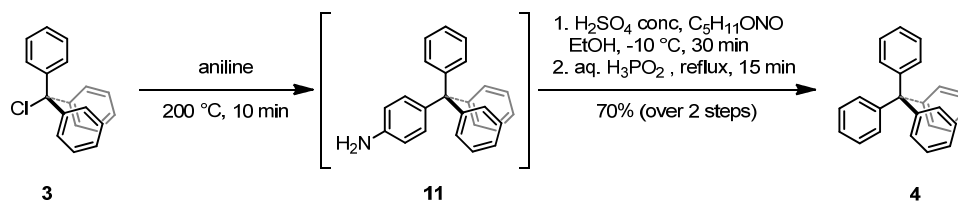*Silica gel 60 F$_{254}$* glass plates with a thickness of 0.25 mm from *Merck* were used. For detection a UV lamp with 254 nm or 366 nm was used.

Microwave Reactions

Microwave reactions were carried out in an *Initiator 8* (400 W) from *Biotage*.

7.2 Synthetic Procedures

Tetraphenylmethane (4)[106]

A mixture of trityl chloride (**3**, 16.7 g, 60 mmol, 1.0 eq.) and aniline (16.4 mL, 16.8 g, 180 mmol, 3.0 eq.) was heated to 200 °C for 10 minutes. After cooling to room temperature hydrochloric acid (2M, 100 mL) and methanol (90 mL) were added and the reaction mixture was heated to reflux for 5 minutes. Cooling to room temperature was followed by filtration. The residue was washed with water and dissolved in a mixture of ethanol (130 mL) and concentrated sulfuric acid (20 mL). Isoamyl nitrite (15 mL) was added at -10 °C. After stirring at this temperature for 30 minutes hypophosphorous acid (50%, 30 mL) was added and the mixture was heated again to reflux for 15 minutes. The resulting precipitate was collected by filtration and the crude was recrystallized from DMF to afford pure tetraphenylmethane (**4**, $C_{25}H_{20}$, 13.5 g) as an off-white solid in a yield of 70%.

^{1}H-NMR (400 MHz, CDCl$_3$, δ/ppm): 7.27 – 7.17 (*m*, 20H, Aryl-*H*).
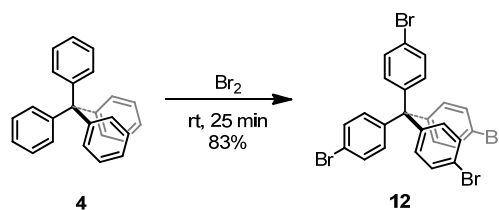
^{13}C-NMR (101 MHz, CDCl$_3$, δ/ppm): 146.8, 131.2, 127.4, 125.9, 65.0.

MS (EI, m/z): 320 (31%, M$^+$), 243 (100%).

EA: calculated: C = 93.71, H = 6.29, found: C = 93.51, H = 6.50.

UV/Vis (CHCl$_3$): λ$_{max}$ = 241 nm.

Tetrakis(4-bromophenyl)methane (12)[106]

Tetraphenylmethane (1.80 g, 5.58 mmol, 1.0 eq.) was added to a 50-mL-three-necked flask equipped with a magnetic stirring bar and an outlet adapter connected via rubber tubing to a pipet that is immersed in an aqueous sodium hydroxide solution (1M, 200 mL). Bromine (2.50 mL, 7.80 g, 48.8 mmol, 8.8 eq.) was added slowly over a period of five minutes. The dark-orange slurry was stirred for an additional 20 minutes and the resulting slurry was poured into ethanol (20 mL) cooled in a dry ice acetone bath. The precipitated solid was filtered and washed with an aqueous sodium bisulfite solution. The crude material was recrystallized from a mixture of chloroform and ethanol to afford pure tetrakis(4-bromophenyl)methane (12, $C_{25}H_{16}Br_4$, 2.93 g) as a yellow crystalline solid in a yield of 83%.

TLC: R_f = 0.40 (hexane).

^{1}H-NMR (400 MHz, CDCl$_3$, δ/ppm): 7.41 – 7.37 (*m*, 8H, Aryl-*H*), 7.03 – 6.99 (*m*, 8H, Aryl-*H*).
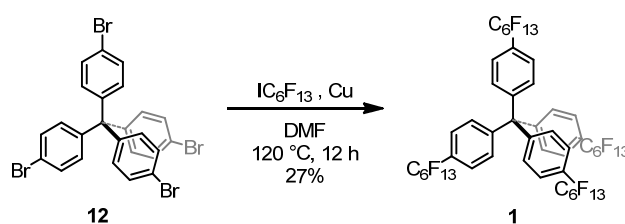
^{13}C-NMR (101 MHz, CDCl$_3$, δ/ppm): 144.4, 132.3, 131.1, 120.8, 63.6.

MS (EI, m/z): 636 (29%, M$^+$), 479 (100%).

T$_M$: 312 °C – 315 °C.

EA: calculated: C = 47.21, H = 2.54, found: C = 46.83, H = 2.45.

Tetrakis(4-(perfluorohexylphenyl)methane (1)

A few crystals of iodine were added under stirring to a suspension of copper (960 mg, 15.1 mmol, 12.0 eq.) in acetone. After 15 minutes the liquid phase was eliminated and the copper was washed with hydrochloric acid in acetone, followed by acetone alone. The activated copper and tetrakis(4-bromophenyl)methane (**12**, 800 mg, 1.26 mmol, 1.0 eq.) were added to dry DMF (10 mL) under an argon atmosphere at 70 °C. The suspension was stirred at 70 °C and *n*-perfluorohexyliodide (1.63 mL, 3.37 g, 7.55 mmol, 6.0 eq.) was added dropwise to the suspension over a period of five minutes. After stirring at 120 °C overnight, the mixture was cooled to room temperature, diluted with water and Et$_2$O and filtered through a plug of Celite. The solid residue was washed with Et$_2$O and the aqueous phase was extracted with Et$_2$O. The combined organic layers were washed with brine and dried over MgSO$_4$. After evaporating the solvent, the crude was purified by column chromatography using silica gel and hexane as eluent to give tetrakis(4-perfluorohexylphenyl)methane (**1**, 549 mg, C$_{49}$H$_{16}$F$_{52}$, 1592.57 g/mol, 27%) as a white solid.

^{1}H-NMR (400 MHz, CDCl$_3$, δ/ppm): 7.56 (*m*, 8H, Aryl-*H*), 7.33 (*m*, 8H, Aryl-*H*).

^{19}F-NMR (377 MHz, CDCl$_3$, δ/ppm): -82.0 (*m*, 12F, C*F*$_3$), -112.0 (*m*, 8F, C*F*$_2$), -122.7 (*m*, 8F, C*F*$_2$), -123.0 (*m*, 8F, C*F*$_2$), -124.0 (*m*, 8F, C*F*$_2$), -127.3 (*m*, 8F, C*F*$_2$).
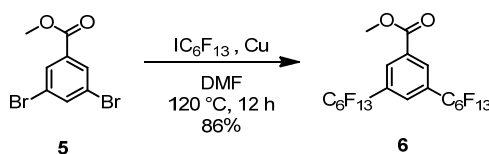
^{13}C-NMR (101 MHz, CDCl$_3$, δ/ppm): 148.6, 130.9, 127.8, 126.9, 65.0.

MS (MALDI-ToF, m/z): 1592 (11%, M$^+$), 1197 (100%).

T$_M$: 104 °C – 105 °C.

EA: calculated: C = 36.96, H = 1.01, found: C = 37.09, H = 0.99.

UV/Vis (CHCl$_3$): λ$_{max}$ = 241, 267, 275 nm.

Methyl-3,5-bis(perfluorohexyl)benzoate (6)

5   **6**

A few crystals of iodine were added under stirring to a suspension of copper (1.98 g, 31.1 mmol, 6.0 eq.) in acetone (5 mL). After 15 minutes the liquid phase was eliminated and the copper washed with hydrochloric acid in acetone, followed by acetone alone. The activated copper was added to 10 mL dry DMF under an argon atmosphere. The suspension was heated under stirring to 70 °C and *n*-perfluorohexyliodide (2.81 mL, 5.78 g, 3.89 mmol, 2.5 eq.) was then added dropwise to the suspension over five minutes. The mixture was heated to 120 °C and a solution of 3,5-dibromo-4-methylbenzoate (**5**, 1.52 g, 5.18 mmol, 1.0 eq.) was added. After stirring overnight at 120 °C, the mixture was cooled to room temperature, diluted with water and Et$_2$O and filtered through a Celite plug. The solid residue was washed with Et$_2$O. The aqueous phase was extracted with Et$_2$O. The combined organic layers were washed with brine and dried over MgSO$_4$. After evaporating the solvent the pale yellow crude was purified by column chromatography using silica gel (ethyl acetate/hexane 1:5) to give methyl-3,5-bis(perfluorohexyl)benzoate (**6**, C$_{20}$H$_6$F$_{26}$O$_2$, 3.35 g) as a white solid in 86% yield.

^{1}H-NMR (400 MHz, CDCl$_3$, δ/ppm): 8.49 (*s*, 2H, Aryl-*H*), 7.98 (*s*, 1H, Aryl-*H*), 4.02 (*s*, 3H, C*H*$_3$).

^{19}F-NMR (377 MHz, CDCl$_3$, δ/ppm): -82.0 (*t*, *J* = 10 Hz, 6F, C*F*$_3$), -112.2 (*m*, 4F, C*F*$_2$), -122.5 (*m*, 4F, C*F*$_2$), -122.9 (*m*, 4F, C*F*$_2$), -124.0 (*m*, 4F, C*F*$_2$), -127.3 (*m*, 4F, C*F*$_2$).

^{13}C-NMR (101 MHz, CDCl$_3$, δ/ppm): 164.4, 132.2, 131.6 (*m*), 130.8 (*t*, $^2J_{C-F}$ = 25 Hz), 129.4, 53.1 (*m*).

MS (EI, m/z): 772 (2%, M$^+$); 741 (56%), 503 (100%).

T$_M$: 58 °C – 60 °C.

EA: calculated: C = 31.11, H = 0.78, found: C = 31.01, H = 0.93.

3,5-Bis(perfluorohexyl)benzylic alcohol (13)
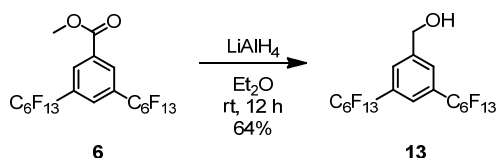
A solution of ester **6** (17.2 g, 22.2 mmol, 1.0 eq.) in Et_2O (150 mL) was added dropwise to a suspension of $LiAlH_4$ (1.27 g, 33.4 mmol, 1.5 eq.) in Et_2O (50 mL). This mixture was stirred at room temperature under an argon atmosphere for 16 hours, before ethyl acetate (4 mL) was added. After 15 minutes, H_2SO_4 (10%, 5 mL) was slowly dropped into the reaction mixture, which was stirred for another 15 minutes. The organic phase was removed and the aqueous phase was extracted with Et_2O. The combined organic layers were washed with brine and dried over $MgSO_4$. Evaporation of the solvent afforded a pale yellow solid that was recrystallized from hexane to give pure 3,5-bis(perfluorohexyl)benzylic alcohol (**13**, $C_{19}H_6F_{26}O$, 10.7 g) as a white solid in 64% yield.

^{1}H-NMR (400 MHz, $CDCl_3$, δ/ppm): 7.83 (s, 2H, Aryl-H), 7.72 (s, 1H, Aryl-H), 4.89 (d, $^3J_{HH}$ = 5.7 Hz, 2H, CH_2), 2.02 (t, $^3J_{HH}$ = 5.7 Hz, 1H, OH).

^{19}F-NMR (377 MHz, $CDCl_3$, δ/ppm): -82.0 (t, J = 10 Hz, 6F, CF_3), -112.2 (m, 4F, CF_2), -122.6 (m, 4F, CF_2), -123.0 (m, 4F, CF_2), -124.0 (m, 4F, CF_2), -127.4 (m, 4F, CF_2).

^{13}C-NMR (101 MHz, $CDCl_3$, δ/ppm): 143.1 (s), 138.9 (s), 128.4 (m), 124.6 (m), 130.3 (t, $^2J_{C-F}$ = 25 Hz), 63.8 (s).

MS (EI, m/z): 744 (16%, M$^+$), 475 (100%), 425 (36%).

T_M: 58 °C – 59 °C.

EA: calculated: C = 30.66, H = 0.81, found: C = 30.71, H = 0.90.

3,5-Bis(perfluorohexyl)benzaldehyde (7)
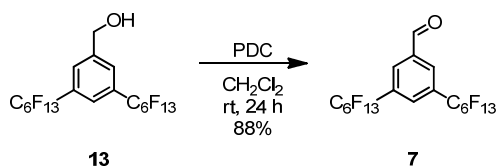
To a solution of alcohol **13** (7.05 g, 9.47 mmol, 1.0 eq.) in dichloromethane (300 mL) pyridinium dichromate (5.35 g, 14.2 mmol, 1.5 eq.) was added. The reaction mixture was stirred at room temperature under atmosphere of argon for 24 h, before Et_2O (30 mL) was added. Filtration of the reaction mixture and evaporation of the solvent afforded a pale yellow solid that was purified by column chromatography using silica gel (ethyl acetate/hexane 1:5) to give 3,5-bis(perfluorohexyl)benzaldehyde (**7**, $C_{19}H_4F_{26}O$, 6.21 g) as a white solid in 88% yield.

^{1}H-NMR (400 MHz, CDCl$_3$, δ/ppm): 10.16 (*s*, 1H, C*H*O), 8.34 (*s*, 2H, Aryl-*H*), 8.05 (*s*, 1H, Aryl-*H*).

^{19}F-NMR (377 MHz, CDCl$_3$, δ/ppm): -81.9 (*t*, $J = 10$ Hz, 6F, C*F*$_3$), -112.3 (*m*, 4F, C*F*$_2$), -122.5 (*m*, 4F, C*F*$_2$), -122.8 (*m*, 4F, C*F*$_2$), -123.9 (*m*, 4F, C*F*$_2$), -127.3 (*m*, 4F, C*F*$_2$).

^{13}C-NMR (101 MHz, CDCl$_3$, δ/ppm): 189.0, 137.3, 131.6 (t, $^2J_{C-F} = 25$ Hz), 131.2 (*m*), 130.5 (*m*).

MS (EI, m/z): 742 (2%, M$^+$), 723 (7%), 473 (100%).

1-(2,2-Dibromovinyl)-3,5-bis(perfluorohexyl)benzene (14)
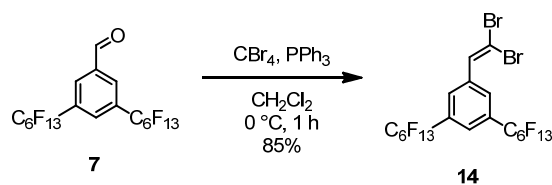
A solution of carbon tetrabromide (8.10 g, 24.4 mmol, 3.0 eq.) and triphenylphosphine (12.8 g, 48.8 mmol, 6.0 eq.) in degassed dichloromethane (250 mL) was cooled to 0 °C. To this yellow solution was added dropwise a solution of aldehyde **7** (6.04 g, 8.14 mmol, 1.0 eq.) in degassed dichloromethane (100 mL). The reaction mixture was stirred at 0 °C under an argon atmosphere for 1 hour. Evaporation of the solvent and purification by column chromatography using silica gel (ethyl acetate/hexane 1:10) yielded the desired dibromoolefin **14** ($C_{20}H_4Br_2F_{26}$, 6.22 g) as a colorless oil in a yield of 85%.

^{1}H-NMR (500 MHz, CDCl$_3$, δ/ppm): 7.97 (*s*, 2H, Aryl-*H*), 7.76 (*s*, 1H, Aryl-*H*), 7.58 (*s*, 1H, ArC*H*CBr$_2$).

^{19}F-NMR (377 MHz, CDCl$_3$, δ/ppm): -81.1 (*t*, $J = 10$ Hz, 6F, CF_3), -111.4 (*m*, 4F, CF_2), -121.6 (*m*, 4F, CF_2), -122.1 (*m*, 4F, CF_2), -123.0 (*m*, 4F, CF_2), -126.4 (*m*, 4F, CF_2).

^{13}C-NMR (126 MHz, CDCl$_3$, δ/ppm): 137.2, 133.9, 130.4 (*t*, $^2J_{\text{C-F}} = 25$ Hz), 130.3 (*m*), 125.1 (*m*), 94.7.

MS (EI, m/z): 898 (86%, M$^+$), 629 (100%), 469 (66%).

EA: calculated: C = 26.75, H = 0.45, found: C = 26.92, H = 0.55.

5-Ethynyl-1,3-bis(perfluorohexyl)benzene (8)
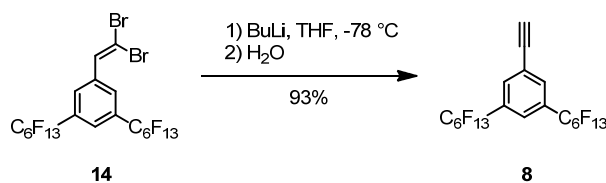
n-Butyllithium (1.6 M in hexane, 2.69 mL, 6.0 eq.) was slowly added to a solution of the dibromoolefin **14** (1.36 g, 1.51 mmol, 1.0 eq.) in THF (40 mL) at -78 °C. After one hour stirring at this temperature, the mixture was left to warm up to room temperature, and the stirring was continued for another 2 hours. The reaction was quenched by the addition of a saturated aqueous ammonium chloride solution (20 mL), and the mixture was diluted with hexane (100 mL). The organic phase was washed with water and dried over magnesium sulfate. Purification by column chromatography using silica gel and hexane as eluent afforded acetylene **8** ($C_{20}H_4F_{26}$, 1.04 g) as a white solid in 93% yield.

^{1}H-NMR (400 MHz, CDCl$_3$, δ/ppm): 7.91 (*s*, 2H, Aryl-*H*), 7.76 (*s*, 1H, Aryl-*H*), 3.29 (*s*, 1H, CC*H*).

^{19}F-NMR (377 MHz, CDCl$_3$, δ/ppm): -82.0 (*t*, *J* = 10 Hz, 6F, C*F*$_3$), -112.5 (*m*, 4F, C*F*$_2$), -122.6 (*m*, 4F, C*F*$_2$), -123.0 (*m*, 4F, C*F*$_2$), -124.0 (*m*, 4F, C*F*$_2$), -127.3 (*m*, 4F, C*F*$_2$).

^{13}C-NMR (126 MHz, CDCl$_3$, δ/ppm): 133.8 (*m*), 130.5 (*t*, $^2J_{C\text{-}F}$ = 25 Hz), 125.4 (*m*), 124.5, 81.0, 80.5.

MS (EI, m/z): 738 (18%, M$^+$), 469 (100%).

T$_M$: 51 °C – 52 °C.

EA: calculated: C = 32.54, H = 0.55, found: C = 32.35, H = 0.70.

1-Ethyl-2,5-diiodo-4-methylbenzene (10)
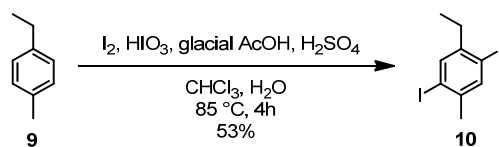
4-Ethyltoluene (**9**, 1.39 mL, 1.20 g, 10.0 mmol, 1.0 eq.), iodine (2.03 g, 8.00 mmol, 0.8 eq.) and iodic acid (774 mg, 4.40 mmol, 0.44 eq.) were dissolved in glacial acetic acid (5 mL), concentrated sulfuric acid (0.5 mL), water (0.5 mL) and chloroform (0.5 mL). The reaction mixture was stirred at 85 °C for 4 hours and then poured into an aqueous NaHSO₃ solution (10 wt%, 20 mL). After extracting with Et₂O the solvent was evaporated. Purification by column chromatography using silica gel and hexane as eluent followed by recrystallization from methanol yielded 1-ethyl-2,5-diiodo-4-methylbenzene (**10**, $C_9H_{10}I_2$, 1.97 g) as white crystals in 53% yield.

^{1}H-NMR (500 MHz, CDCl₃, δ/ppm): 7.65 (*s*, 1H, Aryl-*H*), 7.61 (*s*, 1H, Aryl-*H*), 2.64 (*q*, $^3J_{HH}$ = 7.5 Hz, 2H, ArC*H₂*CH₃), 2.34 (*s*, 3H, Aryl-*H*), 1.17 (*t*, $^3J_{HH}$ = 7.5 Hz, 3H, ArC*H₃*).

^{13}C-NMR (126 MHz, CDCl₃, δ/ppm): 145.8, 140.8, 139.7, 138.2, 101.0, 99.9, 33.1, 26.9, 14.5.

MS (EI, m/z): 372 (100%, M⁺), 357 (39%).

EA: calculated: C = 29.06, H = 2.71, found: C = 29.12, H = 2.61.

2,5-Di((3',5'-diperfluorohexylphenyl)ethynyl)-4-ethyltoluene (2)
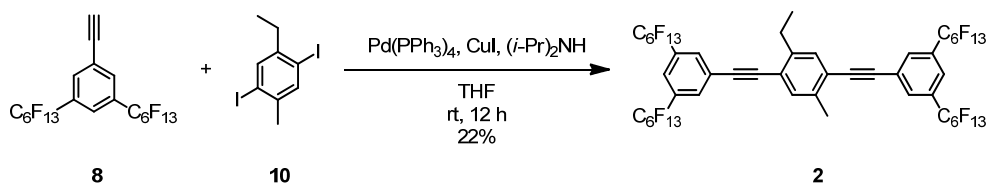
1-Ethynyl-3,5-bis(perfluorohexyl)benzene (**8**, 1.50 g, 2.03 mmol, 2.0 eq.) and 1-ethyl-2,5-diiodo-4-methylbenzene (**10**, 378 mg, 1.02 mmol, 1.0 eq.) was added to a solution of dry THF (10 mL) and (*i*-Pr)$_2$NH (2 mL). The solution was degassed before Pd(PPh$_3$)$_4$ (117 mg, 102 μmol, 10 mol%) and CuI (19.3 mg, 102 μmol, 10 mol%) were added. The reaction mixture was stirred at room temperature overnight. The solvent was evaporated and the crude was purified by column chromatography using silica gel and hexane/acetone (500:1) as eluent yielding the OPE **2** (C$_{49}$H$_{16}$F$_{52}$, 357 mg) as a white solid in a yield of 22%.

^{1}H-NMR (400 MHz, CDCl$_3$,/C$_6$F$_6$, δ/ppm): 8.04 – 7.99 (*m*, 4H, Aryl-*H*), 7.86 – 7.83 (*m*, 2H, Aryl-*H*), 7.41 (*s*, 1H, Aryl-*H*), 7.39 (*s*, 1H, Aryl-*H*), 2.91 (*q*, $^3J_{HH}$ = 7.5 Hz, 2H, Aryl-C*H$_2$*CH$_3$), 2.54 (*s*, 3H, Aryl-C*H$_3$*), 1.37 (*t*, $^3J_{HH}$ = 7.5 Hz, 3H, Aryl-CH$_2$C*H$_3$*).

^{19}F-NMR (377 MHz, CDCl$_3$/Freon113, δ/ppm): -82.0 (*t*, *J* = 10 Hz, 12F, C*F$_3$*), -112.2 (*m*, 8F, C*F$_2$*), -122.1 (*m*, 8F, C*F$_2$*), -122.3 (*m*, 8F, C*F$_2$*), -123.5 (*m*, 8F, C*F$_2$*), -127.0 (*m*, 8F, C*F$_2$*).

MS: (MALDI-ToF, m/z): 1592 (100%, M$^+$).

UV/Vis (CHCl$_3$): λ$_{max}$ = 241, 333 nm.

4-Methylquaterphenyl (15)
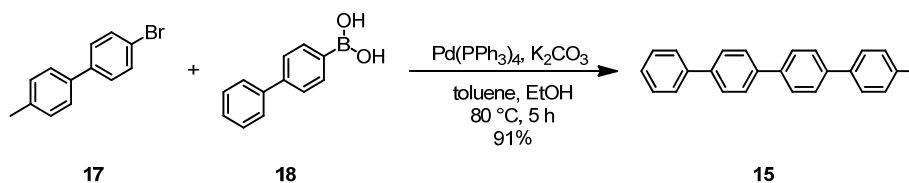
4-Bromo-4'-methylbiphenyl (**17**, 100 mg, 404 µmol, 1.0 eq.), 4-biphenylboronic acid (**18**, 88 mg, 445 µmol, 1.1 eq.) and potassium carbonate (671 g, 4.86 mmol, 8.0 eq.) were added to a solvent mixture of toluene (8 mL) and ethanol (2 mL). This mixture was degassed by bubbling argon through the solution for 15 minutes. After the addition of $Pd(PPh_3)_4$ (42 mg, 40.5 µmol, 10 mol%), the reaction mixture was stirred under argon at 80 °C for 5 hours. Cooling to room temperature was followed by the addition of water and extraction with dichloromethane. The combined organic layers were washed with brine and dried over $MgSO_4$. After evaporation of the solvent the crude was purified by column chromatography using dichloromethane/hexane (1:1) as eluent to afford pure 4-methylquaterphenyl (**15**, $C_{25}H_{20}$, 118 mg) as a white solid in a yield of 91%.

TLC: R_f = 0.58 (hexane/dichloromethane 1:1).

^{1}H-NMR (400 MHz, $CDCl_3$, δ/ppm): 7.74 – 7.65 (*m*, 10H, Aryl-*H*), 7.56 (*d*, $^3J_{HH}$ = 8.1 Hz, 2H, Aryl-*H*), 7.47 (*t*, $^3J_{HH}$ = 7.5 Hz, 2H, Aryl-*H*), 7.37 (*m*, 1H), 7.28 (*d*, $^3J_{HH}$ = 7.9 Hz, 2H, Aryl-*H*), 2.42 (*s*, 3H, C*H*$_3$).

^{13}C-NMR (101 MHz, $CDCl_3$, δ/ppm): 137.2, 129.6, 128.8, 127.5, 127.3, 127.0, 126.9, 21.1 (*not all expected carbon signals were detected due to the low solubility of the compound*).

MS: (EI, m/z): 320 (100%, M$^+$).

EA: calculated: C = 93.71, H = 6.29, found: C = 93.77, H = 6.38.

UV/Vis ($CHCl_3$): λ_{max} = 299 nm.

2,7-Diphenyl-9*H*-fluorene (16)
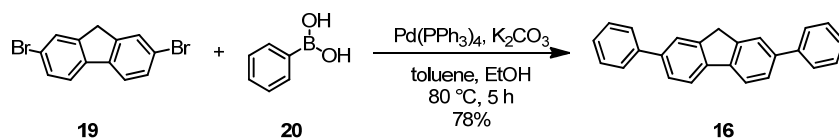
2,7-Dibromofluorene (**19**, 2.79 g, 8.61 mmol, 1.0 eq.), phenylboronic acid (**20**, 2.31 g, 18.9 mmol, 2.2 eq.) and potassium carbonate (8.33 g, 60.3 mmol, 7.0 eq.) were added to a solvent mixture of toluene (30 mL) and ethanol (10 mL). This mixture was degassed by bubbling argon through the solution for 15 minutes. After the addition of Pd(PPh$_3$)$_4$ (711 mg, 689 µmol, 8 mol%), the reaction mixture was stirred under argon at 80 °C for 5 hours. Cooling to room temperature, addition of H$_2$O and extraction with TBME followed. The combined organic layers were washed with brine and dried over MgSO$_4$. After evaporation of the solvent the crude was purified by column chromatography using dichloromethane/hexane (1:1) as eluent to afford the title compound **16** (C$_{25}$H$_{18}$, 2.13 g) as a white solid in a yield of 78%. This compound can be sublimated at 200 °C and 0.5 mbar.

^{1}H-NMR (400 MHz, CDCl$_3$, δ/ppm): 7.87 (*d*, $^3J_{HH}$ = 8.0 Hz, 2H, Aryl-*H*), 7.80 (*s*, 2H, Aryl-*H*), 7.67 (*d*, $^3J_{HH}$ = 8.0 Hz, 4H, Aryl-*H*), 7.64 (*d*, $^3J_{HH}$ = 8.0 Hz, 2H, Aryl-*H*), 7.51 – 7.43 (*m*, 4H, Aryl-*H*), 7.36 (*t*, $^3J_{HH}$ = 7.4 Hz, 2H, Aryl-*H*), 4.03 (*s*, 2H, C*H*$_2$).

^{13}C-NMR (101 MHz, CDCl$_3$, δ/ppm): 144.2, 141.5, 140.6, 139.9, 128.8, 127.2, 127.1, 126.1, 123.8, 120.2, 37.1.

MS: (EI, m/z): 318 (100%, M$^+$).

EA: calculated: C = 94.30, H = 5.70, found: C = 94.04, H = 5.83.

UV/vis (CHCl$_3$): λ$_{max}$ = 240, 305, 323 nm.

Methyl 4-methyl-3,5-bis(perfluorohexyl)benzoate (30)
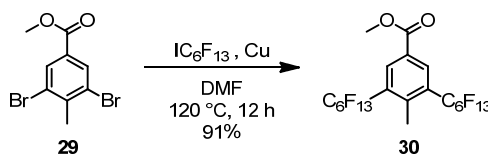
A few crystals of iodine were added under stirring to a suspension of copper (7.43 g, 117 mmol, 6.0 eq.) in acetone (20 mL). After 15 minutes the liquid phase was eliminated and the copper washed with hydrochloric acid in acetone, followed by acetone alone. The activated copper and methyl-3,5-dibromo-4-methylbenzoate (29, 6.00 g, 19.5 mmol, 1.0 eq.) were added to dry DMF (50 mL) under an argon atmosphere. The suspension was heated under stirring to 95 °C and n-perfluorohexyliodide (16.9 mL, 34.8 g, 77.9 mmol, 4.0 eq.) was then added dropwise to the suspension over 45 minutes. After stirring overnight at 125 °C, the mixture was cooled to room temperature, diluted with water and diethylether and filtered through a Celite plug. The solid residue was washed with diethylether. The aqueous phase was extracted with diethylether. The combined organic layers were washed with brine and dried over magnesium sulfate. After evaporating the solvent the pale yellow crude was purified by column chromatography using silica gel (ethyl acetate/hexane 1:4) to give methyl 4-methyl-3,5-bis(perfluorohexyl)benzoate (30, $C_{21}H_8F_{26}O_2$, 13.9 g) as a white solid in a yield of 91%.

TLC: R_f = 0.82 (hexane/ethyl acetate 5:1).

^{1}H-NMR (400 MHz, CDCl$_3$, δ/ppm): 8.42 (s, 2H, Aryl-H), 3.99 (s, 3H, COOCH_3), 2.63 (s, 3H, Aryl-CH_3).

^{19}F-NMR (377 MHz, CDCl$_3$, δ/ppm): -81.9 (t, J = 10 Hz, 6F, CF_3), -104.6 (m, 4F, CF_2), -121.0 (m, 4F, CF_2), -122.7 (m, 4F, CF_2), -123.8 (m, 4F, CF_2), -127.2 (m, 4F, CF_2).

^{13}C-NMR (101 MHz, CDCl$_3$, δ/ppm): 164.6, 144.5, 133.6 (t, $^3J_{CF}$ = 10 Hz), 130.5 (t, $^2J_{CF}$ = 22 Hz), 128.8, 52.9, 16.6.

MS (EI, m/z): 786 (6%, M$^+$), 755 (45%), 517 (100%).

EA: calculated: C = 32.08, H = 1.03, found: C = 32.12, H = 1.00.

4-Methyl-3,5-bis(perfluorohexyl)benzylic alcohol (31)
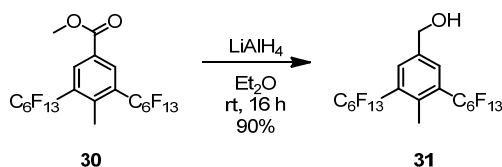
A solution of ester **30** (10.3 g, 13.1 mmol, 1.0 eq.) in diethylether (125 mL) was added dropwise to a suspension of lithium aluminium hydride (746 mg, 19.7 mmol, 1.5 eq.) in diethylether (50 mL). This mixture was stirred at room temperature under an atmosphere of argon for 12 hours, before ethyl acetate (4 mL) was added. After 15 minutes, an aqueous sulfuric acid solution (10%, 10 mL) was slowly added to the stirred reaction mixture, which was then stirred for another 10 minutes. The organic phase was removed and the aqueous phase was extracted with diethylether. The combined organic layers were washed with brine and dried over magnesium sulfate. Evaporation of the solvent afforded a pale yellow solid that was recrystallized from hexane to give pure alcohol **31** ($C_{20}H_8F_{26}O$, 8.97 g) as a white solid in a yield of 90%.

TLC: R_f = 0.31 (hexane/ethyl acetate 5:1).

^{1}H-NMR (400 MHz, CDCl$_3$, δ/ppm): 7.77 (s, 2H, Aryl-H), 4.81 (d, $^3J_{HH}$ = 5.8 Hz, 2H, CH_2), 2.55 (s, 3H, CH_3), 1.85 (t, $^3J_{HH}$ = 5.8 Hz, 1H, OH).

^{19}F-NMR (377 MHz, CDCl$_3$, δ/ppm): -81.9 (t, J = 10 Hz, 6F, CF_3), -104.5 (m, 4F, CF_2), -121.1 (m, 4F, CF_2), -122.8 (m, 4F, CF_2), -123.8 (m, 4F, CF_2), -127.2 (m, 4F, CF_2).

^{13}C-NMR (101 MHz, d_6-acetone, δ/ppm): 143.9, 138.9, 132.6 (t, $^3J_{CF}$ = 10 Hz), 130.8 (t, $^2J_{CF}$ = 21 Hz), 63.9, 17.2.

MS (EI, m/z): 758 (16%, M$^+$), 489 (100%), 439 (30%).

EA: calculated: C = 31.68, H = 1.06, found: C = 31.47, H = 1.04.

4-Methyl-3,5-bis(perfluorohexyl)benzoic acid (32)
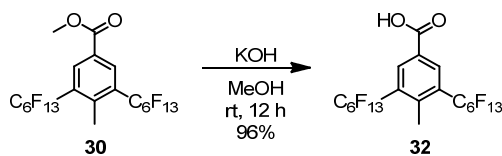
Ester **30** (200 mg, 254 μmol, 1.0 eq.) and potassium hydroxide (500 mg, 8.91 mmol, 35 eq.) were added to methanol (20 mL). The suspension was stirred at room temperature for 12 hours. The solvent was removed under reduced pressure. Water was added and the mixture was acidified with concentrated hydrochloric acid. An extraction with TBME followed. The combined organic layers were dried over magnesium sulfate. Evaporation of the solvent under reduced pressure and purification by recrystallization from acetone afforded the fluorous acid **32** ($C_{20}H_6F_{26}O_2$, 189 mg) as colorless crystals in a yield of 96%.

^{1}H-NMR (400 MHz, d_6-acetone, δ/ppm): 12.14 (*br*, 1H, COO*H*), 8.49 (*s*, 2H, Aryl-*H*), 2.71 (*s*, 3H, Aryl-C*H*$_3$).

^{19}F-NMR (377 MHz, d_6-acetone, δ/ppm): -80.9 (*t*, J = 10 Hz, 6F, C*F*$_3$), -103.1 (*m*, 4F, C*F*$_2$), -119.7 (*m*, 4F, C*F*$_2$), -121.4 (*m*, 4F, C*F*$_2$), -122.5 (*m*, 4F, C*F*$_2$), -126.0 (*m*, 4F, C*F*$_2$).

^{13}C-NMR (126 MHz, d_6-acetone, δ/ppm): 165.0, 145.0, 134.4 (*t*, $^3J_{CF}$ = 10 Hz), 130.8 (*t*, $^2J_{CF}$ = 22 Hz), 130.7, 17.0.

MS (EI, m/z): 772 (3%, M$^+$), 503 (100%).

EA: calculated: C = 31.11, H = 0.78, found: C = 31.24, H = 0.82.

Bis(perfluoroheptylmethyl) malonate (26)
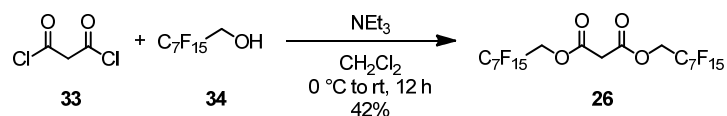
1*H*,1*H*-Perfluoro-1-octanol (**34**, 3.12 g, 7.80 mmol, 2.2 eq.) and triethylamine (1.14 mL, 826 mg, 8.16 mmol, 2.3 eq.) were dissolved in dry dichloromethane (10 mL) under an atmosphere of argon at 0 °C. A solution of malonyl dichloride (**33**, 345 μL, 500 mg, 3.55 mmol, 1.0 eq.) in dry dichloromethane (10 mL) was slowly added and the reaction mixture was allowed to warm to room temperature. After stirring at room temperature for 12 hours the solvent was removed under reduced pressure. Diethylether (100 mL) was added and the solution was washed with hydrochloric acid (1M), a saturated aqueous solution of sodium hydrogen carbonate and water. The organic phase was dried over magnesium sulfate. The crude was purified by column chromatography using silica gel and dichloromethane as eluent. The malonate **26** ($C_{19}H_6F_{30}O_4$, 1.29 g) was isolated as a white solid in a yield of 42%.

^{1}H-NMR (400 MHz, CDCl$_3$, δ/ppm): 4.66 (*t*, $^3J_{HF}$ = 13.3 Hz, 4H, C*H*$_2$CF$_2$), 3.61 (*s*, 2H, C*H*$_2$).

^{19}F-NMR (377 MHz, CDCl$_3$, δ/ppm): -81.0 (*t*, *J* = 10 Hz, 6F, C*F*$_3$), -119.8 (*m*, 4F, C*F*$_2$), -122.3 (*m*, 8F, C*F*$_2$), -123.0 (*m*, 4F, C*F*$_2$), -123.6 (*m*, 4F, C*F*$_2$), -126.4 (*m*, 4F, C*F*$_2$).

^{13}C-NMR (101 MHz, CDCl$_3$, δ/ppm): 194.3, 60.4 (*t*, $^2J_{CF}$ = 27 Hz), 40.2.

MS (MALDI, m/z): 867 (100%, [M-H]$^-$).

EA: calculated: C = 26.29, H = 0.70, found: C = 26.23, H = 0.77.

Bis(3-perfluorooctylpropyl) malonate (27)
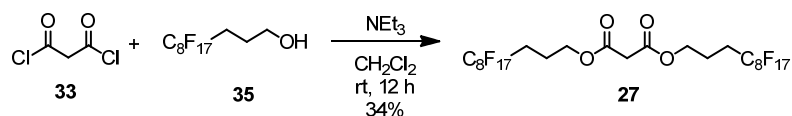
The fluorous alcohol **35** (2.99 g, 6.24 mmol, 2.2 eq.) and triethylamine (905 µL, 660 mg, 6.53 mmol, 2.3 eq.) were dissolved in dry dichloromethane (25 mL) under an atmosphere of argon. Malonyl dichloride (**33**, 276 µL, 400 mg, 2.84 mmol, 1.0 eq.) was added dropwise and the reaction mixture was stirred at room temperature for 12 hours. The solvent was removed under reduced pressure, diethylether was added and the solution was washed with hydrochloric acid (1M), a saturated aqueous solution of sodium hydrogen carbonate and water. The organic phase was dried over magnesium sulfate. The crude was purified by column chromatography using silica gel and a mixture of dichloromethane and hexane (1:1) as eluent. The malonate **27** ($C_{25}H_{14}F_{34}O_4$, 1.00 g) was isolated as a white solid in a yield of 34%.

^{1}H-NMR (400 MHz, CDCl$_3$, δ/ppm): 4.24 (t, $^3J_{HH}$ = 6.3 Hz, 4H, COOCH_2), 3.43 (s, 2H, CH_2), 2.26 – 2.10 (m, 4H, CH_2CF$_2$), 2.04 – 1.94 (m, 4H, CH_2CH$_2$CF$_2$).

^{19}F-NMR (377 MHz, CDCl$_3$, δ/ppm): -81.1 (t, J = 10 Hz, 6F, CF_3), -114.7 (m, 4F, CF_2), -122.0 (m, 4F, CF_2), -122.2 (m, 8F, CF_2), -123.0 (m, 4F, CF_2), -123.7 (m, 4F, CF_2), -126.4 (m, 4F, CF_2).

^{13}C-NMR (101 MHz, CDCl$_3$, δ/ppm): 166.2, 64.0, 41.3, 27.7 (t, $^2J_{CF}$ = 22 Hz), 19.9.

MS (MALDI, m/z): 1047 (100%, [M+Na]$^+$).

Bis(4-methyl-3,5-bis(perfluorohexyl)benzyl) malonate (28)
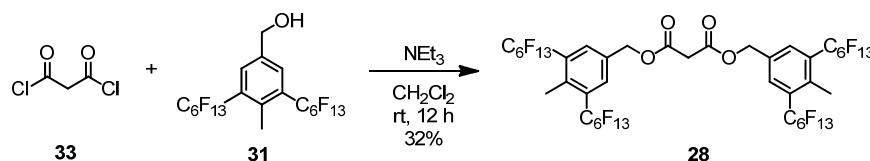
Alcohol **31** (158 mg, 209 μmol, 2.1 eq.) and triethylamine (32 μL, 23 mg, 228 μmol, 2.3 eq.) were dissolved in dry dichloromethane (20 mL) under an atmosphere of argon. Malonyl dichloride (**33**, 10 μL, 14 mg, 99 μmol, 1.0 eq.) was added dropwise and the reaction mixture was stirred at room temperature for 12 hours. The solvent was removed under reduced pressure, diethylether was added to the residue and the solution was washed with hydrochloric acid (1M), a saturated aqueous solution of sodium hydrogen carbonate and water. The organic phase was dried over magnesium sulfate. The crude was purified by column chromatography using silica gel and a mixture of dichloromethane and hexane (1:1) as eluent. The malonate **28** ($C_{43}H_{16}F_{52}O_4$, 50 mg) was isolated as a white solid in a yield of 32%.

^{1}H-NMR (400 MHz, CDCl$_3$, δ/ppm): 7.72 (s, 4H, Aryl-*H*), 5.26 (s, 4H, ArC*H*$_2$), 3.53 (s, 2H, C*H*$_2$), 2.54 (s, 6H, C*H*$_3$).

^{19}F-NMR (377 MHz, CDCl$_3$, δ/ppm): -81.1 (t, $J = 10$ Hz, 12F, C*F*$_3$), -103.8 (m, 8F, C*F*$_2$), -120.3 (m, 8F, C*F*$_2$), -122.0 (m, 8F, C*F*$_2$), -123.0 (m, 8F, C*F*$_2$), -126.4 (m, 8F, C*F*$_2$).

^{13}C-NMR (126 MHz, CDCl$_3$, δ/ppm): 165.7, 139.6, 133.8, 132.0 (m), 130.2 (m), 65.5, 41.2, 16.0.

MS (MALDI, m/z): 1607 (100%, [M+Na]$^+$).

Fluorous methano[60]fullerene-dicarboxylate derivative 38[124]
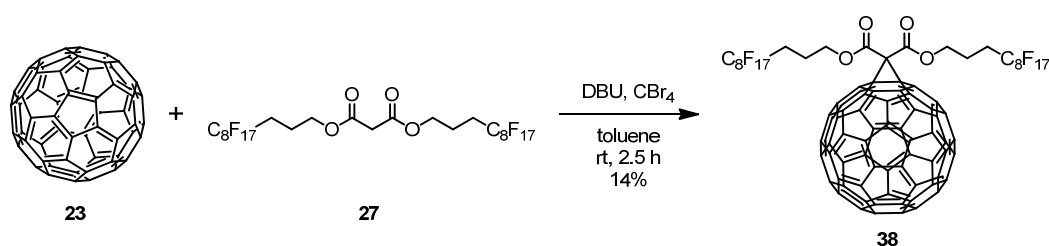
C_{60} (**23**, 100 mg, 139 µmol, 1.0 eq.) was dissolved in toluene (60 mL) under an atmosphere of argon at room temperature. The fluorous malonate **27** (213 mg, 208 µmol, 1.5 eq.), carbon tetrabromide (69 mg, 208 µmol, 1.5 eq.) and DBU (415 µL, 423 mg, 2.78 mmol, 20 eq.) were added and the reaction mixture was stirred for 2.5 hours. The reaction was quenched with water. The organic layer was separated and evaporated to dryness. The crude was purified by column chromatography using silica gel and a mixture of toluene and hexane (1:1) as eluent. The monoadduct **38** ($C_{85}H_{12}F_{34}O_4$, 34 mg) was isolated as a brown solid in a yield of 14%.

TLC: R_f = 0.53 (hexane/toluene 1:1).

¹H-NMR (400 MHz, CDCl₃/Freon113, δ/ppm): 4.58 (t, $^3J_{HH}$ = 6.1 Hz, 4H, COOCH_2), 2.32 – 2.14 (m, 8H, CH_2).

¹⁹F-NMR (377 MHz, CDCl₃, δ/ppm): -81.0 (t, J = 10 Hz, 6F, CF_3), -114.6 (m, 4F, CF_2), -121.9 (m, 4F, CF_2), -122.2 (m, 8F, CF_2), -123.0 (m, 4F, CF_2), -123.5 (m, 4F, CF_2), -126.4 (m, 4F, CF_2).

MS (MALDI, m/z): 1742 (100%, M⁺).

Fluorous methano[60]fullerene-dicarboxylate derivative 39
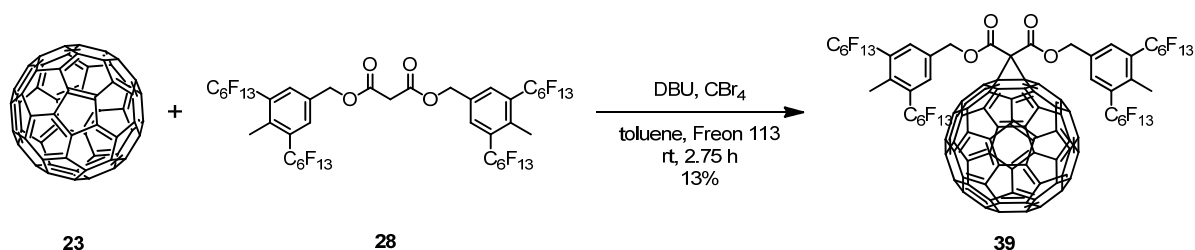
C_{60} (100 mg, 139 μmol, 1.0 eq.) was dissolved in a solvent mixture of toluene (60 mL) and Freon 113 (15 mL) under an atmosphere of argon at room temperature. The fluorous malonate **28** (242 mg, 153 μmol, 1.1 eq.), carbon tetrabromide (51 mg, 153 μmol, 1.1 eq.) and DBU (207 μL, 211 mg, 1.39 mmol, 10 eq.) were added and the reaction mixture was stirred using a glass coated magnetic stirring bar for 2.75 hours. The reaction was quenched with water. The organic layer was separated and evaporated to dryness. The crude was purified by column chromatography using silica gel and a mixture of toluene and cyclohexane (1:4) as eluent. The fluorous monoadduct **39** ($C_{103}H_{14}F_{52}O_4$, 43 mg) was isolated as a brown solid in a yield of 13%.

^{1}H-NMR (400 MHz, CDCl$_3$, δ/ppm): 7.85 (*s*, 4H, Aryl-*H*), 5.55 (*s*, 4H, ArC*H$_2$*), 2.56 (s, 6H, C*H$_3$*).

^{19}F-NMR (377 MHz, CDCl$_3$, δ/ppm): -80.8 (*t*, *J* = 10 Hz, 12F, C*F$_3$*), -103.5 (*m*, 8F, C*F$_2$*), -119.9 (*m*, 8F, C*F$_2$*), -121.6 (*m*, 8F, C*F$_2$*), -122.7 (*m*, 8F, C*F$_2$*), -126.1 (*m*, 8F, C*F$_2$*).

MS (MALDI, m/z): 2303 (100%, M$^+$).

4-Methyl-3,5-bis(perfluorohexyl)benzyl thioacetate (61)
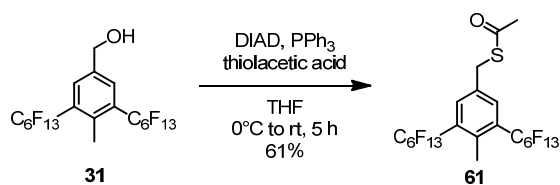
Triphenylphosphine (1.73 g, 6.59 mmol, 2.0 eq.) and DIAD (1.29 mL, 1.33 g, 6.59 mmol, 2.0 eq.) were dissolved in dry THF (25 mL) under an argon atmosphere at 0 °C. This solution was stirred at 0 °C for two hours before a solution of the benzylic alcohol **31** (2.50 g, 3.30 mmol, 1.0 eq.) and thiolacetic acid (469 μL, 502 mg, 6.59 mmol, 2.0 eq.) in dry THF (25 mL) was added. The reaction mixture was stirred for 1.5 hours at 0 °C followed by 1.5 hours at room temperature. After evaporation of the solvent the crude was purified by column chromatography using silica gel (ethyl acetate/cyclohexane 1:20) to give pure 4-methyl-3,5-bis(perfluorohexyl)benzyl thioacetate (**61**, $C_{22}H_{10}F_{26}OS$, 1.65 g) as a colourless oil in a yield of 61%.

TLC: R_f = 0.40 (hexane/ethyl acetate 20:1).

^{1}H-NMR (400 MHz, CDCl$_3$, δ/ppm): 7.69 (s, 2H, Aryl-*H*), 4.14 (s, 2H, C*H*$_2$), 2.52 (s, 3H, Aryl-C*H*$_3$), 2.37 (s, 3H, SCOC*H*$_3$).

^{19}F-NMR (377 MHz, CDCl$_3$, δ/ppm): -81.0 (t, J = 10 Hz, 6F, C*F*$_3$), -103.7 (m, 4F, C*F*$_2$), -120.3 (m, 4F, C*F*$_2$), -121.9 (m, 4F, C*F*$_2$), -122.9 (m, 4F, C*F*$_2$), -126.3 (m, 4F, C*F*$_2$).

^{13}C-NMR (126 MHz, CDCl$_3$, δ/ppm): 194.3, 138.3, 136.6, 132.9 (t, $^3J_{CF}$ = 10 Hz), 130.0 (t, $^2J_{CF}$ = 21 Hz), 32.4, 30.3, 15.9.

MS (EI, m/z): 816 (4%, M$^+$), 741 (26%).

EA: calculated: C = 32.37, H = 1.23, found: C = 32.41, H = 1.29.

4-Methyl-3,5-bis(perfluorohexyl)benzyl thiol (49)
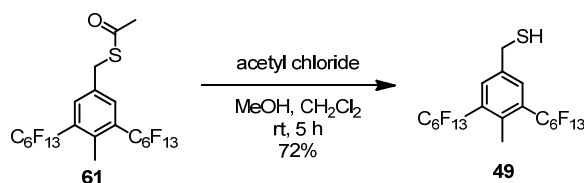
4-Methyl-3,5-bis(perfluorohexyl)benzyl thioacetate (**61**, 270 mg, 331 µmol, 1.0 eq.) was dissolved in a mixture of CH_2Cl_2 (5 mL) and methanol (10 mL). The mixture was degassed by purging argon through the solution for 10 minutes. Acetyl chloride (2.5 mL) was added in portions of 0.5 mL every hour. After a reaction time of five hours the solvent was evaporated. The crude was purified by column chromatography using silica gel (CH_2Cl_2/cyclohexane 1:6) to give pure 4-methyl-3,5-bis(perfluorohexyl)benzyl thiol (**49**, $C_{20}H_8F_{26}S$, 184 mg) as a white solid in a yield of 72%.

^{1}H-NMR (400 MHz, CDCl$_3$, δ/ppm): 7.73 (*s*, 2H, Aryl-*H*), 3.81 (*d*, $^3J_{HH}$ = 7.9 Hz, 2H, C*H*$_2$), 2.53 (*s*, 3H, C*H*$_3$), 1.83 (*t*, $^3J_{HH}$ = 7.9 Hz, 1H, S*H*).

^{19}F-NMR (377 MHz, CDCl$_3$, δ/ppm): -81.0 (*t*, J = 10 Hz, 6F, C*F*$_3$), -103.7 (*m*, 4F, C*F*$_2$), -120.3 (*m*, 4F, C*F*$_2$), -121.9 (*m*, 4F, C*F*$_2$), -122.9 (*m*, 4F, C*F*$_2$), -126.3 (*m*, 4F, C*F*$_2$).

^{13}C-NMR (126 MHz, CDCl$_3$, δ/ppm): 139.6, 138.1, 132.2 (*t*, $^3J_{CF}$ = 10 Hz), 130.0 (*t*, $^2J_{CF}$ = 22 Hz), 28.0, 15.9.

MS (EI, m/z): 774 (9%, M$^+$), 741 (100%).

EA: calculated: C = 31.02, H = 1.04, found: C = 31.04, H = 1.15.

N-(4-methyl-3,5-bis(perfluorohexyl)benzyl)phthalimide (63)
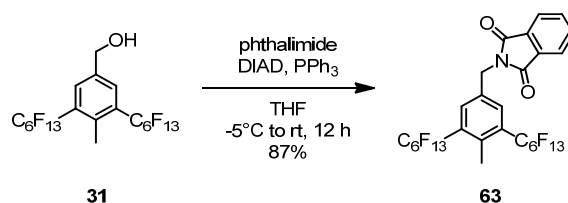
A solution of DIAD (587 µL, 603 mg, 2.98 mmol, 1.2 eq.) in dry THF (10 mL) was added dropwise to a solution of alcohol **31** (1.88 g, 2.48 mmol, 1.0 eq.), phthalimide (439 mg, 2.98 mmol, 1.2 eq.) and triphenylphosphine (782 mg, 2.98 mmol, 1.2 eq.) in THF (20 ml) at -5 °C. This mixture was stirred at room temperature under argon for 12 hours. After evaporating the solvent the residue was dissolved in diethylether and washed with an aqueous sodium hydroxide solution (1M). The organic layer was washed with brine and dried over magnesium sulfate. Evaporation of the solvent and purification by column chromatography using silica gel (ethyl acetate/hexane 1:2) afforded the product **63** ($C_{28}H_{11}F_{26}NO_2$, 1.91 g) as a white solid in a yield of 87%.

TLC: R_f = 0.39 (hexane/ethyl acetate 5:1).

¹H-NMR (400 MHz, CDCl$_3$, δ/ppm): 7.85 − 7.82 (m, 4H, Aryl-H), 7.75 - 7.72 (m, 2H, Aryl-H), 4.90 (s, 2H, CH$_2$), 2.51 (s, 3H, CH$_3$).

¹⁹F-NMR (377 MHz, CDCl$_3$, δ/ppm): -81.9 (t, J = 10 Hz, 6F, CF$_3$), -104.5 (m, 4F, CF$_2$), -121.2 (m, 4F, CF$_2$), -122.8 (m, 4F, CF$_2$), -123.8 (m, 4F, CF$_2$), -127.2 (m, 4F, CF$_2$).

¹³C-NMR (101 MHz, CDCl$_3$, δ/ppm): 167.7, 139.1, 134.8, 134.3, 133.1 (t, $^3J_{CF}$ = 10 Hz), 131.9, 130.2 (t, $^2J_{CF}$ = 22 Hz), 123.7, 40.7, 16.0.

MS (EI, m/z): 887 (100%, M$^+$), 618 (42%), 568 (57%).

EA: calculated: C = 37.90, H = 1.25, N = 1.58, found: C = 37.85, H = 1.26, N = 1.54.

4-Methyl-3,5-bis(perfluorohexyl)benzylamine (50)
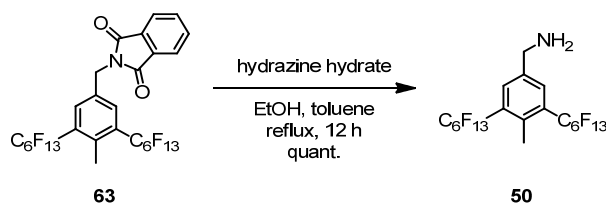
A solution of compound **63** (2.00 g, 2.25 mmol, 1.0 eq.) and hydrazine hydrate (1.0 mL) in a solvent mixture of ethanol (20 mL) and toluene (20 mL) was stirred at reflux under argon overnight. After addition of CH_2Cl_2 the reaction mixture was washed with an aqueous sodium hydroxide solution (1M). The aqueous phase was extracted with CH_2Cl_2 and the combined organic layers were washed with brine and dried over magnesium sulfate. After evaporation of the solvent amine **50** ($C_{20}H_9F_{26}N$, 1.71 g) was obtained as a white solid in a quantitative yield.

^{1}H-NMR (400 MHz, CDCl$_3$, δ/ppm): 7.74 (*s*, 2H, Aryl-*H*), 3.98 (*s*, 2H, C*H$_2$*), 2.52 (*s*, 3H, C*H$_3$*), 1.47 (*s*, br, 2H, N*H$_2$*).

^{19}F-NMR (377 MHz, CDCl$_3$, δ/ppm): -81.9 (*t*, $J = 10$ Hz, 6F, C*F$_3$*), -104.4 (*m*, 4F, C*F$_2$*), -121.2 (*m*, 4F, C*F$_2$*), -122.8 (*m*, 4F, C*F$_2$*), -123.9 (*m*, 4F, C*F$_2$*), -127.3 (*m*, 4F, C*F$_2$*).

^{13}C-NMR (101 MHz, CDCl$_3$, δ/ppm): 141.4, 137.6, 131.2 (*t*, $^3J_{CF} = 9$ Hz), 129.7 (*t*, $^2J_{CF} = 22$ Hz), 45.3, 15.8.

MS (FAB, m/z): 758 (100%, [M+H]$^+$), 741 (63%).

EA: calculated: C = 31.72, H = 1.20, N = 1.85, found: C = 32.19, H = 1.36, N = 1.88.

2,2-Bis(3-perfluorohexylpropyl)malonic diethylester (64)[156]
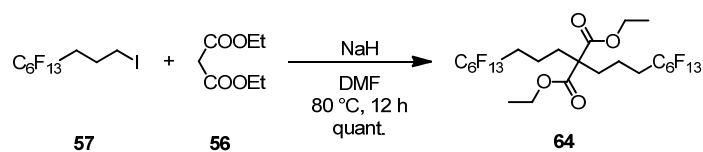
A solution of diethyl malonate (**56**, 720 mg, 4.50 mmol, 1.0 eq.) in dry DMF (14 mL) was added under an atmosphere of argon to a suspension of sodium hydride (freshly washed, 324 mg, 13.5 mmol, 3.0 eq.) in dry DMF (30 mL). The mixture was stirred at room temperature for one hour. A solution of 3-(perfluorohexyl)propyl iodide (**57**, 4.98 g, 10.2 mmol, 2.3 eq.) in dry DMF (14 mL) was slowly added. The temperature was raised to 80 °C and the mixture was stirred for 12 hours. After cooling to room temperature, the reaction was quenched with water. Extraction with diethylether was followed by washing of the combined organic layers with brine. The organic phase was dried over magnesium sulfate. Filtration and evaporation of the solvent under reduced pressure afforded diester **64** ($C_{25}H_{22}F_{26}O_4$, 3.96 g) as a yellow oil in quantitative yield.

^{1}H-NMR (250 MHz, CDCl$_3$, δ/ppm): 4.22 (q, $^3J_{HH}$ = 7.1 Hz, 4H, CH_2CH$_3$), 2.24 − 1.91 (m, 8H), 1.63 − 1.45 (m, 4H), 1.26 (t, $^3J_{HH}$ = 7.1 Hz, 6H, CH$_2$CH_3).

^{19}F-NMR (377 MHz, CDCl$_3$, δ/ppm): -81.1 (t, J = 10 Hz, 6F, CF_3), -114.5 (m, 4F, CF_2), -122.2 (m, 4F, CF_2), -123.2 (m, 4F, CF_2), -123.8 (m, 4F, CF_2), -126.4 (m, 4F, CF_2).

MS (FAB, m/z): 881 (3%, [M+H]$^+$), 154 (100%).

2,2-Bis(3-perfluorohexylpropyl)malonic acid (65)[156]
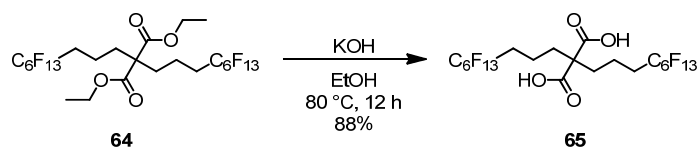
Diester **64** (3.96 g, 4.50 mmol, 1.0 eq.) was dissolved in a mixture of ethanol (30 mL) and an aqueous solution of potassium hydroxide (30 mL, 50 wt%). The reaction mixture was heated to 80 °C for 12 hours. After cooling to room temperature the mixture was acidified by the addition of concentrated hydrochloric acid. The resulting precipitate was filtered off and washed with water. The solid was dissolved in ethyl acetate and dried over magnesium sulfate. After evaporation of the solvent the crude was recrystallized from toluene to afford diacid **65** ($C_{21}H_{14}F_{26}O_4$, 3.28 g) as yellowish solid in a yield of 88%.

^{1}H-NMR (500 MHz, CD$_3$OD, δ/ppm): 2.29 – 2.13 (*m*, 4H, C*H$_2$*C$_6$F$_{13}$), 2.02 – 1.91 (m, 4H, C*H$_2$*CH$_2$C$_6$F$_{13}$), 1.72 – 1.53 (*m*, 4H,C*H$_2$*CH$_2$CH$_2$C$_6$F$_{13}$).

^{19}F-NMR (377 MHz, CD$_3$OD, δ/ppm): -81.9 (*t*, J = 10 Hz, 6F, C*F$_3$*), -114.6 (*m*, 4F, C*F$_2$*), -122.5 (*m*, 4F, C*F$_2$*), -123.4 (*m*, 4F, C*F$_2$*), -124.0 (*m*, 4F, C*F$_2$*), -126.9 (*m*, 4F, C*F$_2$*).

^{13}C-NMR (101 MHz, CD$_3$OD, δ/ppm): 174.6, 58.4, 33.5, 32.0 (*t*, $^2J_{CF}$ = 20 Hz), 16.9.

1,7-Diperfluorohexyl-4-carboxyheptane (66)[156]
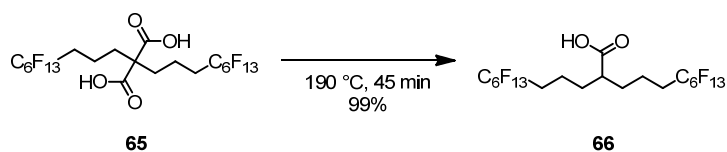
Diacid **65** (6.02 g, 7.30 mmol, 1.0 eq.) was heated to 190 °C for 45 minutes. After cooling to room temperature the crude was dissolved in chloroform. After filtration of insoluble impurities the solvent was removed under reduced pressure to afford acid **66** ($C_{20}H_{14}F_{26}O_2$, 5.67 g) as an off-white solid in a yield of 99%.

^{1}H-NMR (500 MHz, CDCl$_3$, δ/ppm): 2.48 – 2.42 (*m*, 1H, C*H*COOH), 2.18 – 1.99 (*m*, 4H, C*H$_2$*C$_6$F$_{13}$), 1.81 – 1.57 (*m*, 8H).

^{19}F-NMR (377 MHz, CDCl$_3$, δ/ppm): -81.1 (*t*, *J* = 10 Hz, 6F, C*F$_3$*), -114.6 (*m*, 4F, C*F$_2$*), -122.2 (*m*, 4F, C*F$_2$*), -123.2 (*m*, 4F, C*F$_2$*), -123.8 (*m*, 4F, C*F$_2$*), -126.4 (*m*, 4F, C*F$_2$*).

^{13}C-NMR (126 MHz, CDCl$_3$, δ/ppm): 180.7, 44.8, 31.3, 30.7 (*t*, $^2J_{CF}$ = 22 Hz), 18.2.

1,7-Diperfluorohexyl-4-hydroxymethylheptane (67)[156]
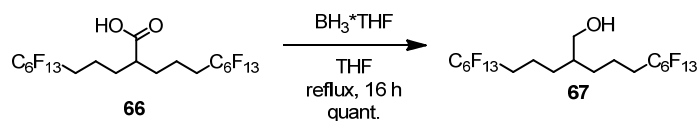
Acid **66** (5.60 g, 7.18 mmol, 1.0 eq.) was dissolved in dry THF (14 mL). A solution of borane-THF complex in THF (1M, 35.9 mL, 35.9 mmol, 5.0 eq.) was added dropwise under an atmosphere of argon. The reaction mixture was heated to reflux for 16 hours. After cooling to room temperature an aqueous hydrochloric acid solution (20 vol%, 70 mL) was carefully added. Water was added and the mixture was extracted with diethylether. The combined organic layers were washed with water and brine, dried over magnesium sulfate. After filtration the solvent was removed under reduced pressure and the alcohol **67** ($C_{20}H_{16}F_{26}O$, 5.50 g) was obtained as a white solid in quantitative yield.

^{1}H-NMR (500 MHz, CDCl$_3$, δ/ppm): 3.65 – 3.56 (*m*, 2H, C*H*$_2$OH), 2.16 – 1.99 (*m*, 4H), 1.70 – 1.60 (*m*, 4H), 1.59 – 1.36 (*m*, 6H).

^{19}F-NMR (377 MHz, CDCl$_3$, δ/ppm): -81.0 (*t*, J = 10 Hz, 6F, C*F*$_3$), -114.5 (*m*, 4F, C*F*$_2$), -122.2 (*m*, 4F, C*F*$_2$), -123.1 (*m*, 4F, C*F*$_2$), -123.8 (*m*, 4F, C*F*$_2$), -126.4 (*m*, 4F, C*F*$_2$).

^{13}C-NMR (126 MHz, CDCl$_3$, δ/ppm): 64.7, 40.0, 31.2 (*t*, $^2J_{CF}$ = 23 Hz), 30.4, 17.7.

MS (EI, m/z): 748 (31%, [M-H$_2$O]$^+$), 388 (100%).

1,7-Diperfluorohexyl-4-((trifluoromethanesulfonylhydroxy)methyl)heptane (58)[156]
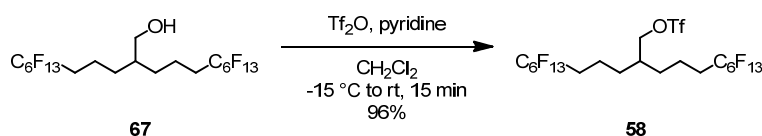
Trifluoromethansulfonic acid anhydride (731 µL, 1.23 g, 4.35 mmol, 1.5 eq.) was added to dry dichloromethane (35 mL). The mixture was cooled to -15 °C with a dry ice/acetone ice bath. A solution of alcohol **67** (2.22 g, 2.90 mmol, 1.0 eq.) and pyridine (233 µL, 229 mg, 1.0 eq.) in dry dichloromethane (25 mL) was slowly added under an atmosphere of argon. The reaction mixture was allowed to warm to room temperature. After evaporation of the solvent the crude was purified by column chromatography using silica gel and dichloromethane as solvent. Pure triflate **58** ($C_{21}H_{15}F_{29}O_3S$, 2.50 g) was obtained as a colorless oil in a yield of 96%.

^{1}H-NMR (500 MHz, CDCl$_3$, δ/ppm): 4.48 (*d*, $^3J_{HH}$ = 4.9 Hz, 2H, C*H$_2$*OTf), 2.19 – 2.01 (*m*, 4H, CH2C6F13), 1.93 – 1.82 (*m*, 1H, C*H*), 1.74 – 1.61 (*m*, 4H, C*H$_2$*CH$_2$C$_6$F$_{13}$), 1.57 – 1.47 (*m*, 4H, C*H*2CH$_2$CH$_2$C$_6$F$_{13}$).

^{19}F-NMR (377 MHz, CDCl$_3$, δ/ppm): -74.8 (*s*, 3F, OSO$_2$C*F$_3$*), -81.1 (*t*, *J* = 10 Hz, 6F, C*F$_3$*), -114.5 (*m*, 4F, C*F$_2$*), -122.2 (*m*, 4F, C*F$_2$*), -123.1 (*m*, 4F, C*F$_2$*), -123.8 (*m*, 4F, C*F$_2$*), -126.4 (*m*, 4F, C*F$_2$*).

^{13}C-NMR (126 MHz, CDCl$_3$, δ/ppm): 78.2, 38.1, 30.9 (*t*, $^2J_{CF}$ = 23 Hz), 29.8, 17.5.

MS (EI, m/z): 748 (31%, [M-OTf]$^+$), 735 (100%).

1,7-Diperfluorohexyl-4-((tritylthio)methyl)heptane (68)
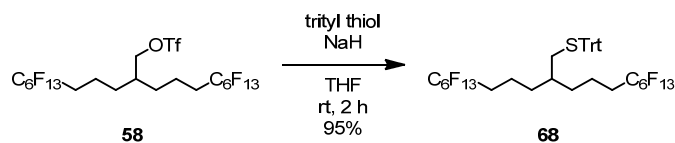
Triflate **58** (1.00 g, 1.11 mmol, 1.0 eq.) and trityl thiol (492 mg, 1.78 mmol, 1.6 eq.) were dissolved in dry THF (15 mL) under an atmosphere of argon. To this solution was added sodium hydride (178 mg, 60% dispersion in mineral oil, 4.45 mmol, 4.0 eq.) at room temperature. The reaction mixture was stirred for 2 hours at room temperature and. After quenching with water it was extracted with CH_2Cl_2. The combined organic phases were washed with brine, dried over magnesium sulfate, filtered and evaporated to dryness. Purification by column chromatography (silica gel, cyclohexane/CH_2Cl_2 4:1) gave the title compound **68** ($C_{39}H_{30}F_{26}S$, 1.08 g) as a colorless oil in a yield of 95%.

TLC: R_f = 0.69 (hexane/dichloromethane 3:1).

^{1}H-NMR (500 MHz, CDCl$_3$, δ/ppm): 7.44 – 7.40 (*m*, 6H, Aryl-H_{ortho} of trityl group), 7.30 – 7.26 (*m*, 6H, Aryl-H_{meta} of trityl group), 7.23 – 7.19 (*m*, 3H, Aryl-H_{para} of trityl group), 2.16 – 2.14 (*m*, 2H, CH_2STrt), 2.03 – 1.89 (*m*, 4H, CH_2CF$_2$), 1.44 – 1.24 (*m*, 9H).

^{19}F-NMR (377 MHz, CDCl$_3$, δ/ppm): -81.0 (*t*, *J* = 10 Hz, 6F, CF_3), -114.5 (*m*, 4F, CF_2), -122.3 (*m*, 4F, CF_2), -123.1 (*m*, 4F, CF_2), -123.8 (*m*, 4F, CF_2), -126.4 (*m*, 4F, CF_2).

^{13}C-NMR (126 MHz, CDCl$_3$, δ/ppm): 144.7, 129.6, 127.9, 126.7, 66.7, 37.7, 35.3, 32.7, 31.0 (*t*, $^2J_{CF}$ = 22 Hz), 17.3.

MS (ESI-Q-ToF, m/z): 1047 (100%, [M+Na]$^+$).

EA: calculated: C = 45.71, H = 2.95, found: C = 45.66, H = 2.85.

1,7-Diperfluorohexyl-4-((hydrothio)methyl)heptane (51)
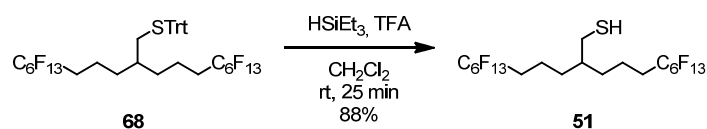
1,7-Diperfluorohexyl-4-((tritylthio)methyl)heptane **68** (1.00 g, 976 µmol, 1.0 eq.) and triethylsilane (236 µL, 170 mg, 1.46 mmol, 1.5 eq.) were dissolved in dry CH_2Cl_2 (20 mL) under an atmosphere of argon. Trifluoroacetic acid (800 µL) was added dropwise and the reaction mixture was stirred for 25 minutes at room temperature. The reaction was quenched by the addition of a saturated aqueous solution of sodium hydrogen carbonate. After completion of the gas formation, the phases were separated and the aqueous phase was extracted with CH_2Cl_2. The combined organic fractions were dried over magnesium sulfate, filtered and evaporated to dryness. After purification by column chromatography (silica gel, cyclohexane/CH_2Cl_2 4:1), the thiol **51** ($C_{20}H_{16}F_{26}S$, 669 mg) was obtained as a colorless oil in a yield of 88%.

TLC: R_f = 0.80 (hexane/dichloromethane 3:1).

^{1}H-NMR (500 MHz, CDCl$_3$, δ/ppm): 2.61 – 2.56 (*m*, 2H, C*H$_2$*SH), 2.13 - 2.03 (*m*, 4H, C*H$_2$*CF$_2$), 1.67-1.37 (*m*, 9H), 1.21 (*t*, $^3J_{HH}$ = 8.1 Hz, 1H, S*H*).

^{19}F-NMR (377 MHz, CDCl$_3$, δ/ppm): -81.0 (*t*, J = 10 Hz, 6F, C*F$_3$*), -114.5 (*m*, 4F, C*F$_2$*), -122.2 (*m*, 4F, C*F$_2$*), -123.1 (*m*, 4F, C*F$_2$*), -123.8 (*m*, 4F, C*F$_2$*), -126.4 (*m*, 4F, C*F$_2$*).

^{13}C-NMR (126 MHz, CDCl$_3$, δ/ppm): 39.8, 31.7, 31.1 (*t*, $^2J_{CF}$ = 22 Hz), 27.9, 17.5.

MS (EI, m/z): 782 (3%, M$^+$), 389 (87%), 375 (100%).

EA: calculated: C = 30.70, H = 2.06, found: C = 31.04, H = 2.24.

(3,5-Bis(bromomethyl)benzyl)(trityl)sulfane (60)
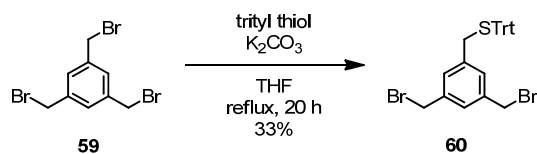
1,3,5-Tris(bromomethyl)benzene (**59**, 5.00 g, 14.0 mmol, 1.0 eq.) and triphenylmethanethiol (3.87 g, 14.0 mmol, 1.0 eq.) were dissolved in dry tetrahydrofuran (40 mL) under an atmosphere of argon. Potassium carbonate (2.90 g, 21.0 mmol, 1.5 eq.) was added and the mixture was heated to reflux for 20 hours. After cooling to room temperature, water was added and the mixture was extracted with *tert*-butyl methyl ether. The combined organic fractions were washed with brine, dried over magnesium sulfate and evaporated to dryness. After purification by column chromatography (silica gel, hexane/dichloromethane 3:1), the product **60** ($C_{28}H_{24}Br_2S$, 2.55 g) was obtained as colorless solid in a yield of 33%.

TLC: R_f = 0.24 (hexane/dichloromethane 3:1).

^{1}H-NMR (400 MHz, CDCl$_3$, δ/ppm): 7.47 − 7.42 (*m*, 6H, Aryl-*H*), 7.35 − 7.20 (*m*, 10H, Aryl-*H*), 7.01 (*s*, 2H, Aryl-*H*), 4.39 (*s*, 4H, ArC*H*$_2$Br), 3.33 (*s*, 2H, ArC*H*$_2$STrt).

^{13}C-NMR (101 MHz, CDCl$_3$, δ/ppm): 144.5, 138.7, 138.4, 129.7, 129.6, 128.2, 128.0, 126.8, 67.3, 36.4, 32.6.

MS (ESI-Q-ToF, m/z): 575 (31%, [M+Na]$^+$), 217 (100%).

EA: calculated: C = 60.89, H = 4.38, found: C = 60.53, H = 4.50.

((5-((Tritylthio)methyl)-1,3-phenylene)bis(methylene))bis((2-perfluorooctylethyl)sulfane) (69)
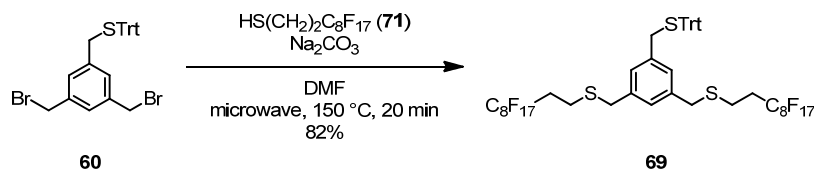
Three microwave vials (Biotage microwave vial 10-20 mL) were each charged with the following mixture. (3,5-Bis(bromomethyl)benzyl)(trityl)sulfane (**60**, 150 mg, 272 μmol, 1.0 eq.), 1*H*,1*H*,2*H*,2*H*-perfluorodecanethiol (233 μL, 391 mg, 815 μmol, 3.0 eq.) and sodium carbonate (86 mg, 815 μmol, 3.0 eq.) were added to dry DMF (12 mL) in a microwave vial. The sealed tubes were heated in a microwave apparatus (Biotage, Initiator 8) to 150 °C for 20 minutes. After cooling to room temperature the three reaction mixtures were diluted with water and diethylether and subsequently combined. The organic phase was separated, washed with brine and dried over magnesium sulfate. After evaporation of the solvent under reduced pressure the crude was purified by column chromatography using silica gel (eluent: dichloromethane/cyclohexane 1:3) to afford the desired compound **69** ($C_{48}H_{32}F_{34}S_3$, 898 mg) as an off-white solid in a yield of 82%.

TLC: R_f = 0.35 (hexane/dichloromethane 3:1).

^{1}H-NMR (400 MHz, CDCl$_3$, δ/ppm): 7.49 − 7.42 (*m*, 6H, Aryl-*H*), 7.33 − 7.27 (*m*, 6H, Aryl-*H*), 7.25 − 7.19 (*m*, 3H, Aryl-*H*), 7.07 (*s*, 1H, Aryl-*H*), 6.95 (*s*, 2H, Aryl-*H*), 3.66 (*s*, 4H, ArC*H$_2$*SC*H$_2$*), 3.29 (*s*, 2H, C*H$_2$*STrt), 2.61 − 2.53 (*m*, 4H, C*H$_2$*CH$_2$C$_8$F$_{17}$), 2.35 − 2.17 (*m*, 4H, C*H$_2$*C$_8$F$_{17}$).

^{19}F-NMR (377 MHz, CDCl$_3$, δ/ppm): -81.0 (*t*, *J* = 10 Hz, 6F, C*F$_3$*), -114.7 (*m*, 4F, C*F$_2$*), -122.0 (*m*, 4F, C*F$_2$*), -122.2 (*m*, 8F, C*F$_2$*), -123.0 (*m*, 4F, C*F$_2$*), -123.7 (*m*, 4F, C*F$_2$*), -126.4 (*m*, 4F, C*F$_2$*).

^{13}C-NMR (126 MHz, CDCl$_3$, δ/ppm): 144.6, 138.4, 138.3, 129.6, 128.6, 128.0, 127.9, 126.8, 67.6, 36.6, 36.1, 31.7 (*t*, $^2J_{CF}$ = 22 Hz), 21.9.

MS (MALDI, m/z): 1373 (100%, [M+Na]$^+$), 1350 (32%, M$^+$).

EA: calculated: C = 42.68, H = 2.39, found: C = 42.90, H = 2.59.

(3,5-Bis(((2-perfluoroocytlethyl)thio)methyl)phenyl)methanethiol (52)
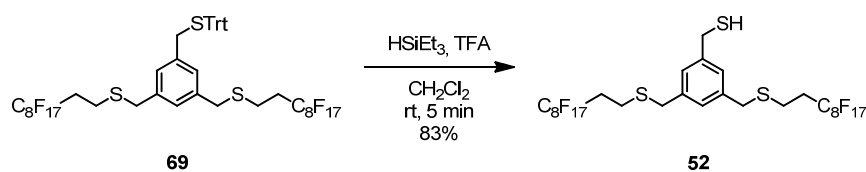
Compound **69** (790 mg, 0.58 mmol, 1.0 eq.) and triethylsilane (142 µL, 102 mg, 0.88 mmol, 1.5 eq.) were dissolved in dry dichloromethane (15 mL). Trifluoroacetic acid (600 µL) was added dropwise and the reaction mixture was stirred for five minutes at room temperature. The reaction was quenched by the addition of a saturated aqueous solution of sodium hydrogen carbonate. After completion of the gas formation, the phases were separated and the aqueous phase was extracted with dichloromethane. The combined organic fractions were dried over magnesium sulfate, filtered and evaporated to dryness. After purification by column chromatography (silica gel, cyclohexane/dichloromethane 2:1), the thiol **52** ($C_{29}H_{18}F_{34}S_3$, 540 mg) was obtained as a white solid in a yield of 83%.

TLC: R_f = 0.32 (hexane/dichloromethane 3:1).

^{1}H-NMR (500 MHz, CDCl$_3$, δ/ppm): 7.19 (*s*, 2H, Aryl-*H*), 7.14 (*s*, 1H, Aryl-*H*), 3.77 – 3.68 (*m*, 6H, C*H*$_2$SH and ArC*H*$_2$SCH$_2$), 2.67 – 2.56 (*m*, 4H, C*H*$_2$CH$_2$C$_8$F$_{17}$), 2.36 – 2.20 (*m*, 4H, C*H*$_2$C$_8$F$_{17}$), 1.75 (*t*, $^3J_{HH}$ = 7.6 Hz, 1H, S*H*).

^{19}F-NMR (377 MHz, CDCl$_3$, δ/ppm): -81.2 (*t*, *J* = 10 Hz, 6F, C*F*$_3$), -114.8 (*m*, 4F, C*F*$_2$), -122.1 (*m*, 4F, C*F*$_2$), -122.3 (*m*, 8F, C*F*$_2$), -123.1 (*m*, 4F, C*F*$_2$), -123.7 (*m*, 4F, C*F*$_2$), -126.5 (*m*, 4F, C*F*$_2$).

^{13}C-NMR (126 MHz, CDCl$_3$, δ/ppm): 142.5, 138.8, 128.2, 127.8, 36.4, 31.9 (*t*, $^2J_{CF}$ = 22 Hz), 28.8, 22.1.

EA: calculated: C = 31.42, H = 1.64, found: C = 31.59, H = 1.75.

(3,5-Bis((3-perfluorooctylpropoxy)methyl)benzyl)(trityl)sulfane (70)
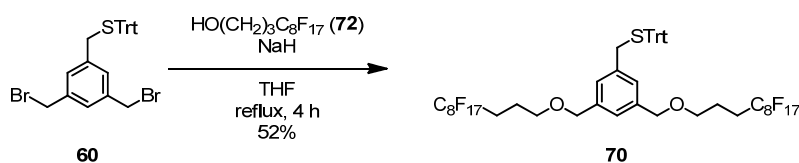
3-(Perfluorooctyl)propanol (**72**, 2.16 g, 4.53 mmol, 5.0 eq.) was dissolved in dry tetrahydrofuran (10 mL) under an atmosphere of argon. This solution was added to a suspension of sodium hydride (freshly washed, 109 mg, 4.53 mmol, 5.0 eq.) in dry tetrahydrofuran (5 mL) at 0 °C. After 15 minutes the mixture was allowed to warm to room temperature and then a solution of (3,5-bis(bromomethyl)benzyl)(trityl)sulfane (**60**, 500 mg, 0.91 mmol, 1.0 eq.) in dry tetrahydrofuran (20 mL) was added dropwise. The reaction mixture was stirred for 4 hours at reflux. After cooling to room temperature it was quenched with an saturated aqueous ammonium chloride solution. The mixture was extracted with diethylether and the organic fractions were washed with brine, dried over magnesium sulfate, filtered and evaporated to dryness. Purification by column chromatography (silica gel, cyclohexane/dichloromethane 1:1) gave the title compound **70** ($C_{50}H_{36}F_{34}O_2S$, 632 mg) as a white solid in a yield of 52%.

TLC: R_f = 0.55 (hexane/dichloromethane 1:1).

^{1}H-NMR (500 MHz, CDCl$_3$, δ/ppm): 7.48 − 7.44 (*m*, 6H, Aryl-*H*), 7.32 − 7.26 (*m*, 6H, Aryl-*H*), 7.24 − 7.21 (*m*, 3H, Aryl-*H*), 7.14 (*s*, 1H, Aryl-*H*), 6.99 (*s*, 2H, Aryl-*H*), (*s*, 4H, ArC*H$_2$*OCH$_2$), 3.51 (*t*, $^3J_{HH}$ = 5.9 Hz, 4H, ArCH$_2$OC*H$_2$*), 3.31 (*s*, 2H, C*H$_2$*STrt), 2.24 − 2.14 (*m*, 4H, C*H$_2$*C$_8$F$_{17}$), 1.92 − 1.87 (*m*, 4H, C*H$_2$*CH$_2$C$_8$F$_{17}$).

^{19}F-NMR (377 MHz, CDCl$_3$, δ/ppm): -81.0 (*t*, *J* = 10 Hz, 6F, C*F$_3$*), -114.7 (*m*, 4F, C*F$_2$*), -122.0 (*m*, 4F, C*F$_2$*), -122.2 (*m*, 8F, C*F$_2$*), -123.0 (*m*, 4F, C*F$_2$*), -123.7 (*m*, 4F, C*F$_2$*), -126.4 (*m*, 4F, C*F$_2$*).

^{13}C-NMR (126 MHz, CDCl$_3$, δ/ppm): 144.7, 138.7, 137.5, 129.6, 128.0, 127.7, 126.8, 125.5, 72.7, 68.8, 67.5, 36.8, 28.0, 20.8.

MS (ESI-Q-ToF, m/z): 1369 (54%, [M+Na]$^+$), 685 (100%).

EA: calculated: C = 44.59, H = 2.69, found: C = 44.83, H = 2.65.

(3,5-Bis((3-perfluorooctylpropoxy)methyl)phenyl)methanethiol (53)
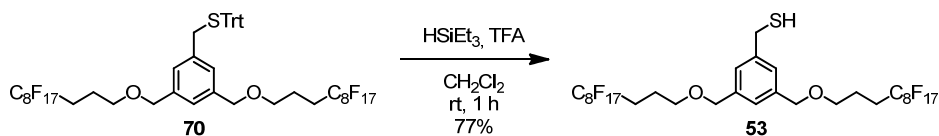
(3,5-Bis((3-perfluorooctyl-propoxy)methyl)benzyl)(trityl)sulfane (**70**, 650 mg, 0.48 mmol, 1.0 eq.) and triethylsilane (117 µL, 84 mg, 0.72 mmol, 1.5 eq.) were dissolved in dry dichloromethane (20 mL). Trifluoroacetic acid (800 µL) was added dropwise and the reaction mixture was stirred for one hour at room temperature. The reaction was quenched by the addition of a saturated aqueous solution of sodium hydrogen carbonate. After completion of the gas formation, the phases were separated and the aqueous phase was extracted with dichloromethane. The combined organic fractions were dried over magnesium sulfate, filtered and evaporated to dryness. After purification by column chromatography (silica gel, cyclohexane/dichloromethane 2:1, then 1:1, then 1:2), the thiol **53** ($C_{31}H_{22}F_{34}O_2S$, 413 mg) was obtained as white solid in a yield of 77%.

^{1}H-NMR (500 MHz, CDCl$_3$, δ/ppm): 7.21 (*s*, 2H, Aryl-*H*), 7.18 (*s*, 1H, Aryl-*H*), 4.50 (*s*, 4H, ArC*H*$_2$OCH$_2$), 3.75 (*d*, $^3J_{HH}$ = 7.6 Hz, 2H, C*H*$_2$SH), 3.55 (*t*, $^3J_{HH}$ = 6.0 Hz, 4H, ArCH$_2$OC*H*$_2$), 2.27 – 2.16 (*m*, 4H, C*H*$_2$C$_8$F$_{17}$), 1.95 – 1.89 (*m*, 4H, C*H*$_2$CH$_2$C$_8$F$_{17}$), 1.77 (*t*, $^3J_{HH}$ = 7.6 Hz, 1H, S*H*).

^{19}F-NMR (377 MHz, CDCl$_3$, δ/ppm): -81.0 (*t*, *J* = 10 Hz, 6F, C*F*$_3$), -114.7 (*m*, 4F, C*F*$_2$), -122.0 (*m*, 4F, C*F*$_2$), -122.2 (*m*, 8F, C*F*$_2$), -123.0 (*m*, 4F, C*F*$_2$), -123.7 (*m*, 4F, C*F*$_2$), -126.4 (*m*, 4F, C*F*$_2$).

^{13}C-NMR (126 MHz, CDCl$_3$, δ/ppm): 141.6, 139.0, 126.6, 125.4, 72.7, 68.9, 28.8, 28.0, 20.8.

MS (ESI-Q-ToF, m/z): 1127 (100%, [M+Na]$^+$).

EA: calculated: C = 33.71, H = 2.01, found: C = 33.74, H = 2.05.

(3,5-Bis(((4-methyl-3,5-bis(perfluorohexyl)benzyl)thio)methyl)benzyl)-(trityl)sulfane (73)
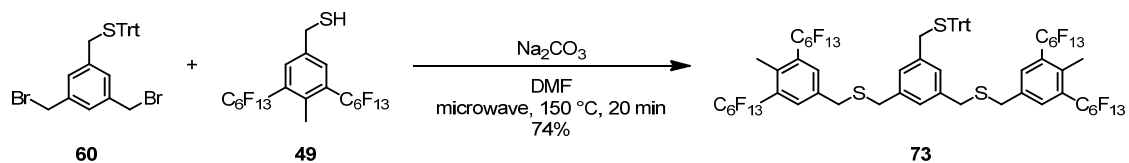
(3,5-Bis(bromomethyl)benzyl)(trityl)sulfane (**60**, 27 mg, 48.9 μmol, 1.0 eq.), thiol **49** (94 mg, 122 μmol, 2.5 eq.) and sodium carbonate (16 mg, 147 μmol, 3.0 eq.) were added to dry DMF (12 mL) in a microwave vial (Biotage microwave vial 10-20 mL). The sealed tube was heated in a microwave apparatus (Biotage, Initiator 8) to 150 °C for 20 minutes. After cooling to room temperature the reaction mixture was diluted with water and diethylether. The organic phase was separated, washed with brine and dried over magnesium sulfate. After evaporation of the solvent under reduced pressure the crude was purified by column chromatography using silica gel (eluent: dichloromethane/hexane 1:3) to afford the desired compound **73** ($C_{68}H_{38}F_{52}S_3$, 70 mg) as an off-white solid in a yield of 74%.

^{1}H-NMR (400 MHz, CDCl$_3$, δ/ppm): 7.64 (*s*, 4H, Aryl-*H*), 7.48 – 7.42 (*m*, 6H, Aryl-*H*$_{ortho}$ of trityl group), 7.33 – 7.27 (*m*, 6H, Aryl-*H*$_{meta}$ of trityl group), 7.24 – 7.19 (*m*, 3H, Aryl-*H*$_{para}$ of trityl group), 6.93 (*s*, 2H, Aryl-*H*), 6.90 (*s*, 1H, Aryl-*H*), 3.58 (*s*, 4H, C*H*$_2$), 3.49 (*s*, 4H, C*H*$_2$) 3.30 (*s*, 2H, ArC*H*$_2$STrt), 2.51 (*s*, 6H, C*H*$_3$).

^{19}F-NMR (377 MHz, CDCl$_3$, δ/ppm): -81.1 (*t*, *J* = 10 Hz, 6F, C*F*$_3$), -103.7 (*m*, 4F, C*F*$_2$), -120.3 (*m*, 4F, C*F*$_2$), -121.9 (*m*, 8F, C*F*$_2$), -123.0 (*m*, 4F, C*F*$_2$), -126.4 (*m*, 4F, C*F*$_2$).

(3,5-Bis(((4-methyl-3,5-bis(perfluorohexyl)benzyl)oxy)methyl)benzyl)-(trityl)sulfane (74)
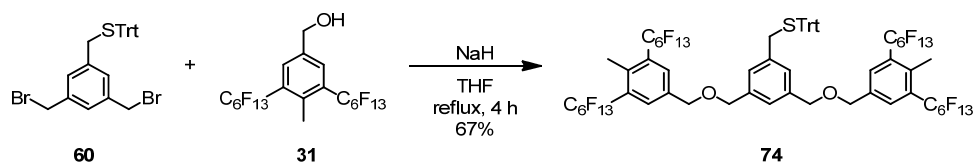
Alcohol **31** (892 mg, 1.88 mmol, 2.6 eq.) and (3,5-bis(bromomethyl)benzyl)-(trityl)sulfane (**60**, 250 mg, 453 µmol, 1.0 eq.) were dissolved in dry THF (20 mL) under an atmosphere of argon. Sodium hydride (60% dispersion in mineral oil, 108 mg, 2.72 mmol, 6.0 eq.) was added and the reaction mixture was stirred for 4 hours at reflux. After cooling to room temperature it was quenched with a saturated aqueous ammonium chloride solution. The mixture was extracted with diethylether and the organic fractions were washed with brine, dried over magnesium sulfate, filtered and evaporated to dryness. Purification by column chromatography (silica gel, hexane/acetone 12:1) gave the title compound **74** ($C_{68}H_{38}F_{52}O_2S$, 580 mg) as a colorless oil in a yield of 67%.

TLC: R_f = 0.70 (hexane/acetone 12:1).

^{1}H-NMR (400 MHz, CDCl$_3$, δ/ppm): 7.72 (*s*, 4H, Aryl-*H*), 7.47 – 7.44 (*m*, 6H, Aryl-*H$_{ortho}$* of trityl group), 7.31 – 7.26 (*m*, 6H, Aryl-*H$_{meta}$* of trityl group), 7.23 – 7.19 (*m*, 3H, Aryl-*H$_{para}$* of trityl group), 7.18 (*s*, 1H, Aryl-*H*), 7.05 (*s*, 2H, Aryl-*H*), 4.56 (*s*, 4H, C*H$_2$*), 4.52 (*s*, 4H, C*H$_2$*) 3.33 (*s*, 2H, ArC*H$_2$*STrt), 2.53 (*s*, 6H, C*H$_3$*).

^{19}F-NMR (377 MHz, CDCl$_3$, δ/ppm): -81.1 (*t*, *J* = 10 Hz, 12F, C*F$_3$*), -103.6 (*m*, 8F, C*F$_2$*), -120.3 (*m*, 8F, C*F$_2$*), -122.0 (*m*, 8F, C*F$_2$*), -123.0 (*m*, 8F, C*F$_2$*), -126.4 (*m*, 8F, C*F$_2$*).

^{13}C-NMR (126 MHz, CDCl$_3$, δ/ppm): 144.8, 138.7, 138.4, 138.2, 137.0, 131.6 (*t*, $^3J_{CF}$ = 10 Hz), 130.0 (*t*, $^2J_{CF}$ = 22 Hz), 129.8, 128.4, 128.1, 126.9, 126.1, 72.5, 70.7, 67.7, 36.9, 16.0.

MS (ESI-Q-ToF, m/z): 1929 (89%, [M+Na]$^+$), 686 (100%).

EA: calculated: C = 42.83, H = 2.01, found: C = 43.11, H = 2.16.

(3,5-Bis(((4-methyl-3,5-bis(perfluorohexyl)benzyl)oxy)methyl)phenyl)-methanethiol (55)
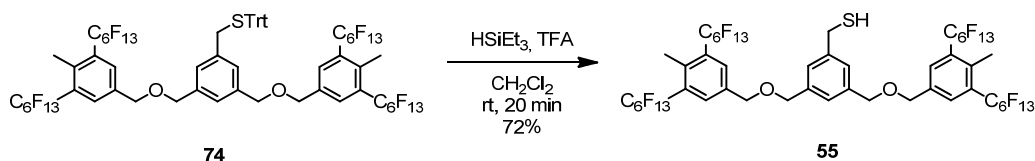
Compound **74** (675 mg, 0.35 mmol, 1.0 eq.) and triethylsilane (86 µL, 62 mg, 0.53 mmol, 1.5 eq.) were dissolved in dry CH_2Cl_2 (25 mL). Trifluoroacetic acid (1.0 mL) was added dropwise and the reaction mixture was stirred for 20 minutes at room temperature. The reaction was quenched by the addition of a saturated aqueous solution of sodium hydrogen carbonate. After completion of the gas formation, the phases were separated and the aqueous phase was extracted with CH_2Cl_2. The combined organic fractions were dried over magnesium sulfate, filtered and evaporated to dryness. After purification by column chromatography (silica gel, hexane/CH_2Cl_2 2:1), the thiol **55** ($C_{49}H_{24}F_{52}O_2S$, 425 mg) was obtained as a white solid in a yield of 72%.

TLC: R_f = 0.48 (hexane/dichloromethane 2:1).

^{1}H-NMR (500 MHz, CDCl$_3$, δ/ppm): 7.75 (s, 4H, Aryl-*H*), 7.28 (s, 2H, Aryl-*H*), 7.22 (s, 1H, Aryl-*H*), 4.61 (s, 4H, C*H*$_2$), 4.57 (s, 4H, C*H*$_2$), 3.74 (d, $^3J_{HH}$ = 7.7 Hz, 2H, Ar-C*H*$_2$SH), 2.54 (s, 6H, C*H*$_3$), 1.76 (t, $^3J_{HH}$ = 7.7 Hz, 1H, S*H*).

^{19}F-NMR (377 MHz, CDCl$_3$, δ/ppm): -81.1 (t, *J* = 10 Hz, 12F, C*F*$_3$), -103.6 (m, 8F, C*F*$_2$), -120.3 (m, 8F, C*F*$_2$), -121.9 (m, 8F, C*F*$_2$), -123.0 (m, 8F, C*F*$_2$), -126.4 (m, 8F, C*F*$_2$).

^{13}C-NMR (126 MHz, CDCl$_3$, δ/ppm): 142.0, 138.6, 138.5, 136.8, 131.5 (t, $^3J_{CF}$ = 10 Hz), 129.8 (t, $^2J_{CF}$ = 22 Hz), 127.1, 125.9, 72.3, 70.6, 28.7, 15.9.

MS (ESI-Q-ToF, m/z): 1687 (100%, [M+Na]$^+$).

EA: calculated: C = 35.35, H = 1.45, found: C = 35.26, H = 1.54.

5,10,15,20-Tetrakis[4-(2-perfluorooctylethylthio)-2,3,5,6-tetrafluorophenyl]-porphyrin (40)
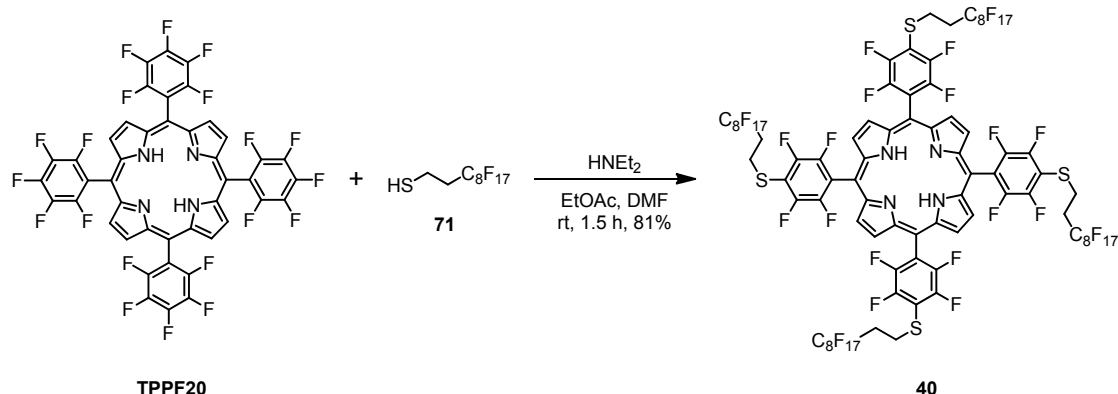
Thiol **71** (704 μL, 1.18 g, 2.46 mmol, 8.0 eq.) was added under an atmosphere of argon to a mixture of ethyl acetate (60 mL) and dry DMF (20 mL). To this solution was added diethylamine (0.45 mL) and a solution of **TPPF20** (300 mg, 308 μmol, 1.0 eq.) in dry DMF (30 mL). The reaction mixture was stirred under argon at room temperature for 1.5 hours and was then quenched by the addition of water and subsequently diluted with diethylether. After phase separation the aqueous phase was extracted with diethylether. The combined organic phases were washed with brine and evaporated to dryness. The crude was purified by column chromatography using silica gel (hexane/acetone 9:1) to give porphyrin **40** ($C_{84}H_{26}F_{84}N_4S_4$, 700 mg) as purple solid in a yield of 81%.

TLC: R_f = 0.62 (hexane/acetone 9:1).

^{1}H-NMR (400 MHz, CDCl$_3$, δ/ppm): 8.91 (*s*, 8H, β-*H*), 3.51 – 3.47 (*m*, 8H, C*H*$_2$), 2.77 – 2.64 (*m*, 8H, C*H*$_2$), -2.87 (*s*, 2H, N*H*).

^{19}F-NMR (377 MHz, CDCl$_3$, δ/ppm): -81.0 (*t*, *J* = 10 Hz, 12F, C*F*$_3$), -114.1 (*m*, 8F, C*F*$_2$), -121.8 (*m*, 8F, C*F*$_2$), -122.1 (*m*, 16F, C*F*$_2$), -123.0 (*m*, 8F, C*F*$_2$), -123.4 (*m*, 8F, C*F*$_2$), -126.4 (*m*, 8F, C*F*$_2$), -133.9 (*m*, 8F, Aryl-*F*), -136.3 (*m*, 8F, Aryl-*F*).

MS (MALDI-ToF, m/z): 2814 (100%, M$^+$).

EA: calculated: C = 35.84, H = 0.93, N = 1.99, found: C = 35.79, H = 1.10, N = 2.16.

HPLC (Fluoro*Flash*; 1.4 mL/min; 24 bar; 100% THF; 50 °C): R_t = 1.82 min (97.6%).

UV/Vis (CH$_2$Cl$_2$): λ$_{max}$ = 415, 508, 536, 584 nm.

5,10,15,20-Tetrakis[4-(4-methyl-3,5-bis(perfluorohexyl)benzylthio)-2,3,5,6-tetrafluoro-phenyl]-porphyrin (42)
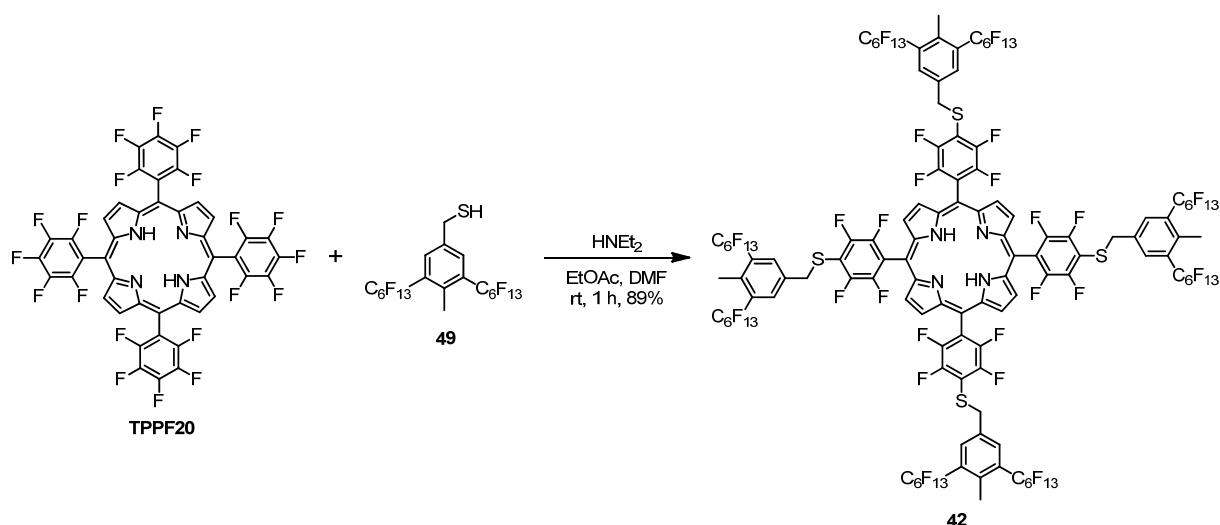
4-Methyl-3,5-bis(perfluoro-hexyl)benzyl thiol (**49**, 143 mg, 184 µmol, 6.0 eq.) was added under an atmosphere of argon to a mixture of ethyl acetate (4 mL) and DMF (2 mL). Diethylamine (60 µL) and a solution of **TPPF20** (30 mg, 30.8 µmol, 1.0 eq.) in DMF (3 mL) was added. The reaction mixture was stirred under argon at room temperature for 1.5 hours and was then quenched by the addition of water and subsequently diluted with diethylether. After phase separation the aqueous phase was extracted with diethylether. The combined organic phases were washed with brine and evaporated to dryness. The crude was purified by column chromatography using silica gel (hexane/acetone 9:1). Porphyrin **42** ($C_{124}H_{38}F_{120}N_4S_4$, 109 mg) was obtained as a purple solid in a yield of 89%.

TLC: R_f = 0.29 (hexane/acetone 9:1).

^{1}H-NMR (400 MHz, CDCl$_3$, δ/ppm): 8.69 (*s*, 8H, β-*H*), 7.91 (*s*, 8H, Aryl-*H*), 4.49 (*s*, 8H, C*H$_2$*), 2.64 (*s*, 12H, C*H$_3$*), -2.96 (*s*, 2H, N*H*).

^{19}F-NMR (377 MHz, CDCl$_3$, δ/ppm): -81.2 (*t*, *J* = 10 Hz, 24F, C*F$_3$*), -103.6 (*m*, 16F, C*F$_2$*), -120.2 (*m*, 16F, C*F$_2$*), -121.9 (*m*, 16F, C*F$_2$*), -123.0 (*m*, 16F, C*F$_2$*), -126.5 (*m*, 16F, C*F$_2$*), -134.0 (*m*, 8F, Aryl-*F*), -136.9 (*m*, 8F, Aryl-*F*).

MS (MALDI-ToF, m/z): 3990 (100%, M$^+$).

HPLC (Fluoro*Flash*; 1.4 mL/min; 24 bar; 100% THF; 50 °C): R_t = 7.07 min (97.2%).

UV/Vis (CH$_2$Cl$_2$): λ_{max} = 415, 508, 536, 584 nm.

5,10,15,20-Tetrakis[4-(2,2-di(3-perfluorohexylpropyl)ethylthio)-2,3,5,6-tetrafluoro-phenyl]-porphyrin (44)
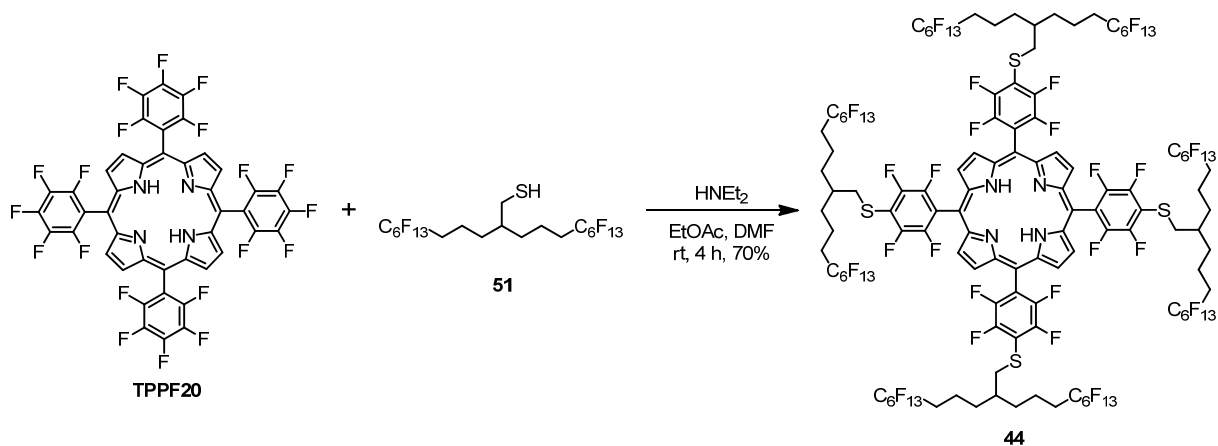
1,7-Diperfluorohexyl-4-((hydrothio)-methyl)heptane (**51**, 321 mg, 410 μmol, 10.0 eq.) was added under an atmosphere of argon to a mixture of ethyl acetate (1.5 mL) and DMF (6 mL). Diethylamine (150 μL) and a solution of 5,10,15,20-tetrakis(pentafluorophenyl)-porphyrin (**TPPF20**, 40 mg, 41.0 μmol, 1.0 eq.) in DMF (4 mL) was added. The reaction mixture was stirred under argon at room temperature for 4 hours and was then quenched by the addition of water and subsequently diluted with diethylether. After phase separation the aqueous phase was extracted with diethylether. The combined organic phases were washed with brine and evaporated to dryness. The crude was purified by column chromatography using silica gel (hexane/acetone 12:1) to afford the title compound **44** ($C_{124}H_{70}F_{120}N_4S_4$, 116 mg) as a purple solid in a yield of 70%.

1H-NMR (400 MHz, $CDCl_3$, δ/ppm): 8.90 (*s*, 8H, Aryl-*H*), 3.28 (*d*, $^3J_{HH}$ = 6.0 Hz, 8H, ArSC*H₂*), 2.27 − 2.10 (*m*, 16H, C*H₂*CF_2), 1.94 − 1.83 (*m*, 4H, ArSCH₂C*H*), 1.81 − 1.62 (*m*, 32H, C*H₂*), -2.87 (*s*, 2H, N*H*).

19F-NMR (377 MHz, $CDCl_3$, δ/ppm): -81.2 (*t*, *J* = 10 Hz, 24F, C*F₃*), -114.5 (*m*, 16F, C*F₂*), -122.2 (*m*, 16F, C*F₂*), -123.2 (*m*, 16F, C*F₂*), -123.8 (*m*, 16F, C*F₂*), -126.5 (*m*, 16F, C*F₂*), -134.3 (*m*, 8F, Ar-*F*), -137.0 (*m*, 8F, Ar-*F*).

MS (MALDI-ToF, m/z): 4022 (100%, M⁺).

HPLC (Fluoro*Flash*; 1.4 mL/min; 24 bar; 100% THF; 50 °C): R_t = 7.12 min (97.7%).

UV/Vis (CH_2Cl_2): λ_{max} = 415, 508, 536, 584 nm.

5,10,15,20-Tetrakis[4-((3,5-bis((3-perfluorooctylpropoxy)methyl)phenyl)methanethio)-2,3,5,6-tetrafluorophenyl]porphyrin (46)
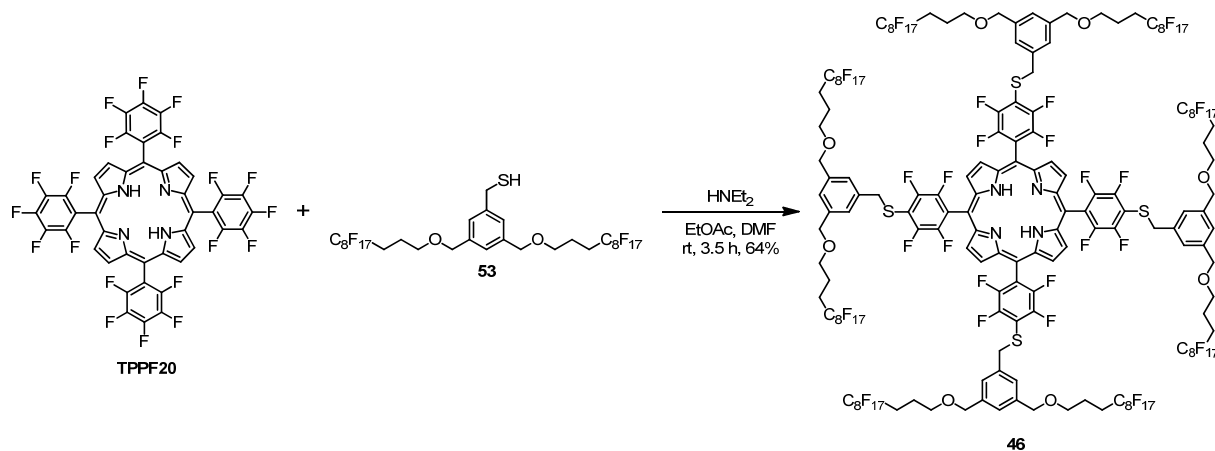
Thiol **53** (136 mg, 123 μmol, 8.0 eq.) was added under an atmosphere of argon to a mixture of ethyl acetate (2 mL) and dimethylformamide (1 mL). Diethylamine (100 μL) and a solution of **TPPF20** (15 mg, 15.4 μmol, 1.0 eq.) in dimethylformamide (2 mL) were subsequently added. The reaction mixture was stirred under argon at room temperature for 3.5 hours and was then quenched by the addition of water and subsequently diluted with diethylether. After phase separation the aqueous phase was extracted with diethylether. The combined organic phases were washed with brine and evaporated to dryness. The crude was purified by column chromatography using silica gel (hexane/acetone 8:1). Porphyrin **46** ($C_{168}H_{94}F_{152}N_4O_8S_4$, 52 mg) was obtained as a purple solid in a yield of 64%.

TLC: R_f = 0.18 (hexane/acetone 5:1).

^{1}H-NMR (400 MHz, CDCl$_3$, δ/ppm): 8.75 (*s*, 8H, Aryl-*H*), 7.42 (*s*, 8H, Aryl-*H*), 7.36 (*s*, 4H, Aryl-*H*), 4.61 (*s*, 16H, ArC*H$_2$*OC*H$_2$*), 4.48 (*s*, 8H, ArC*H$_2$*S), 3.55 (*t*, $^3J_{HH}$ = 6.0 Hz, 16H), 2.21 − 2.05 (*m*, 16H, C*H$_2$*CF$_2$), 1.89 − 1.81 (*m*, 16H, C*H$_2$*CH$_2$CF$_2$), -2.94 (*s*, 2H, N*H*).

^{19}F-NMR (377 MHz, CDCl$_3$, δ/ppm): -81.2 (*t*, *J* = 10 Hz, 24F, C*F$_3$*), -114.9 (*m*, 16F, C*F$_2$*), -122.2 (*m*, 16F, C*F$_2$*), -122.4 (*m*, 32F, C*F$_2$*), -123.1 (*m*, 16F, C*F$_2$*), 123.9 (*m*, 16F, C*F$_2$*), -126.5 (*m*, 16F, C*F$_2$*), -133.8 (*m*, 8F, Ar-*F*), -137.7 (*m*, 8F, Ar-*F*).

MS (MALDI-ToF, m/z): 5310 (100%, M$^+$).

HPLC (Fluoro*Flash*; 1.4 mL/min; 24 bar; 100% THF; 50 °C): R$_t$ = 21.70 min (97.6%).

UV/Vis (CH$_2$Cl$_2$): λ$_{max}$= 415, 508, 537, 585 nm.

5,10,15,20-Tetrakis[4-((3,5-bis(((4-methyl-3,5-bis(perfluorohexyl)benzyl)oxy)methyl)-phenyl)methanethio)-2,3,5,6-tetrafluorophenyl]-porphyrin (48)
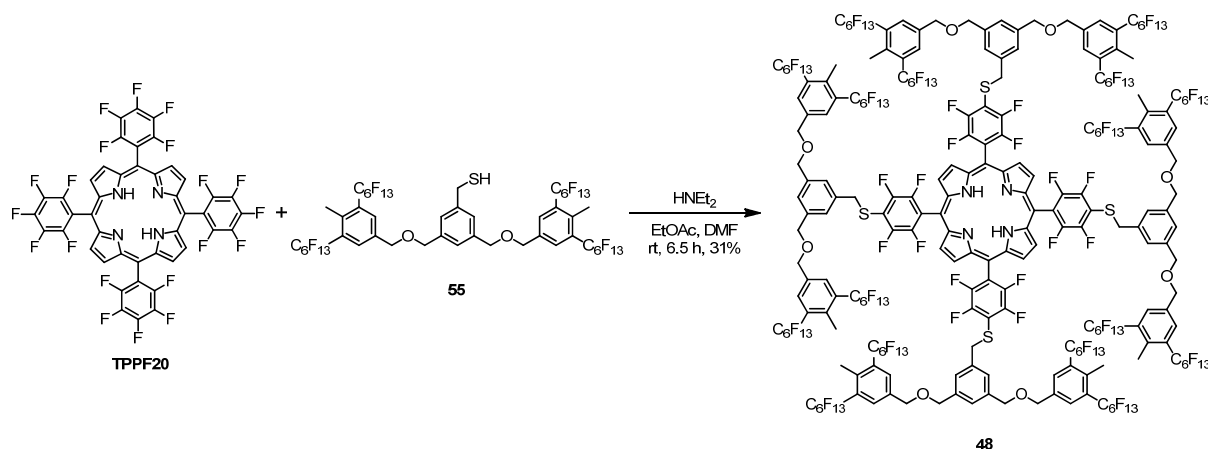
Thiol **55** (150 mg, 90.3 μmol, 8.0 eq.) was added under an atmosphere of argon to a mixture of ethyl acetate (5 mL) and DMF (5 mL). Diethylamine (100 μL) and a solution of 5,10,15,20-tetrakis(pentafluorophenyl)-porphyrin (**TPPF20**, 11 mg, 11.3 μmol, 1.0 eq.) in DMF (4 mL) was added. The reaction mixture was stirred under argon at room temperature for 3.5 hours and was then quenched by the addition of water and subsequently diluted with diethylether. After phase separation the aqueous phase was extracted with diethylether. The combined organic phases were washed with brine and evaporated to dryness. After purification by a short column chromatography using silica gel (hexane/acetone 12:1) the obtained compound mixture was further purified by recycling gel permeations chromatography (flow rate: 2.0 mL/min, 34 cycles). The desired porphyrin **48** ($C_{240}H_{102}F_{224}N_4O_8S_4$, 26 mg) was obtained as a purple solid in a yield of 31%.

TLC: R_f = 0.79 (hexane/acetone 5:1).

^{1}H-NMR (400 MHz, CDCl$_3$, δ/ppm): 8.78 (*s*, 8H, β-*H*), 7.71 (*s*, 16H, Aryl-*H*), 7.47 (*s*, 8H, Aryl-*H*), 7.39 (*s*, 4H, Ar-*H*), 4.65 (*s*, 16H, C*H$_2$*), 4.59 (*s*, 16H, C*H$_2$*), 4.45 (*s*, 8H, ArSC*H$_2$*), 2.46 (*s*, 24H, C*H$_3$*), -2.95 (*s*, 2H, N*H*).

^{19}F-NMR (377 MHz, CDCl$_3$, δ/ppm): -81.1 (*t*, *J* = 10 Hz, 48F, C*F$_3$*), -103.6 (*m*, 32F, C*F$_2$*), -120.2 (*m*, 32F, C*F$_2$*), -121.9 (*m*, 32F, C*F$_2$*), -123.0 (*m*, 32F, C*F$_2$*), -126.4 (*m*, 32F, C*F$_2$*), -133.8 (*m*, 8F, Aryl-*F*), -137.5 (*m*, 8F, Aryl-*F*).

MS (MALDI-ToF, m/z): 7550 (100%, M$^+$).

UV/Vis (CH$_2$Cl$_2$): λ_{max} = 415, 508, 536, 585 nm.

5,10,15,20-Tetrakis[4-(3-perfluorooctylpropylamino)-2,3,5,6-tetra-fluorophenyl]-porphyrin (41)
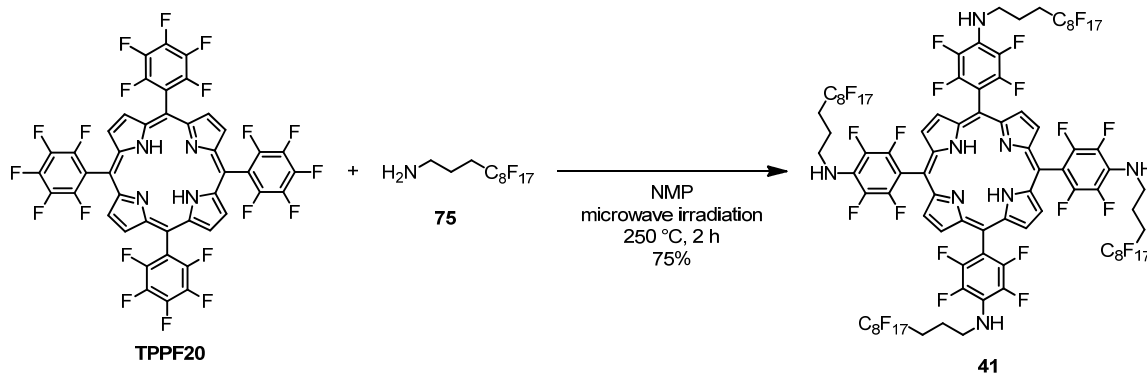
5,10,15,20-Tetrakis(pentafluoro-phenyl)-porphyrin (**TPPF20**, 100 mg, 103 µmol, 1.0 eq.) and 3-(perfluorooctyl)propylamine (**75**, 490 mg, 1.03 mmol, 10.0 eq.) were added to a microwave vial (Biotage microwave vial 10-20 mL). The mixture was dissolved in NMP (10 mL) and the sealed tube was heated in a microwave apparatus (Biotage, Initiator 8) to 250 °C for two hours. After cooling to room temperature the reaction mixture was diluted with diethylether and water. The organic phase was separated and washed with brine. After evaporation of the solvent under reduced pressure the crude was purified by column chromatography using silica gel (eluent: acetone/hexane 1:9 then 1:6) to afford the desired compound **41** ($C_{88}H_{38}F_{84}N_8$, 214 mg) as a purple solid in a yield of 75%.

¹H-NMR (400 MHz, CDCl$_3$, δ/ppm): 8.94 (*s*, 8H, Aryl-*H*), 4.31 − 4.23 (*m*, 4H, ArN*H*CH$_2$), 3.82 − 3.73 (*m*, 8H, C*H*$_2$), 2.45 − 2.29 (*m*, 8H, C*H*$_2$), 2.21 − 2.11 (*m*, 8H, C*H*$_2$), -2.85 (*s*, 2H, N*H*).

¹⁹F-NMR (377 MHz, CDCl$_3$, δ/ppm): -81.0 (*t*, *J* = 10 Hz, 12F, C*F*$_3$), -114.2 (*m*, 8F, C*F*$_2$), -121.8 (*m*, 8F, C*F*$_2$), -122.1 (*m*, 16F, C*F*$_2$), -122.9 (*m*, 8F, C*F*$_2$), -123.5 (*m*, 8F, C*F*$_2$), -126.3 (*m*, 8F, C*F*$_2$), -140.2 (*m*, 8F, Aryl-*F*), -160.9 (m, 8F, Aryl-*F*).

MS (MALDI-ToF, m/z): 2802 (100%, M⁺).

HPLC (Fluoro*Flash*; 1.4 mL/min; 24 bar; 100% THF; 50 °C): R$_t$ = 1.52 min (97.0%).

UV/Vis (CH$_2$Cl$_2$): λ_{max} = 420, 511, 545, 586 nm.

5,10,15,20-Tetrakis[4-(4-methyl-3,5-bis(perfluorohexyl)benzylamino)-2,3,5,6-tetrafluoro-phenyl]-porphyrin (43)
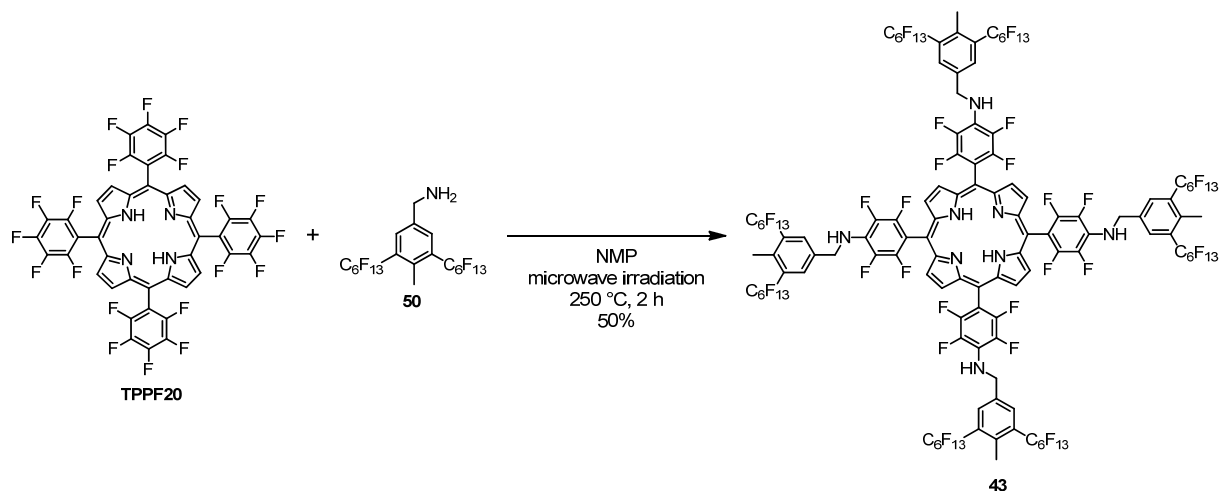
5,10,15,20-Tetrakis(pentafluoro-phenyl)-porphyrin (**TPPF20**, 80 mg, 82.1 µmol, 1.0 eq.) and 4-methyl-3,5-bis(perfluorohexyl)benzylamine (**50**, 622 mg, 821 µmol, 10.0 eq.) were added to a microwave vial (Biotage microwave vial 10-20 mL). The mixture was dissolved in NMP (10 mL) and the sealed tube was heated in a microwave apparatus (Biotage, Initiator 8) to 250 °C for two hours. After cooling to room temperature the reaction mixture was diluted with diethylether and water. The organic phase was separated and washed with brine. After evaporation of the solvent under reduced pressure the crude was purified by column chromatography using silica gel (eluent: acetone/hexane 1:9) to afford the desired compound **43** ($C_{124}H_{42}F_{120}N_8$, 162 mg) as a purple solid in a yield of 50%.

^{1}H-NMR (400 MHz, CDCl$_3$, δ/ppm): 8.84 (*s*, 8H, β-*H*), 7.95 (*s*, 8H, Aryl-*H*), 4.93 (*d*, $^3J_{HH} = 6.6$ Hz, 8H, ArC*H*$_2$NHAr), 4.77 – 4.68 (*m*, 4H, ArCH$_2$N*H*Ar), 2.64 (*s*, 12H, C*H*$_3$), -2.91 (*s*, 2H, N*H*).

^{19}F-NMR (377 MHz, CDCl$_3$, δ/ppm): -81.2 (*t*, *J* = 10 Hz, 24F, C*F*$_3$), -103.7 (*m*, 16F, C*F*$_2$), -120.3 (*m*, 16F, C*F*$_2$), -121.9 (*m*, 16F, C*F*$_2$), -122.9 (*m*, 16F, C*F*$_2$), -126.4 (*m*, 16F, C*F*$_2$), -139.9 (*m*, 8F, Aryl-*F*), -160.0 (*m*, 8F, Aryl-*F*).

MS (MALDI-ToF, m/z): 3922 (100%, M$^+$).

HPLC (Fluoro*Flash*; 1.4 mL/min; 24 bar; 100% THF; 50 °C): R$_t$ = 6.63 min (97.1%).

UV/Vis (CH$_2$Cl$_2$): λ_{max} = 419, 510, 542, 586 nm.

1st Generation porphyrin library: TPPF20-x+17x
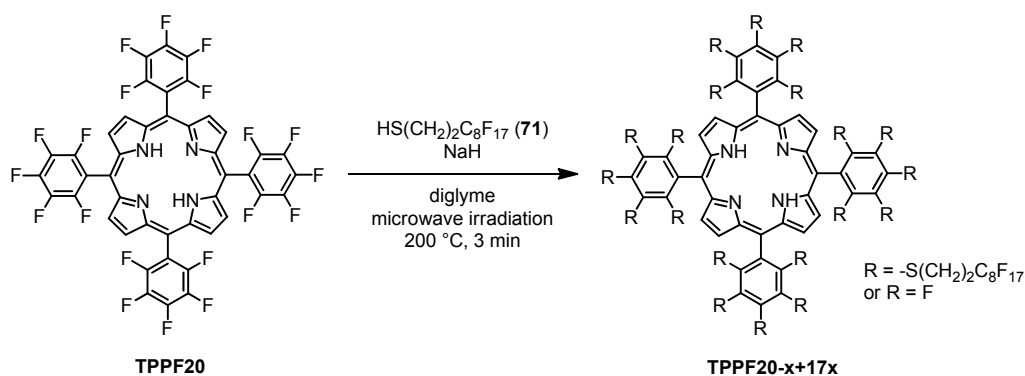
TPPF20   **TPPF20-x+17x**

5,10,15,20-Tetrakis(pentafluoro-phenyl)-porphyrin (**TPPF20**, 4.0 mg, 4.10 µmol, 1.0 eq.), 1*H*,1*H*,2*H*,2*H*-perfluorodecane-1-thiol (**71**, 138 mg, 287 µmol, 70 eq.) and sodium hydride (60% dispersion in mineral oil, 16.4 mg, 410 µmol, 100 eq.) were added to diglyme (4 mL) in a microwave vial. The sealed tube was heated under microwave irradiation to 200 °C for 3 minutes. After cooling to room temperature the reaction mixture was quenched with water and subsequently extracted with diethylether. The organic layer was washed with brine and water, dried over sodium sulfate and evaporated to dryness. The resulting product mixture (85 mg) was analyzed by MALDI-ToF mass spectrometry.

MS (MALDI-ToF, m/z): 5 577 (12%), 6 048 (23%), 6 496 (57%), 6 957 (91%), 7 416 (100%), 7 877 (89%), 8 337 (78%), 8 797 (45%), 9 257 (31%), 9 637 (16%).

2nd Generation porphyrin library: TPPF20-x+26x
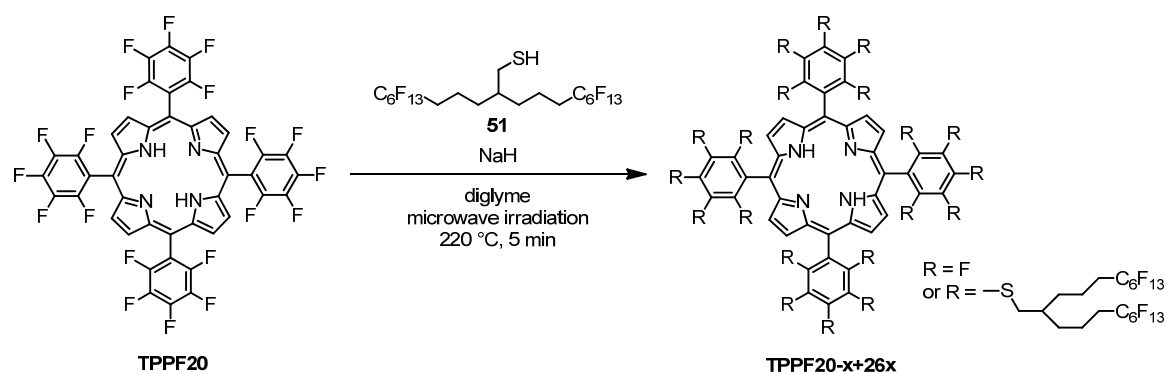
5,10,15,20-Tetrakis(pentafluoro-phenyl)-porphyrin (**TPPF20**, 4.0 mg, 4.10 µmol, 1.0 eq.), thiol **51** (193 mg, 246 µmol, 60 eq.) and sodium hydride (60% dispersion in mineral oil, 14.8 mg, 369 µmol, 90 eq.) were added to diglyme (4 mL) in a microwave vial. The sealed tube was heated under microwave irradiation to 220 °C for 5 minutes. After cooling to room temperature the reaction mixture was quenched with water and subsequently extracted with diethylether. The organic layer was washed with brine and water, dried over sodium sulfate and evaporated to dryness. The resulting product mixture (183 mg) was analyzed by MALDI-ToF mass spectrometry.

MS (MALDI-ToF, m/z): 12 403 (29%), 11 645 (52%), 10 884 (100%), 10 121 (78%), 9 339 (15%), 8 597 (7%).

5,10,15,20-Tetrakis(4-phenoxy-2,3,5,6-tetrafluorophenyl)porphyrin (80)
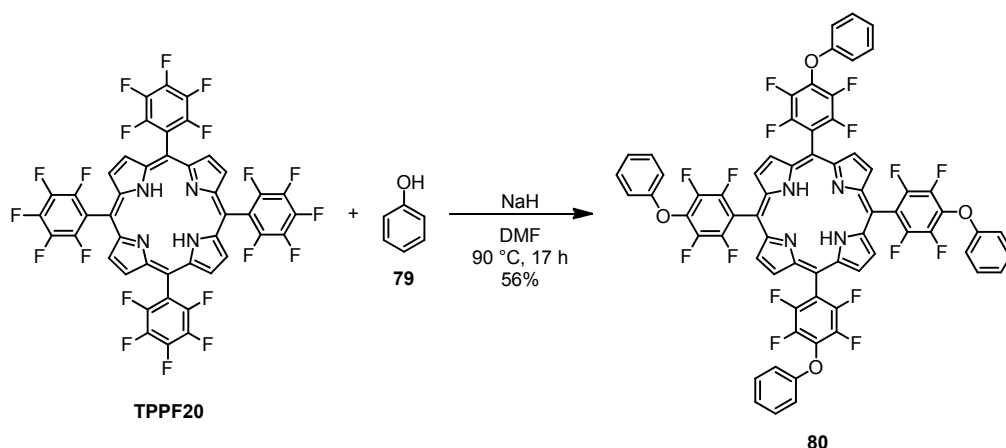
Phenol (**79**, 14.5 mg, 154 µmol, 5.0 eq.) was added under an atmosphere of argon to a suspension of sodium hydride (60% dispersion in mineral oil, 11 mg, 462 µmol, 15 eq.) in dry DMF (4 mL). The mixture was stirred at room temperature for 20 minutes. 5,10,15,20-Tetrakis(pentafluorophenyl)-porphyrin (**TPPF20**, 30 mg, 30.8 µmol, 1.0 eq.) was added and the reaction mixture was stirred at 90 °C for 17 hours. After cooling to room temperature, the solvent was evaporated and the crude was purified by column chromatography using silica gel and a mixture of dichloromethane and hexane (1:1) as eluent. Porphyrin **80** ($C_{68}H_{30}F_{16}N_4O_4$, 22 mg) was obtained as a purple solid in a yield of 56%.

TLC: R_f = 0.67 (hexane/dichloromethane 1:1).

^{1}H-NMR (500 MHz, d_6-acetone, δ/ppm): 9.49 (*s*, br, 8H, β-*H*), 7.59 – 7.55 (*m*, 8H, Aryl-*H*), 7.54 – 7.51 (*m*, 8H, Aryl-*H*), 7.31 (*tt*, $^3J_{HH}$ = 7.4 Hz, $^4J_{HH}$ = 1.2 Hz, 4H, Aryl-*H*), -2.83 (*s*, br, 2H, N*H*).

^{19}F-NMR (377 MHz, d_6-acetone, δ/ppm): -140.3 (*dd*, *J* = 22 Hz, *J* = 8 Hz, 8F, Aryl-*F*), 156.5 (*dd*, *J* = 22 Hz, *J* = 8 Hz, 8F, Aryl-*F*).

MS (MALDI-ToF, m/z): 1270 (100%, M$^+$).

5,10,15,20-Tetrakis[4-(3,4,5-trifluorophenoxy)-2,3,5,6-tetrafluorophenyl]porphyrin (TPPF28)
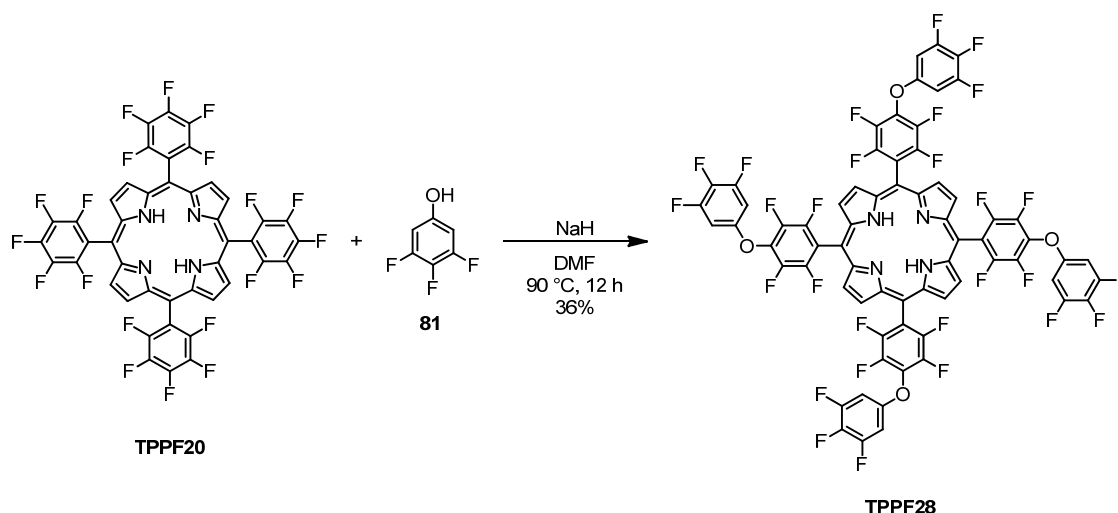
3,4,5-Trifluorophenol (**81**, 213 mg, 1.44 mmol, 7.0 eq.) was added under an atmosphere of argon to a suspension of sodium hydride (60% dispersion in mineral oil, 123 mg, 3.08 mmol, 15 eq.) in dry DMF (25 mL). The mixture was stirred at room temperature for 20 minutes. 5,10,15,20-Tetrakis(pentafluorophenyl)-porphyrin (**TPPF20**, 200 mg, 205 μmol, 1.0 eq.) was added and the reaction mixture was stirred at 90 °C for 12 hours. After cooling to room temperature, the solvent was evaporated and the crude was dissolved in acetone and absorbed on silica gel. Purification by column chromatography using silica gel and a mixture of acetone and hexane (1:6) as eluent and subsequently recrystallization from acetone afforded **TPPF28** ($C_{68}H_{18}F_{28}N_4O_4$, 109 mg) as purple crystals in a yield of 36%.

^{1}H-NMR (400 MHz, d_6-acetone, δ/ppm): 9.51 (*s*, br, 8H, β-*H*), 7.57 − 7.49 (*m*, 8H, Aryl-*H*), -2.83 (*s*, br, 2H, N*H*).

^{19}F{^{1}H}-NMR (377 MHz, d_6-acetone, δ/ppm): -134.0 (*d*, *J* = 21 Hz, 8F, Aryl-*F*), -139.5 (*m*, 8F, Aryl-*F*), -156.2 (*m*, 8F, Aryl-*F*), -168.7 (*t*, *J* = 21 Hz, 4F, Aryl-*F*).

MS (MALDI-ToF, m/z): 1486 (100%, M$^+$).

UV/Vis (CH$_2$Cl$_2$): λ_{max} = 413, 507, 583 nm.

Crystal data for **TPPF28**: formula $C_{76.26}H_{34.52}F_{28.00}N_4O_{6.75}$, M = 1646.78, F(000) = 3304.435, colourless needle, size $0.020 \cdot 0.030 \cdot 0.220$ mm^3, monoclinic, space group C 2/c , Z = 4, a = 36.8024(11) Å, b = 9.7053(3) Å, c = 24.1038(7) Å, α = 90°, β = 123.4190(10)°, γ = 90°, V = 7185.9(4) Å^3, $D_{calc.}$ = 1.522 Mg $\cdot$ m^{-3}. The crystal was measured on a Bruker Kappa Apex2 diffractometer at 123K using graphite-monochromated Mo K_α-radiation with λ = 0.71073 Å, Θ_{max} = 33.141°. Minimal/maximal transmission 1.00/1.00, μ = 0.147 mm^{-1}. The Apex2 suite has been used for datacollection and integration. From a total of 106513 reflections, 13669 were independent (merging r = 0.031). From these, 10693 were considered as observed (I>2.0σ(I)) and were used to refine 742 parameters. The structure was solved by Other methods using the program Superflip. Least-squares refinement against F was carried out on all non-hydrogen atoms using the program CRYSTALS. R = 0.0784 (observed data), wR = 0.1177 (all data), GOF = 1.0458. Minimal/maximal residual electron density = -1.16/1.44 e Å^{-3}. Chebychev polynomial weights were used to complete the refinement. Plots were produced using CAMERON.
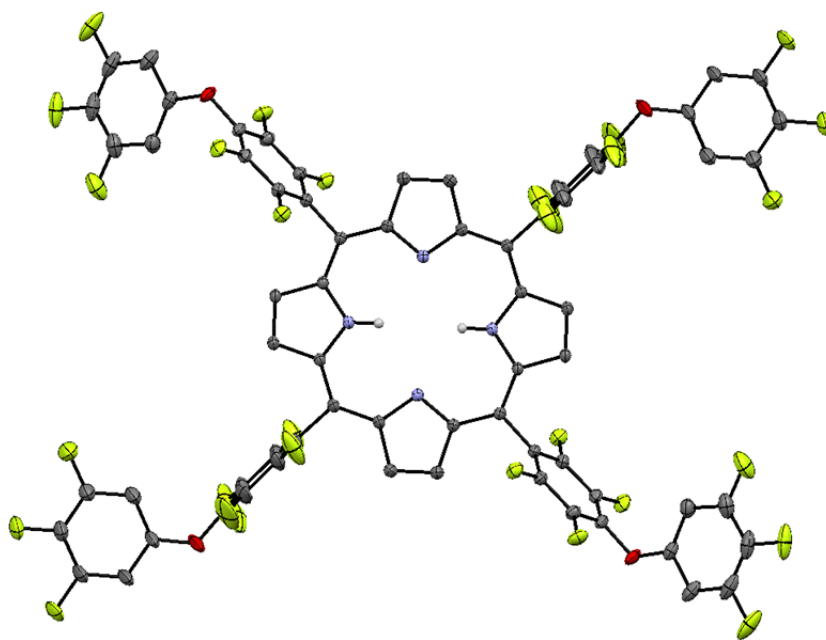
3rd Generation porphyrin library: TPPF28-x+17x
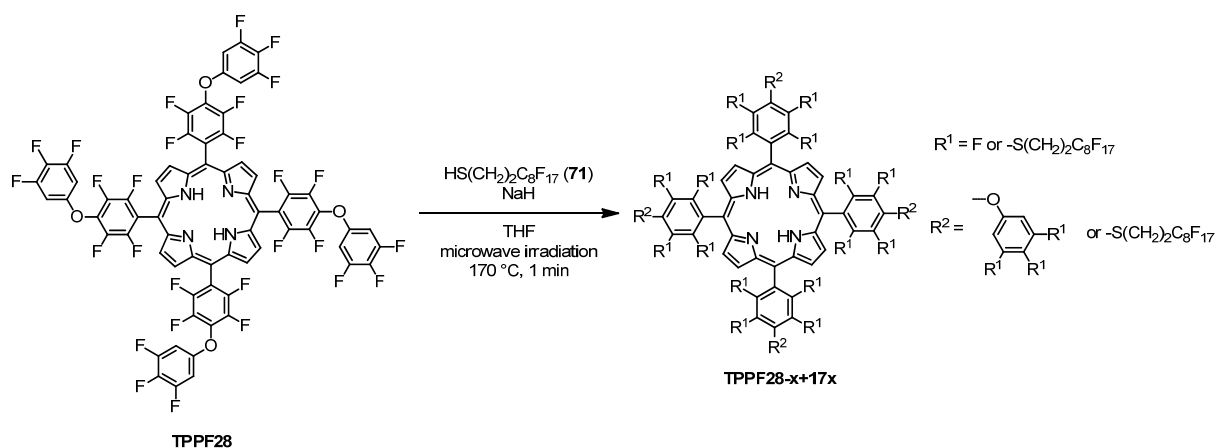
Porphyrin derivative **TPPF28** (4.0 mg, 2.69 µmol, 1.0 eq.), 1*H*,1*H*,2*H*,2*H*-perfluorodecane-1-thiol (**71**, 207 mg, 430 µmol, 160 eq.) and sodium hydride (60% dispersion in mineral oil, 12.9 mg, 323 µmol, 120 eq.) were added to tetrahydrofuran (4 mL) in a microwave vial. The sealed tube was heated under microwave irradiation to 170 °C for 1 minute. After cooling to room temperature the reaction mixture was quenched with water and subsequently extracted with diethylether. The organic layer was washed with brine and water, dried over sodium sulfate and evaporated to dryness. The resulting product mixture (180 mg) was analyzed by MALDI-ToF mass spectrometry.

MS (MALDI-ToF, m/z): 6 625 (25%), 7 086 (48%), 7 214 (56%), 7 343 (24%), 7 548 (33%), 7 675 (100%), 7 803 (54%), 8 135 (83%), 8 264 (96%), 8 595 (57%), 8 723 (92%), 8 854 (51%), 9 186 (68%), 9 313 (56%), 9 772 (49%).

4th Generation porphyrin library: TPPF28-x+26x
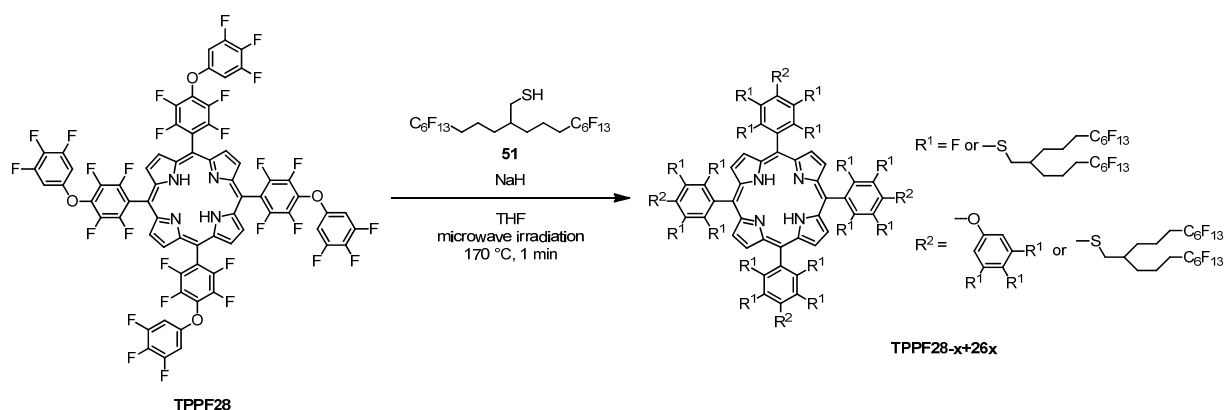
Porphyrin derivative **TPPF28** (4.0 mg, 2.69 µmol, 1.0 eq.), thiol **51** (168 mg, 215 µmol, 80 eq.) and sodium hydride (60% dispersion in mineral oil, 9.7 mg, 242 µmol, 90 eq.) were added to tetrahydrofuran (4 mL) in a microwave vial. The sealed tube was heated under microwave irradiation to 170 °C for 1 minute. After cooling to room temperature the reaction mixture was quenched with water and subsequently extracted with diethylether. The organic layer was washed with brine and water, dried over sodium sulfate and evaporated to dryness. The resulting product mixture (165 mg) was finally analyzed by MALDI-ToF mass spectrometry.

MS (MALDI-ToF, m/z): 7 960 (11%), 8 723 (26%), 8 849 (14%), 9 484 (43%), 9 612 (63%), 9 739 (14%), 10 247 (21%), 10 374 (100%), 10 502 (50%), 11 137 (61%), 11 265 (93%), 11 392 (15%), 11 897 (16%), 12 027 (79%), 12 155 (34%), 12 790 (30%), 12 918 (44%), 13 681 (20%).

N,N'-Di-(4'-methyl-3',5'-bis(perfluorohexyl)benzyl)-2,6-dichloronaphthalene-1,4,5,8-tetracarboxylic acid diimide (87)
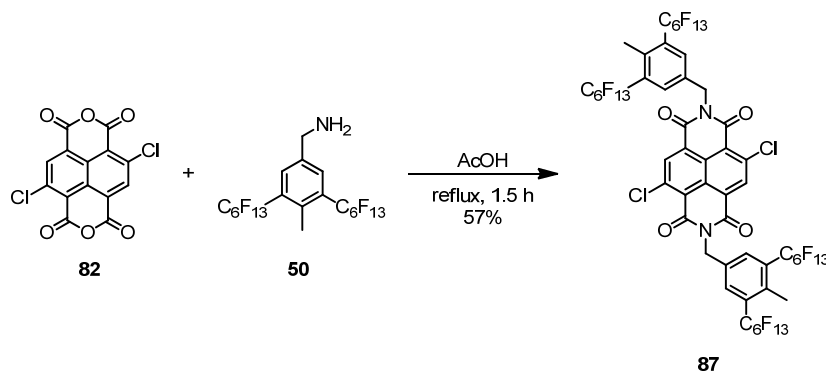
Amine **50** (840 mg, 1.11 mmol, 2.2 eq.) and 2,6-dichloronaphthalene-1,4,5,8-tetracarboxylic acid dianhydride (**82**, 170 mg, 504 µmol, 1.0 eq.) were added to acetic acid (15 mL). The mixture was heated to reflux for 90 minutes. While the mixture was allowed to cool to room temperature a pale orange solid formed. The precipitate was filtered off and subsequently washed with cold acetic acid and cold water. The pale yellow solid was dried under high vacuum to afford the fluorous NDI **87** ($C_{54}H_{16}Cl_2F_{52}N_2O_4$, 526 mg) as a yellowish solid in a yield of 57%. The product was used without any further purification for the next reaction steps.

MS (MALDI-ToF, m/z): 1815 (100%, $[M+H]^+$).

N,N′-Di-(4′-methyl-3′,5′-bis(perfluorohexyl)benzyl)-2,6-di-*n*-pentylaminonaphthalene-1,4,5,8-tetracarboxylic acid diimide (84)
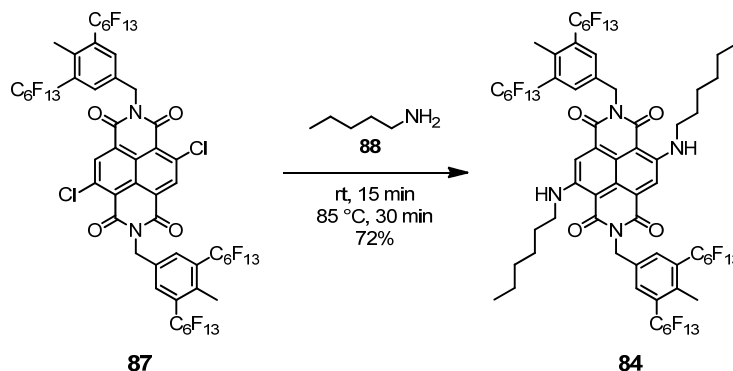
The fluorous NDI **87** (250 mg, 138 μmol, 1.0 eq.) was suspended in *n*-pentylamine (**88**, 5 mL). The mixture was stirred under an atmosphere of argon at room temperature for 15 minutes. The color of the reaction mixture turned from colorless to red. The temperature was raised to 85 °C, which was accompanied by a color change from red to blue. After 30 minutes at this temperature the mixture was allowed to cool to room temperature. The crude was dissolved in dichloromethane, absorbed on silica gel, evaporated to dryness and chromatographed using silica gel and a mixture of dichloromethane and hexane (1:1) as eluent. Target structure **84** ($C_{66}H_{44}F_{52}N_4O_4$, 194 mg) was isolated as a blue solid in a yield of 72%.

TLC: R_f = 0.51 (hexane/dichloromethane 1:1).

^{1}H-NMR (600 MHz, C_6D_6, δ/ppm): 9.35 (*t*, $^3J_{HH}$ = 5.1 Hz, 2H, N*H*), 8.26 (*s*, 4H, Aryl-*H*), 8.20 (*s*, 2H, naphthalene-*H*), 5.15 (*s*, 4H, C*H$_2$*), 2.87 – 2.82 (*m*, 4H, C*H$_2$*), 2.35 (*s*, 6H, C*H$_3$*). *The residual protons of the pentyl chain could not be assigned as signals originating from traces of the solvents used for chromatography overlap with the pentyl signals.*

^{19}F-NMR (377 MHz, $CDCl_3$, δ/ppm): -81.9 (*t*, *J* = 10 Hz, 12F, C*F$_3$*), -104.5 (*m*, 8F, C*F$_2$*), -121.1 (*m*, 8F, C*F$_2$*), -122.8 (*m*, 8F, C*F$_2$*), -123.9 (*m*, 8F, C*F$_2$*), -127.3 (*m*, 8F, C*F$_2$*).

MS (MALDI-ToF, m/z): 1944 (100%, M$^+$).

UV/Vis (CH_2Cl_2): λ_{max} = 279, 347, 364, 580, 622 nm.

Attempted synthesis of *N*,*N*'-**Di-(4'-methyl-3',5'-bis(perfluorohexyl)benzyl)-2,6-di-(1''***H***,1''***H***,2''***H***,2''***H***-perfluorodecanethio)naphthalene-1,4,5,8-tetracarboxylic acid diimide (85)**
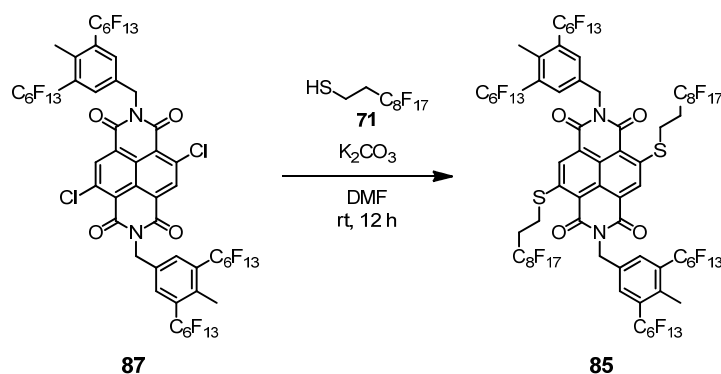
To a suspension of the diimide derivative **87** (80 mg, 44 µmol, 1.0 eq.) and potassium carbonate (37 mg, 264 µmol, 6.0 eq.) as base in DMF (20 mL) was added 1*H*,1*H*,2*H*,2*H*-perfluorodecanethiol (**71**, 76 µL, 127 mg, 264 µmol, 6.0 eq.). The mixture was stirred under an atmosphere of argon at room temperature for 12 hours. Already after a few minutes the reaction mixture turned from colorless to red. After cooling to room temperature a triphasic extraction using water, dichloromethane and perfluorohexane was performed. The dark red colored fluorous phase was evaporated to dryness and the crude was purified by column chromatography using silica gel and a solvent mixture of ethyl acetate and hexane (1:5). Subsequently the crude was further purified by column chromatography using a fluorous silica gel. The column was conditioned with a mixture of acetonitrile and diethylether (1:1). The diethylether content was gradually increased to 100%. At a solvent ration of 80/20 (Et$_2$O/MeCN) the product was eluted. The isolated red solid containing product **85** (C$_{74}$H$_{24}$F$_{86}$N$_2$O$_4$S$_2$, 10 mg) was poorly soluble in common organic solvents and showed still several side products.

MS (MALDI-ToF, m/z): 2707 (100%, M$^+$), 2258 (77%, [M$_{\text{side product}}$]$^+$).

UV/Vis (FC-72): λ_{max} = 263, 290, 367, 489, 522 nm.

Attempted synthesis of N,N'-Di-(4'-methyl-3',5'-bis(perfluorohexyl)benzyl)-2,6-di-(4''-methyl-3'',5''-bis(perfluorohexyl)benzylamino)naphthalene-1,4,5,8-tetracarboxylic acid diimide (86)
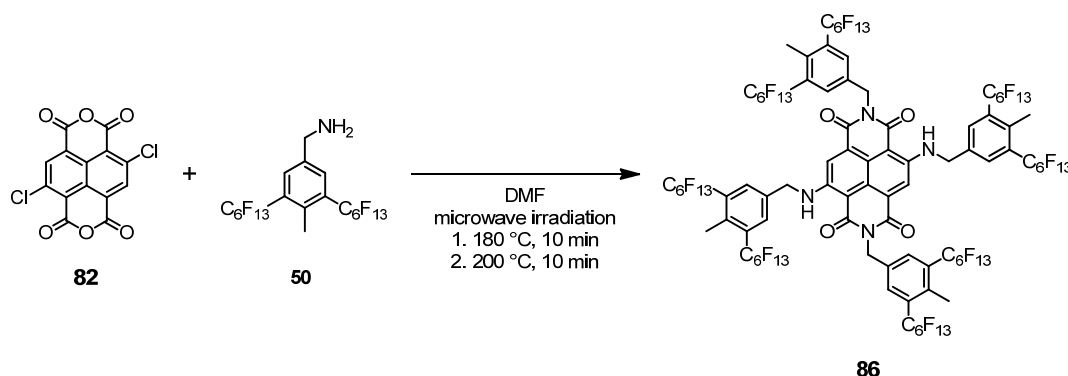
Dianhydride **82** (30 mg, 89 μmol, 1.0 eq.), amine **50** (337 mg, 445 μmol, 5.0 eq.) and DMF (15 mL) were added to a microwave vial (Biotage microwave vial 10-20 mL). The sealed tube was heated in a microwave apparatus (Biotage, Initiator 8) to 180 °C for 10 minutes. After checking the conversion by TLC (silica gel, dichloromethane/hexane 1:1) it was decided to heat to 200 °C for another 10 minutes. The mixture was cooled to room temperature and it was extracted with water and perfluorohexane. The fluorous phase was evaporated to dryness. The crude was chromatographed with FRPSG (perfluorohexyl functionalized silica gel from the group of Prof. Bannwarth). The obtained blue solid obtained the desired product **86** ($C_{94}H_{32}F_{104}N_4O_4$), as indicated by MALDI-ToF-MS, but the purity could not be analyzed because of the very poor solubility of the obtained sample.

¹H-NMR (500 MHz, CDCl₃, δ/ppm): 9.80 (t, $^3J_{HH}$ = 5.5 Hz, 2H, N*H*), 8.10 (s, 2H, naphthalene-*H*), 7.95 (s, 4H, Aryl-*H*), 7.80 (s, 4H, Aryl-*H*), 5.36 (s, 4H, C*H₂*), 4.83 (d, $^3J_{HH}$ = 5.5 Hz, 4H, C*H₂*NH), 2.55 (s, 6H, C*H₃*), 2.49 (s, 6H, C*H₃*).

MS (MALDI-ToF, m/z): 3255 (100%, M⁺), 2515 (29%).

5,10,15,20-Tetrakis[4-(2-perfluorooctylethylthio)-2,3,5,6-tetrafluorophenyl]-porphyrin zinc (89)
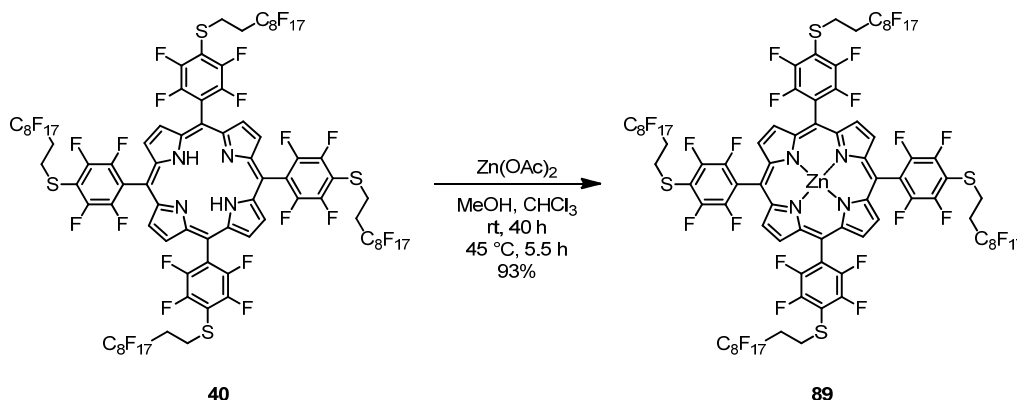
Porphyrin derivative **40** (134 mg, 47.6 µmol, 1.0 eq.) and zinc acetate (17.5 mg, 95.2 µmol, 2.0 eq.) were dissolved under an atmosphere of argon in a mixture of chloroform (20 mL) and methanol (4 mL). The mixture was stirred at room temperature. TLC control after 24 hours revealed still unreacted starting material. Another two equivalents of zinc acetate, chloroform (10 mL) and methanol (1 mL) were added, and the mixture was stirred for another 16 hours at room temperature. Subsequently, the temperature was increased to 45 °C, another two equivalents of zinc acetate were added and the mixture was stirred for 5.5 hours. After cooling to room temperature the reaction mixture was evaporated to dryness and chromatographed using silica gel and a mixture of cyclohexane and acetone (5:1). The metalloporphyrin **89** ($C_{84}H_{24}F_{84}N_4S_4Zn$, 127 mg) was isolated as a pink solid in a yield of 93%.

TLC: R_f = 0.33 (cyclohexane/acetone 5:1).

^{1}H-NMR (400 MHz, CDCl$_3$, δ/ppm): 9.00 (*s*, 8H, β-*H*), 3.52 – 3.45 (*m*, 8H, C*H*$_2$), 2.79 – 2.62 (*m*, 8H, C*H*$_2$).

^{19}F-NMR (377 MHz, CDCl$_3$, δ/ppm): -81.0 (*t*, *J* = 10 Hz, 12F, C*F*$_3$), -114.0 (*m*, 8F, C*F*$_2$), -121.8 (*m*, 8F, C*F*$_2$), -122.1 (*m*, 16F, C*F*$_2$), -122.9 (*m*, 8F, C*F*$_2$), -123.4 (*m*, 8F, C*F*$_2$), -126.4 (*m*, 8F, C*F*$_2$), -134.1 (*m*, 8F, Aryl-*F*), -136.5 (*m*, 8F, Aryl-*F*).

MS (MALDI-ToF, m/z): 2876 (100%, M$^+$).

EA: calculated: C = 35.05, H = 0.84, N = 1.95, found: C = 34.90, H = 1.02, N = 2.12.

UV/Vis (CH$_2$Cl$_2$): λ$_{max}$ = 416, 544, 578 nm.

4,5-Bis(2,2,2-trifluoroethoxy)phthalonitrile (90)
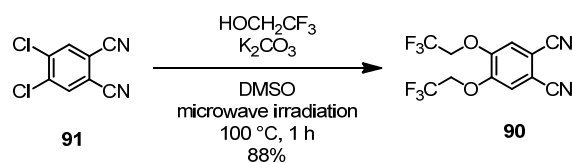
4,5-Dichlorophthalonitrile (**91**, 200 mg, 1.02 mmol, 1.0 eq.), 2,2,2-trifluoroethanol (609 mg, 6.09 mmol, 6.0 eq.) and potassium carbonate (842 mg, 6.09 mmol, 6.0 eq,) were added to dry DMSO (10 mL) in a microwave vial (Biotage microwave vial 10-20 mL). The sealed tube was heated in a microwave apparatus to 100 °C for one hour. After cooling to room temperature water was added to the reaction mixture. The mixture was extracted with dichloromethane. The combined organic phases were washed with brine and subsequently dried over magnesium sulfate. After evaporation of the solvent under reduced pressure the crude was purified by column chromatography (silica gel; cyclohexane/ethyl acetate, 4:1) to afford 4,5-bis(2,2,2-trifluoroethoxy)phthalonitrile (**90**, $C_{12}H_6F_6N_2O_2$, 291 mg) as a white solid in a yield of 88%.

TLC: R_f = 0.40 (hexane/ethylacetate 4:1).

^{1}H-NMR (400 MHz, CDCl$_3$, δ/ppm): 7.33 (s, 2H, Aryl-*H*), 4.51 (q, $^3J_{HH}$ = 7.7 Hz, 4H, C*H$_2$*).

^{19}F-NMR (377 MHz, CDCl$_3$, δ/ppm): -73.7 (t, J = 7.7 Hz, 6F, C*F$_3$*).

^{13}C-NMR (101 MHz, CDCl$_3$, δ/ppm): 151.0, 122.6 (q, J = 278 Hz), 120.2, 114.7, 111.6, 67.4 (q, J = 37 Hz).

MS (EI-QMS, m/z): 324 (100%, M$^+$), 241 (25%), 171 (35%), 83 (45%).

2,3,9,10,16,17,23,24-Octakis(2,2,2-trifluoroethoxy)phthalocyaninatozinc(II) (F24PcZn)
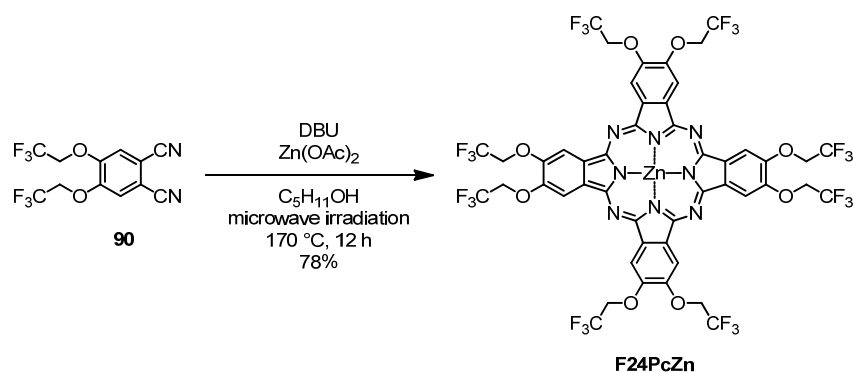
4,5-Bis(2,2,2-trifluoroethoxy)phthalonitrile (**90**, 100 mg, 308 µmol, 1.0 eq.), zinc acetate (14.2 mg, 77.1 µmol, 0.25 eq.) and 1,8-diazabicyclo[5.4.0]undec-7-ene (DBU, 46 µL, 47 mg, 308 µmol, 1.0 eq.) were added to pentanol (3.5 mL) in a microwave vial (Biotage microwave vial 2-5 mL). The sealed tube was heated in a microwave apparatus to 170 °C for 12 hours. After cooling to room temperature the solvent was removed by distillation at ambient pressure. Diethylether was added and the solution was washed successively with water and brine. The organic phase was dried over magnesium sulfate. After evaporation of the solvent under reduced pressure, the crude was purified by column chromatography (silica gel; diethylether/hexane 8:2 then 9:1) to afford 2,3,9,10,16,17,23,24-octakis(2,2,2-trifluoroethoxy)phthalocyaninatozinc(II) (**F24PcZn**, $C_{48}H_{24}F_{24}N_8O_8Zn$, 82 mg) as a blue solid in a yield of 78%.

^{1}H-NMR (400 MHz, d_6-acetone, δ/ppm): 8.50 (*s*, br, 8H), 5.40 – 5.20 (*m*, 16H).

^{19}F{^{1}H} -NMR (377 MHz, d_6-acetone, δ/ppm): -74.3 (*s*, 24F, C*F*$_3$).

MS (MALDI-ToF, m/z): 1360 (100%, M$^+$).

UV/Vis (acetone): λ_{max} = 360, 600, 635, 664 nm.

2,3,9,10,16,17,23,24-Octakis(2,2,2-trifluoroethoxy)phthalocyaninato-magnesium(II) (F24PcMg)
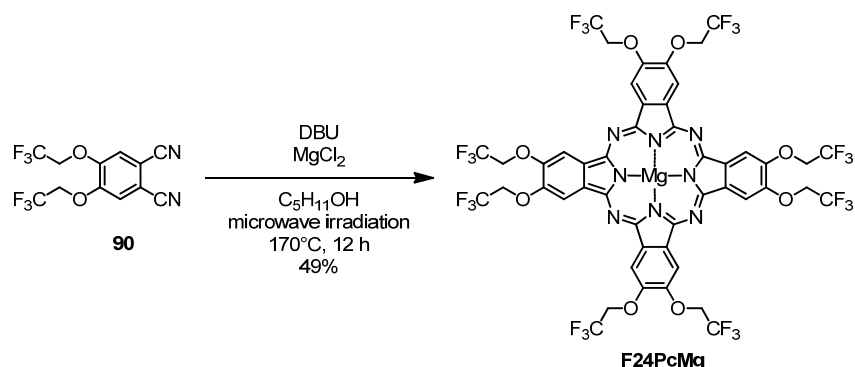
4,5-Bis(2,2,2-trifluoroethoxy)phthalonitrile (**90**, 75 mg, 231 µmol, 1.0 eq.), magnesium dichloride (5.5 mg, 57.8 µmol, 0.25 eq.) and 1,8-diazabicyclo[5.4.0]undec-7-ene (DBU, 35 µL, 35 mg, 231 µmol, 1.0 eq.) were added to pentanol (3.0 mL) in a microwave vial (Biotage microwave vial 2-5 mL). The sealed tube was heated in a microwave apparatus to 170 °C for 12 hours. After cooling to room temperature the solvent was removed by distillation at ambient pressure. The crude was purified by column chromatography (silica gel; acetone/hexane 1:1) to afford the title compound **F24PcMg** ($C_{48}H_{24}F_{24}MgN_8O_8$, 37 mg) as a blue solid in a yield of 49%.

TLC: R_f = 0.67 (hexane/acetone 1:1).

^{1}H-NMR (400 MHz, d_6-acetone, δ/ppm): 8.62 (s, br, 8H), 5.46 – 5.09 (m, 16H).

^{19}F{H} -NMR (377 MHz, d_6-acetone, δ/ppm): -74.4 (s, 24F, CF_3).

MS (MALDI-ToF, m/z): 1320 (100%, M$^+$).

UV/Vis (acetone): λ_{max} = 356, 600, 635, 663 nm.

2,3,9,10,16,17,23,24-Octakis(2,2,2-trifluoroethoxy)phthalocyanine (F24PcH2)
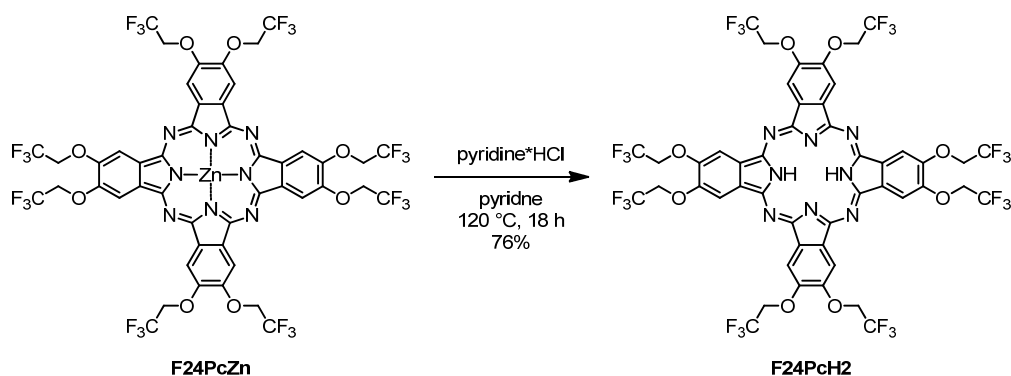
2,3,9,10,16,17,23,24-Octakis(2,2,2-trifluoroethoxy)phthalocyaninatozinc(II)   (**F24PcZn**, 70 mg, 51.4 µmol, 1.0 eq.) and pyridine hydrochloride (1.50 g) were added to dry pyridine (3 mL). The mixture was stirred under argon at 120 °C for 18 hours. Water (15 mL) was added to the hot reaction mixture. After cooling to room temperature the resulting precipitate was collected by centrifugation. The dark blue precipitate was washed successively with water, methanol, acetone and diethylether, and subsequently dried under high vacuum to yield **F24PcH2** ($C_{48}H_{26}F_{24}N_8O_8$, 51 mg) as a blue solid in a yield of 76%. The metal-free phthalocyanine **F24PcH2** is completely insoluble in common organic solvents and was thus exclusively characterized by solid-state analytical methods like MALDI-ToF mass spectrometry and elemental analysis.

MS (MALDI-ToF, m/z): 1298 (100%, M$^+$).

EA: calculated: C = 44.39, H = 2.02, N = 8.63, found: C = 44.42, H = 2.16, N = 8.77.

8   Abbreviations

Ac	acetyl
amu	atomic mass unit
aq.	aqueous
br	broad
bu	butyl
CC	column chromatography
CMOS	complementary metal oxide semiconductor
conc	concentrated
d	duplet
DBU	1,8-diazabicyclo[5.4.0]undec-7-ene
DCM	dichloromethane
DIAD	diisopropyl azodicarboxylate
DIBAL	diisobutyl aluminum hydride
diglyme	diethylene glycol dimethyl ether
DMAC	dimethylacetamide
DMAP	4-dimethylaminopyridine
DMF	*N,N*-dimethylformamide
DMI	1,3-dimethyl-2-imidazolidinone
DMSO	dimethylsulfoxide
DU	degree of unsaturation
EA	elemental analysis
EI	electron impact
EMCCD	electron multiplying charge-coupled device
eq.	equivalent
ESI	electrospray ionization
Et	ethyl
F-	perfluoro-
FBC	fluorous biphasic catalysis

FAB	fast atom bombardment
FMS	fluorous mixture synthesis
FRPSG	fluorous reverse phase silica gel
GPC	gel permeation chromatography
h	hour
HMPA	hexamethylphosphoramide
HPLC	high-performance liquid chromatography
K	Kelvin
KDTLI	Kapitza-Dirac-Talbot-Lau interferometer
m	multiplet
M	molar
m	milli
m/z	mass per charge
MALDI	matrix-assisted laser desorption ionization
Me	methyl
min	minute
MS	mass spectrometry
MUPI	multi-photon ionization
M_W	molecular weight
n	nano
NDI	naphthalene diimide
NMP	*N*-methyl-pyrrolidone
NMR	nuclear magnetic resonance
NP	nanoparticle
OPE	oligo phenylene ethynylene
OPV	oligo phenylene vinylene
OTf	triflate
p	piko
PDC	pyridinium dichromate
PDT	photodynamic therapy

PFMC	perfluoro(methylcyclohexane)
PG	protecting group
Ph	phenyl
ppm	parts per million
q	quartet
QB	quartz balance
QIE	quantum interference experiments
QMS	quadrupole mass spectrometry
quant.	quantitative
R_f	retention factor
R_t	retention time
rt	room temperature
s	singlet
sat	saturated
S_NAr	nucleophilic aromatic substitution
STM	scanning tunneling microscopy
t	triplet
TBME	tert-butyl methyl ether
Tf_2O	trifluoromethanesulfonic anhydride
TFA	trifluoroacetic acid
THF	tetrahydrofuran
TLC	thin layer chromatography
TLD	thermal laser desorption
TLI	Talbot-Lau interferometer
T_M	melting point
TMS	tetramethylsilane
ToF	time of flight
TPP	tetraphenylporphyrin
Trt	trityl
UV	ultra violet

V	volt
Vis	visible
vol.-%	volume percent
W	watt
wt%	weight percent
ε	extinction coefficient
μ	micro

9   Literature

[1]   L. De Broglie, *Nature* **1923**, *112*, 540.
[2]   C. Davisson, L. H. Germer, *Nature* **1927**, *119*, 558–560.
[3]   I. Estermann, O. Stern, *Zeitschrift für Physik* **1930**, *61*, 95–125.
[4]   H. von Halban, P. Preiswerk, *Comptes Rendus de l'Académie des Sciences - Paris* **1936**, *203*, 73–5.
[5]   T. Young, *Lectures on Natural Philosophy* **1807**, 1.
[6]   D. Meschede, *Optik, Licht und Laser*, Vieweg Teubner In Gwv Fachverlage, Wiesbaden, **2008**.
[7]   C. Jönsson, *Zeitschrift für Physik* **1961**, *161*, 454–474.
[8]   A. Zeilinger, R. Gähler, C. G. Shull, W. Treimer, W. Mampe, *Reviews of Modern Physics* **1988**, *60*, 1067–1073.
[9]   O. Carnal, A. Faulstich, J. Mlynek, *Applied Physics B Photophysics and Laser Chemistry* **1991**, *53*, 88–91.
[10]   D. W. Keith, M. L. Schattenburg, H. I. Smith, D. E. Pritchard, *Physical Review Letters* **1988**, *61*, 1580–1583.
[11]   W. Schöllkopf, J. P. Toennies, *Science* **1994**, *266*, 1345 –1348.
[12]   C. J. Bordé, N. Courtier, F. du Burck, A. N. Goncharov, M. Gorlicki, *Physics Letters A* **1994**, *188*, 187–197.
[13]   M. S. Chapman, C. R. Ekstrom, T. D. Hammond, R. A. Rubenstein, J. Schmiedmayer, S. Wehinger, D. E. Pritchard, *Physical Review Letters* **1995**, *74*, 4783.
[14]   C. Lisdat, M. Frank, H. Knöckel, M.-L. Almazor, E. Tiemann, *The European Physical Journal D* **2000**, *12*, 235–240.
[15]   T. Reisinger, A. A. Patel, H. Reingruber, K. Fladischer, W. E. Ernst, G. Bracco, H. I. Smith, B. Holst, *Physical Review A* **2009**, *79*, 053823.
[16]   M. Arndt, O. Nairz, J. Vos-Andreae, C. Keller, G. van der Zouw, A. Zeilinger, *Nature* **1999**, *401*, 680–682.
[17]   J. F. Clauser, S. Li, *Physical Review A* **1994**, *49*, R2213–R2216.
[18]   O. Nairz, M. Arndt, A. Zeilinger, *Journal of Modern Optics* **2000**, *47*, 2811–2821.
[19]   O. Nairz, M. Arndt, A. Zeilinger, *American Journal of Physics* **2003**, *71*, 319.
[20]   M. Arndt, O. Nairz, J. Petschinka, A. Zeilinger, *Comptes Rendus de l'Académie des Sciences - Series IV - Physics* **2001**, *2*, 581–585.
[21]   O. Nairz, B. Brezger, M. Arndt, A. Zeilinger, *Physical Review Letters* **2001**, *87*, 160401.
[22]   P. L. Kapitza, P. a. M. Dirac, *Mathematical Proceedings of the Cambridge Philosophical Society* **1933**, *29*, 297–300.
[23]   P. E. Moskowitz, P. L. Gould, S. R. Atlas, D. E. Pritchard, *Physical Review Letters* **1983**, *51*, 370–373.
[24]   A. D. Cronin, J. Schmiedmayer, D. E. Pritchard, *Reviews of Modern Physics* **2009**, *81*, 1051–1129.
[25]   D. L. Freimund, K. Aflatooni, H. Batelaan, *Nature* **2001**, *413*, 142–143.
[26]   T. Juffmann, S. Nimmrichter, M. Arndt, H. Gleiter, K. Hornberger, *Foundations of Physics* **2010**, *42*, 98–110.
[27]   K. Hornberger, S. Gerlich, P. Haslinger, S. Nimmrichter, M. Arndt, *Reviews of Modern Physics* **2012**, *84*, 157–173.
[28]   H. F. Talbot, *Philosophical Magazine* **1836**, *9*, 401–407.
[29]   E. Lau, *Annalen der Physik* **1948**, *437*, 417–423.
[30]   W. B. Case, M. Tomandl, S. Deachapunya, M. Arndt, *Optics Express* **2009**, *17*, 20966–20974.
[31]   B. Brezger, M. Arndt, A. Zeilinger, *Journal of Optics B: Quantum and Semiclassical Optics* **2003**, *5*, S82.
[32]   M. Arndt, L. Hackermüller, E. Reiger, *Brazilian Journal of Physics* **2005**, *35*, 216–223.
[33]   B. Brezger, L. Hackermüller, S. Uttenthaler, J. Petschinka, M. Arndt, A. Zeilinger, *Physical Review Letters* **2002**, *88*, 100404.
[34]   L. Hackermüller, S. Uttenthaler, K. Hornberger, E. Reiger, B. Brezger, A. Zeilinger, M. Arndt, *Physical Review Letters* **2003**, *91*, 090408.
[35]   A. Stibor, A. Stefanov, F. Goldfarb, E. Reiger, M. Arndt, *New Journal of Physics* **2005**, *7*, 224.

[36]   S. Gerlich, L. Hackermüller, K. Hornberger, A. Stibor, H. Ulbricht, M. Gring, F. Goldfarb, T. Savas, M. Muri, M. Mayor, u. a., *Nature Physics* **2007**, *3*, 711–715.

[37]   K. Hornberger, S. Gerlich, H. Ulbricht, L. Hackermüller, S. Nimmrichter, I. V Goldt, O. Boltalina, M. Arndt, *New Journal of Physics* **2009**, *11*, 043032.

[38]   L. Hackermüller, K. Hornberger, B. Brezger, A. Zeilinger, M. Arndt, *Nature* **2004**, *427*, 711–714.

[39]   K. Hornberger, L. Hackermüller, M. Arndt, *Physical Review A* **2005**, *71*, 023601.

[40]   K. Hornberger, S. Uttenthaler, B. Brezger, L. Hackermüller, M. Arndt, A. Zeilinger, *Physical Review Letters* **2003**, *90*, 160401.

[41]   L. Hackermüller, K. Hornberger, B. Brezger, A. Zeilinger, M. Arndt, *Applied Physics B: Lasers and Optics* **2003**, *77*, 781–787.

[42]   A. Stibor, K. Hornberger, L. Hackermüller, A. Zeilinger, M. Arndt, *Laser Physics* **2005**, *15*, 10–17.

[43]   C. R. Ekstrom, J. Schmiedmayer, M. S. Chapman, T. D. Hammond, D. E. Pritchard, *Physical Review A* **1995**, *51*, 3883–3888.

[44]   A. Stefanov, M. Berninger, M. Arndt, *Measurement Science and Technology* **2008**, *19*, 055801.

[45]   M. Berninger, A. Stefanov, S. Deachapunya, M. Arndt, *Physical Review A* **2007**, *76*, 013607.

[46]   H. Ulbricht, M. Berninger, S. Deachapunya, A. Stefanov, M. Arndt, *Nanotechnology* **2008**, *19*, 045502.

[47]   L. Hackermüller, K. Hornberger, S. Gerlich, M. Gring, H. Ulbricht, M. Arndt, *Applied Physics B* **2007**, *89*, 469–473.

[48]   S. Nimmrichter, K. Hornberger, H. Ulbricht, M. Arndt, *Physical Review A* **2008**, *78*, 063607.

[49]   M. Gring, S. Gerlich, S. Eibenberger, S. Nimmrichter, T. Berrada, M. Arndt, H. Ulbricht, K. Hornberger, M. Müri, M. Mayor, u. a., *Physical Review A* **2010**, *81*, 031604.

[50]   J. Van Vleck, J. Hasbrouck, *The theory of electric and magnetic susceptibilities.*, Oxford University Press, **1965**.

[51]   M. Marksteiner, G. Kiesewetter, L. Hackermüller, H. Ulbricht, M. Arndt, *Acta Physica Hungarica A) Heavy Ion Physics* **2006**, *26*, 87–94.

[52]   E. Reiger, L. Hackermüller, M. Berninger, M. Arndt, *Optics Communications* **2006**, *264*, 326–332.

[53]   S. Deachapunya, P. J. Fagan, A. G. Major, E. Reiger, H. Ritsch, A. Stefanov, H. Ulbricht, M. Arndt, *The European Physical Journal D* **2007**, *46*, 307–313.

[54]   P. J. Fagan, P. J. Krusic, C. N. McEwen, J. Lazar, D. H. Parkert, N. Herron, E. Wasserman, *Science* **1993**, *262*, 404 –407.

[55]   T. Juffmann, S. Truppe, P. Geyer, A. G. Major, S. Deachapunya, H. Ulbricht, M. Arndt, *Physical Review Letters* **2009**, *103*, 263601.

[56]   A. Stefanov, A. Stibor, A. Dominguez-Clarimon, M. Arndt, *The Journal of Chemical Physics* **2004**, *121*, 6935.

[57]   F. Goldfarb, S. Deachapunya, A. Stefanov, A. Stibor, E. Reiger, M. Arndt, *Journal of Physics: Conference Series* **2005**, *19*, 125–133.

[58]   A. Dreas-Wlodarczak, M. Müllneritsch, T. Juffmann, C. Cioffi, M. Arndt, M. Mayor, *Langmuir* **2010**, *26*, 10822–10826.

[59]   S. I. Troyanov, P. A. Troshin, O. V. Boltalina, I. N. Ioffe, L. N. Sidorov, E. Kemnitz, *Angewandte Chemie International Edition* **2001**, *40*, 2285–2287.

[60]   O. V. Boltalina, A. Y. Borschevskii, L. N. Sidorov, J. M. Street, R. Taylor, *Chemical Communications* **1996**, 529–530.

[61]   O. V. Boltalina, V. Y. Markov, A. Y. Borschevskii, N. A. Galeva, L. N. Sidorov, G. Gigli, G. Balducci, *The Journal of Physical Chemistry B* **1999**, *103*, 3828–3832.

[62]   E. Kissa, *Fluorinated surfactants and repellents*, Marcel Dekker, New York, **2001**.

[63]   I. T. Horváth, J. Rábai, *Science* **1994**, *266*, 72 –75.

[64]   J. H. Hildebrand, D. R. F. Cochran, *Journal of the American Chemical Society* **1949**, *71*, 22–25.

[65]   A. P. Dobbs, M. R. Kimberley, *Journal of Fluorine Chemistry* **2002**, *118*, 3–17.

[66]   A. Endres, G. Maas, *Chemie in unserer Zeit* **2000**, *34*, 382–393.

[67]   I. Klement, H. Lütjens, P. Knochel, *Angewandte Chemie* **1997**, *109*, 1605–1607.

[68]   S. Schneider, W. Bannwarth, *Angewandte Chemie International Edition* **2000**, *39*, 4142–4145.

[69]   T. Soós, B. L. Bennett, D. Rutherford, L. P. Barthel-Rosa, J. A. Gladysz, *Organometallics* **2001**, *20*, 3079–3086.

[70]   J. Gladysz, *Handbook of fluorous chemistry*, Wiley-vch, Weinheim, **2004**.

[71]   A. Studer, S. Hadida, R. Ferritto, S.-Y. Kim, P. Jeger, P. Wipf, D. P. Curran, *Science* **1997**, *275*, 823 –826.

[72]   A. Ogawa, D. P. Curran, *The Journal of Organic Chemistry* **1997**, *62*, 450–451.

[73]   J. J. Maul, P. J. Ostrowski, G. A. Ublacker, B. Linclau, D. P. Curran, in *Modern Solvents in Organic Synthesis* (Hrsg.: P. Knochel), Springer Berlin Heidelberg, Berlin, Heidelberg, **1999**, S. 79–105.

[74]   G. E. Berendsen, K. A. Pikaart, L. De Galan, C. Olieman, *Analytical Chemistry* **1980**, *52*, 1990–1993.

[75]   D. P. Curran, *Synlett* **2001**, *2001*, 1488–1496.

[76]   D. P. Curran, S. Hadida, M. He, *The Journal of Organic Chemistry* **1997**, *62*, 6714–6715.

[77]   Z. Luo, Q. Zhang, Y. Oderaotoshi, D. P. Curran, *Science* **2001**, *291*, 1766 –1769.

[78]   W. Zhang, *Tetrahedron* **2003**, *59*, 4475–4489.

[79]   P. C. de Visser, M. van Helden, D. V. Filippov, G. A. van der Marel, J. W. Drijfhout, J. H. van Boom, D. Noort, H. S. Overkleeft, *Tetrahedron Letters* **2003**, *44*, 9013–9016.

[80]   H. Jian, J. M. Tour, *The Journal of Organic Chemistry* **2005**, *70*, 3396–3424.

[81]   H. Glatz, C. Blay, H. Engelhardt, W. Bannwarth, *Chromatographia* **2004**, *59*, 567–570.

[82]   B. Neal O., *Journal of Fluorine Chemistry* **1999**, *93*, 1–25.

[83]   B. Neal O., *Journal of Fluorine Chemistry* **1999**, *96*, 101–127.

[84]   V. C. R. Mcloughlin, J. Thrower, *Tetrahedron* **1969**, *25*, 5921–5940.

[85]   O. A. Tomashenko, V. V. Grushin, *Chemical Reviews* **2011**, *111*, 4475–4521.

[86]   Q.-Y. Chen, Z.-Y. Yang, Y.-B. He, *Journal of Fluorine Chemistry* **1987**, *37*, 171–176.

[87]   G. J. Chen, C. Tamborski, *Journal of Fluorine Chemistry* **1989**, *43*, 207–228.

[88]   G. J. Chen, L. S. Chen, K. C. Eapen, *Journal of Fluorine Chemistry* **1993**, *63*, 113–123.

[89]   G. J. Chen, L. S. Chen, K. C. Eapen, *Journal of Fluorine Chemistry* **1993**, *65*, 59–65.

[90]   D. J. Burton, Z.-Y. Yang, *Tetrahedron* **1992**, *48*, 189–275.

[91]   J.-C. Xiao, C. Ye, J. M. Shreeve, *Organic Letters* **2005**, *7*, 1963–1965.

[92]   S. Purser, P. R. Moore, S. Swallow, V. Gouverneur, *Chemical Society Reviews* **2008**, *37*, 320–330.

[93]   J.-A. Ma, D. Cahard, *Chemical Reviews* **2008**, *108*, PR1–PR43.

[94]   B. Bhhatarai, P. Gramatica, *Environmental Science & Technology* **2010**, *45*, 8120–8128.

[95]   P. J. Krusic, A. A. Marchione, F. Davidson, M. A. Kaiser, C.-P. C. Kao, R. E. Richardson, M. Botelho, R. L. Waterland, R. C. Buck, *The Journal of Physical Chemistry A* **2005**, *109*, 6232–6241.

[96]   A. M. A. Dias, C. M. B. Gonçalves, A. I. Caço, L. M. N. B. F. Santos, M. M. Piñeiro, L. F. Vega, J. A. P. Coutinho, I. M. Marrucho, *Journal of Chemical & Engineering Data* **2005**, *50*, 1328–1333.

[97]   N. L. Stock, D. A. Ellis, L. Deleebeeck, D. C. G. Muir, S. A. Mabury, *Environmental Science & Technology* **2004**, *38*, 1693–1699.

[98]   X. Feng, X. Xu, H. Lin, Y. Duan, *Fluid Phase Equilibria* **2010**, *290*, 127–136.

[99]   S. Wu, M. T. Gonzalez, R. Huber, S. Grunder, M. Mayor, C. Schönenberger, M. Calame, *Nature Nanotechnology* **2008**, *3*, 569–574.

[100]   R. Huber, M. T. González, S. Wu, M. Langer, S. Grunder, V. Horhoiu, M. Mayor, M. R. Bryce, C. Wang, R. Jitchati, u. a., *Journal of the American Chemical Society* **2007**, *130*, 1080–1084.

[101]   M. Mayor, C. von Hänisch, H. B. Weber, J. Reichert, D. Beckmann, *Angewandte Chemie International Edition* **2002**, *41*, 1183–1186.

[102]   E. Lörtscher, M. Elbing, M. Tschudy, C. von Hänisch, H. B. Weber, M. Mayor, H. Riel, *ChemPhysChem* **2008**, *9*, 2252–2258.

[103]   D. Vonlanthen, A. Mishchenko, M. Elbing, M. Neuburger, T. Wandlowski, M. Mayor, *Angewandte Chemie International Edition* **2009**, *48*, 8886–8890.

[104]   M. Badertscher, K. Bischofberger, M. E. Munk, E. Pretsch, *Journal of Chemical Information and Computer Sciences* **2001**, *41*, 889–893.

[105]   M. J. Frisch, *Gaussian 03W*, Gaussian Inc., Pittsburgh, **2003**.

[106]   P. Ganesan, X. Yang, J. Loos, T. J. Savenije, R. D. Abellon, H. Zuilhof, E. J. R. Sudhölter, *Journal of the American Chemical Society* **2005**, *127*, 14530–14531.

[107]   R. Rathore, C. L. Burns, I. A. Guzei, *The Journal of Organic Chemistry* **2004**, *69*, 1524–1530.

[108]   T. D. Nelson, R. D. Crouch, in *Organic Reactions* (Hrsg.: John Wiley & Sons, Inc.), John Wiley & Sons, Inc., Hoboken, NJ, USA, **2004**.

[109]   R. Brückner, *Reaktionsmechanismen: organische Reaktionen, Stereochemie, moderne Synthesemethoden*, Spektrum Akad. Verl., Berlin, **2007**.

[110]   J. Clayden, N. Greeves, S. Warren, *Organic chemistry*, Oxford University Press, Oxford, **2001**.

[111]   E. J. Corey, G. Schmidt, *Tetrahedron Letters* **1979**, *20*, 399–402.

[112]   E. J. Corey, P. L. Fuchs, *Tetrahedron Letters* **1972**, *13*, 3769–3772.

[113]   A. de Meijere, F. Diederich, *Metal-catalyzed cross-coupling reactions*, Wiley-vch, Weinheim, **2004**.

[114]   L. Kürti, B. Czako, *Strategic applications of named reactions in organic synthesis: background and detailed mechanisms*, Elsevier Academic Press, Amsterdam; Boston, **2005**.

[115]   N. M. Jenny, M. Mayor, T. R. Eaton, *European Journal of Organic Chemistry* **2011**, *2011*, 4965–4983.

[116]   N. E. Leadbeater, B. J. Tominack, *Tetrahedron Letters* **2003**, *44*, 8653–8656.

[117]   I. Compagnon, R. Antoine, D. Rayane, M. Broyer, P. Dugourd, *Physical Review Letters* **2002**, *89*, 253001.

[118]   J. Tüxen, S. Gerlich, S. Eibenberger, M. Arndt, M. Mayor, *Chemical Communications* **2010**, *46*, 4145–4147.

[119]   M. J. Frisch, *Gaussian 09*, Gaussian Inc., Wallingford CT, **2009**.

[120]   S. Schneider, W. Bannwarth, *Helvetica Chimica Acta* **2001**, *84*, 735–742.

[121]   A. Hirsch, *Angewandte Chemie International Edition* **1993**, *32*, 1138–1141.

[122]   C. Bingel, *Chemische Berichte* **1993**, *126*, 1957–1959.

[123]   A. Hirsch, I. Lamparth, T. Groesser, H. R. Karfunkel, *Journal of the American Chemical Society* **1994**, *116*, 9385–9386.

[124]   S. R. Wilson, M. E. Yurchenko, D. I. Schuster, E. N. Yurchenko, O. Sokolova, S. E. Braslavsky, G. Klihm, *Journal of the American Chemical Society* **2002**, *124*, 1977–1981.

[125]   S. R. Wilson, V. Cayetano, M. Yurchenko, *Tetrahedron* **2002**, *58*, 4041–4047.

[126]   H. Nagashima, K. Hosoda, T. Abe, S. Iwamatsu, T. Sonoda, *Chemistry Letters* **1999**, 469–470.

[127]   S. J. Tavener, J. H. Clark, *Journal of Fluorine Chemistry* **2003**, *123*, 31–36.

[128]   U. Schurath, *Chemie in unserer Zeit* **1977**, *11*, 181–189.

[129]   A. Hirsch, O. Vostrowsky, *European Journal of Organic Chemistry* **2001**, *2001*, 829–848.

[130]   A. Hirsch, *Synthesis* **1995**, *1995*, 895–913.

[131]   K. Kadish, K. M. Smith, R. Guilard, Hrsg., *The Porphyrin Handbook Volume 4*, Academic Press, **1999**.

[132]   S. Deachapunya, A. Stefanov, M. Berninger, H. Ulbricht, E. Reiger, N. L. Doltsinis, M. Arndt, *The Journal of Chemical Physics* **2007**, *126*, 164304.

[133]   S. Eibenberger, S. Gerlich, M. Arndt, J. Tüxen, M. Mayor, *New Journal of Physics* **2011**, *13*, 043033.

[134]   G. Pozzi, F. Montanari, S. Quici, *Chemical Communications* **1997**, 69–70.

[135]   G. Pozzi, I. Colombani, M. Miglioli, F. Montanari, S. Quici, *Tetrahedron* **1997**, *53*, 6145–6162.

[136]   O. Paleta, M. Beneš, J. Koutníková, V. Král, *Tetrahedron Letters* **2002**, *43*, 6827–6831.

[137]   G. Pozzi, L. Mercs, O. Holczknecht, F. Martimbianco, F. Fabris, *Advanced Synthesis & Catalysis* **2006**, *348*, 1611–1620.

[138]   J. I. T. Costa, A. C. Tomé, M. G. P. M. S. Neves, J. A. S. Cavaleiro, *Journal of Porphyrins and Phthalocyanines* **2011**, *15*, 1116.

[139]   C. R. Becer, R. Hoogenboom, U. S. Schubert, *Angewandte Chemie International Edition* **2009**, *48*, 4900–4908.

[140]   M. Suzuki, S. Shimizu, J.-Y. Shin, A. Osuka, *Tetrahedron Letters* **2003**, *44*, 4597–4601.

[141]   J. Kvíčala, M. Beneš, O. Paleta, V. Král, *Journal of Fluorine Chemistry* **2010**, *131*, 1327–1337.

[142] K. M. Kadish, B. C. Han, M. M. Franzen, C. Araullo-McAdams, *Journal of the American Chemical Society* **1990**, *112*, 8364–8368.

[143] P. Battioni, O. Brigaud, H. Desvaux, D. Mansuy, T. G. Traylor, *Tetrahedron Letters* **1991**, *32*, 2893–2896.

[144] J. Králová, T. Bříza, I. Moserová, B. Dolenský, P. Vašek, P. Poučková, Z. Kejík, R. Kaplánek, P. Martásek, M. Dvořák, u. a., *Journal of Medicinal Chemistry* **2008**, *51*, 5964–5973.

[145] F. da C. Santos, A. C. Cunha, M. C. B. V. de Souza, A. C. Tomé, M. G. P. M. S. Neves, V. F. Ferreira, J. A. S. Cavaleiro, *Tetrahedron Letters* **2008**, *49*, 7268–7270.

[146] V. V. Serra, F. Camoes, S. I. Vieira, M. A. F. Faustino, J. P. C. Tomé, D. C. G. A. Pinto, M. G. Neves, A. C. Tomé, A. M. S. Silva, E. F. C. e Silva, u. a., *Acta Chimica Slovenica* **2009**, *56*, 603–611.

[147] M. Suarez, E. Salfran, R. I. Rodriguez Curiel, F. Gaudemer, J. Elguero, *Bulletin des Sociétés Chimiques Belges* **1997**, 323–326.

[148] L. F. Pedrosa, M. C. de Souza, M. A. F. Faustino, M. G. P. M. S. Neves, A. M. S. Silva, A. C. Tomé, V. F. Ferreira, J. A. S. Cavaleiro, *Australian Journal of Chemistry* **2011**, *64*, 939–944.

[149] M. C. A. F. Gotardo, H. C. Sacco, J. C. S. Filho, A. G. Ferreira, A. C. Tedesco, M. D. Assis, *Journal of Porphyrins and Phthalocyanines* **2003**, *07*, 399.

[150] R. Breslow, Z. Fang, *Tetrahedron Letters* **2002**, *43*, 5197–5200.

[151] S. Hirohara, M. Nishida, K. Sharyo, M. Obata, T. Ando, M. Tanihara, *Bioorganic & Medicinal Chemistry* **2010**, *18*, 1526–1535.

[152] R. Breslow, B. Gabriele, J. Yang, *Tetrahedron Letters* **1998**, *39*, 2887–2890.

[153] T. Bříza, R. Kaplánek, M. Havlík, B. Dolenský, Z. Kejík, P. Martásek, V. Král, *Supramolecular Chemistry* **2008**, *20*, 237–242.

[154] D. Samaroo, M. Vinodu, X. Chen, C. M. Drain, *Journal of Combinatorial Chemistry* **2007**, *9*, 998–1011.

[155] A. Varotto, L. Todaro, M. Vinodu, J. Koehne, G. Liu, C. M. Drain, *Chemical Communications* **2008**, 4921–4923.

[156] R. Kaplánek, T. Bříza, M. Havlík, B. Dolenský, Z. Kejík, P. Martásek, V. Král, *Journal of Fluorine Chemistry* **2006**, *127*, 386–390.

[157] R. P. Volante, *Tetrahedron Letters* **1981**, *22*, 3119–3122.

[158] O. Mitsunobu, M. Yamada, *Bulletin of the Chemical Society of Japan* **1967**, *40*, 2380–2382.

[159] H. R. Ing, R. H. F. Manske, *J. Chem. Soc.* **1926**, 2348–2351.

[160] L. J. Alvey, R. Meier, T. Soós, P. Bernatis, J. A. Gladysz, *European Journal of Inorganic Chemistry* **2000**, *2000*, 1975–1983.

[161] C. Rocaboy, D. Rutherford, B. L. Bennett, J. A. Gladysz, *Journal of Physical Organic Chemistry* **2000**, *13*, 596–603.

[162] X. Moreau, J.-M. Campagne, *The Journal of Organic Chemistry* **2003**, *68*, 5346–5350.

[163] T. Peterle, Benzylthioether stabilized gold nanoparticles: towards novel hybrid superstructures, Dissertation, University of Basel, **2009**.

[164] D. Samaroo, C. E. Soll, L. J. Todaro, C. M. Drain, *Organic Letters* **2006**, *8*, 4985–4988.

[165] N. Srinivasan, C. A. Haney, J. S. Lindsey, W. Zhang, B. T. Chait, *Journal of Porphyrins and Phthalocyanines* **1999**, *3*, 283–291.

[166] P. J. Spellane, M. Gouterman, A. Antipas, S. Kim, Y. C. Liu, *Inorganic Chemistry* **1980**, *19*, 386–391.

[167] K. Kalyanasundaram, *Photochemistry of polypyridine and porphyrin complexes*, Academic Press, London; San Diego, **1992**.

[168] M. E. Peach, A. M. Smith, *Journal of Fluorine Chemistry* **1974**, *4*, 399–408.

[169] B. C. Musial, M. E. Peach, *Journal of Fluorine Chemistry* **1976**, *7*, 459–469.

[170] R. D. Chambers, W. K. R. Musgrave, J. S. Waterhouse, D. L. H. Williams, J. Burdon, W. B. Hollyhead, J. C. Tatlow, *Journal of the Chemical Society, Chemical Communications* **1974**, 239–240.

[171] T. R. Crowell, M. E. Peach, *Journal of Fluorine Chemistry* **1982**, *21*, 469–477.

[172] D. O'Hagan, *Chemical Society Reviews* **2008**, *37*, 308–319.

[173] W. Zhang, in *Microwave Methods in Organic Synthesis*, Springer Berlin Heidelberg, **2006**, S. 145–166.

[174] M. Gingras, J. Raimundo, Y. M. Chabre, *Angewandte Chemie* **2006**, *118*, 1718–1745.

[175]   J. N. Lowe, D. A. Fulton, S.-H. Chiu, A. M. Elizarov, S. J. Cantrill, S. J. Rowan, J. F. Stoddart, *The Journal of Organic Chemistry* **2004**, *69*, 4390–4402.

[176]   M. Mayor, J. Lehn, K. M. Fromm, D. Fenske, *Angewandte Chemie International Edition* **1997**, *36*, 2370–2372.

[177]   M. Mayor, M. Büschel, K. M. Fromm, J. Lehn, J. Daub, *Chemistry - A European Journal* **2001**, *7*, 1266–1272.

[178]   A. Pažitný, T. Solčán, D. Végh, *Journal of Fluorine Chemistry* **2009**, *130*, 267–294.

[179]   O. Carnal, J. Mlynek, *Physical Review Letters* **1991**, *66*, 2689–2692.

[180]   B. S. Zhao, G. Meijer, W. Schöllkopf, *Science* **2011**, *331*, 892–894.

[181]   R. P. Crease, *The most beautiful experiment in physics. Phys. World* **2002**.

[182]   A. Tonomura, *American Journal of Physics* **1989**, *57*, 117.

[183]   P. G. Merli, *American Journal of Physics* **1976**, *44*, 306.

[184]   G. Kaiser, T. Jarrosson, S. Otto, Y. Ng, A. D. Bond, J. K. M. Sanders, *Angewandte Chemie International Edition* **2004**, *43*, 1959–1962.

[185]   S. A. Vignon, T. Jarrosson, T. Iijima, H.-R. Tseng, J. K. M. Sanders, J. F. Stoddart, *Journal of the American Chemical Society* **2004**, *126*, 9884–9885.

[186]   G. D. Fallon, M. A.-P. Lee, S. J. Langford, P. J. Nichols, *Organic Letters* **2004**, *6*, 655–658.

[187]   G. J. Gabriel, B. L. Iverson, *Journal of the American Chemical Society* **2002**, *124*, 15174–15175.

[188]   A. J. Zych, B. L. Iverson, *Journal of the American Chemical Society* **2000**, *122*, 8898–8909.

[189]   J. Jazwinski, A. J. Blacker, J.-M. Lehn, M. Cesario, J. Guilhem, C. Pascard, *Tetrahedron Letters* **1987**, *28*, 6060.

[190]   S. Brochsztain, M. A. Rodrigues, G. J. F. Demets, M. J. Politi, *Journal of Materials Chemistry* **2002**, *12*, 1250–1255.

[191]   P. Mukhopadhyay, Y. Iwashita, M. Shirakawa, S. Kawano, N. Fujita, S. Shinkai, *Angewandte Chemie International Edition* **2006**, *45*, 1592–1595.

[192]   H. N. Lee, Z. Xu, S. K. Kim, K. M. K. Swamy, Y. Kim, S.-J. Kim, J. Yoon, *Journal of the American Chemical Society* **2007**, *129*, 3828–3829.

[193]   W. S. Horne, N. Ashkenasy, M. R. Ghadiri, *Chemistry - A European Journal* **2005**, *11*, 1137–1144.

[194]   S. Alp, Ş. Erten, C. Karapire, B. Köz, A. O. Doroshenko, S. İçli, *Journal of Photochemistry and Photobiology A: Chemistry* **2000**, *135*, 103–110.

[195]   M. Licchelli, A. Orbelli Biroli, A. Poggi, *Organic Letters* **2006**, *8*, 915–918.

[196]   F. Würthner, S. Ahmed, C. Thalacker, T. Debaerdemaeker, *Chemistry - A European Journal* **2002**, *8*, 4742–4750.

[197]   A. Błaszczyk, M. Fischer, C. von Hänisch, M. Mayor, *Helvetica Chimica Acta* **2006**, *89*, 1986–2005.

[198]   I. Pugliesi, P. Krok, S. Lochbrunner, A. Błaszczyk, C. von Hänisch, M. Mayor, E. Riedle, *Journal of Physical Chemistry A* **2010**, *114*, 12555–12560.

[199]   S. V. Bhosale, C. H. Jani, S. J. Langford, *Chemical Society Reviews* **2008**, *37*, 331–342.

[200]   C. Thalacker, C. Röger, F. Würthner, *The Journal of Organic Chemistry* **2006**, *71*, 8098–8105.

[201]   S. Gabutti, S. Schaffner, M. Neuburger, M. Fischer, G. Schäfer, M. Mayor, *Organic & Biomolecular Chemistry* **2009**, *7*, 3222–3229.

[202]   N. Sakai, J. Mareda, E. Vauthey, S. Matile, *Chemical Communications* **2010**, *46*, 4225–4237.

[203]   F. Chaignon, M. Falkenström, S. Karlsson, E. Blart, F. Odobel, L. Hammarström, *Chemical Communications* **2006**, 64–66.

[204]   H. Vollmann, H. Becker, M. Corell, H. Streeck, *Justus Liebigs Annalen der Chemie* **1937**, *531*, 1–159.

[205]   S. Gabutti, An Investigation of Naphthalenediimides as Central Building Blocks in Model Compounds for Scanning Tunneling Microscope Induced Light Emission Experiments and Förster Resonance Energy Transfer Studies, Dissertation, University of Basel, **2009**.

[206]   J. Weiss, *Journal of Inclusion Phenomena and Macrocyclic Chemistry* **2001**, *40*, 1–22.

[207]   P. Hambright, *Coordination Chemistry Reviews* **1971**, *6*, 247–268.

[208]   F. Da Cruz, K. Driaf, C. Berthier, J.-M. Lameille, F. Armand, *Thin Solid Films* **1999**, *349*, 155–161.

[209]   Z. Zhang, S. Hou, Z. Zhu, Z. Liu, *Langmuir* **2000**, *16*, 537–540.

[210]   M. T. Brumbach, A. K. Boal, D. R. Wheeler, *Langmuir* **2009**, *25*, 10685–10690.
[211]   M. Nappa, J. S. Valentine, *Journal of the American Chemical Society* **1978**, *100*, 5075–5080.
[212]   H. Zollinger, *Color chemistry: syntheses, properties and applications of organic dyes and pigments*, Vch, Weinheim; New York, **1987**.
[213]   A. Ebadi, N. Safari, M. H. Peyrovi, *Applied Catalysis A: General* **2007**, *321*, 135–139.
[214]   Y. Ooyama, Y. Harima, *European Journal of Organic Chemistry* **2009**, *2009*, 2903–2934.
[215]   A. Hirth, U. Michelsen, D. Wöhrle, *Chemie in unserer Zeit* **1999**, *33*, 84–94.
[216]   E. A. Lukyanets, *Journal of Porphyrins and Phthalocyanines* **1999**, *3*, 424–432.
[217]   B. A. Bench, W. W. Brennessel, H. Lee, S. M. Gorun, *Angewandte Chemie International Edition* **2002**, *41*, 750–754.
[218]   T. M. Keller, J. R. Griffith, *Journal of Fluorine Chemistry* **1979**, *13*, 73–77.
[219]   B. A. Bench, A. Beveridge, W. M. Sharman, G. J. Diebold, J. E. van Lier, S. M. Gorun, *Angewandte Chemie International Edition* **2002**, *41*, 747–750.
[220]   R. Minnes, R. Minnes, *Photochemistry and Photobiology* **2006**, *82*, 593.
[221]   T. Qiu, X. Xu, X. Qian, *Journal of Chemical Technology and Biotechnology* **2009**, *84*, 1051–1055.
[222]   T. Qiu, X. Xu, J. Liu, X. Qian, *Dyes and Pigments* **2009**, *83*, 127–133.
[223]   İ. Gürol, M. Durmuş, V. Ahsen, *European Journal of Inorganic Chemistry* **2010**, *2010*, 1220–1230.
[224]   G. Pozzi, S. Quici, M. C. Raffo, C. A. Bignozzi, S. Caramori, M. Orlandi, *Journal of Physical Chemistry C* **2011**, *115*, 3777–3788.
[225]   G. Löbbert, *Ullmann's Encyclopedia of Industrial Chemistry* **2000**.
[226]   B. I. Kharisov, U. Ortiz Méndez, J. L. Almaraz Garza, J. R. Almaguer Rodríguez, *New Journal of Chemistry* **2005**, *29*, 686.
[227]   Y. Gök, H. Kantekin, A. Bilgin, D. Mendil, I. Degirmencioglu, *Chemical Communications* **2001**, 285–286.
[228]   T. Muto, T. Temma, M. Kimura, K. Hanabusa, H. Shirai, *Chemical Communications* **2000**, 1649–1650.
[229]   J. Rusanova, M. Pilkington, S. Decurtins, *Chemical Communications* **2002**, 2236–2237.
[230]   D. Wöhrle, G. Schnurpfeil, G. Knothe, *Dyes and Pigments* **1992**, *18*, 91–102.
[231]   J. Alzeer, P. J. C. Roth, N. W. Luedtke, *Chemical Communications* **2009**, 1970–1971.
[232]   T. Juffmann, A. Milic, M. Müllneritsch, P. Asenbaum, A. Tsukernik, J. Tüxen, M. Mayor, O. Cheshnovsky, M. Arndt, *Nature Nanotechnology* **2012**, *7*, 297–300.
[233]   S. Gerlich, M. Gring, H. Ulbricht, K. Hornberger, J. Tüxen, M. Mayor, M. Arndt, *Angewandte Chemie International Edition* **2008**, *47*, 6195–6198.
[234]   J. Tüxen, S. Eibenberger, S. Gerlich, M. Arndt, M. Mayor, *European Journal of Organic Chemistry* **2011**, 4823–4833.
[235]   S. Gerlich, S. Eibenberger, M. Tomandl, S. Nimmrichter, K. Hornberger, P. J. Fagan, J. Tüxen, M. Mayor, M. Arndt, *Nature Communications* **2011**, *2*, 263.

10 Appendix

10.1 Contributions

All molecules were synthesized and characterized by Jens Tüxen. The described quantum interference experiments were performed in the group of Prof. Markus Arndt mainly by Dr. Stefan Gerlich, Sandra Eibenberger and Thomas Juffmann.

10.2 Publications

Parts of the work presented in this thesis have been published in the following articles:

Thomas Juffmann, Adriana Milic, Michael Müllneritsch, Peter Asenbaum, Alexander Tsukernik, Jens Tüxen, Marcel Mayor, Ori Cheshnovsky, Markus Arndt
Real-time single-molecule imaging of quantum interference
Nature Nanotechnology, **2012**, 7, 297.

Jens Tüxen, Sandra Eibenberger, Stefan Gerlich, Markus Arndt, Marcel Mayor
Highly Fluorous Porphyrins as Model Compounds for Molecule Interferometry
European Journal of Organic Chemistry, **2011**, 4823.

Sandra Eibenberger, Stefan Gerlich, Markus Arndt, Jens Tüxen, Marcel Mayor
Electric moments in molecule interferometry
New Journal of Physics, **2011**, *13*, 043033.

Stefan Gerlich, Sandra Eibenberger, Mathias Tomandl, Stefan Nimmrichter, Klaus Hornberger, Paul Fagan, Jens Tüxen, Marcel Mayor, Markus Arndt
Quantum interference of large organic molecules
Nature Communications, **2011**, *2*, 263.

Jens Tüxen, Stefan Gerlich, Sandra Eibenberger, Markus Arndt, Marcel Mayor
Quantum interference distinguishes between constitutional isomers
Chemical Communications, **2010**, *46*, 4145.

Stefan Gerlich, Michael Gring, Hendrik Ulbricht, Klaus Hornberger, Jens Tüxen, Marcel Mayor, Markus Arndt
Matter-Wave Metrology as a Complementary Tool for Mass Spectrometry
Angewandte Chemie International Edition, **2008**, *47*, 6195

10.3 Cover Design

The background of the book cover displays an interference pattern obtained in far-field experiments using phthalocyanine molecules. The same image was used for the cover design of the May 2012 issue of the journal *Nature Nanotechnology*.

Curriculum Vitae

Personal Information

Name	Jens Tüxen
Date/place of birth	February 14, 1983 in Lörrach, Germany
Citizenship	German

Education

06/2008 – 05/2012	**PhD** work at the University of Basel, Department of Chemistry, Switzerland. Thesis: "Highly Fluorinated Model Compounds for Matter-Wave Interferometry". Supervisor: Prof. Dr. Marcel Mayor.
04/2007 – 04/2008	**Master of Science** (MSc) in Chemistry, Institute of Organic Chemistry, University of Basel, Switzerland. Thesis: "Synthesis of Tailor-Made Molecules for Quantum Interference Experiments". Supervisor: Prof. Dr. Marcel Mayor.
10/2003 – 03/2007	**Bachelor of Science** (BSc) in Chemistry, University of Basel, Switzerland.
1993 – 2002	**Abitur** at the Kant-Gymnasium in Weil am Rhein, Germany.

Publications

• **Real-time single-molecule imaging of quantum interference**, T. Juffmann, A. Milic, M. Müllneritsch, P. Asenbaum, A. Tsukernik, J.Tüxen, M. Mayor, O. Cheshnovsky, M. Arndt, *Nature Nanotechnology*, **2012**, 7, 297.

• **Highly Fluorous Porphyrins as Model Compounds for Molecule Interferometry**, J. Tüxen, S. Eibenberger, S. Gerlich, M. Arndt, M. Mayor, *European Journal of Organic Chemistry*, **2011**, 4823.

• **Electric moments in molecule interferometry**, S. Eibenberger, S. Gerlich, M. Arndt, J. Tüxen, Marcel Mayor, *New Journal of Physics*, **2011**, 13, 043033.

• **Quantum interference of large organic molecules**, S. Gerlich, S. Eibenberger, M. Tomandl, S. Nimmrichter, K. Hornberger, P. Fagan, J. Tüxen, M. Mayor, M. Arndt, *Nature Communications*, **2011**, 2, 263.

• **Quantum interference distinguishes between constitutional isomers**, J. Tüxen, S. Gerlich, S. Eibenberger, M. Arndt, M. Mayor, *Chemical Communications*, **2010**, 46, 4145.

• **Amphiphilic Diblock Copolymers for Molecular Recognition: Metal-Nitrilotriacetic Acid Functionalized Vesicles**, R. Nehring, C. G. Palivan, O. Casse, Pa. Tanner, J. Tüxen, W. Meier, *Langmuir*, **2009**, 25, 1122.

• **Matter-Wave Metrology as a Complementary Tool for Mass Spectrometry**, S. Gerlich, M. Gring, H. Ulbricht, K. Hornberger, J. Tüxen, M. Mayor, M. Arndt, *Angewandte Chemie International Edition*, **2008**, 47, 6195.